

USING LIGHT DETECTION AND RANGING (LiDAR) TECHNOLOGY TO ASSESS BIRD-
HABITAT RELATIONSHIPS: A CASE STUDY IN THE NORTHWOODS OF MAINE

A Dissertation
Submitted to the Graduate Faculty
of the
North Dakota State University
of Agriculture and Applied Science

By

Wesley Eugene Newton

In Partial Fulfillment of the Requirements
for the Degree of
DOCTOR OF PHILOSOPHY

Major Department:
Natural Resources Management

April 2012

Fargo, North Dakota

North Dakota State University
Graduate School

Title

Using Light Detection and Ranging (LiDAR) Technology to Assess

Bird-habitat Relationships: A Case Study in the Northwoods of Maine

By

Wesley Eugene Newton

The Supervisory Committee certifies that this *disquisition* complies with North Dakota State University's regulations and meets the accepted standards for the degree of

DOCTOR OF PHILOSOPHY

SUPERVISORY COMMITTEE:

Mario E. Biondini, PhD

Chair

Jay B. Hestbeck, PhD

James W. Grier, PhD

Gary K. Clambey, PhD

Jack E. Norland, PhD

Approved:

19 April 2012

Date

Carolyn E. Grygiel, PhD

Department Chair

ABSTRACT

Airborne light detection and ranging (LiDAR) is a remote sensing technology that quantifies the travel time of photons emitted in pulses from a LiDAR instrument to travel to and reflect back from objects. Knowing the travel time for the photons and accounting for the speed of light, distances to objects from the instrument can be quantified. When LiDAR is acquired over forested areas some of the pulses will find canopy openings and “penetrate” to the ground with others striking the canopy at various heights above the ground, generating an XYZ point-cloud of eastings, northings, and elevations. Capitalizing on the information in these point-clouds from a June, 2003, acquisition in forested areas of Maine, we characterized the vertical profile of the canopy from which we computed LiDAR-derived explanatory variables for empirical modeling of various response variables (i.e., forest stand metrics, bird species abundance). The first aim of the research reported in this study was to assess the ability of LiDAR-derived explanatory variables to predict forest stand structure that can then be used as input in a suite of habitat-models that predict New England wildlife occurrences (called ECOSEARCH). Using regression analyses and field-collected data, we determined that LiDAR does a good job of predicting various forest stand metrics for the over- and understory (Adj. $R^2 > 0.60$ for 14 of 20 models developed). The second aim was to assess the ability of LiDAR-derived explanatory variables to directly predict mean bird abundance within forested areas during their breeding season. We derived a set of minimally correlated LiDAR-derived explanatory variables and used these in regression analyses to predict mean bird abundance from field surveys. Results indicate that LiDAR-derived explanatory variables were useful for predicting the mean abundance of 17 bird species (all with Adj. $R^2 > 0.2$, with 5 models having Adj. $R^2 > 0.4$). The third aim was to utilize the LiDAR-derived habitat-models and apply these

across two study sites under varying management scenarios for assessments and planning purposes. Using a simple Euclidean distance metric and under various but realistic assumptions we were able to ascertain optimal management scenarios for five focal bird species.

ACKNOWLEDGMENTS

I first want to thank Dr. Mario Biondini for offering me the opportunity to pursue a doctorate program at NDSU while accommodating my full-time work schedule, family life, and personal hobbies, fitting this dissertation in when convenient for me, not him. Not many professors would do that, I am much indebted. Second, I want to thank Dr. Jay Hestbeck for allowing me the wonderful opportunity to work in the Northwoods of Maine, to the ECOSEARCH concept, the suggestion for exploring LiDAR, and the need to move away from polygon modeling to a point-intercept approach. I want to thank Drs. James Grier, Gary Clambey, and Donald Kirby for accommodating me in their classes when I could come over from Jamestown, especially through very challenging winters, and of course, their willingness to serve on my graduate committee. I learned much from them, especially the ecology of the northern prairies. In addition, I would like to thank Dr. Jack Norland and his willingness to come on-board my committee with little notice and for discussions we have had through the years about an animal we both hold a great respect for, bison.

I am indebted to my co-workers at Northern Prairie Wildlife Research Center for their support and encouragement over the years. First and foremost, I thank Terry Shaffer for opening the door for me at the Center many years ago, his mentoring and leadership was and still is an aspiration to me. I appreciate Dr. Lawrence Igl for the discussions we had, and the humor we found in those discussion, as we both pursued doctorate programs. I especially thank Larry for much needed editorial reviews on earlier editions. I also want to thank Betty Euliss, Tom Sklebar, and Cady Sijapati for GIS help and preparation of many graphics for presentations. A special thanks to Cady Sijapati for fine-tuning and documenting the SAS programs for depicting and rendering forest stands in 3D (Appendix B). I also thank Dr. Dennis Jorde for allowing me

the opportunity to continue with the Northwoods project and to pursue many other LiDAR-related projects, good things will come of those efforts. I also need to give a thank you to Deborah Buhl and Dr. Glen Sargeant for bouncing-off statistical ideas and approaches, and keeping me grounded in simplicity. Thank you to Dr. Robert Gleason for accepting the Center Director position and allowing me to continue with the LiDAR projects. And of course, a thank you to Mike Schwartz for computer support and also providing much needed editorial comments.

I want to thank my colleague in Maine, Dan McAuley, for his assistance and patience with continuing this project, what a great field biologist and researcher Dan is, I learned a great deal about forest management and Maine wildlife from Dan. I want to thank the staff at Moosehorn National Wildlife Refuge for access to the Refuge to gather needed data, and in particular Maury Mills for seeing the long-term potential of this approach. I also want to thank International Paper, now American Foresters, for access to their lands. This work would not be possible without two great bird surveyors who collected and provided the much needed bird survey data, Marion Bates and Ron Joseph. I also want to thank Stephen Magill for helping with collection of forest stand metrics and keeping me from periodically getting lost in the Northwoods. Other individuals that need to be noted and thanked are Jan Taylor (USFWS) for funding bird surveys, and Robert Kelly (USGS), Tonda Shelton, Karl Heidemann, and Bob Ryan (EarthData, Inc.) for assistance in various ways with contracting for the LiDAR acquisition. Thank you to Robert Lisota for editorial reviews on earlier versions.

A special thanks to Ray Greenwood, friend and mentor, for teaching me innumerable aspects about the northern prairies, and of course, helping me out with the “bufflers.”

Finally, to my wife Robin for tolerating and supporting many days of me being out-of-town and putting in many extra hours at-the-office – thank you. And thank you to my “thwee

wittle girls” who were that when I started this project and now are all grown-up pursuing their own dreams; Darci, Holly, and Rachel.

I dedicate this to my father, Raymond Lee Newton, who taught me the value of hard work, “tough’n it out” and introducing me to the great outdoors and partnering-up with me on a bison ranch. I also dedicate this to my mother, Norma Kaye Fowler-Newton, as an example of what being meek and empathetic are all about.

DEDICATION

This disquisition is dedicated to my father, Ray, and mother, Kaye.

TABLE OF CONTENTS

ABSTRACT.....	iii
ACKNOWLEDGMENTS	v
DEDICATION.....	viii
LIST OF TABLES	xiv
LIST OF FIGURES	xvii
LIST OF APPENDIX TABLES.....	xxi
LIST OF APPENDIX FIGURES.....	xxii
CHAPTER 1. GENERAL INTRODUCTION	1
Background and Justification	1
LiDAR.....	5
Goal and Objectives	10
Organization of Dissertation	10
Literature Cited	11
CHAPTER 2. PREDICTING OVER- AND UNDERSTORY FOREST STAND STRUCTURAL METRICS WITH DISCRETE-RETURN LiDAR IN MIXED FORESTS OF MAINE, USA	16
Abstract	16
Introduction.....	16
Goals and Objectives.....	20
Study Area.....	20
Methods.....	21
Forest Plot Data Metrics	21
Study plots	21
Tree and sapling metrics	23

Canopy closure (field derived).....	28
LiDAR Acquisition and Processing.....	31
Acquisition.....	31
Post-processing.....	32
Canopy closure (LiDAR-derived).....	33
Building classification and extraction.....	36
Digitization of water bodies and sphagnum bogs.....	39
Use of 50×50 m cells for modeling.....	39
LiDAR-derived explanatory variables.....	39
Data analysis and modeling.....	44
Plausible models.....	44
Statistical analysis and modeling.....	45
Results.....	46
Forest Plot Metrics.....	46
Modeling.....	49
Discussion.....	64
Literature Cited.....	67
CHAPTER 3. PREDICTING BREEDING SONGBIRD ABUNDANCE IN MIXED FORESTS OF MAINE (NORTHWOODS) WITH LiDAR.....	75
Abstract.....	75
Introduction.....	75
Goals and Objectives.....	79
Study Area.....	79
Methods.....	80
Bird Surveys.....	80

LiDAR.....	82
Acquisition and processing.....	82
LiDAR-derived explanatory variables.....	82
Data Analysis and Modeling.....	90
Plausible models.....	90
Statistical modeling.....	94
Results.....	95
Bird Surveys.....	95
Models.....	95
Discussion.....	107
Literature Cited.....	114
CHAPTER 4. OPTIMIZATION OF HABITAT MANAGEMENT BASED ON LiDAR- DERIVED FOREST-STAND AND BREEDING-BIRD MODELS: A CASE STUDY FROM THE NORTHWOODS OF MAINE.....	122
Abstract.....	122
Introduction.....	122
Goals and Objectives.....	124
Study Area.....	124
Methods.....	125
LiDAR and Processing.....	125
Hypothetical Age Classes.....	126
Vertical Canopy Profiles.....	126
Classifying 50×50 m Cells.....	130
Harvest Schedules and Spatial Pattern.....	131
Predicting Bird Abundance.....	133

Assessing Optimal Management Scenario.....	134
Results	135
Discussion	142
Literature Cited	145
CHAPTER 5. CONCLUSIONS AND FUTURE DIRECTIONS	147
Conclusions	147
Future Directions.....	148
Literature Cited	150
APPENDIX A. AN EVALUATION OF THE WANDERING POINT-QUARTER METHOD TO ESTIMATE FOREST STAND STRUCTURE WITHIN STUDY PLOTS.....	153
Introduction	153
Methods.....	155
Sampling Methods	155
Simulation of Plot Data to Sample.....	160
Statistical Methods.....	161
Results	162
Discussion	174
Literature Cited	174
APPENDIX B. A SAS PROGRAM FOR THREE-DIMENSIONAL VISUALIZATION OF FOREST HABITAT	177
Background and Justification	177
Methods.....	180
General Process.....	180
Spreadsheet Format.....	180
SAS Programs.....	182

Remarks.....	189
Literature Cited	189
APPENDIX C. SUPPLEMENTARY MATERIAL FOR CHAPTER 3	191

LIST OF TABLES

<u>Table</u>	<u>Page</u>
2.1. Forest metric response variable summary statistics across all study plots and sites (n=69 plots, n=68 for Y13).	28
2.2. LiDAR acquisition summary statistics for International Paper (IP) and Moosehorn National Wildlife Refuge (MH).	31
2.3. Summary statistics for LiDAR-derived explanatory variables within 50×50m study plots across both study sites.	40
2.4. Pair-wise correlations among LiDAR-derived explanatory variables.	42
2.5. Principal Component Analysis (PCA) results among LiDAR-derived explanatory variables.	43
2.6. Plausible models for modeling individual forest stand metrics as a function of LiDAR-derived explanatory variables.	44
2.7. Individual tree and sapling summary statistics from 50×50m study plots for International Paper (30 plots).	47
2.8. Individual tree and sapling summary statistics from 50×50m study plots for Moosehorn National Wildlife Refuge (39 plots).	48
2.9. Pair-wise correlations among individual tree and sapling measurements from 50×50m study plots for International Paper (IP, 30 plots) and Moosehorn National Wildlife Refuge (MH, 39 plots).	49
2.10.a. Pair-wise correlations among forest metrics (n=69 plots, n=68 for correlations with Y20).	50
2.10.b. Pair-wise correlations among tree forest metrics with sapling forest metrics (n=69 plots).	51
2.11. Modeling results for trees (n=69 plots).	52
2.12. Model parameter estimates for tree metrics for selected model(s) based on results from 2.11.	58
2.13. Modeling results for saplings (n=69 plots).	60
2.14. Model parameter estimates for sapling metrics for selected model(s) based on results from 2.12.	61

3.1.a.	Description of LiDAR-derived explanatory variables for modeling bird species abundance derived from the center 50×50 m cell of 3×3- and 5×5 blocks of 50×50 m cells (see Fig. 3.2 for visual reference).	84
3.1.b.	Description of LiDAR-derived explanatory variables for modeling bird species abundance derived from concentric radii bands (see Fig. 3.2 for visual reference).	88
3.2.	Summary statistics of selected explanatory variables combined across IP (n = 99) and MH (n = 114) for the central 50×50 m cell and surrounding concentric 50 m radii (see Fig. 3.2 for visual reference).	89
3.3.a.	Correlations among relevant combinations of explanatory variables, center 50×50 m cell (see Fig. 3.2 for visual reference).	89
3.3.b.	Correlations among relevant combinations of explanatory variables, surrounding 3×3 grid of 50×50 m cells (see Fig. 3.2 for visual reference).	90
3.3.c.	Correlations among relevant combinations of explanatory variables, surrounding 5×5 grid of 50×50 m cells (see Fig. 3.2 for visual reference).	91
3.3.d.	Correlations among relevant combinations of explanatory variables, surrounding concentric 50-m radii (see Fig. 3.2 for visual reference).	91
3.4.a.	Plausible bird models using 50×50 m cells at three different scales (see Fig. 3.2 for visual reference).	92
3.4.b.	Plausible bird models using concentric 50-m radii (see Fig. 3.1 for visual reference, model numbers are a continuation of those from Table 3.4.a.)	93
3.5.	Bird species frequency of occurrence at International Paper (IP; n = 99) and Moosehorn National Wildlife Refuge (MH; n = 114) for species that were detected ≥ 1 in either 2002, 2003, or 2004.	96
3.6.	Summary of best bird models for which Adj. R ² were greater than 0.20.	105
4.1.	Percent of LiDAR returns expected from hypothetical vertical canopy profiles for incremental increasing successional age classes assumed from the mixed softwoods-hardwood trajectory in bottom panel of Fig. 4.1.	128
4.2.	Summary of classification and enumeration of the number of 50×50 m cells from International Paper (IP) and Moosehorn National Wildlife Refuge (MH) study sites into successional age classes based on LiDAR-derived 3-m vertical vegetation profiles from 2003 acquisition year (age classes vertical profiles are per Table 4.1).	136
4.3.	Percent of 50×50 m cells at International Paper (IP) and Moosehorn National Wildlife Refuge (MH) for each level of increasing predicted mean species abundance (number/0.25 ha) using models developed in Chapter 3 using 2003 LiDAR acquisition.	139

4.4.a.	Percent of 50×50 m cells with predicted mean abundance (number of birds/0.25 ha) > 0.50 for five bird species based on “best” model selected in Chapter 3 under hypothetical management scenarios at International Paper.	140
4.4.b.	Percent of 50×50 m cells with predicted mean abundance (number of birds/0.25 ha) > 0.25 for five focal bird species based on “best” model selected Chapter 3 under hypothetical management scenarios at Moosehorn National Wildlife Refuge.....	141
4.5.	Comparison of Euclidean distances for percent occurrence (%) of five bird species based on the results from three hypothetical management goals at International Paper (IP) and Moosehorn National Wildlife Refuge (MH) (Tables 4.4.a. and 4.4.b)....	143

LIST OF FIGURES

<u>Figure</u>	<u>Page</u>
1.1. Sketch of flying and acquiring LiDAR (UL), illustration of sources for multiple returns (UR), format of delivered XYZ data set (LL), and subsequent point-cloud plot of XYZ values colored by height elevation (LR).	7
2.1. Study site locations within Maine (Blue=International Paper, Red=Moosehorn National Wildlife Refuge).....	22
2.2.a. International Paper (IP) study site; dark-gray circles are locations of 99 50 m radii bird survey points (not drawn to scale), green squares are locations of 30 50×50 m forest stand plots (two forest stand plots are not centered on a bird survey point).....	24
2.2.b. Moosehorn National Wildlife Refuge (MH) study site; dark-gray circles are locations of 114 50 m radii bird survey points (not drawn to scale), green squares are locations of 40 50×50 m forest stand plots (two forest stand plots are not centered on a bird survey point).....	25
2.3. Illustration of conducting a wandering point-quarter (WQ) sampling method within quadrants of a 50×50 m plot (0.25 ha) of trees (total trees in plot = 50, n=18 selected for WQ, with 3 distances censored and represented by *); plot is centered on 50 m radius bird point (see text for more details).	26
2.4. Example of digital photographic images and calibration curve for adjusting mean camera canopy closure estimates across five images to account for hemispheric digital photographic estimates.	30
2.5. TIN-interpolated (2 m) shaded relief digital elevation model (DEM) estimate for International Paper (IP) and Moosehorn National Wildlife Refuge (MH) (not drawn to scale, see Fig. 2.2.a and 2.2.b for scale of boundary for IP and MH respectively).	33
2.6.a. TIN-interpolated (2 m) canopy height model (CHM) and gray-scale intensity image for International Paper (left panel: dark green being 0 m heights to light green being 30 m heights; not drawn to scale, see Fig. 2.2.a for scale of boundary).	34
2.6.b. TIN-interpolated (2 m) canopy height model (CHM) and gray-scale intensity image for Moosehorn National Wildlife (left panel: dark green being 0 m heights to light green being 30 m heights; not drawn to scale, see Fig. 2.2.b for scale of boundary).	35

2.7.	Illustration of processing steps for deriving a digital elevation model (DEM) from raw (2D) point-cloud (UL), deriving digital surface model (DSM), highest open circles within each 2-m cell, and canopy height model (CHM) (UR, solid black points being those classified as ground and where CHM=DSM-DEM), classifying and tallying LiDAR returns into ground and above ground height categories (LL), and deriving 3-m vertical height profiles and computing percent canopy closure estimates within a 50×50 m plot (LR).	37
2.8.	Illustration of the process for digitizing, classifying, and removing buildings from total canopy closure estimates (UL – TIN-interpolated shaded relief from first return LiDAR, buildings circled in white, grid cells are 50×50 m, UR – 2D scatterplot of first return LiDAR data with yellow representing ground classified, purple represents vegetation, LL - black values represent identified LiDAR returns from buildings, LR – buildings “removed” by coloring yellow).	38
2.9.a.	Relationship between observed forest metrics and LiDAR predicted forest metrics; dashed line represents 1:1 correspondence; Y1-Y4 and Y14-Y17 are defined in Table 2.1.	54
2.9.b.	Relationship between observed forest metrics and LiDAR predicted forest metrics; dashed line represents 1:1 correspondence; Y6-Y8 and Y18-Y20 are defined in Table 2.1.	55
2.9.c.	Relationship between observed forest metrics and LiDAR predicted forest metrics; dashed line represents 1:1 correspondence; Y9-Y13 are defined in Table 2.1.....	56
2.10.a.	Predicted maps for stem densities (Y1, 14), mean canopy heights (Y4, Y17) and total volumes (Y7, Y20) at International Paper (blue=water, gray=sphagnum bog); see Table 2.1 for definitions of Y1, Y4, Y7, Y14, Y17, and Y20.	62
2.10.b.	Predicted maps for stem densities (Y1, 14), mean canopy heights (Y4, Y17) and total volumes (Y7, Y20) at Moosehorn National Wildlife Refuge (blue=water, gray=bog); see Table 2.1 for definitions of Y1, Y4, Y7, Y14, Y17, and Y20.	63
2.11.	Example associations of binning LiDAR when individual tree type is known or proportion of hardwoods:softwoods is estimated from fusion of LiDAR with image-classified and geo-rectified data (e.g., Quickbird imagery at 2.4 m pixels across a 50 m pixel); top panel is 10:90, middle panel is 50:50, and bottom panel is 90:10 hardwoods:softwoods).	66
3.1.	Forest plot (50×50 m, top panel) juxtaposed within a homogeneous landscape of like plots (middle panel) and within a heterogeneous landscape (bottom panel).	85

3.2.	An example of 50×50 m vertical height profiles in a homogeneous forest and a heterogeneous forest.	86
3.3.a.	Observed versus LiDAR-predicted bird abundance at two forest study sites in Maine (dashed lines indicate 1-to-1 correspondence, species codes are in Table C.1.).....	98
3.3.b.	Observed versus LiDAR-predicted bird abundance at two forest study sites in Maine (dashed lines indicate 1-to-1 correspondence, species codes are in Table C.1.).....	99
3.3.c.	Observed versus LiDAR-predicted bird abundance at two forest study sites in Maine (dashed lines indicate 1-to-1 correspondence, species codes are in Table C.1.).....	100
3.3.d.	Observed versus LiDAR-predicted bird abundance at two forest study sites in Maine (dashed lines indicate 1-to-1 correspondence, species codes are in Table C.1.).....	101
3.3.e.	Observed versus LiDAR-predicted bird abundance at two forest study sites in Maine (dashed lines indicate 1-to-1 correspondence, species codes are in Table C.1.).....	102
3.3.f.	Observed versus LiDAR-predicted bird abundance at International Paper only (dashed lines indicate 1-to-1 correspondence, species codes are in Table C.1.).....	103
3.4.	Observed vs LiDAR-predicted species richness and diversity at two forest study sites in Maine (dashed lines indicate 1-to-1 correspondence).	104
3.5.	LiDAR-derived TIN-interpolated shaded-relief surface model for nine example bird survey points for 3 levels of Palm Warbler (PAWA) abundance at International Paper lands in Maine (O=observed, P=predicted; images are 400×400 m centered on 50 m radii bird survey point, see Table C.1 for species code).....	109
3.6.	LiDAR-derived vertical height profiles at 9 example bird survey points for 3 levels of Palm Warbler (PAWA) abundance at International Paper lands in Maine (O=observed, P=predicted; cells are 50×50 m with center cell centered on 50 m radii bird survey point, see Table C.1 for species code).....	110
3.7.	Three-dimensional visualization of simulated Palm Warbler at the center 50×50 m stands from Figure 3.5 using SAS program described in Appendix B (assumed mixed softwoods and hardwoods).	111
3.8.	Example predicted maps for PAWA, COYE, and OVEN at International Paper (IP) (6.4×12.0 km) and Moosehorn National Wildlife Refuge (MH) (7.9×13.1 km); not drawn to scale, cells represent 50×50 m (0.25 ha), species codes for PAWA, COYE, and OVEN are in Table C.1.....	113

4.1.	Hypothetical forest stand succession for softwood (top), hardwood (middle), and mixed hardwood-softwood (bottom).	127
4.2.	Vertical vegetation profiles (%) for hypothetical forest stand succession in Fig. 4.1 (purple bars are 3-m vertical profiles, bottom black-hashed bar is percent ground, assumed to be 10% for all age classes; all bars combined sum to 100%).	129
4.3.	Hypothetical harvest-schedules and spatial patterns for management scenarios juxtaposed on the landscape within either square blocks (top four configurations) or harvest strips (bottom four configurations).....	132
4.4.a.	Projected forest stand ages for International Paper over a 100-year period from 2003 (LiDAR acquisition year) to 2103, in 20-year increments (study site is 6.4×12.0 km).	137
4.4.b.	Projected forest stand ages for Moosehorn National Wildlife Refuge over a 100-year period from 2003 (LiDAR acquisition year) to 2103, in 20-year increments (study site is 7.9×13.1 km).....	138

LIST OF APPENDIX TABLES

<u>Table</u>	<u>Page</u>
A.1. Parameter estimates and correlations evaluating the linear relationship between simulated population size of total trees (N) within 50×50 m plots and estimated population size using a Wandering Quarter (WQ) method and a Belt Transect (BT) method for three spatial distributions.	164
A.2. Parameter estimates and correlations evaluating the linear relationship between simulated population size of total saplings (N) within 50×50 m plots and estimated population size using a Wandering Quarter (WQ) method and a Belt Transect (BT) method for three spatial distributions.	166
A.3. Parameter estimates and correlations evaluating the linear relationship between simulated population size of total trees (N) within 88×88 m plots and estimated population size using a Wandering Quarter (WQ) method and Forest Inventory and Analysis Plots (FIA) method for three spatial distributions.	168
C.1. Bird species observed at tow mixed forests in Maine Northwoods: species are listed alphabetically by their American Ornithologists’ Union (AOU) species code.	191
C.2. Bird modeling results for International Paper (IP) and Moosehorn National Wildlife Refuge (MH) sorted by the most encountered species to least encountered (see Table 3.5; bolded Adj. R ² indicate a reasonable best model selected based on Akaike’s weights and Adj. R ² ≥ 0.2).	193
C.3. Estimated model parameters for best bird selected models only and with Adj.R ² ≥0.20 at International Paper (IP) and Moosehorn National Wildlife Refuge (MH).	202

LIST OF APPENDIX FIGURES

<u>Figure</u>	<u>Page</u>
A.1. Illustration of conducting a Wandering Quarter (WQ) sampling method within a 50×50 m plot (0.25 ha) of trees (total trees in plot = 50, n=18 selected for WQ, with 3 distances censored and represented by *).	157
A.2. Belt transect (BT) versus Wandering Quarter (WQ) sampling within a 50×50 m plot (0.25 ha) of trees: centered crossing S-N and W-E lines represent 2 m wide BT; thick open circles are selected trees using WQ only, solid circles are selected with BT only, stars are selected in both WQ and BT, with thin open circles being unsampled (N=50 total random distribution of trees, n=18 sampled for WQ, n=5 for BT).	158
A.3. Forest Inventory and Analysis (FIA) plots versus Wandering Quarter (WQ) sampling within a 88×88 m plot (0.77 ha): large circles represent location of 7.31 m radius FIA plots; thick open circles are selected using WQ only, solid circles are selected with FIA, stars are selected in both WQ and FIA, thin open circles being unsampled by either method (N=100 total random distribution of trees, n=23 sampled for WQ, n=5 for FIA).	159
A.4. Comparison of the relationship between simulated population size of total trees (all N levels) and estimated total trees for two sampling methods (WQ=Wandering Quarter, BT=Belt Transect) for three spatial distributions within 50×50 m plots (0.25 ha); dashed line is 1-to-1 correspondence.	163
A.5. Comparison of the relationship between simulated population size of total trees (only N levels < 125) and estimated total trees for two sampling methods (WQ=Wandering Quarter, BT=Belt Transect) for three spatial distributions within 50×50 m plots (0.25 ha); dashed line is 1-to-1 correspondence.	165
A.6. Comparison of the relationship between simulated population size of total trees (all N levels) and estimated total trees for two sampling methods (WQ=Wandering Quarter, FIA=Forest Inventory and Analysis) for three spatial distributions within 88×88 m plots (0.77 ha); dashed line is 1-to-1 correspondence.	167
A.7. Comparison of the relationship between simulated population size of total trees (all N levels < 125) and estimated total trees for two sampling methods (WQ=Wandering Quarter, FIA=Forest Inventory and Analysis) for three spatial distributions within 88×88 m plots (0.77 ha); dashed line is 1-to-1 correspondence.	169
A.8. Comparison of sampling intensities between Wandering Quarter (WQ) and Belt Transect (0.25 ha plots) and WQ and Forest Inventory and Analysis (FIA) plots (0.77 ha plots) sampling methods for increasing simulated total trees for three spatial distributions (dashed-line represents maximum number of stems sampled by WQ across the four quadrants).	170

A.9.	Comparison of mean difference between sampled mean canopy heights and simulated population mean canopy heights within 50×50 m plots (0.25 ha) for Wandering Quarter (WQ) and Belt Transect (BT) methods for three spatial distributions (dashed-lines are ±2 m for reference only).....	171
A.10.	Comparison of mean difference between sampled mean canopy heights and simulated population mean canopy heights within 88×88 m plots (0.77 ha) for Wandering Quarter (WQ) and Forest Inventory and Analysis (FIA) methods for three spatial distributions (dashed-lines are ±2 m for reference only).....	172
A.11.	Distribution of variance-to-mean ratio distances for trees and saplings sampled from known random (R), uniform (U), and clumped (C) spatial distributions within 50×50 m plots (0.25 ha) as a result of increasing sample sizes using Wandering Quarter sampling method: here Ratio=variance of distances between trees (or saplings) to their respective mean distance (note: numbers of saplings sampled for uniform and random increased from 13-24 range to 37-48 range; vertical dashed-line represents variance-to-mean ratio of 1.0 implying random distribution of stems).....	173
B.1.	Basic data flow chart illustrating three-dimensional visualization of 50×50 m plot using SAS program(s) from field or simulated data, estimated field data from empirical wildlife models, or those modeled from LiDAR-derived data (see text for details, spreadsheet units are in meters).....	181
B.2.	Pseudocode of SAS programs used two render in 3D forest stand metrics.....	183
B.3.	Basic steps used to draw a single tree at a specific location within a 50×50 m plot, and then add additional trees as per specific data set.....	184
B.4.	Examples of 50×50 m forest plots positioned on a digital elevation model: UL represents a thinned early successional mixed-type (hardwood:softwood) plot, UR represents an early successional softwood plot, ML represents a mature softwood plot with low density understory, MR represents a mixed-type plot with moderately dense understory, LL represents highly thinned mid-story plot that maybe have experience a recent burn, and LR represents a dense mid-story plot with no understory.	186
B.5.	Examples of tree stands juxtaposed on 50×50 m forest plots within a landscape.	187
B.6.	General modification tools available in the visualization program developed using SAS.	188

CHAPTER 1. GENERAL INTRODUCTION

Background and Justification

Ecosystem management has become the goal and contemporary approach to management of natural resources that has been embraced by many if not most land owners and management agencies, including public, non-profit, and private entities (e.g., USDA Forest Service - Thomas 1995, International Paper Company 2011). Ecosystem management has been defined in various ways, entails many factors, and is implemented at various scales (Brussard et al. 1998, Grumbine 1994). One definition of ecosystem management from an ecological perspective supported by the Ecological Society of America is “Ecosystem management is management driven by explicit goals, executed by policies, protocols, and practices, and made adaptable by monitoring and research based on our best understanding of the ecological interactions and processes necessary to sustain ecosystem composition, structure, and function” (Christensen et al. 1996). Therefore, one aspect or outcome of ecosystem management entails conserving, restoring, and maintaining wildlife species diversity either directly (e.g., hunting) or through direct or indirect habitat management (Hunter 1999, Lindenmayer and Franklin 2002).

To effectively manage forest ecosystems from a wildlife perspective in the 21st century and beyond requires a comprehensive multifaceted and multiscaled approach (Kohm and Franklin 1997), typically in an adaptive framework (Walters 1986, Ringold et al. 1996). One of several challenges for resource managers is that forest ecosystems often are partitioned into artificially bounded tracts under varying ownerships and sizes with competing interests making it difficult to meet ecosystem management objectives (Boyce and Haney 1997). This difficulty is mostly due to private and public holders of forest lands making daily decisions concerning management on their respective tracts within the larger matrix of tracts of a landscape with little

understanding about the consequences to wildlife both on and adjacent to surrounding tracts (Wear et al. 1996). Therefore, one important tool for ecosystem management is the development and verification of spatially-explicit wildlife-habitat models that can predict the occurrence(s) or other demographic metrics (e.g., abundance, survival) of wildlife species as a function of changing habitat conditions under different land ownerships and/or management activities (DeGraaf et al. 1992). Such wildlife-habitat models, even if only qualitative (e.g., HSI - Habitat Suitability Index models, US Fish and Wildlife Service 1981), may enable managers with the ability to predict effects of management activities on a particular species habitat and distribution and make projections under varying future scenarios (Schamberger and O'Neil 1984). For actively managed forests certifying a forest tract as being managed sustainably often requires documenting impacts or potential impacts to wildlife (Vogt et al. 2000). Making these wildlife assessments effectively from an ecosystem management perspective relies heavily on qualitative and empirically-based models, with confidence in the models gained through field testing.

One such suite of wildlife-habitat models developed for forests in New England is ECOSEARCH (Short et al. 2001). The goal of ECOSEARCH is for it to be used as a tool that allows managers of forests in New England to better balance the often conflicting demands of economics (e.g., maximizing profits from commercial forests) and conservation (e.g., maximizing habitat for select species) (Buongiorno and Gilless 2003). ECOSEARCH's intent is also to provide a means by which small and large land holders can link their management goals with those of larger umbrella initiatives such as Partners-In-Flight (Carter et al. 2000). One question managers can ask is "How should the tract I'm responsible for best be managed relative

to the landscape it is juxtaposed in?” ECOSEARCH was developed as a tool to assist with answering such questions.

ECOSEARCH is a computer program containing species-habitat models for 331 wildlife species generating spatially-explicit predictions of occurrences, with predicted occurrence assumed to imply potential habitat for each species. ECOSEARCH, as Version 1, is a 50-m pixel-based modeling procedure using natural history-habitat selection cross-walk models described in DeGraaf and Rudis (1986). Predictions made with ECOSEARCH rely on Geographic Information Systems (GIS) data for wetlands, soils, topography, and vegetation structure. Information for wetlands, soils, and topography comes from readily available U.S. Fish and Wildlife Service (USFWS) National Wetland Inventory (NWI) maps, U.S. Department of Agriculture (USDA) Natural Resources Conservation Service (NRCS) maps, and U.S. Geological Survey (USGS) maps, respectively. Vegetation structure of trees and saplings, representing over-, mid-, and understory canopy and heights, is estimated by first gridding, geo-rectifying, and imprinting 50×50 m grid cells on a clear plastic overlay (Mylar). The plastic grid is then overlaid on an aerial photograph, preferably a 1:40,000 color infrared. Vegetation structure at the center within each 50-m cell (i.e., point-intercept) is visually interpreted and classified into one of approximately 94 vertical habitat descriptors (e.g., man-made structures, upland tree canopy, wetland tree canopy – see pages 16-17 in Short et al. 2001 for complete list). Although the models are not statistically based but are natural-history based (i.e., based on known habitat needs), ECOSEARCH can yield reasonable predictions based on natural history attributes alone (Giorgi 1999). Updating or simulating changes with the input GIS data layers to ECOSEARCH provides managers with the opportunity to assess not only the current status of species occurrences and habitat but any future changes in occurrence as a function of planned

(or unplanned) activities in “what-if” scenarios. Also, managers and stakeholders can explore mixings of habitat types and sizes in maximization-minimization problems (e.g., maximize amount of habitat for a few species while minimizing habitat loss for others).

Although single-species habitat models such as those used in ECOSEARH are in many cases not the most ideal and are not unbiased (e.g., they often do not take into account species interactions such as competition), they can and are viewed as a foundation to be improved upon and currently, really, the only available tool (e.g., Guisan and Zimmerman 2000, Franklin 2009). However, most wildlife-habitat models can be improved with increased knowledge about individual species biology and ecology, and refining the ability to more accurately and precisely derive explanatory variables used to predict individual species demographics (Morrison et al 2006). Improvement also comes from calibrating models using field data on species demographics by accounting for detection and/or encounter probabilities (e.g., Rosenstock et al. 2002, MacKenzie et al. 2006).

Short et al. (2001) described three areas as future directions for improving ECOSEARCH: (1) movement towards empirical models (i.e., statistical) that predict abundance or at least probability of occurrence as opposed to occurrence-only from species-habitat cross-walks based on natural history alone, (2) use continuous grids based on point-intercept data instead of arbitrary polygons of discrete habitat classes, and (3) take advantage of increasing resolution of remotely sensed data and types that can be more easily and readily processed on desktop computers. Addressing the first can be done by strategically collecting field survey data for wildlife species of interest and relating those to relevant potential explanatory variables using one of several statistical modeling methods available for calibration (e.g., Austin 2002, Hirzel and Guisan 2002). Addressing the second can partially be done with increasing pixel resolution

by using higher resolution imagery, particularly satellite-based that cover broad landscapes (e.g., QuickBird - Toutin and Cheng 2002). Addressing the third is being done with each new processing technology and is already available for desktop computers. Deriving the vertical structure (typically considered fine-scale metrics) across broad landscapes can be challenging, especially since most remote sensing technologies provide only two-dimensional (2D) data, albeit with improved resolution.

As mentioned above, three of four GIS data layers required by ECOSEARCH (soils, wetlands, topography) are readily available and require no acquisition of aerial photographs. Although vegetative cover types can be delineated from aerial images, the vertical vegetative structure typically cannot or is difficult at best because of its three-dimensional (3D) characteristic. This is unfortunate because most studies of habitat selection, particularly for birds, have found that vertical structure, and how it varies across space and through time, to be one of the most critical factors influencing niche-partitioning among bird species (James 1971, DeGraaf et al. 1998). As pointed out in Short et al. (2001) in referencing Hilden (1965), Lack (1933), and Willson (1974), “vegetation structure is the most important factor affecting habitat selection by temperate forest birds.” The seminal work by MacArthur and MacArthur (1961) pointed out the strong association between the diversity of breeding forest birds and foliage height diversity. Therefore, a tool that can describe and characterize spatially and explicitly the vegetation structure (in 3D) across an ecosystem is needed to improve the models in ECOSEARCH.

LiDAR

One promising yet relatively new technology being used to remotely estimate topography and vegetation structure in a spatially-explicit manner across broad landscapes is light detection

and ranging (LiDAR) systems (Lefsky et al. 2002). There are several different types of LiDAR pulsing and recording systems (e.g., discrete-return, full waveform), using different wavelengths (but usually either green or near-infrared wave bands), and mounted on various platforms (e.g., ground-based tri-pods, mobile systems, satellite-based). However, our primary interest here is in what is typically considered to be the current work-horse of LiDAR acquisitions, that is, small-footprint multiple discrete-return LiDAR mounted as an airborne system (Vosselman and Maas 2010). A detailed description of LiDAR, including the physics, instrumentation, and numerous applications, can be found in Shan and Toth (2009).

Airborne multiple discrete-return LiDAR is a remote sensing technology that emits rapid pulses of light energy (i.e., eye-safe near-infrared laser beams from 80-300 kHz) from a calibrated instrument mounted on an aircraft. The instrument and linked software quantifies the travel time for the emitted photons from each pulse to travel to an object, or the ground, and reflect back to a detector on the aircraft, typically from a scanning instrument (see sketch in upper left panel of Fig. 1.1). Accounting for the speed of light for each emitted pulse (and dividing by 2), knowing the position of the aircraft both in XYZ space from satellite-based Global Positioning System (GPS) and controlling for the inertial measurement unit (IMU) of the aircraft (i.e., pitch, roll, and yaw) at the time of each pulse, accurate elevations of objects encountered (typically above sea-level ± 5 -10 cm) can be computed if a pre-defined and calibrated quantity of photons are detected upon reflection from an object or the ground.

Often, objects encountered by the photos within each pulse are not “solid” (e.g., tree canopies) with some photons being reflected back to the instrument while others “penetrate” through gaps in the canopy until either the ground is encountered (and enough photons are reflected back and detected by the instrument), or a large branch or cluster of leaves are

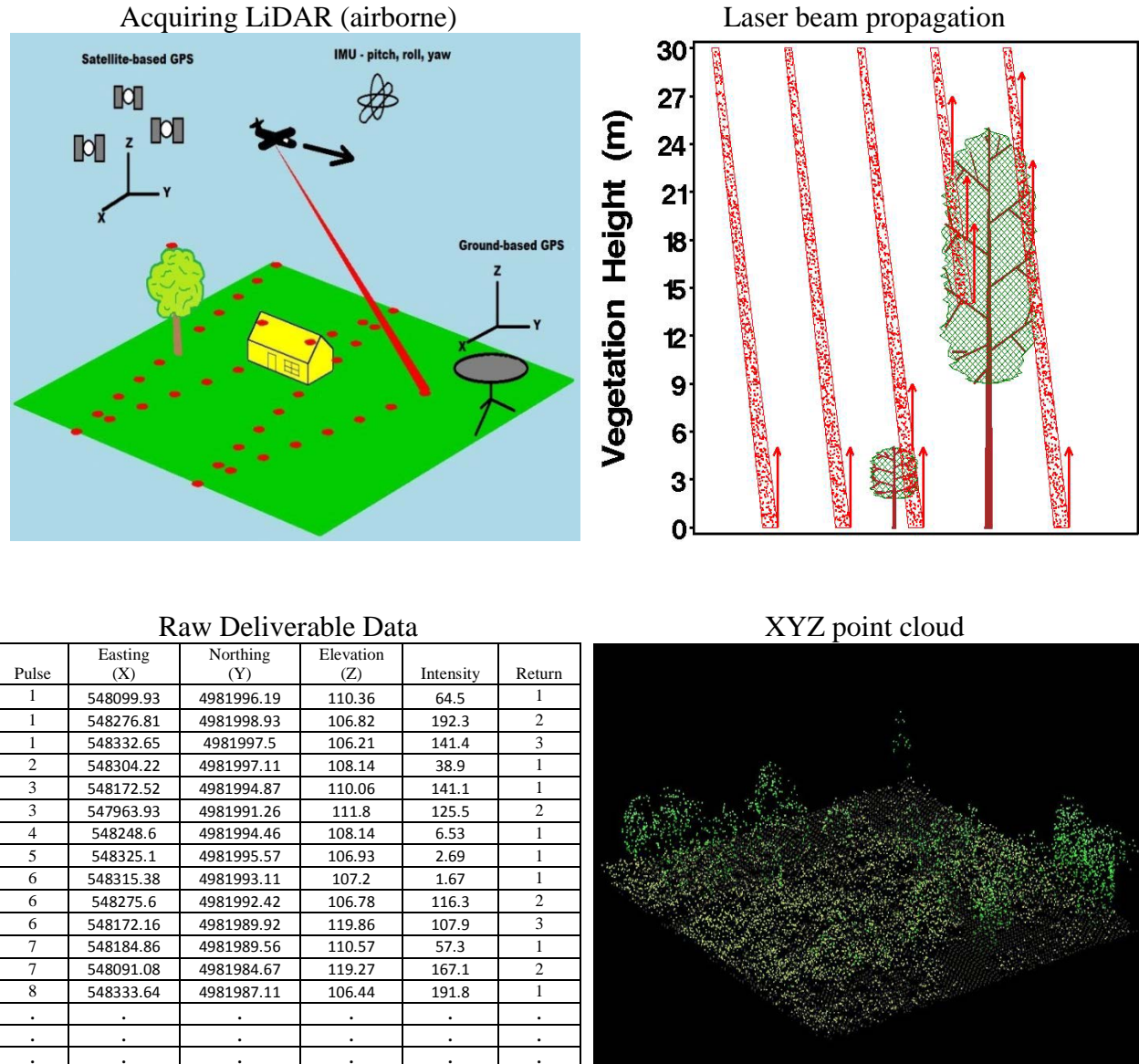


Figure 1.1. Sketch of flying and acquiring LiDAR (UL), illustration of sources for multiple returns (UR), format of delivered XYZ data set (LL), and subsequent point-cloud plot of XYZ values colored by height elevation (LR).

encountered, with no photons penetrating further. These types of LiDAR systems can therefore record several returns from objects encountered, yielding multiple returns as illustrated in the upper right panel of Fig. 1.1. In this panel, the first two pulses from left to right encounter only ground, hence a single return for each pulse. The third pulse from the left encounters a small tree with some photons being reflected back to and detected (i.e., first-return) with the remainder of

photons penetrating and reflecting from the ground (i.e., second-return, and in this case, last-return). The fourth pulse in the upper right panel in Fig. 1.1 illustrates a pulse in which no photons reach the ground, or at least none are reflected and detected by the instrument, with three returns (i.e., elevations) recorded for this single pulse (note: instruments are typically calibrated to detect from 3 to 5 returns). The fifth pulse in the upper right panel of Fig. 1.1 illustrates a pulse with three returns with the third return being the last return encountering the ground. Also recorded for each pulsed return is the intensity (i.e., a measurement of the quantity of reflected photons). Typically the lighter the object encountered the more photons are reflected back, the darker the object the more photons are absorbed by the object but usually with enough photons reflecting back to be detected by the instrument on the aircraft. LiDAR systems are considered active sensors because they generate their own light as opposed to passive sensors that record reflected light from other sources, typically from the sun. The diameter of the pulsed beam encountering only ground is considered the footprint size, typically ≈ 20 cm for aircraft flying 1000-1500 m above the terrain. For comparison, satellite-based LiDAR systems, which typically profile pulses as opposed to scanning, have footprints in the range of 10-30 m diameter on flat terrain, and hence are considered to have “large” footprints. LiDAR systems emitting green spectral band energy typically “penetrate” water and are also useful for bathymetric studies, whereas systems emitting near-infrared typically scatter photons when encountering water with few to no photons detected by the instrument, hence issues arise over bodies of water. Awareness of unreliable returns on bodies of water need to be accounted for when processing LiDAR data because most commercial vendors use near infrared lasers.

Depending on project specific goals, airborne LiDAR systems are currently calibrated and pulse around 80-100+ kHz at aircraft speeds of 70 m/s, altitudes of 1000 m above the terrain,

and with scanning swath widths of 600 m resulting in approximately 2 pulses/m² on the ground (usually defined as the nominal post-spacing). At these specifications and depending on acquisition area, delivered LiDAR data sets quickly become large, often reaching billions of data points (Vosselman and Maas 2010). An example format of deliverable data in ASCII text file is illustrated in the lower left panel of Fig. 1.1 (albeit LiDAR is typically delivered in a binary format (i.e., labeled LAS) usually partitioned into 2×2 km tiles, Graham 2012). These ASCII data sets, often called “XYZ” data are typically a subset of the information in LAS files. They have the most relevant information for analyses which includes a unique pulse number for each pulse, the easting (X), northing (Y), and elevation above sea level (Z) for each return as well as the intensity of the return, and the return number if multiple returns are recorded. The XYZ data set is usually in NAD83 horizontal datum and NADV83 vertical datum using Universal Transverse Mercator (UTM) coordinate system, but project specific datums can also be specified (e.g., counties, World Geodetic System).

Prior to delivery by LiDAR vendors, the data sets go through a rigorous quality check for positional accuracy in XYZ space usually using ground-control locations for calibration (Wehr 2009). Accuracy of a particular data set is usually quantified using a root-mean squared error (RMSE) value under varying conditions (e.g., roads, open canopy, closed canopy). Plotting the XYZ values in 3D results in what is called a raw point-cloud (lower right panel of Fig. 1.1). The level of detail provided from discrete-return LiDAR in capturing vegetation structure and its capability for improving the predictive ability and applications of ECOSEARCH are what I will assess in this dissertation.

Goal and Objectives

The overall goal of this dissertation is to present a case for using airborne discrete-return LiDAR and LiDAR-derived explanatory variables as the base GIS data layer(s) for deriving species occurrence or abundance maps that can be used for habitat assessments using a point-intercept centered approach. If workable, this methodology could be incorporated into a subsequent version of ECOSEARCH.

The three specific objectives are to: (1) develop and assess empirical models for predicting both over- and understory forest stand structure from LiDAR-derived explanatory variables (Chapter 2), (2) develop and assess empirical models for predicting breeding forest bird abundance directly with LiDAR-derived explanatory variables (Chapter 3), and (3) based on the success of results from the two previous objectives, assess the utility of developing optimization and/or management activities, at least for forest birds, under varying scenarios (Chapter 4).

Organization of Dissertation

My dissertation is organized into five chapters. This Chapter serves as a general background and justification for the methods and results presented in Chapters 2-4, each of which will become a stand-alone manuscript with additional co-authors (hence “we” is used throughout the dissertation as opposed to “I”). Although I attempted to minimize redundancy among Chapters 2-4, some information is repeated out of necessity to improve clarity and consistency. Detailed descriptions of LiDAR are provided in this Chapter, briefer descriptions will be included in Chapters 2-4. The final Chapter 5 provides an overall assessment of LiDAR as a base technology for a new version of ECOSEARCH, with a discussion of future research directions and improvements for ecosystem management applications. Appendix A and B are

stand-alone supporting documents relevant for all Chapters with the intent of becoming publishable manuscripts in their own right.

Literature Cited

- Austin, M.P. 2002. Spatial prediction of species distribution: an interface between ecological theory and statistical modelling. *Ecological Modelling* 157:101-118.
- Buongiorno, J., and J.K. Gilless. 2003. Decision methods for forest resource management. Academic Press, San Diego, California.
- Boyce, M.S., and A. Haney. (Editors). 1997. Ecosystem management: applications for sustainable forest and wildlife resources. Yale University Press, New Haven, Connecticut.
- Brussard, P.F., M.J. Reed, and T.C. Richard. 1998. Ecosystem management: what is it really? *Landscape and Urban Planning* 40:9-20.
- Carter, M.F., W.C. Hunter, D.N. Pashley, and K.V. Rosenberg. 2000. Setting conservation priorities for landbirds in the United States: the partners in flight approach. *Auk* 117:541-548.
- Christensen, N.L., A.M. Bartuska, J.H. Brown, S. Carpenter, C. D'Antonio, R. Francis, J.F. Franklin, J.A. MacMahon, R.F. Noss, D.J. Parsons, C.H. Peterson, M.G. Turner, and R.G. Woodmansee. 1996. The report of the Ecological Society of America committee on the scientific basis for ecosystem management. *Ecological Applications* 6:665-691.
- DeGraaf, R.M., and D.D. Rudis. 1986. New England wildlife: habitat, natural history, and distribution. USDA Forest Service, Northeastern Forest Experiment Station, GTR NE-108, Broomall, Pennsylvania.

- DeGraaf, R.M., J.B. Hestbeck, M. Yamasaki. 1998. Associations between breeding bird abundance and stand structure in the White Mountains, New Hampshire and Maine, USA. *Forest Ecology and Management* 103:217-233.
- DeGraaf, R.M., M. Yamasaki, W.B. Leak, and J.W. Lanier. 1992. New England wildlife: management of forested habitats. USDA Forest Service, Northeastern Forest Experiment Station, GTR NE-144, Radnor, Pennsylvania.
- Franklin, J. 2009. Mapping species distributions: spatial inference and prediction. Cambridge University Press, Cambridge, United Kingdom.
- Giorgi, K.S.H. 1999. Evaluation of ECOSEARCH: a wildlife-habitat model for predicting species occurrence. Masters Thesis, Wildlife and Fisheries Conservation, University of Massachusetts-Amherst.
- Grumbine, R.E. 1994. What is ecosystem management? *Conservation Biology* 8:27-38.
- Hirzel, A., and A. Guisan. 2002. Which is the optimal sampling strategy for habitat suitability modelling. *Ecological Modelling* 157:331-341.
- Graham, L. 2012. The LAS 1.4 specification. *Photogrammetric Engineering and Remote Sensing* 78:93-102.
- Guisan, A., and N.E. Zimmerman. 2000. Predictive habitat distribution models in ecology. *Ecological Modelling* 135:147-186.
- Hilden, O. 1965. Habitat selection in birds. *Annales Zoologici Fennici* 2:53-75.
- Hunter, M.L. (Editor). 1999. Maintaining biodiversity in forest ecosystems. Cambridge University Press, Cambridge, United Kingdom.

- International Paper Company. 2011. International Paper 2010 Sustainability Report.
www.internationalpaper.com/documents/EN/Sustainability/SustainabilityReport.pdf.
Accessed 26 March 2012.
- James, F.C. 1971. Ordinations of habitat relationships among breeding birds. *The Wilson Bulletin* 83:215-236.
- Kohm, K.A. and J.F. Franklin. (Editors). 1997. *Creating a forestry for the 21st century: the science of ecosystem management*. Island Press, Washington, District of Columbia.
- Lack, D. 1933. Habitat selection in birds. *Journal of Animal Ecology* 2:239-262.
- Lefsky, M.A., W.B. Cohen, G.G. Parker, and D.J. Harding. 2002. Lidar remote sensing for ecosystem studies. *BioScience* 52:19-30.
- Lindenmayer, D.B. and J.F. Franklin. 2002. *Conserving forest biodiversity: a comprehensive multiscaled approach*. Island Press, Washington, District of Columbia.
- MacArthur, R.H., and J. MacArthur. 1961. On bird species diversity. *Ecology* 42:594-598.
- MacKenzie, D.I., J.D. Nichols, J.A. Royle, K.H. Pollock, L.L. Bailey, and J.E. Hines. 2006. *Occupancy estimation and modeling: inferring patterns and dynamics of species occurrence*. Academic Press, Burlington, Massachusetts.
- Morrison, M.L., B.G. Marcot, and R.W. Mannan. 2006. *Wildlife-habitat relationships: concepts and applications*. Island Press, Washington, District of Columbia.
- Ringold, P.L., J. Alegria, R.L. Czaplewski, B.S. Mulder, T. Tolle, and K. Burnett. 1996. Adaptive monitoring design for ecosystem management. *Ecological Applications* 6:745-747.
- Rosenstock, S.S., D.R. Anderson, K.M. Giessen, T. Leukering, and M.F. Carter. 2002. Landbird counting techniques: current practices and an alternative. *The Auk* 119:56-53.

- Schamberger, M.L., and L.J. O'Neil. 1984. Concepts and constraints of habitat-model testing. Pages 5-10 *in* Wildlife 2000: modeling habitat relationships of terrestrial vertebrates (J. Verner, M.L. Morrison, C.J. Ralph, Editors). The University of Wisconsin Press, Madison, Wisconsin.
- Shan, J., and C.K. Toth. 2009. Topographic laser ranging and scanning: principles and processing. CRC Press, Boca Raton, Florida.
- Short, H.L., J.B. Hestbeck, R.M. DeGraaf. 2001. New England wildlife: a model for ecosystem management – ECOSEARCH (version 1). Northeastern Forest Experiment Station, GTR NE-283, Radnor, Pennsylvania.
- Thomas, J.W. 1995. Agencies' roles in ecosystem management: USDA Forest Service directions. *Natural Resources and Environmental Issues* 5:86-90.
- Toutin, T., and P. Cheng. 2002. QuickBird – a milestone for high-resolution mapping. *Earth Observation Magazine*. 11:14-18.
- US Fish and Wildlife Service. 1981. Standards for the development of suitability index models. Ecological Services Manual 103. USDOJ Fish and Wildlife Service, Division of Ecological Services. Government Printing Office, Washington, D.C.
- Vosselman, G., and H.-G. Maas (Editors). 2010. Airborne and terrestrial laser scanning. CRC Press, Boca Raton, Florida.
- Vogt, K.A., B.C. Larson, J.C. Gordon, D.J. Vogt, and A. Fanzeres. 2000. Forest certification: roots, issues, challenges, and benefits. CRC Press, Boca Raton, Florida.
- Walters, C.J. 1986. Adaptive management of renewable resources. McGraw-Hill, New York, New York.

- Wear, D.N., M.G. Turner, and R.O. Flamm. 1996. Ecosystem management with multiple owners: landscape dynamics in a southern Appalachian watershed. *Ecological Applications* 6:1173-1188.
- Wehr, A. 2009. LiDAR systems and calibration. Pages 129-172 In *Topographic laser ranging and scanning: principles and processing* (J. Shan and C.K. Toth, Editors). CRC Press, Boca Raton, Florida.
- Willson, M.F. 1974. Avian community organization and habitat structure. *Ecology* 55:1017-1029.

CHAPTER 2. PREDICTING OVER- AND UNDERSTORY FOREST STAND STRUCTURAL METRICS WITH DISCRETE-RETURN LiDAR IN MIXED FORESTS OF MAINE, USA

Abstract

Light detection and ranging (LiDAR) is a remote sensing technology that has found utility in quantifying forest canopies. Foresters have exploited LiDAR by quantifying structural metrics useful for forest inventories (e.g., tree volumes). Wildlife professionals are only now beginning to recognize LiDARs' ability to characterize vertical vegetation structure from a habitat assessment perspective. The vertical structure and how it varies across space has been shown to be a strong predictor for assessing wildlife-habitat relationships. ECOSEARCH is a computer program that uses natural-history models to predict New England wildlife habitat. Vertical vegetation structure is one of several data layers required by ECOSEARCH. In this study, we calibrated field-data with LiDAR and found good predictability of several over-and understory forest stand metrics ($\text{Adj. } R^2 > 0.6$). These metrics should be useful for not only improving input data layers to wildlife-habitat models such as ECOSEARCH but also value-add to forest inventories in general.

Introduction

ECOSEARCH is a computer program that uses a suite of natural-history based wildlife-habitat models to spatially and explicitly predict occurrences (i.e., habitat maps) for 331 New England wildlife species as a function of environmental attributes (Short et al. 2001). Predictions are centered on a grid of 50×50 m cells (i.e., rasters) across an entire landscape of interest in a point-intercept context as opposed to artificial habitat polygons comprising broad habitat classes such as a mature forest. Pragmatically the predicted habitat map for each species is done at 50-m pixel resolution using the center of each grid cell as a longitude-latitude (i.e.,

XY) point. However, a continuous map could be derived at essentially every XY point (e.g., every 1 meter across the landscape). The goal of ECOSEARCH is to provide resource managers with a tool to assess the current status of habitat simultaneously for several species across a broad landscape. Having reliable maps of current habitat for each species also allows managers to simulate potential impacts of various management activities and ultimately help guide policy. The ability to make reliable predictions of habitat is one of several criteria required to effectively monitor and quantify the success of ecosystem management which is currently the accepted paradigm for managing ecosystems (Grumbine 1994, Christensen et al. 1996).

As described in Chapter 1, ECOSEARCH requires predictor variables that are input from four basic GIS data layers: topography, soils, water regimes, and forest composition and structure (i.e., primarily vertical structure) that are summarized to a grid of 50×50 m cells (i.e., 50-m pixels). The first three layers are derived from readily available and reliable sources whereas the fourth is estimated through visually interpreting gridded aerial images. Although there are up to 94 vertical habitat descriptors used in ECOSEARCH, those pertaining to forest composition and structure are typically the most relevant, and currently the most challenging to determine. Composition refers to two overstory tree groups: broad-leaved deciduous trees (hardwoods) and needle-leaved evergreens (softwoods). In general, dominance of these two tree types within each 50×50 m cell can reliably be determined from color infrared images, either manually or digitally through georectified images (e.g., Meyer et al. 1996). However, estimating the vertical forest structure component within each 50×50 m cell across the entire landscape of interest is difficult to obtain from interpreting aerial images, even though ECOSEARCH currently only requires two broad height categories, canopy > 6 m and canopy < 6 m.

The ability to estimate the vegetation structure is critical because the occurrence of many wildlife species is determined not only by the overstory canopy but also by the understory. For example, Ovenbirds (*Seiurus aurocapillus*) prefer to nest on the ground in closed-canopy hardwood forests or mixed forests with little to no understory (DeGraaf and Yamasaki 2001). The Hooded Warbler (*Wilsonia citrina*) is associated with hardwood and mixed forests with gap openings and a shrubby understory (DeGraaf and Yamasaki 2001). Structural and compositional constraints are not just limited to only birds. For example, the Delmarva fox squirrel (*Sciurus niger cinereus*), also prefers a similar habitat to Ovenbirds: a closed-canopy hardwood forest with open understory and an abundance of mast trees (Dueser et al. 1988). Overstory structure, such as tree stem densities and canopy closure can be estimated reasonably well from images alone, although it can be time-consuming with the quality of interpretation dependent on the skill of the interpreter. Other overstory metrics such as canopy heights are more difficult to quantify with much confidence. Ascertaining the understory is nearly impossible because currently, understory vegetation is essentially “invisible” from remotely sensed images (McKenzie et al. 2009). Given the importance of these metrics as explanatory variables for successful modeling by ECOSEARCH, the challenge is to find a method that provides detailed forest structural metrics for the both the over- and understory at each 50×50 m cell across the entire landscape of interest. Once these habitat descriptors are reliably determined for each 50×50 m cell, detailed tables (known as a “cross-walk” across natural-history tables) can be constructed regarding the potential occurrence (i.e., likely habitat, not likely habitat) for each of the 331 wildlife species at each 50×50 m cell. Tallying the number of 50×50 m cells then provides an estimate of habitat area for each species.

A relatively new remote sensing tool that has met with good success in forestry applications is light detection and ranging (LiDAR). LiDAR has been demonstrated over the past decade for its use in predicting stand structural metrics such as canopy closure, stem densities, canopy heights, and volumes (e.g., Lim et al. 2003, Woods et al. 2008). Several studies have demonstrated its utility for predicting stem diameter distributions (e.g., Gobakken and Næsset 2005), a prerequisite for forest growth models (e.g., Peng 2000, Pretzsch et al. 2002) and understanding successional trajectories (Oliver and Larson 1996). To date, the general approach is to use regression analyses to model field-collected vegetation structural metrics as a function of LiDAR data. Results vary but most studies report empirical models explaining >75% of total variation between observed field-collected metrics and LiDAR predicted metrics (e.g., Hall et al. 2005, Rooker Jensen et al. 2006).

Currently, the trend for LiDAR acquisitions are for increased point-cloud densities from increased pulse-return rates of 4 to 10 (or more) points per m² allowing for delineation of individual tree crowns (e.g., Falkowski et al. 2006, Koch et al. 2006). Results of these high-density LiDAR acquisitions can be improved further when LiDAR data is combined (i.e., “fused”) with classified digital imagery such as Quickbird (Toutin and Cheng 2002) for mapping not only individual trees and their structural attributes but also individual tree species (e.g., Ke et al. 2010).

As LiDAR acquisition costs have decreased and reliability of predictions have improved, LiDAR has moved from being a research-only tool to an operational inventory tool for foresters (Evans et al. 2006). However, most LiDAR studies thus far have focused on predicting forest structural metrics for the overstory with few attempting to model both the overstory and understory. Anderson et al. (2003) found that for northwest USA forests when a 1.8 m above

ground cut-point is used for defining understory to overstory, the correlations between field-based understory cover estimates and those predicted from LiDAR vary with stand age and type ($r=0.30$ to 0.73). Working in coniferous forests on Vancouver Island, British Columbia, Goodwin et al. (2007) found even stronger correlations between field-based understory cover (to 4 m above ground) and LiDAR-predicted estimates in coniferous forests from British Columbia ($r=0.82$ to 0.93). Martinuzzi et al. (2009) were able to map the presence/absence of understory cover to 83% accuracy in northern Idaho forests. To date, most studies reporting assessments of understory metrics using LiDAR have focused on either percent cover or presence/absence. There is therefore a need to further assess the capabilities of LiDAR as a tool to characterize the over- and understory of forests that can be used for inventory purposes and also for modeling applications such as required by ECOSEARCH.

Goals and Objectives

The overall goal of this study was to assess the utility of discrete-return LiDAR data for spatially and explicitly predicting both over- and understory forest stand structural metrics on 50×50 m cells in mixed forests of Maine (i.e., the Northwoods). The specific objective was to develop and assess empirical models relating seven understory forest stand metrics, 12 overstory stand metrics, and canopy closure from field-collected data to LiDAR-derived explanatory variables. Ultimately, the results from this modeling exercise can be used to create maps of predicted forest structural metrics that can be co-registered and gridded with images and used for better interpretation as needed by ECOSEARCH.

Study Area

We selected two study sites in Maine that are typical of northeastern USA mixed forests representing two diverse forest management objectives. The first study site, located

approximately 30 km east-northeast of Bangor, Maine, is on private land formerly owned by International Paper, Inc. (IP) and encompasses approximately 7,680 ha (Fig. 2.1). The second study site, located approximately 10 km southwest of Calais, Maine, was on the Baring Unit of Moosehorn National Wildlife Refuge (MH) and encompasses approximately 10,350 ha (Fig. 2.1). The IP site is classified as northern hardwoods-spruce forest (*Acer-Betula-Fagus-Picea-Tsuga*) by K uchler (1964) and is actively managed for forestry products. The MH study site falls within the northeastern spruce-fir-forest classification (*Picea-Abies*) (K uchler 1964) and is actively managed to ensure the presence of stands of early successional forest habitat in a mosaic of stands, which provides important habitat for the American Woodcock (*Scolopax minor*) (Dessecker and McAuley 2001). Although the Baring Unit of MH has been cutting and harvesting 40-60 hectares of forest per year in 10-ha blocks since about 1979 to maintain some early successional stages on a rotational schedule, this unit also contains a 2000-ha wilderness area that receives no active management. Both study sites also support the goal of maintaining wildlife diversity by minimizing the impacts of their management activities.

Methods

Forest Plot Data Metrics

Study plots

Breeding bird survey points (50-m radius) were established at MH (n=114) and IP (n=100, but only 99 fell within the LiDAR acquisition area, see below) in 1995 and 2001 respectively, for long-term monitoring (Ralph et al. 1995). Criteria used to establish the survey points included (1) coverage of the full range in heterogeneity of forest composition (proportion of hardwood-to-softwood) and structure (early successional-to-mature forest stands), (2) were located ≥ 250 m apart, and (3) at least 100 m from main bodies of water. A subset of these points

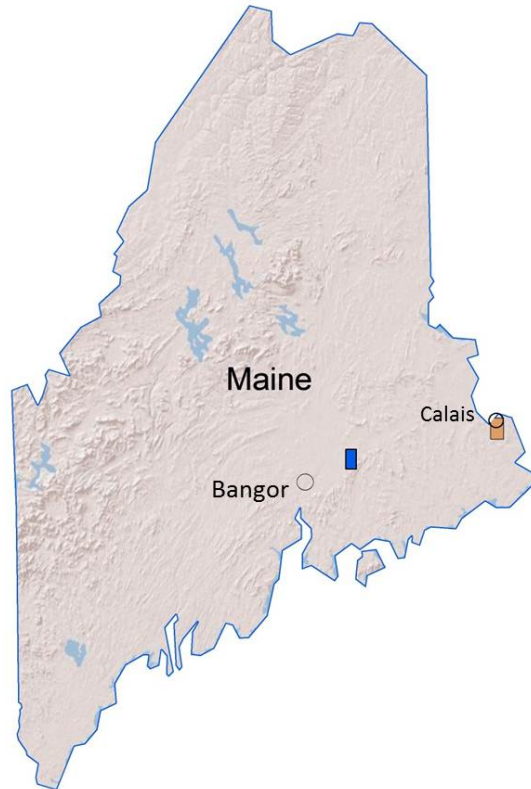


Figure 2.1. Study site locations within Maine (Blue=International Paper, Red=Moosehorn National Wildlife Refuge).

(28 from IP and 38 from MH) were surveyed in August and September of 2003 to estimate total canopy closure and other forest-stand metrics on 50×50 m plots centered within the 50-m radius point (Figs. 2.2.a and 2.2.b). The actual subset of points selected for field sampling was based on an assessment of the stands from a reconnaissance of the points conducted in June, 2003, with the goal of maintaining the range in stand type heterogeneity within the study site (Hirzel and Guisan 2002). To supplement the range in heterogeneity of forest stands, we opportunistically added two additional 50×50 m plots at each of the two study sites that were not centered on a bird survey point but seemed to represent unique forest stands or structure (e.g., tall trees with cleared understory, recent clear-cuts).

Tree and sapling metrics

Each 50×50 m plot was subdivided into 4 quadrants (NE, NW, SW, SE). Within each quadrant we used a wandering point-quarter sampling method (WQ) to subsample, measure, and characterize individual tree and sapling stems (Catana 1963; Fig. 2.3). Trees, for the purposes of this study, are defined as stems ≥ 10 cm (4 in.) in diameter at breast height (DBH \approx 1.6 m above ground), with saplings having DBHs being ≥ 0.635 cm (0.25 in.) but < 10 cm (DeGraaf et al.1998). For saplings, we recorded the actual diameter at 0.305 m (1 ft.) above the ground as sapling “DBH”; saplings are assumed to represent the understory or new growth in early successional stands. The WQ method was conducted separately for trees and saplings within each quadrant.

For each tree (or sapling) encountered we measured the angle and distance from the prior nearest tree (or point center for first tree encountered), DBH, distance from the ground to bottom of live canopy (GTC), canopy height from ground to the canopy top (CH), and the maximum and minimum canopy width radius at the drip-line (CWL and CWS, respectively). For saplings we

IP Study Site (6.4×12.0 km)

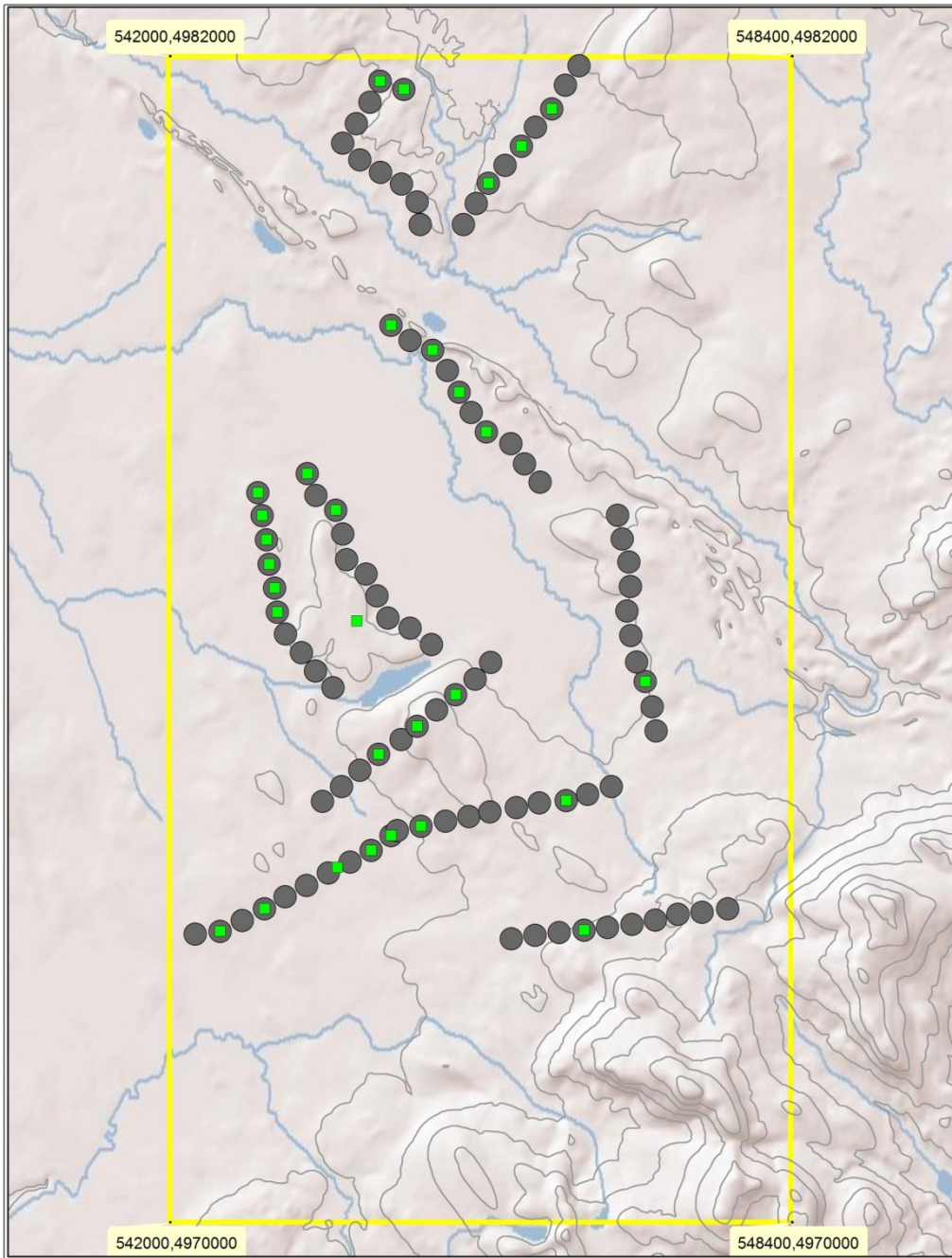


Figure 2.2.a. International Paper (IP) study site; dark-gray circles are locations of 99 50 m radii bird survey points (not drawn to scale), green squares are locations of 30 50×50 m forest stand plots (two forest stand plots are not centered on a bird survey point).

MH Study Site (7.9 × 13.1 km)

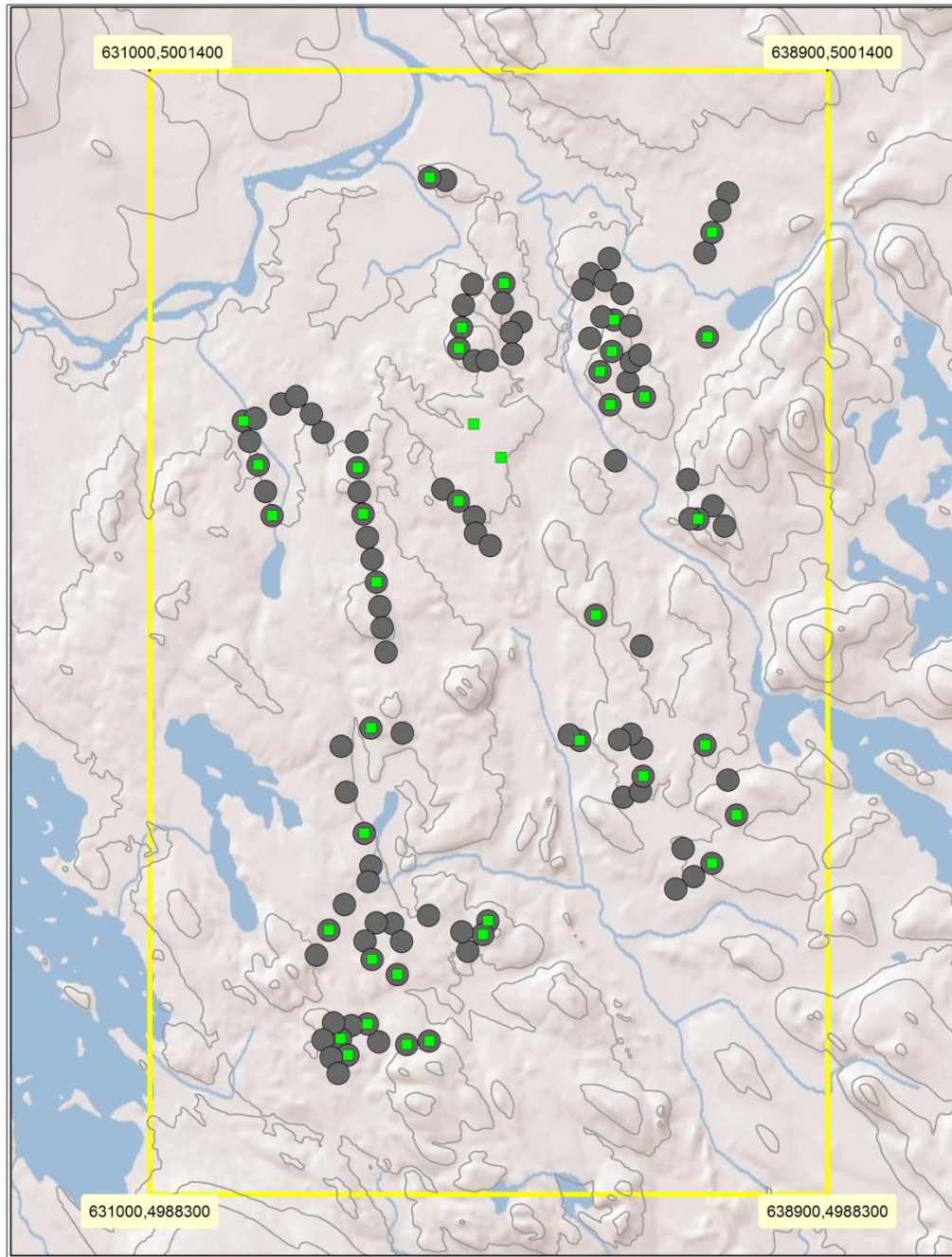


Figure 2.2.b. Moosehorn National Wildlife Refuge (MH) study site; dark-gray circles are locations of 114 50 m radii bird survey points (not drawn to scale), green squares are locations of 40 50×50 m forest stand plots (two forest stand plots are not centered on a bird survey point).

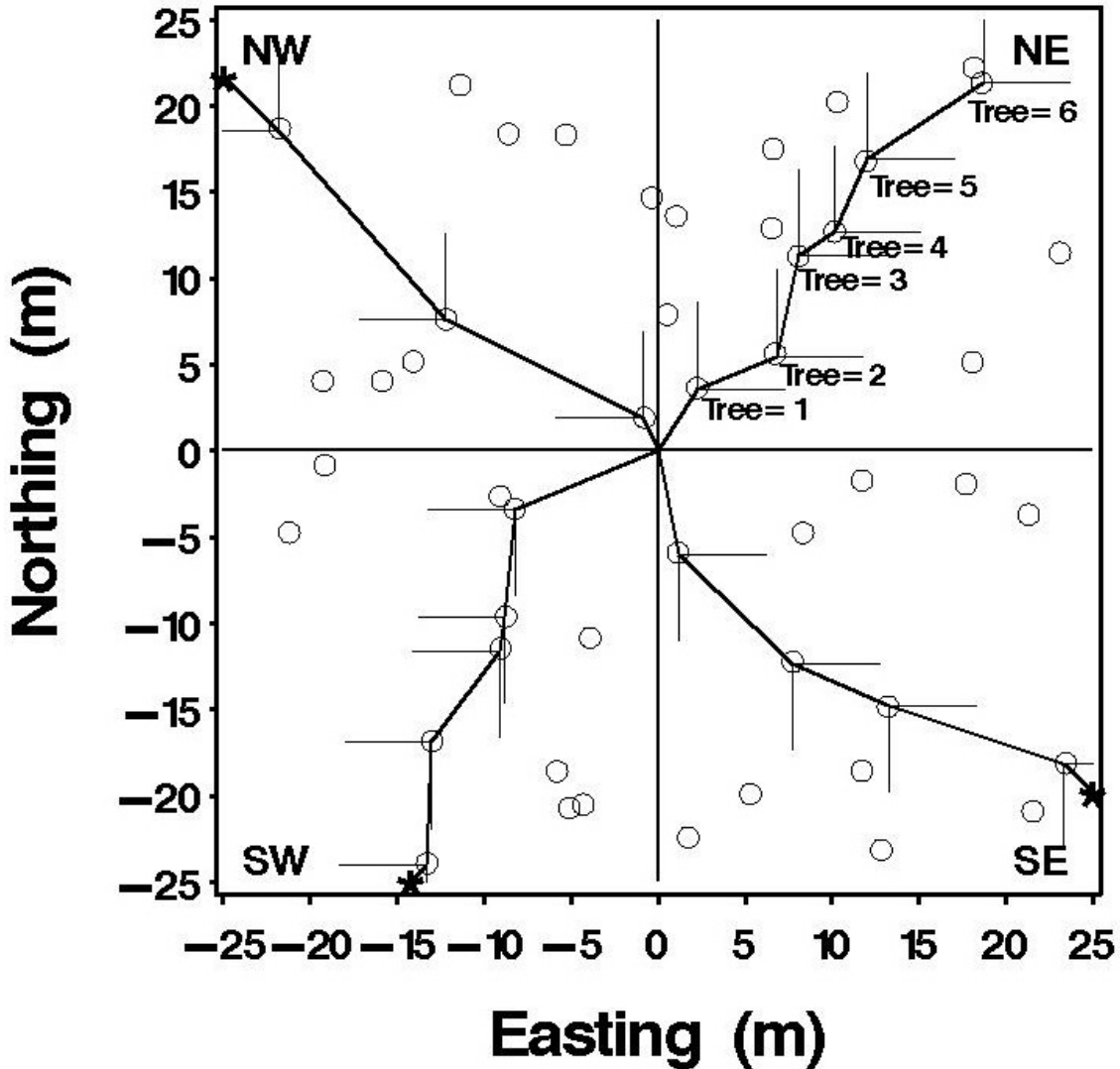


Figure 2.3. Illustration of conducting a wandering point-quarter (WQ) sampling method within quadrants of a 50×50 m plot (0.25 ha) of trees (total trees in plot = 50, n=18 selected for WQ, with 3 distances censored and represented by *); plot is centered on 50 m radius bird point (see text for more details).

did not measure the GTC, CWL, and CWS. For total canopy width (CW), we averaged CWL and CWS and then multiplied by two to get an estimate of full canopy width. A steel tape measure was used to measure DBH, GTC, CH, CWL, and CWS for shorter stems, and a Hypsometer Range Finder was used to measure GTC and CH for taller trees (typically greater than 6 m). Heights were recorded to the nearest 0.305 m (1 ft.) with DBH to the nearest 0.635

cm (0.25 in.). Stems that forked below the DBH were considered separate stems, with those forking above considered as a single stem. Basal area (BA) was computed as $(\frac{1}{2} \times \text{DBH})^2 \times \pi$, with stems assumed to be simple conics; stem volumes were computed as $\frac{1}{3} \times \text{BA} \times \text{CH}$. All measurements were recorded in English units but converted to metric units during data analysis.

Species and wood type (softwood, hardwood) also were recorded as was the status of the upright stems encountered (% dead foliage >80% classified as dead snags). Depending on stem density within each quadrant, data were typically collected for up to six stems for trees and up to 12 for saplings within each quadrant out to a distance of approximately 25 m radius. We censored stems falling outside the 50×50 m plot if the cumulative number of stems quantified was less than six trees (or 12 saplings). Accommodation of the censored distances in estimating stem densities for 50×50 m plots followed Datta (2005) and used PROC SURVIVE in SAS (SAS 2009). The WQ was found in simulation studies to be a rapid yet reasonably efficient technique for estimating stem densities with trivial biases (Engeman et al. 1994) and also can be used to estimate other stand structural attributes such as mean tree height (Brower et al. 1989), mostly on larger stands of forests (i.e., >1 ha). Appendix A summarizes a simulation study investigating and comparing the relative biases and efficiencies between the WQ and a belt transect method for 0.25-ha forest-stands (i.e., study plots) and between the WQ and circular subplots on 0.77-ha stands.

Using the measurements taken on individual trees and saplings we derived 19 forest stand metrics (i.e., response variables) summarized for each 50×50 m plot; 12 stand metrics for trees and seven for saplings (Table 2.1). An estimate of canopy closure within the 50×50 m plots are deemed important and useful for forest inventory purposes (e.g., Avery and Burkhart 2002) and for characterizing wildlife habitat (e.g., DeGraaf et al. 1998, Short et al. 2001).

Table 2.1. Forest metric response variable summary statistics across all study plots and sites (n=69 plots, n=68 for Y13).

Response Var. ¹	Forest metric ²	Mean	SD	Min.	Median	Max.
Trees:						
Y1	Stem density (stems/0.25 ha)	155.8	131.4	0.0	146.0	484.0
Y2	Mean DBH (cm)	14.7	6.7	0.0	15.6	30.9
Y3	Mean BA (cm ²)	241.1	187.8	0.0	216.1	1001.8
Y4	Mean CH (m)	10.2	4.7	0.0	11.2	19.3
Y5	Mean volume (m ³)	0.12	0.12	0.0	0.09	0.7
Y6	Total BA (m ² /0.25 ha)	4.4	4.4	0.0	3.5	15.2
Y7	Total volume (m ³ /0.25 ha)	24.3	28.9	0.0	13.0	124.9
Y8	Mean GTC (m)	5.5	3.7	0.0	5.8	14.1
Y9	Max. CH (m)	15.8	8.5	0.0	16.6	32.8
Y10	SD CH (m)	3.0	2.0	0.0	3.0	7.6
Y11	Max. GTC (m)	10.0	6.4	0.0	10.6	21.9
Y12	SD GTC (m)	2.3	1.5	0.0	2.7	4.6
Y13	Canopy Closure > 2 m (%)	45	29	0.0	50	86
Saplings:						
Y14	Density (stems/0.25 ha)	1603.1	1450.2	0.0	1256.0	7652.0
Y15	Mean DBH (cm)	3.3	1.2	0.0	3.4	6.5
Y16	Mean BA (cm ²)	12.3	7.3	0.0	12.0	37.3
Y17	Mean CH (m)	3.5	1.3	0.0	3.4	6.9
Y18	Mean volume (cm ³)	2285.1	1859.6	0.0	1742.9	10553.9
Y19	Total BA (m ² /0.25 ha)	1.7	1.5	0.0	1.4	7.0
Y20	Total volume (m ³ /0.25 ha)	3.0	3.0	0.0	1.9	13.5

¹Trees = stem \geq 10 cm DBH, sapling = stems < 10 cm DBH (but \geq 0.635 cm).

²DBH=diameter at breast height (saplings at 0.3m), BA=basal area, GTC = ground-to-canopy height refers to distance from ground to the bottom live canopy, SD=standard deviation. also was estimated and used as a response variable (see below). All of these structural metrics

Canopy closure (field derived)

To efficiently estimate total canopy closure at each 50×50 m plot to be related to LiDAR-derived estimates we took five overhead hemispherical photographs using a digital camera, one at the plot center and four in each cardinal direction at approximately 12 m from the plot center. For consistency, the camera was held 2 m above the ground at each photo-point to avoid over-saturation of canopy closure estimates in areas with short- and dense non-woody vegetation. Each photograph was saved as a .jpg file to a computer hard-drive and imported into

MicroImages Software (MicroImages, Inc. 2012). Photographs were converted to images and separated into red, green, and blue .tiff files. The bands that best represented sky and canopy for each image were then used to select a threshold-pixel value. Pixels below the threshold were classified as canopy with those above the threshold being sky. Using this threshold value a binary image was created with all vegetation assigned a value of 1 and sky having a value of 0. A histogram for the binary image provided a count of pixels which was used to calculate percent canopy closure for each image. We averaged the percent closure across the five images to derive a mean canopy closure for each 50×50 m plot. Because overhead photographs of canopies encapsulate a hemispheric representation of canopy leading to biased high estimates and are camera dependent (Frazer et al. 1997; overhead photographs in Fig. 2.4), we developed a calibration curve to adjust our mean estimates. We used a GRS densitometer (Geographic Resource Solutions, 2012) at eight 50×50 m plots ranging from 0 to nearly 80% canopy closure. For consistency with the digital photographs, we held the densitometer at approximately 2 m above the ground and recorded a “hit” (i.e., vegetation) at the center and at 12 locations 1-2 m apart in each cardinal direction for a total of 49 points per plot, computing the percentage of vegetation hits as canopy closure. For these eight calibration points, we built a nonlinear calibration curve relating the densitometer estimates to camera estimates. We used PROC NLIN (SAS Institute, Inc. 2009) to fit the nonlinear curve, forcing it through the points (0, 0%) and (100, 100%) yielding a simple adjustment equation presented in the lower right panel of Fig. 2.4. We applied the calibration adjustment to all mean camera estimates for each 50×50 m plot across both study sites.

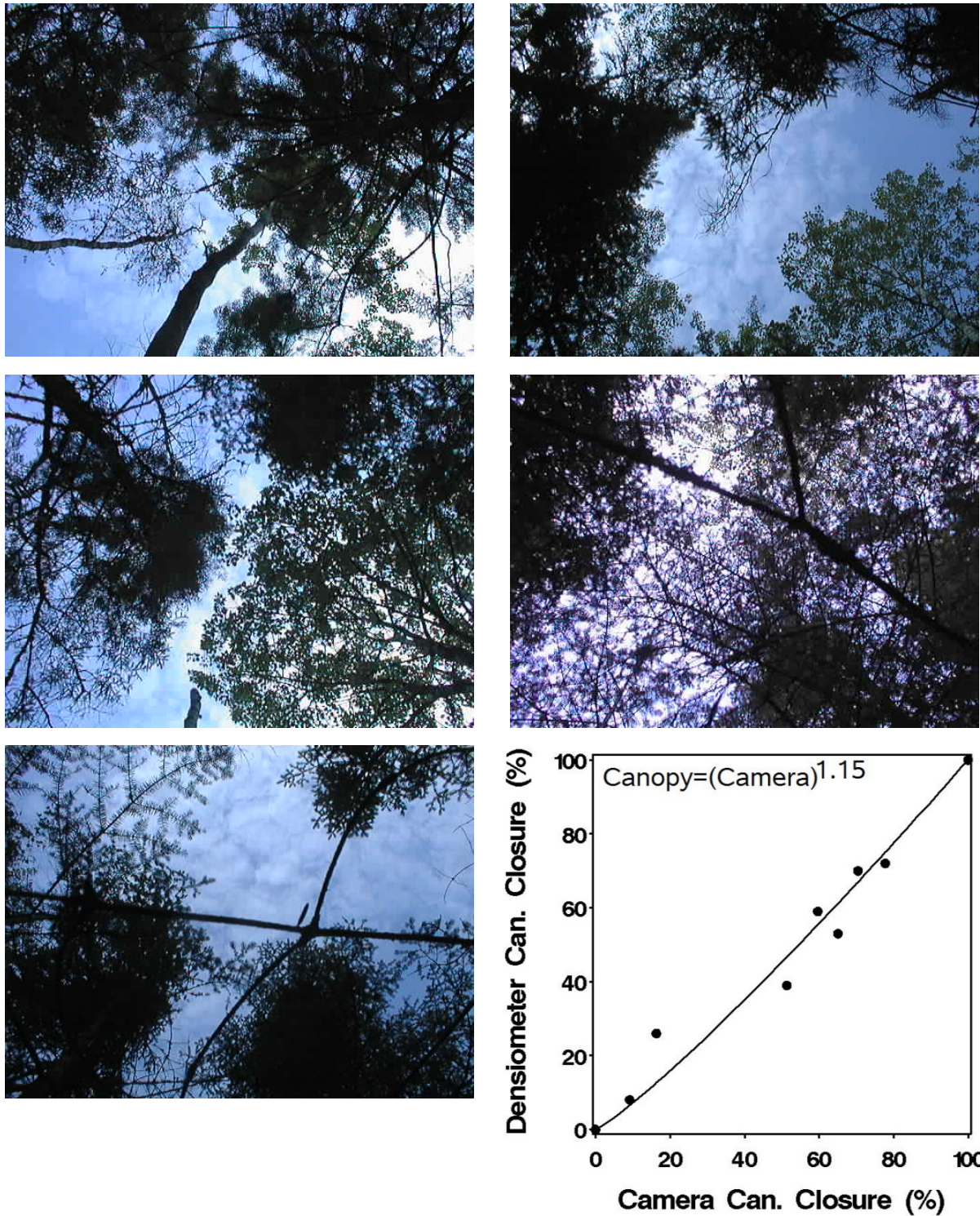


Figure 2.4. Example of digital photographic images and calibration curve for adjusting mean camera canopy closure estimates across five images to account for hemispheric digital photographic estimates.

LiDAR Acquisition and Processing

Acquisition

Discrete-return LiDAR was acquired on IP and MH study sites as delineated by the rectangular boxes in Fig. 2.2.a and 2.2.b respectively on 21 June 2003 (full leaf-on). A Leica ALS40 LiDAR system mounted on an aircraft was used and flown at an average altitude of 1828 m above the terrain. The airspeed was 240 km/hr (130 knots) with a laser pulse rate of 30.5 kHz, a field of view of 45°, scan rate of 19 Hz, and an average swath width of 1515 m. Instruments were calibrated to record up to 3 returns, including intensity values for each return. These flight and instrument parameters yielded a nominal ground pulse spacing of approximately 2 m (0.25 returns/m²) resulting in > 18.9 million returns from IP and > 25.7 million returns from MH (Table 2.2).

Table 2.2. LiDAR acquisition summary statistics for International Paper (IP) and Moosehorn National Wildlife Refuge (MH).

Site ¹	Return	Filtering Classification		Total
		Non-ground	Ground	
IP (7680 ha)	1	12480797	4292970	16773767
	2	860741	1257176	2117917
	3	4761	27727	32487
	Total	13346299	5577873	18924172
MH (10349 ha)	1	17262073	5167876	22429949
	2	1206613	2022825	3229438
	3	7746	46080	53826
	Total	18476432	7236781	25713213

¹IP=International Paper, MH=Moosehorn National Wildlife Refuge.

Ten ground control points dispersed across each site yielded RMSE vertical accuracy of 0.107 m at IP and 0.059 m at MH on open areas (gravel roads and/or short grassy areas). LiDAR data also were quality checked by contracting staff at the USGS Mid-Continent Mapping Center, Rolla, Missouri, prior to acceptance and post-processing. Data were delivered from the vendor as easting, northing, elevation, and intensity (XYZI) ASCII data sets, separated for each of the

three returns and by study site (six total files). The XYZ values were from UTM coordinate system (zone 19) with XY in NAD83 m and Z in NADV88 m. Intensity values were near-infrared waveband and rescaled to range from 0-250 to represent greyscale.

Post-processing

To save on costs and since the study sites are not considered large by today's standards for LiDAR acquisitions, we chose to post-process the raw XYZ data ourselves and not rely on vendor proprietary software. Classifying three-dimensional (3D) LiDAR point-clouds to ground and non-ground is an active area of research with many algorithms available (e.g., Zhang and Whitman 2005). We coded the de-spike algorithm described in Haugerud and Harding (1999) in SAS (SAS Institute, Inc.) and filtered and classified each XYZ point to ground or non-ground using a tolerance of 0.25 m using 10 iterations. However, few changes in classifications were found after approximately 4-5 iterations. A 0.25-m tolerance was used because most saplings that had a "DBH" ≥ 0.635 cm also were > 0.5 m in height, hence our field collected data were not distinguishable from ground below this threshold and doubling the RMSE from the control points which were near 0.25 m. We used the de-spike filtering process centered on each bird survey point in 400×400 m square blocks and across the entire acquisition areas for IP and MH. We used a triangular irregular network (TIN)-like algorithm in SAS (PROC G3GRID, SAS Institute, Inc. 2009) to grid the data to 2-m cells and derived a digital elevation model (DEM) (Fig. 2.5), a digital surface model (DSM) for first returns only (no figures created), and a canopy height model (CHM), where $CHM = DSM - DEM$ (left panels Figs. 2.6.a and 2.6.b). This filtering process yielded approximately 5.7 million and 7.2 million ground returns across all three returns for IP and MH respectively (Table 2.2). We also generated gray-scale images for each site by TIN-interpolating (2 m) using first-return intensity data (right panels Figs. 2.6.a and 2.6.b).

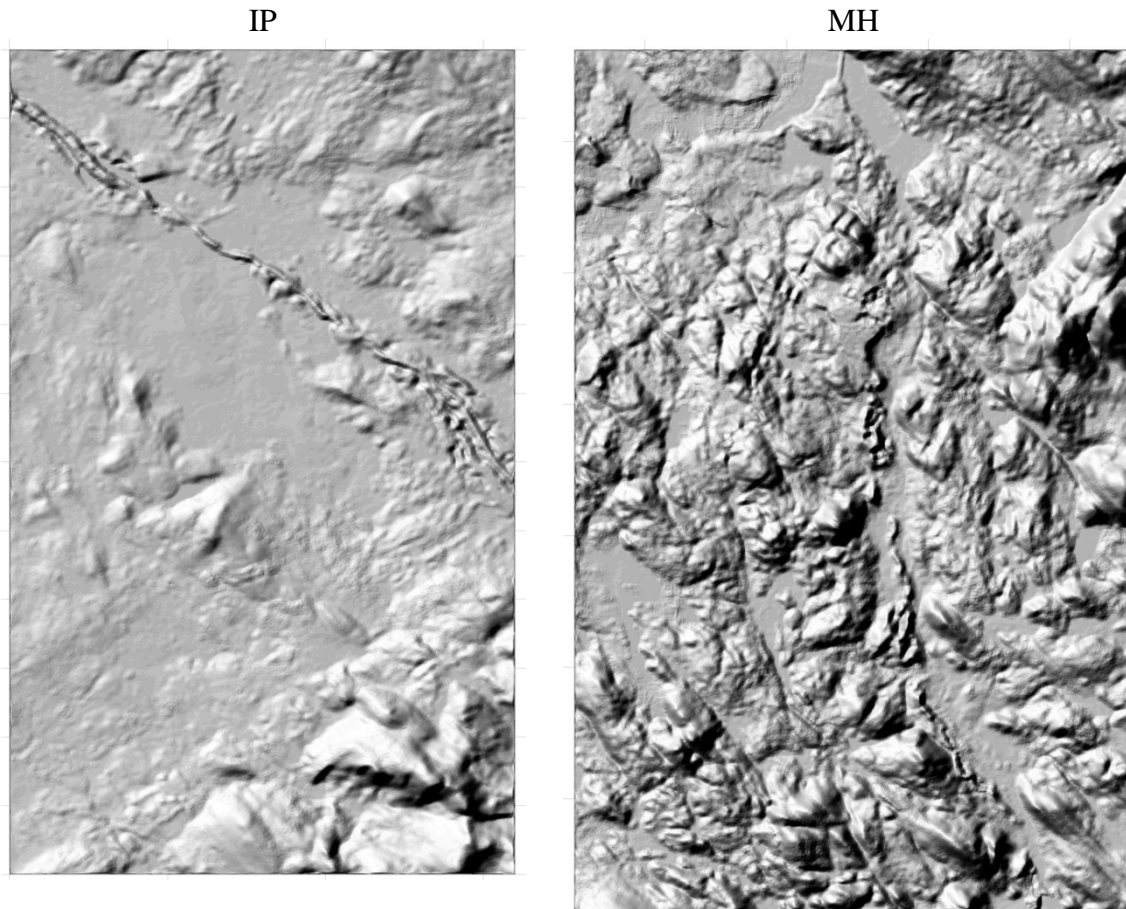
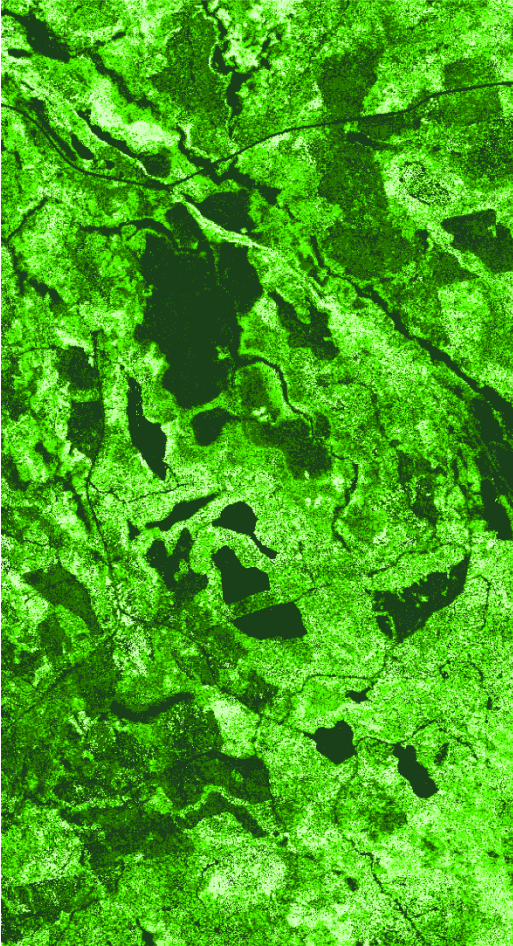


Figure 2.5. TIN-interpolated (2 m) shaded relief digital elevation model (DEM) estimate for International Paper (IP) and Moosehorn National Wildlife Refuge (MH) (not drawn to scale, see Fig. 2.2.a and 2.2.b for scale of boundary for IP and MH respectively).

Canopy closure (LiDAR-derived)

We estimated LiDAR-derived canopy closure (CC) at each 50×50 m cell across the entire study area and at each of the selected bird survey points used for sampling forest structure (i.e., plots). Canopy closure is defined as the penetration and return-detection of emitted photons through the forest canopy for each pulsed LiDAR beam within a 50×50 m cell or plot. To compute CC, we first partitioned each study area into non-overlapping 50×50 m cells. Within each 50×50 m cell, we further stratified each LiDAR point into non-overlapping 1-m cells and subtracted the estimated ground elevation using the DEM from all values to derive

Canopy Height Model



LiDAR Intensity Image

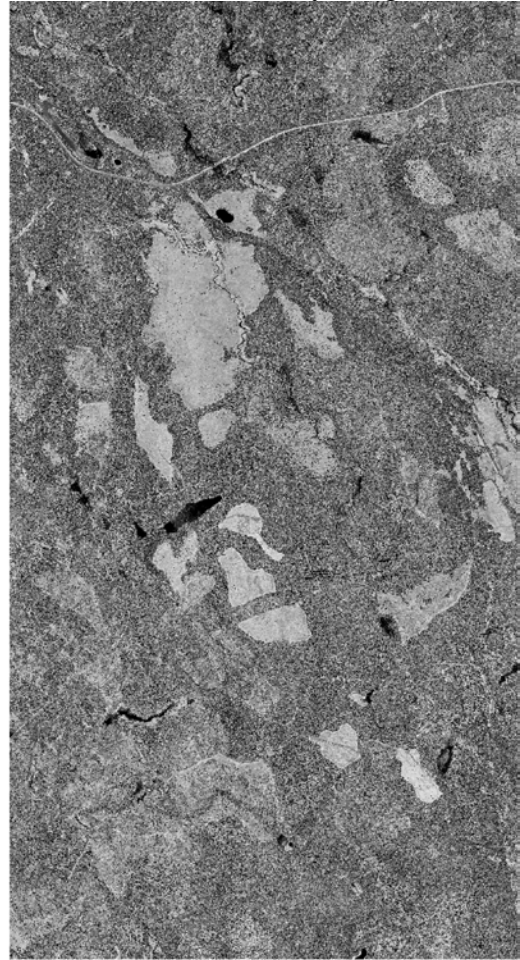
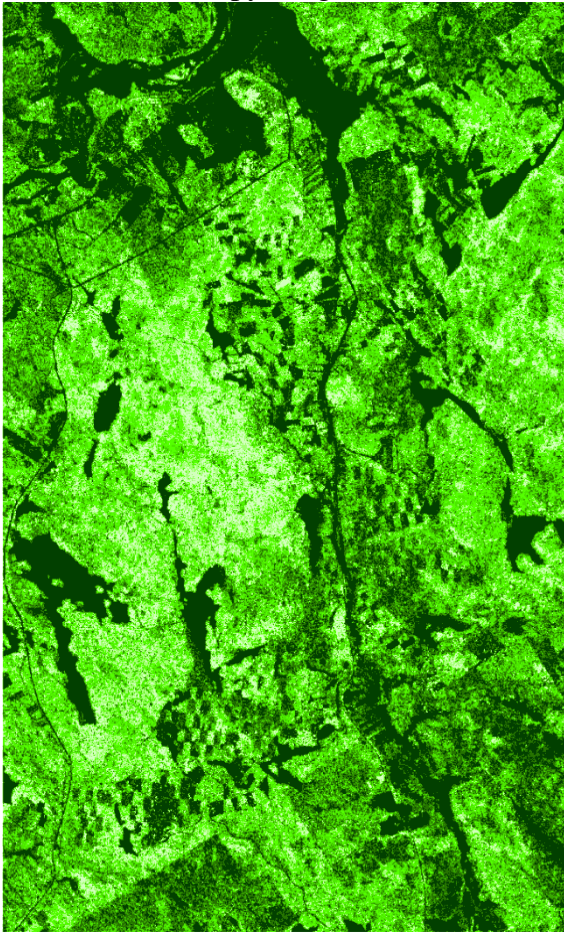


Figure 2.6.a. TIN-interpolated (2 m) canopy height model (CHM) and gray-scale intensity image for International Paper (left panel: dark green being 0 m heights to light green being 30 m heights; not drawn to scale, see Fig. 2.2.a for scale of boundary).

“above-the-ground” heights within each 1-m cell. We then classified each point’s height above ground into 1-m vertical height bins up to 30 m (the 30-m height bin also included all points > 30 m above ground). We tallied the number of LiDAR returns for each vertical height bin across the 50×50 m cells. Dividing each of the 1-m vertical bin counts by the total number of points within each 50×50 m cell yielded the proportion of points at each of 30 vertical bins into a canopy closure profile, labeled CC0, CC1, ... CC30 (CC0 represented the proportion of ground returns, CC1 represents the proportion of returns classified between the ground and 1 m above

Canopy Height Model



LiDAR Intensity

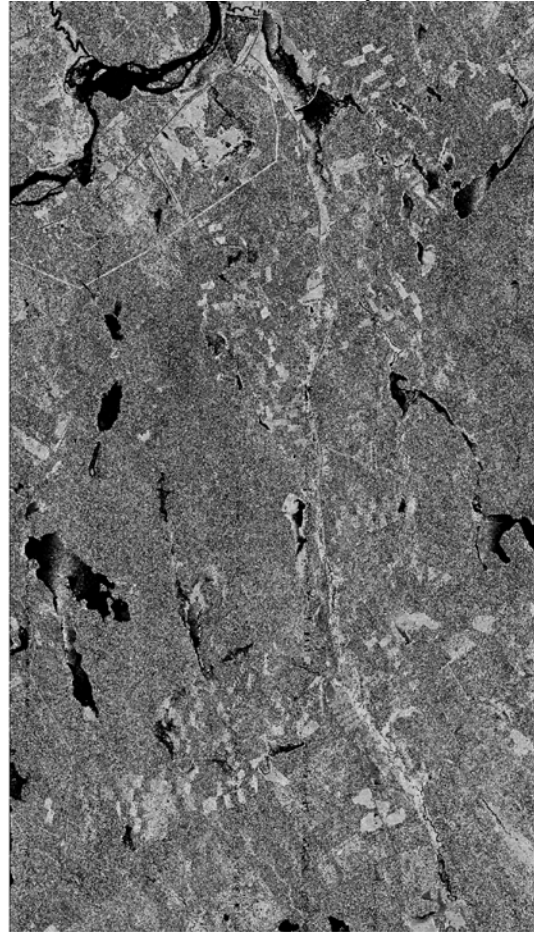


Figure 2.6.b. TIN-interpolated (2 m) canopy height model (CHM) and gray-scale intensity image for Moosehorn National Wildlife (left panel: dark green being 0 m heights to light green being 30 m heights; not drawn to scale, see Fig. 2.2.b for scale of boundary).

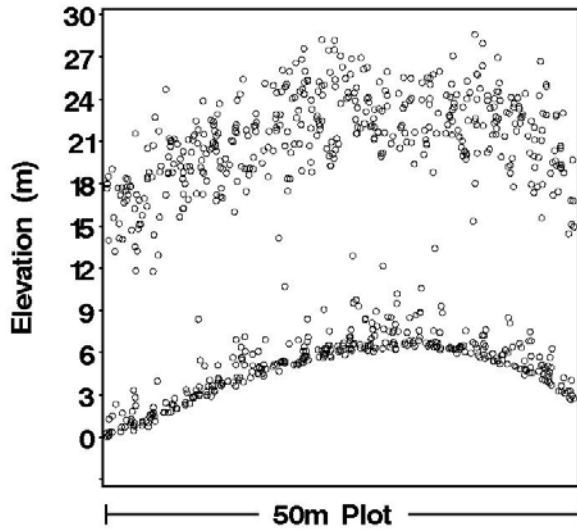
the ground, CC2 represents the proportion of returns classified between 1-2 m, etc.; few trees at either study site exceed 30 m in height). The sum of all ground and non-ground proportions equaled 1.00 (equivalent to 100%). This procedure allowed us to sum proportions within a 50×50 m cell to any desired 1-m canopy closure category (e.g., canopy closure from 6-12 m above ground would be the sum of CC6 through CC12). We used various combinations of these sums for the 50×50 m cells to derive explanatory variables for modeling forest stand metrics. An example of this process is illustrated in Fig. 2.7 in four basic steps: (1) filtering and classifying

raw point cloud data to ground and non-ground, (2) determining height of non-ground points above ground through subtraction (i.e., $CHM=DSM-DEM$), (3) binning each non-ground point height above ground into vertical height bins, and (4) resulting histogram of tallied points, re-scaled to sum to 100%.

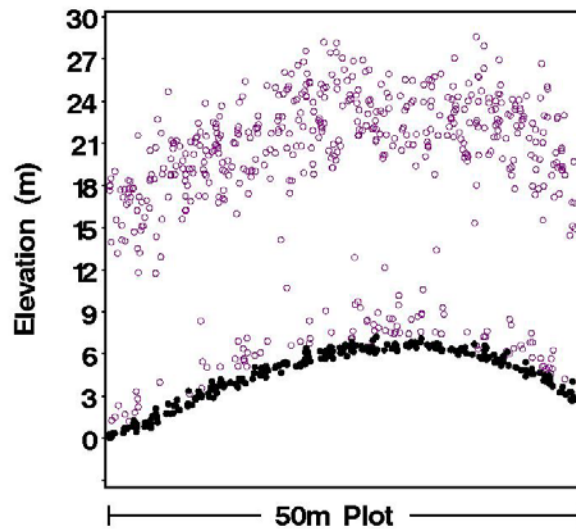
Building classification and extraction

Although both study sites are highly rural, buildings and other man-made structures exist within the acquisition area. We labeled and excluded LiDAR returns that obviously represented buildings or other structures from canopy closure estimates described above. To do so, we TIN gridded all first-returns at 2 m and produced a shaded relief image using Surfer Software (Golden Software, Inc. 2002). From this image we manually digitized the centroid of each detected building or other non-vegetation structures (e.g., upper left panel in Fig. 2.8 with upper right panel illustrating the buildings that would be considered as canopy returns without labeling and removing from canopy closure estimates). We then classified each non-ground classified LiDAR return within 150 m of each centroid as building (or non-vegetation) and conducted a radius search away from the centroid in 5° arcs until the first ground point was encountered, all non-ground returns beyond the first encountered were classified as non-buildings (lower left panel in Fig. 2.8). These building-labeled points were then classified as non-ground non-vegetation and were not used when computing canopy closure estimates within each 50×50 m cells (lower right panel in Fig. 2.8 with building locations now classified and interpolated to ground). Although we manually digitized and excluded buildings, feature extraction is an active area of research with LiDAR data (e.g., Meng et al. 2009).

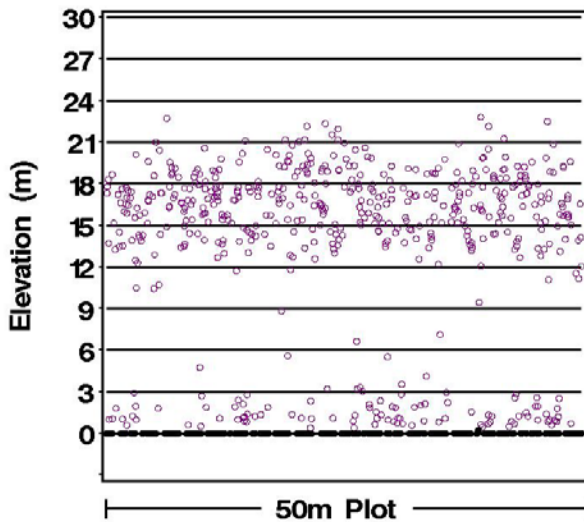
Step 1 – Filter to ground and non-ground.



Step 2 – Determine height above ground.



Step 3 – Bin points into vertical profiles



Step 4 – Tally points within bins for CC

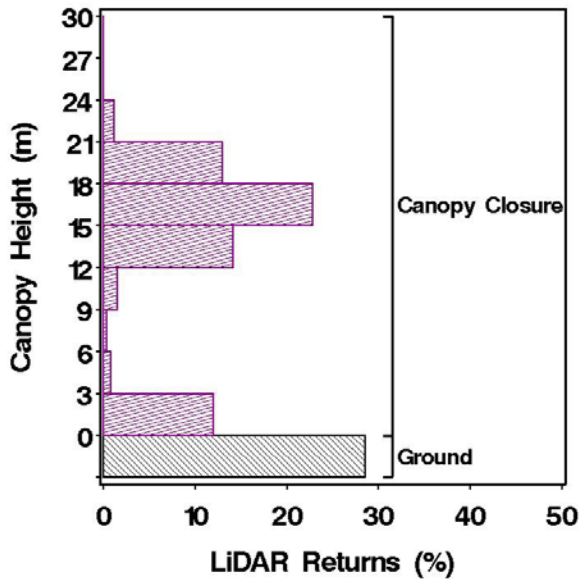


Figure 2.7. Illustration of processing steps for deriving a digital elevation model (DEM) from raw (2D) point-cloud (UL), deriving digital surface model (DSM), highest open circles within each 2-m cell, and canopy height model (CHM) (UR, solid black points being those classified as ground and where CHM=DSM-DEM), classifying and tallying LiDAR returns into ground and above ground height categories (LL), and deriving 3-m vertical height profiles and computing percent canopy closure estimates within a 50×50 m plot (LR).

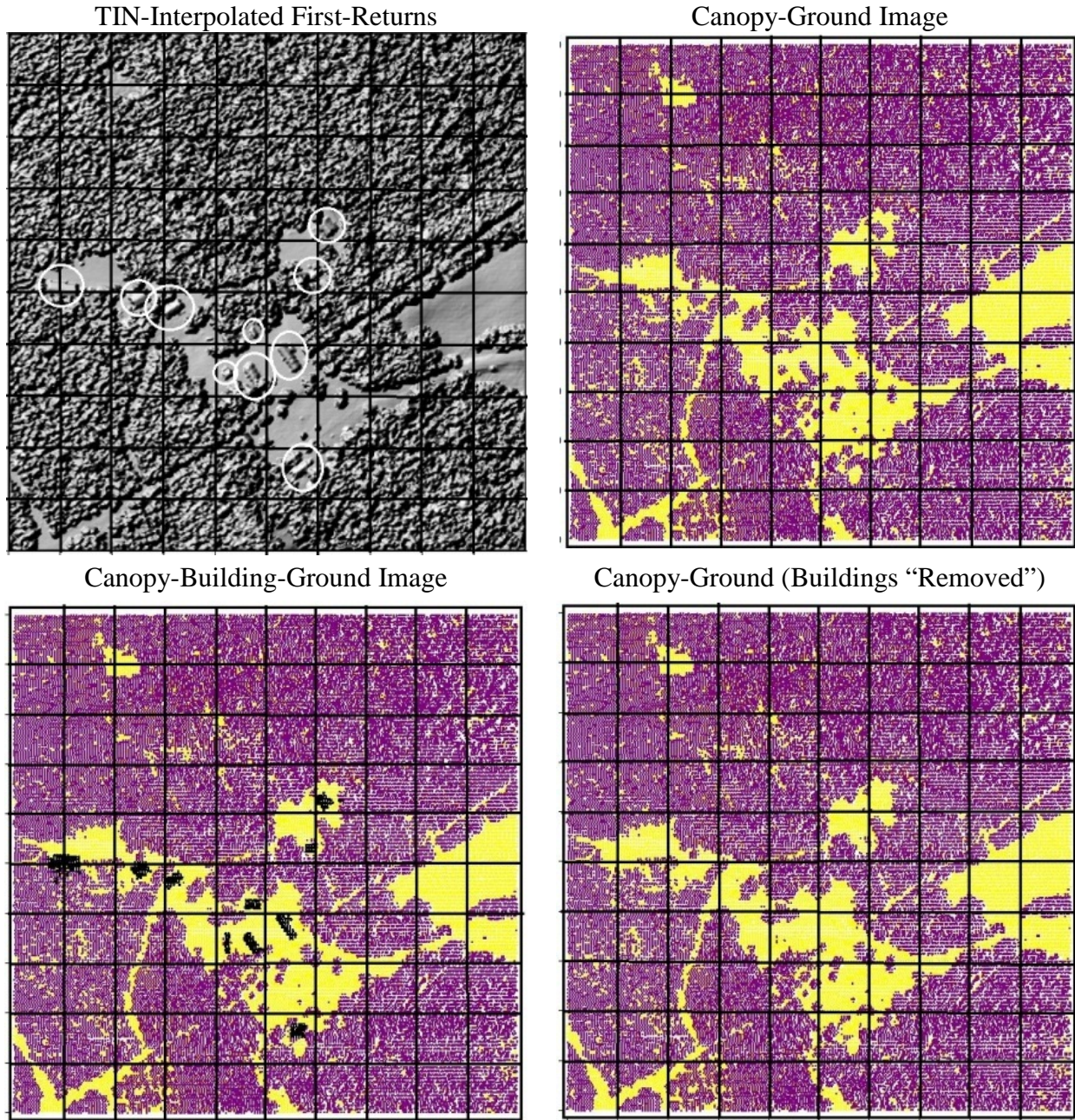


Figure 2.8. Illustration of the process for digitizing, classifying, and removing buildings from total canopy closure estimates (UL – TIN-interpolated shaded relief from first return LiDAR, buildings circled in white, grid cells are 50×50 m, UR – 2D scatterplot of first return LiDAR data with yellow representing ground classified, purple represents vegetation, LL - black values represent identified LiDAR returns from buildings, LR – buildings “removed” by coloring yellow).

Digitization of water bodies and sphagnum bogs

We used the intensity images (right panels in Figs. 2.6.a and 2.6.b) to digitize obvious water bodies and bogs as polygons and exclude these areas for predicting forest stand metrics with LiDAR (see below modeling). If the center of a 50×50 m cell fell within the water (or bog) polygon, we classified the entire cell as water.

Use of 50×50 m cells for modeling

The decision to use 50×50 m plots (0.25-ha) as the sampling unit for modeling forest stand metrics (and bird modeling in Chapter 3 of this dissertation) was based on three criteria. The first criterion was that a sufficient number of LiDAR returns are required from a 3-dimensional XYZ point-cloud to bin returns into vertical height classes necessary to create a vegetation profile above the DEM. A 50×50 m plot with an average two-m nominal post-spacing (0.25 returns/m²) contained > 625 total returns, which was sufficient to construct vertical vegetation profiles. Smaller plots (e.g., 10×10 m) did not contain a sufficient number of LiDAR returns to construct vegetation profiles, whereas larger plots (e.g., 100×100 m) regressed to the mean of the entire stand and thereby substantially reduced heterogeneity in explanatory variables. The second criterion was that 50×50 m plots center well within a 50-m radius bird survey point, thereby allowing description of habitat heterogeneity at the bird survey points and surrounding cells that can be used for other assessments (Chapter 3 of this dissertation uses the center cell as well as surrounding cell information to model bird abundance). The third reason is that this is currently the pixel size used by ECOSEARCH, Version 1.

LiDAR-derived explanatory variables

As described above, we tallied the proportion of LiDAR returns within each 50×50 m cell into 31 one-m vertical height CC bins, with the first bin being ground returns (labeled CC0). To

develop and assess empirical models for modeling the 20 forest metrics described above and listed in Table 2.1 as a function of LiDAR, we generated LiDAR-derived explanatory variables from the 31 CC bins. To do so, and to reduce the number to a manageable number, we combined the 30 non-ground 1-m CC bins into 10 3-m CC bins as proportions and considered these as one set of plausible explanatory variables (labeled P0 to P10 in Table 2.3, with summary statistics

Table 2.3. Summary statistics for LiDAR-derived explanatory variables within 50×50m study plots across both study sites.

Explan. Var.	Description ¹	Summary Statistic ²				
		Mean	SD	Min.	Median	Max.
P0	Proportion classified on ground	0.317	0.225	0.06	0.23	0.99
P1	(0 < CC ≤ 3 m above ground)	0.186	0.141	0.00	0.15	0.57
P2	(3 < CC ≤ 6 m above ground)	0.142	0.120	0.00	0.11	0.51
P3	(6 < CC ≤ 9 m above ground)	0.099	0.101	0.00	0.08	0.53
P4	(9 < CC ≤ 12 m above ground)	0.090	0.088	0.00	0.08	0.32
P5	(12 < CC ≤ 15 m above ground)	0.083	0.089	0.00	0.05	0.27
P6	(15 < CC ≤ 18 m above ground)	0.058	0.080	0.00	0.01	0.27
P7	(18 < CC ≤ 21 m above ground)	0.019	0.033	0.00	0.00	0.13
P8	(21 < CC ≤ 24 m above ground)	0.004	0.012	0.00	0.00	0.08
P9	(24 < CC ≤ 27 m above ground)	0.001	0.004	0.00	0.00	0.02
P10	(CC > 27 m above ground)	0.000	0.001	0.00	0.00	0.01
X1	log((P1+0.001)/(P0+0.001))	-0.743	1.290	-5.09	-0.39	1.15
X2	log((P2+0.001)/(P0+0.001))	-1.131	1.805	-6.83	-0.71	1.48
X3	log((P3+0.001)/(P0+0.001))	-1.766	2.173	-6.83	-0.97	1.51
X4	log((P4+0.001)/(P0+0.001))	-2.280	2.616	-6.90	-1.14	1.01
X5	log((P5+0.001)/(P0+0.001))	-2.645	2.696	-6.90	-1.63	0.87
X6	log((P6+0.001)/(P0+0.001))	-3.170	2.539	-6.90	-3.45	0.79
X7	log((P7+0.001)/(P0+0.001))	-4.009	2.083	-6.90	-4.61	-0.12
X8	log((P8+0.001)/(P0+0.001))	-4.893	1.488	-6.90	-5.28	-0.51
X9	log((P9+0.001)/(P0+0.001))	-5.314	1.068	-6.90	-5.43	-1.75
X10	log((P10+0.001)/(P0+0.001))	-5.484	0.763	-6.90	-5.43	-2.86
PRIN1P	PCA variable 1 among P0 to P10	0.00	2.03	-2.31	-0.35	5.98
PRIN2P	PCA variable 2 among P0 to P10	0.00	1.51	-3.65	-0.16	3.75
PRIN3P	PCA variable 3 among P0 to P10	0.00	1.33	-2.41	-0.09	4.20
PRIN1X	PCA variable 1 among X1 to X10	0.00	2.54	-5.34	0.79	4.51
PRIN2X	PCA variable 2 among X1 to X10	0.00	1.33	-3.04	0.10	2.60

¹CC = canopy closure at each vertical height bin is the proportion of all LiDAR data falling within the intervals, PCA = principal components analysis.

²SD=standard deviation, summary statistics are computed across both study sites.

being computed across both study sites). Here, P1 and P2 are at the appropriate heights to represent the amount of understory or early successional vegetation. This “deciling” approach has been done with much success in many LiDAR studies that relate LiDAR data to forest overstory metrics (e.g., Li et al. 2008). However, because these P0 to P10 proportions are constrained to sum-to-one this can create problems when using these as explanatory variables in regression analyses (Becker 1969). Therefore, one transformation that can accommodate the sum-to-one constraint is to combine the proportions as ratios using a base value for all ratios and computing the log of this ratio, thus reducing the number of explanatory variables by one (Aitchison 1986). Doing this for P0 to P10, using P0 as the base and adding a small value of 0.001 to accommodate zero values, yields a second suite of potential explanatory variables labeled X1 to X10 in Table 2.3.

Graham (2003), among many others, raised concerns with using collinear (i.e., correlated) explanatory variables in regression analyses. Computing pairwise correlations among the variables P0 to P10 and X1 to X10 revealed strong correlations in our LiDAR-derived explanatory variables, especially between adjacent height classes (Table 2.4). Therefore, as one way to reduce these correlations and derive uncorrelated explanatory variables, we conducted separate principal components analyses (PCA) using PROC PRINCOMP in SAS (SAS Institute, Inc., 2009) for P0 to P10 and for X1 to X10 as recommended by Graham (2003). Results of the PCA revealed that we could reduce P0 to P10 to three PCA variables and X1 to X10 to two PCA variables while still accounting for 75% and 82% of the variation among them respectively (Table 2.5). Labeling these PCA variables as PRIN1P-PRIN3P computed from P0 to P10 and PRIN1X-PRIN2X computed from X1 to X10 and summarizing these PCA variables across both study sites indicates reasonable range for modeling purposes (Table 2.3; Hirzel and Guisan

Table 2.4. Pair-wise correlations among LiDAR-derived explanatory variables.

Var. ¹	P0	P1	P2	P3	P4	P5	P6	P7	P8	P9	P10
P0		0.05	-0.49	-0.53	-0.47	-0.45	-0.33	-0.25	-0.22	-0.20	-0.13
P1			0.42	-0.38	-0.63	-0.62	-0.49	-0.33	-0.17	-0.13	-0.09
P2				-0.31	-0.22	-0.39	-0.42	-0.34	-0.18	-0.14	-0.09
P3					0.52	0.06	-0.11	-0.18	-0.10	-0.09	-0.06
P4						0.64	0.24	0.07	0.08	0.10	0.11
P5							0.78	0.52	0.28	0.26	0.27
P6								0.84	0.44	0.30	0.17
P7									0.71	0.52	0.11
P8										0.90	0.33
P9											0.54
P10											

	X1	X2	X3	X4	X5	X6	X7	X8	X9	X10
X1		0.70	0.25	0.02	-0.03	-0.01	0.10	0.24	0.37	0.45
X2			0.76	0.50	0.35	0.28	0.30	0.39	0.54	0.70
X3				0.88	0.69	0.58	0.51	0.51	0.60	0.75
X4					0.91	0.79	0.69	0.61	0.61	0.70
X5						0.94	0.83	0.68	0.61	0.65
X6							0.93	0.76	0.63	0.61
X7								0.85	0.69	0.61
X8									0.88	0.74
X9										0.87

¹ See Table 2.3 for descriptions, bolded correlations indicate those where $r \geq 0.50$.

2002). Examining the eigenvector “loadings” in Table 2.5 we can interpret PRIN1P and PRIN1X as contrasting shorter vegetation with taller vegetation with PRIN2P and PRIN2X representing the mid-story vegetation. PRIN3P could be interpreted as being ground contrasted with all other vegetation, especially the understory and taller overstory canopy. In essence, all of these potential LiDAR-derived explanatory variables “capture” most of the information available in the point-cloud and cover reasonably wide ranges in values, a prerequisite to increase the potential for successful modeling (Hirzel and Guisan 2002). Unless stated otherwise, all processing of LiDAR was done using the data step and macro facilities provided in SAS (SAS Institute, Inc., 2009).

Table 2.5. Principal Component Analysis (PCA) results among LiDAR-derived explanatory variables.

	Principal Component Variables				
	Prin1	Prin2	Prin3	Prin4	Prin5
PCA results for P0-P10:					
Eigenvalue	4.13	2.29	1.78	1.11	0.79
Proportion	0.38	0.21	0.16	0.10	0.07
Cum. Proportion	0.38	0.58	0.75	0.85	0.92
Variable ¹	Eigenvectors				
P0	-0.204	0.380	-0.437	0.302	-0.221
P1	-0.314	0.244	0.341	-0.193	0.279
P2	-0.212	-0.229	0.540	-0.231	0.078
P3	0.043	-0.556	0.160	0.127	-0.373
P4	0.266	-0.447	-0.123	0.252	-0.013
P5	0.411	-0.157	-0.173	-0.081	0.396
P6	0.412	0.070	-0.141	-0.382	0.199
P7	0.391	0.222	0.027	-0.391	-0.158
P8	0.342	0.270	0.322	0.055	-0.397
P9	0.312	0.260	0.380	0.294	-0.228
P10	0.193	0.124	0.250	0.586	0.552
PCA results for X1-X10:					
Eigenvalue	6.44	1.78	0.91	0.43	0.18
Proportion	0.64	0.18	0.09	0.04	0.02
Cum. Proportion	0.64	0.82	0.91	0.96	0.97
Variable ¹	Eigenvectors				
X1	0.119	0.632	0.260	0.499	0.282
X2	0.252	0.510	-0.254	0.156	-0.391
X3	0.325	0.138	-0.516	-0.146	-0.305
X4	0.346	-0.144	-0.414	-0.048	0.140
X5	0.346	-0.281	-0.165	0.228	0.345
X6	0.340	-0.315	0.063	0.355	0.102
X7	0.335	-0.248	0.279	0.353	-0.279
X8	0.337	-0.068	0.451	-0.185	-0.431
X9	0.339	0.115	0.340	-0.490	0.069
X10	0.348	0.209	0.054	-0.355	0.507

¹ See Table 2.3 for variable descriptions; bolded values represent proportion of variation explained ≥ 0.75 .

Data analysis and modeling

Plausible models

Because stepwise regression methods have been shown to have biases, among other concerns (Whittingham et al. 2006), we used an Information-Theoretic (IT) model development and selection approach for assessing empirical models relating the 20 forest metrics (Table 2.1) to the potential suite of LiDAR-derived explanatory variables in Table 2.3. The IT approach advocates more thought to developing a suite of competing models (i.e., hypotheses) than what stepwise or other similar methods require (Burnham and Anderson 2002). Therefore, we derived a suite of 8 plausible models that are parsimonious (i.e., minimized as much as possible the number of parameters involved) and minimized the amount of correlations among explanatory variables within each model (Table 2.6).

Table 2.6. Plausible models for modeling individual forest stand metrics as a function of LiDAR-derived explanatory variables.

Model		
No.	k ¹	Model Parameters (Explanatory Variables ²)
1	2	β_0
2	8	$\beta_0 + \beta_1(P0) + \beta_2(P2) + \beta_3(P4) + \beta_4(P6) + \beta_5(P8) + \beta_6(P10)$
3	8	$\beta_0 + \beta_2(P1) + \beta_3(P3) + \beta_4(P5) + \beta_5(P7) + \beta_6(P9)$
4	4	$\beta_0 + \beta_1(\text{PRIN1P}) + \beta_2(\text{PRIN2P})$
5	5	$\beta_0 + \beta_1(\text{PRIN1P}) + \beta_2(\text{PRIN2P}) + \beta_3(\text{PRIN3P})$
6	5	$\beta_0 + \beta_1(X1) + \beta_2(X3) + \beta_3(X6)$
7	5	$\beta_0 + \beta_1(X2) + \beta_2(X5) + \beta_3(X8)$
8	4	$\beta_0 + \beta_1(\text{PRIN1X}) + \beta_2(\text{PRIN2X})$

¹k=number of parameters estimated in model plus one for estimate of error variance.

²See Table 2.3 for description of explanatory variables.

Model 1 in Table 2.6 is simply a null model stating the forest metric of interest is not associated with any of the LiDAR variables. Model 2 states the the forest metric can be predicted from the proportion of ground returns (P0) and alternating relatively uncorrelated 3-m incremental bins above the ground beginning with P2 (3-6 m). The

third model excludes the ground returns but includes alternating bins beginning with short understory P1 to P9. The fourth model expresses a composite of understory to overstory computed from PCA variables and a separate parameter accommodating the mid-story. Model 5 is Model 4 but also includes the third PCA variable which deems the amount of ground returns (i.e., total canopy closure) is relevant. Models 6-8 are analogous to models 2-4 except “compete” with them by using the proportion of ground returns as a base in all definitions of the explanatory variables and linear combinations of them computed from the PCA.

Statistical analysis and modeling

We used univariate multiple regression techniques (Neter et al. 1996) to model the relationship between the forest stand metrics and LiDAR-derived explanatory variables. We modeled each of the 20 response variables separately and log-transformed if necessary to reduce influences of extreme values. An information-theoretic model selection process (Burnham and Anderson 2002) was used to obtain evidence for which of the eight plausible models best described variation in forest stand metrics. We used ΔAIC_C and Akaike’s weights (ω_i) to judge model adequacy among competing models. To increase sample size for modeling purposes, we combined the two data sets from IP (n = 30 plots) and MH (n = 39 plots) which should be reasonable since the forests at the two sites are structurally similar. Even after combining plots from both sites, we did not have enough to adequately split the data sets into training and test data sets and still have adequate coverage in structural heterogeneity within the forests (Snee 1977). Therefore, we assessed the “best” model(s) fit with two statistics: adjusted R^2 and adjusted PRESS R^2 , the latter a measure of “fit” by computing an adjusted R^2 by leaving one observation

out at a time (Myers et al. 2002). We also plotted observed forest metric versus LiDAR-predicted to further assess model fit for the “best” model and assess biases, if any (Piñeiro et al. 2008). We used PROC REG (SAS Institute, Inc. 2009) to fit each of the multiple regression models. We report the top three competing models for each modeled forest metric and where applicable made predictions across both study sites for each 50×50 m cell for wall-to-wall maps. If there was more than one competing model, we used Akaike’s weights (ω_i) to derive a weighted prediction but only when cumulative weights become > 0.5 .

Results

Forest Plot Metrics

We sampled and measured 1032 trees and 2247 saplings across both study sites (Table 2.7 and 2.8). Twenty seven percent of the trees were hardwoods, 58% softwoods, 14% were unknown snags. Hardwoods, softwoods, and unknown dead accounted for 39%, 54%, and 7% of the saplings respectively. The maximum height of a tree encountered was 32.0 m, one softwood at each each site. Mean heights of hardwoods tended to be higher than mean heights of softwoods at both sites for both trees and saplings. Summarizing the individual tree measurements within and then across the 50×50 m plots resulted in stem densities (stems/0.25 ha) ranging from 0 to 484 for trees and 0 to 7652 for saplings (Table 2.1). Estimated canopy closure at 2 m above the ground ranged from 0 to 86% with a median of 50%. Total volumes of trees ranged from 0 to 124.9 m³/0.25 ha and 0 to 13.5 m³/0.25 ha for saplings. All of the forest metric summaries indicated our coverage of the heterogeneity at both IP and MH was broad. Because it is currently difficult to distinguish between hardwoods and softwoods with

Table 2.7. Individual tree and sapling summary statistics from 50×50m study plots for International Paper (30 plots).

Stage ¹	Type ²	Metric ³	n ⁴	Mean	SD	Min.	Med.	Max.
T	H	DBH (cm)	107	17.7	6.3	9.7	17.1	38.1
		CH (m)	107	14.0	3.9	4.9	14.0	22.0
		GTC (m)	107	8.3	3.7	2.1	7.9	17.7
		CW (m)	107	4.3	1.7	1.0	4.0	10.4
	S	DBH (cm)	276	17.8	7.6	9.7	15.2	58.4
		CH (m)	276	11.7	4.9	2.4	11.0	32.0
		GTC (m)	276	5.6	4.6	0.3	4.6	17.7
		CW (m)	276	3.6	1.4	1.8	3.0	9.8
	X	DBH (cm)	61	16.0	5.3	9.7	14.6	36.8
		CH (m)	61	9.5	4.3	2.4	10.4	18.0
		CW (m)	61	0.0	0.0	0.0	0.0	0.0
	S	H	DBH (cm)	374	2.3	1.4	1.3	1.9
CH (m)			374	3.3	1.7	0.9	3.0	10.4
S		DBH (cm)	584	3.5	2.1	1.3	2.8	9.1
		CH (m)	584	3.0	1.7	0.9	2.7	12.2
X		DBH (cm)	58	4.3	2.2	1.3	4.4	8.9
		CH (m)	58	4.0	2.5	1.2	3.0	15.8

¹T=trees (DBH≥10cm), S=saplings (DBH<10cm).

²H=hardwood, S=softwood, X=unknown dead.

³DBH=diameter at breast height (saplings at 0.3m), CH=canopy height, GTC=ground to live canopy, CW=canopy width (full diameter at drip line).

⁴n=number of individual trees or saplings measured across all study plots.

LiDAR data alone (e.g., intensity values), and this is an active area of research (e.g., Donoghue et al. 2007, Holmgren et al. 2008), we combined individual tree and sapling metrics across hardwoods and softwoods since our main objective was structure and not composition.

Pair-wise correlations among individual tree and sapling metrics were strong at both IP and MH, especially among DBH, GTC, and CH, as would be expected (Table 2.9). CW was only weakly correlated with other metrics. Pairwise correlations among the forest plot metrics when summarized across individual tree and sapling

Table 2.8. Individual tree and sapling summary statistics from 50×50m study plots for Moosehorn National Wildlife Refuge (39 plots).

Stage ¹	Type ²	Metric ³	n ⁴	Mean	SD	Min.	Med.	Max.
T	H	DBH (cm)	173	15.9	6.7	9.7	14.0	51.3
		CH (m)	173	13.5	3.7	4.9	13.7	27.1
		GTC (m)	173	8.3	3.3	2.1	7.9	15.8
		CW (m)	173	4.1	1.3	0.0	4.0	9.1
	S	DBH (cm)	332	17.5	10.5	9.7	14.0	88.9
		CH (m)	332	11.9	4.8	3.0	11.0	32.0
		GTC (m)	332	5.9	3.8	0.3	5.5	21.3
		CW (m)	332	4.3	1.6	1.2	4.0	9.8
	X	DBH (cm)	83	14.9	7.0	9.7	14.0	66.0
		CH (m)	83	7.8	3.8	1.5	6.4	18.6
		CW (m)	83	0.1	0.5	0.0	0.0	4.9
	S	H	DBH (cm)	496	3.4	2.0	0.6	2.8
CH (m)			496	4.1	2.3	0.9	3.7	14.0
S		DBH (cm)	633	3.6	1.9	1.3	3.3	8.9
		CH (m)	633	3.2	1.9	0.9	2.7	13.7
X		DBH (cm)	102	4.6	2.1	1.3	3.9	9.1
		CH (m)	102	4.4	2.3	1.2	4.0	12.8

¹T=trees (DBH≥10cm), S=saplings (DBH<10cm).

²H=hardwood, S=softwood, X=unknown dead.

³DBH=diameter at breast height (saplings at 0.3m), CH=canopy height, GTC=ground to live canopy, CW=canopy width (full diameter at drip line).

⁴n=number of individual trees or saplings measured across all study plots.

measurements within plots were also strong, including stem densities (Table 2.10.a).

However, and somewhat surprisingly, pairwise correlations between sapling and tree metrics were not strong across study plots, albeit the correlations were in the expected direction (Table 2.10.b). This indicates knowing the overstory structure as represented by trees does not ensure knowing the understory as represented by saplings, hence providing a strong justification to develop models separately for trees and saplings.

Table 2.9. Pair-wise correlations among individual tree and sapling measurements from 50×50m study plots for International Paper (IP, 30 plots) and Moosehorn National Wildlife Refuge (MH, 39 plots).

Stage ¹	Type ²	Metric	IP Metric (m)			MH Metric (m)				
			n ³	CH	GTC	CW	n ³	CH	GTC	CW
T	H	DBH (cm)	107	0.80	0.64	0.53	173	0.67	0.63	0.45
		CH (m)			0.83	0.41			0.80	0.41
		GTC (m)				0.24				0.33
	S	DBH (cm)	276	0.82	0.60	0.66	332	0.84	0.56	0.61
		CH (m)			0.82	0.45			0.81	0.45
		GTC (m)				0.20				0.14
	X	DBH (m)	61	-0.07			83	0.21		
S	H	DBH (cm)	374	0.85			496	0.84		
	S	DBH (cm)	584	0.90			633	0.84		
	X	DBH (m)	58	0.71			102	0.57		

¹T=trees (DBH≥10cm), S=saplings (DBH<10cm).

²H=hardwood, S=softwood, X=unknown dead.

³n=number of individual trees or saplings measured across all study plots.

⁴DBH=diameter at breast height (saplings at 0.3m), CH=canopy height, GTC=ground to live canopy, CW=canopy width (full diameter at drip line).

Modeling

Tree models selected and their predictive ability varied little for each response variable, most likely because of the strong correlations among the tree metrics (Table 2.11). Model 6 surfaced as the the “best” model for 10 of 12 response variables for tree metrics, all having Akaike weights (ω_i) > 0.55, with 8 of the 10 having weights > 0.8 (Table 2.11). Examination of adjusted R^2 , adjusted PRESS R^2 , and bivariate plots of the observed metric with the LiDAR-predicted metric (Figs. 2.9.a-2.9.c) show strong predictive ability for 10 of the 12 forest metrics (all having adjusted R^2 > 0.6). The other two of the 12 forest metrics, Y2 (mean DBH) and Y3 (mean BA), still indicate the models were able to explain 42% of the variation in these metrics. These models would

Table 2.10.a. Pair-wise correlations among forest metrics (n=69 plots, n=68 for correlations with Y20).

Stage	FM ¹	Forest Metric (FM ¹)											
		Y2	Y3	Y4	Y5	Y6	Y7	Y8	Y9	Y10	Y11	Y12	Y13
Trees	Y1	0.43	0.27	0.56	0.33	0.81	0.66	0.64	0.64	0.62	0.71	0.62	0.72
	Y2		0.88	0.87	0.78	0.61	0.59	0.73	0.81	0.70	0.72	0.67	0.48
	Y3			0.63	0.90	0.59	0.64	0.61	0.65	0.62	0.58	0.55	0.33
	Y4				0.68	0.66	0.63	0.89	0.90	0.76	0.83	0.74	0.69
	Y5					0.73	0.82	0.67	0.74	0.71	0.62	0.56	0.43
	Y6						0.96	0.74	0.79	0.78	0.76	0.67	0.69
	Y7							0.70	0.78	0.77	0.69	0.61	0.60
	Y8								0.86	0.78	0.91	0.78	0.71
	Y9									0.92	0.90	0.83	0.68
	Y10										0.86	0.89	0.62
	Y11											0.93	0.68
	Y12												0.62
Saplings	Y14												
	Y15												
	Y16												
	Y17												
	Y18												
	Y19												
	Y20												

¹FM=forest metric, see Table 2.1 for description of each forest metric variable, bolded correlations indicated those where $r \geq 0.50$.

Table 2.10.b. Pair-wise correlations among tree forest metrics with sapling forest metrics (n=69 plots).

FM	Forest Metric (FM ¹)												
	Y1	Y2	Y3	Y4	Y5	Y6	Y7	Y8	Y9	Y10	Y11	Y12	Y13
Y14	-0.31	-0.22	-0.24	-0.22	-0.33	-0.39	-0.37	-0.32	-0.20	-0.17	-0.24	-0.11	-0.17
Y15	0.36	-0.04	-0.18	0.11	-0.14	0.19	0.13	0.13	0.12	0.14	0.16	0.16	0.39
Y16	0.36	0.03	-0.10	0.16	-0.07	0.20	0.14	0.19	0.15	0.17	0.19	0.16	0.39
Y17	0.28	-0.11	-0.25	0.12	-0.22	0.07	0.02	0.13	0.06	0.05	0.12	0.11	0.44
Y18	0.37	0.05	-0.08	0.23	-0.04	0.21	0.16	0.29	0.18	0.16	0.23	0.16	0.44
Y19	-0.13	-0.18	-0.29	-0.10	-0.32	-0.30	-0.32	-0.25	-0.11	-0.10	-0.16	-0.01	0.10
Y20	-0.07	-0.16	-0.28	-0.03	-0.30	-0.26	-0.28	-0.17	-0.06	-0.08	-0.11	0.01	0.22

¹FM=forest metric, see Table 2.1 for description of each forest metric variable, bolded correlations indicated those where $r \geq 0.50$.

Table 2.11. Modeling results for trees (n=69 plots).¹

Model No.	k	RSS	AIC _C	ΔAIC _C	ω _i	Adj. R ²	Adj. PRESS
Y1=log[Stem density (stems/0.25ha)+1.0]:							
6	5	77.47	18.94	0.00	0.99	0.72	0.69
4	4	102.06	35.63	16.70	<0.01	0.64	0.61
5	5	99.95	36.52	17.58	<0.01	0.64	0.60
Y2=Mean DBH (cm):							
6	5	1722.28	232.95	0.00	0.57	0.42	0.32
8	4	1810.78	234.08	1.13	0.32	0.40	0.32
7	5	1818.46	236.70	3.75	0.09	0.38	0.29
Y3=log[Mean basal area (cm ²)+1.0]:							
6	5	126.77	52.92	0.00	0.95	0.42	0.33
8	4	144.85	59.80	6.88	0.03	0.35	0.26
7	5	142.19	60.84	7.92	0.02	0.35	0.25
Y4=Mean canopy height (m):							
6	5	496.54	147.13	0.00	0.93	0.66	0.60
8	4	556.55	152.67	5.55	0.06	0.62	0.58
7	5	567.06	156.29	9.16	0.01	0.61	0.55
Y5=Mean volume (m ³):							
2	8	0.354	-345.4	0.00	0.99	0.62	0.37
4	4	0.484	-333.64	11.76	<0.01	0.51	0.42
5	5	0.481	-331.68	13.72	<0.01	0.51	0.30
Y6=log[Total basal area (m ² /0.25 ha)+1.0]:							
6	5	12.52	-106.78	0.00	0.83	0.78	0.76
8	4	13.66	-103.12	3.68	0.13	0.77	0.75
7	5	13.68	-100.72	6.08	0.04	0.76	0.74
Y7=log[Total volume (m ³ /0.25 ha)+1.0]:							
6	5	29.91	-46.73	0.00	0.85	0.82	0.80
8	4	32.60	-43.12	3.61	0.14	0.81	0.79
7	5	33.81	-38.28	8.45	0.01	0.80	0.77
Y8=Ground to live canopy (m):							
6	5	215.21	89.44	0.00	0.55	0.76	0.72
3	7	201.31	89.72	0.28	0.36	0.77	0.72
8	4	228.98	91.39	1.95	0.15	0.75	0.72

Table 2.11. Continued.¹

Model No.	k	RSS	AIC _C	ΔAIC _C	ω _i	Adj. R ²	Adj. PRESS
Y9=Max. CH (m):							
8	4	1223.07	207.00	0.00	0.89	0.74	0.72
6	5	1258.97	211.32	4.32	0.10	0.73	0.70
7	5	1350.73	216.18	9.18	0.01	0.71	0.68
Y10=SD CH (m):							
6	5	80.56	21.64	0.00	0.86	0.70	0.66
8	4	87.81	25.26	3.62	0.14	0.68	0.65
7	5	94.01	32.30	10.66	<0.01	0.65	0.61
Y11=Max. GTC (m):							
6	5	565.66	156.12	0.00	0.99	0.79	0.76
7	5	645.27	165.21	9.09	0.01	0.75	0.73
8	4	720.66	170.50	14.38	<0.01	0.73	0.71
Y12=SD Ground to live canopy (m):							
6	5	46.76	-15.89	0.00	0.99	0.68	0.65
8	4	58.88	-2.32	13.58	<0.01	0.61	0.57
7	5	57.39	-1.76	14.13	<0.01	0.61	0.57

¹See Table 2.6 for plausible models; k=number of parameters, RSS=regression residual sums-of-squares, AIC_C=Akaike's Information Criteria corrected for small sample sizes, ΔAIC_C=difference from minimum AIC_C, ω_i=Akaike's model weight; see Table 2.1 for descriptions of response variables.

be improved if two obvious outliers for Y2, which were from plots with few but large diameter trees, and from plots with no trees (i.e., mean DBH = 0) were removed (Fig. 2.9.a). However, we were reluctant to do this as it would be difficult to distinguish these plots with LiDAR flown at the 2 m nominal post-spacing. Examination of the model parameter estimates and their directions reveal that the tree metrics are generally negatively related to those explanatory variables utilizing ground or near-ground LiDAR returns (Table 2.12). Explanatory variables with more LiDAR returns at higher canopy heights (i.e., > 6 m) tended to be positively associated with each tree metric. Total canopy closure > 2 m (Y13) had Model 5 as the “best” model among candidate models with Model 3 being recognized as a reasonable candidate model

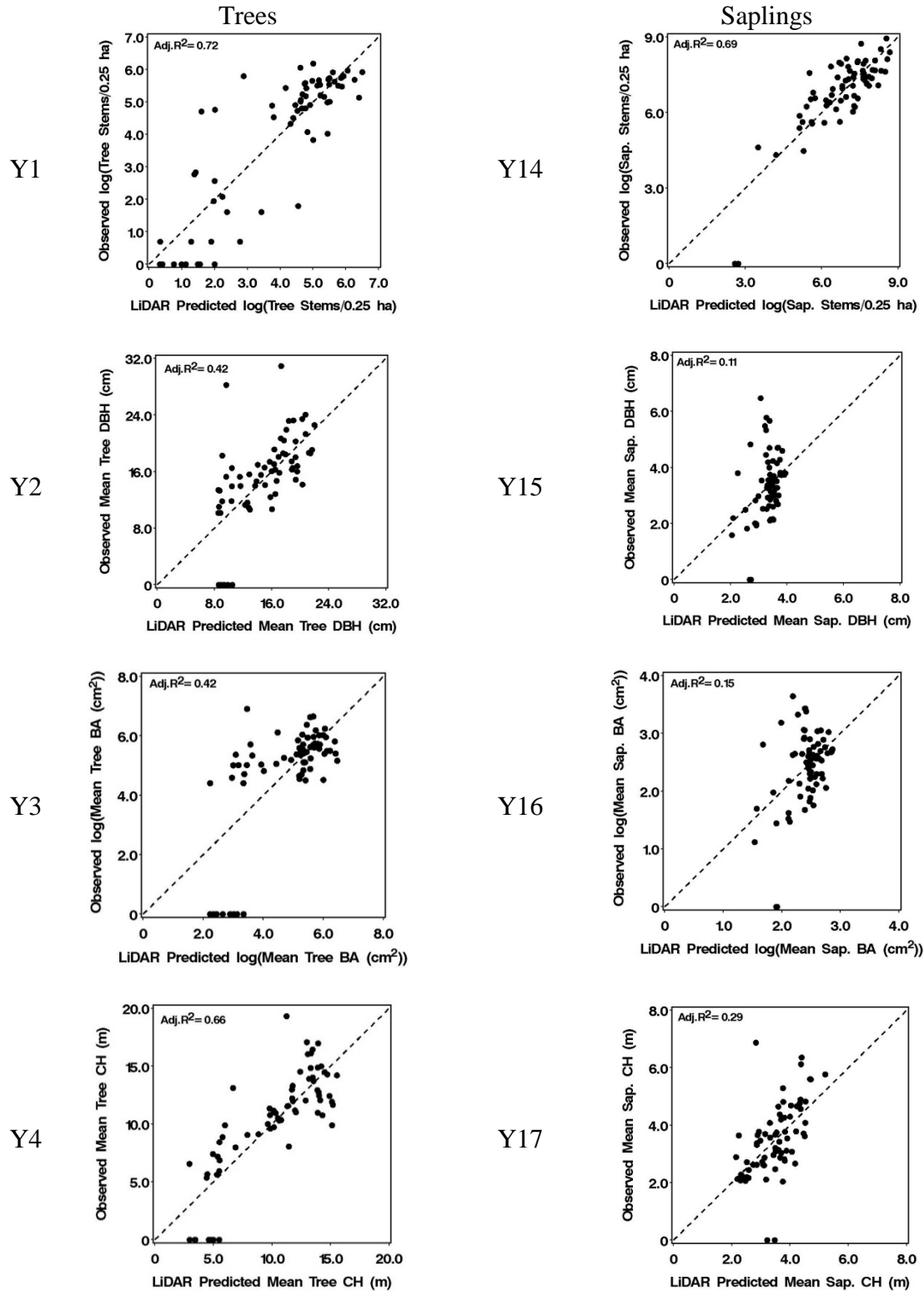


Figure 2.9.a. Relationship between observed forest metrics and LiDAR predicted forest metrics; dashed line represents 1:1 correspondence; Y1-Y4 and Y14-Y17 are defined in Table 2.1.

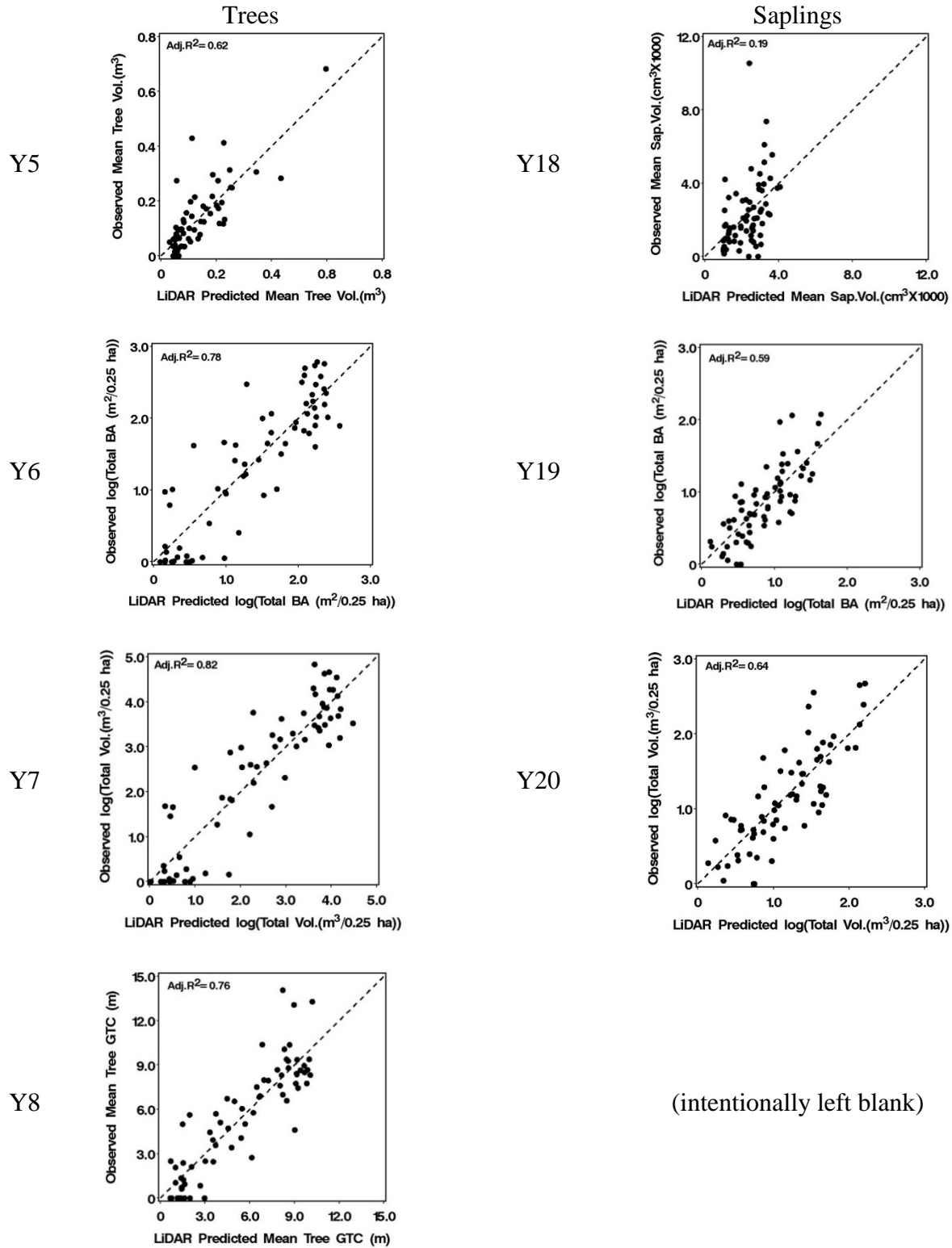


Figure 2.9.b. Relationship between observed forest metrics and LiDAR predicted forest metrics; dashed line represents 1:1 correspondence; Y6-Y8 and Y18-Y20 are defined in Table 2.1.

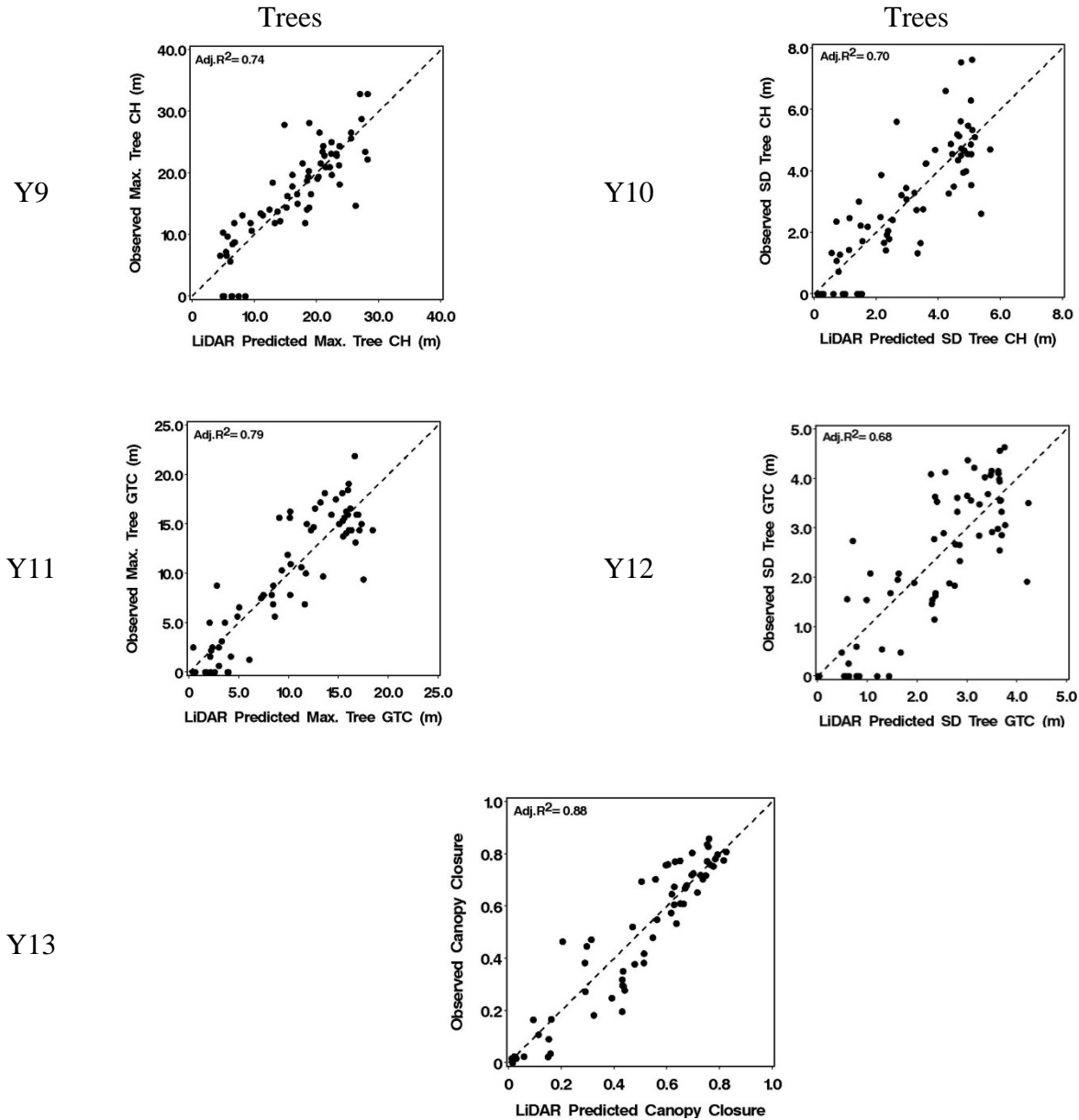


Figure 2.9.c. Relationship between observed forest metrics and LiDAR predicted forest metrics; dashed line represents 1:1 correspondence; Y9-Y13 are defined in Table 2.1.

as well, both models accounting for > 82% of the variation (Table 2.12, Fig. 2.9.c). As a measure of model validation, adjusted PRESS R² values indicate all models do at least a reasonable job of predicting forest metrics on 50×50 m plots with some doing what would be considered exceptional (i.e., adjusted PRESS R² > 0.75).

Models selected for saplings varied a great deal as did their predictive ability (Table 2.13). Models for Y14 (stem density) and Y20 (total volume) all had a single model surface as “best” (with Akaike weights > 0.97 , adjusted R^2 and PRESS $R^2 \geq 0.59$). Mean sapling height (Y17) and total basal area (Y19) had reasonably good models as well implying both these metrics are predictable from LiDAR. These results can be visualized in the right columns of Figs. 2.9.a and 2.9.b. Although mean DBH (Y15), mean BA (Y16), and mean volume (Y18) of saplings did not have any models that were selected and had good predictive ability based on adjusted R^2 , by being able to predict total sapling volume, total sapling BA, and sapling stem densities reasonably well, and taking advantage of the strong correlations among these variables (Table 2.10.a), we can back-compute estimates of these metrics using the following relationships (first converting all units to meters as necessary):

$$\text{Predicted Y18} = \left(\frac{\text{Predicted Total Volume}}{\text{Predicted Stem Density}} \right)$$

$$\text{Predicted Y16} = \left(\frac{\text{Predicted Total BA}}{\text{Predicted Stem Density}} \right)$$

$$\text{Predicted Y15} = 2 \times \sqrt{\frac{\text{Predicted Mean BA}}{\pi}}$$

Correlating these back-predicted predicted estimates with the field estimated metrics, and excluding the two obvious outliers with density estimates (Y14) of 0.0 in Fig. 2.9.a. we found reasonable correlations of $r=0.43$, 0.38 , and 0.48 for back-estimated mean volume (Y18), mean BA (Y16), and mean DBH (Y15) respectively for saplings. Therefore, although we were not able to model these three sapling metrics directly, reasonable estimates can be back-computed from others that can be modeled. As with tree metric models, parameter estimates are generally

Table 2.12. Model parameter estimates for tree metrics for selected model(s) based on results from Table 2.11.¹

Model		
No.	ω_i	Model (parameter estimate SE are in “()” below parameters)
Y1=log[Stem density (stems/0.25ha)+1.0]:		
6	0.99	Y1=5.91 - 0.18(X1) + 0.53(X3) + 0.34(X6) (0.23) (0.11) (0.08) (0.07)
Y2=Mean tree DBH (cm):		
6	0.42	Y2=19.45 - 0.90(X1) + 0.79(X3) + 1.27(X6) (1.96) (0.51) (0.40) (0.31)
8	0.32	Y2=14.71 + 1.50(P1N1X) - 1.55(P1N2X) (0.63) (0.25) (0.48)
Y3=log[Mean tree basal area (cm ²)+1.0]:		
6	0.95	Y3=6.05 - 0.17(X1) + 0.40(X3) + 0.21(X6) (0.29) (0.14) (0.10) (0.08)
Y4=Mean tree canopy height (m):		
6	0.93	Y4=14.34 - 0.64(X1) + 0.82(X3) + 1.01(X6) (0.57) (0.27) (0.20) (0.16)
Y5=Mean tree volume (m ³):		
2	0.99	Y5=0.09 - 0.05(P0) - 0.10(P2) + 0.10(P4) + 0.67(P6) + 0.58(P8) + (0.08) (0.10) (0.18) (0.17) (0.21) (0.90) 54.42(P10) (9.01)
Y6=log[Total basal area (m ² /0.25 ha)+1.0]:		
6	0.83	Y6=2.31 - 0.06(X1) + 0.08(X3) + 0.29(X6) (0.09) (0.04) (0.03) (0.03)
Y7=log[Total volume (m ³ /0.25 ha)+1.0]:		
6	0.82	Y7=4.01 - 0.14(X1) + 0.15(X3) + 0.49(X6) (0.14) (0.07) (0.05) (0.04)
Y8=Ground to live canopy (m):		
6	0.55	Y8=8.92 - 0.70(X1) + 0.26(X3) + 1.10(X6) (0.38) (0.18) (0.13) (0.11)
3	0.36	Y8=1.77 - 0.24(P1) + 9.56(P3) + 24.71(P5) + 49.72(P7) -175.04(P9) (0.79) (2.21) (2.50) (3.43) (9.00) (67.94)

Table 2.12. Continued.¹

Model			
No.	ω_i	Model (parameter estimate SE's are in "()" below parameters)	
Y9=Max. CH (m):			
8	0.89	Y9=15.83 + 2.69(PRIN1X) – 2.09(PRIN2X)	
		(0.52) (0.21)	(0.39)
Y10=SD CH (m):			
6	0.86	Y10=5.14 + 0.02(X1) + 0.11(X3) + 0.62(X6)	
		(0.23) (0.11)	(0.08) (0.07)
Y11=Max. GTC (m):			
6	0.99	Y11=16.64 – 0.54(X1) + 0.72(X3) + 1.82(X6)	
		(0.61) (0.29)	(0.21) (0.18)
Y12=SD GTC (m):			
6	0.99	Y12=3.87 + 0.05(X1) + 0.20(X3) + 0.37(X6)	
		(0.17) (0.08)	(0.06) (0.37)
Y13=Canopy Closure > 2m (%):			
5	0.63	Y13=0.45 + 0.10(PRIN1P) – 0.11(PRIN2P) + 0.04(PRIN3P)	
		(0.02) (0.01)	(0.01) (0.01)

¹See Table 2.6 for plausible models; ω_i =Akaike's model weight.

in the direction one would expect. For example, increasing amount of total sapling densities (Y14) and volume (Y20) are related positively with increase LiDAR returns in 0-6 meters above ground (Table 2.14). Also as a validation of models based on adjusted PRESS R^2 , models Y14 (sapling densities), Y19 (sapling total BA), and Y20 (total sapling volume), LiDAR does a good job of predicting these metrics (Table 2.12).

Figures 2.10.a and 2.10.b present the results of applying the empirical models for three tree metrics (Y1, Y4, and Y7) and their equivalent sapling metrics (Y14, Y17, and Y20) across the entire study site of 30,720 50×50 m cells for IP and 41,396 50×50 m cells for MH respectively (less water and bog classified cells). These maps represent not only the current status inventories of the 20 forest stand metrics, but also photo interpreters can now use these

Table 2.13. Modeling results for saplings (n=69 plots).¹

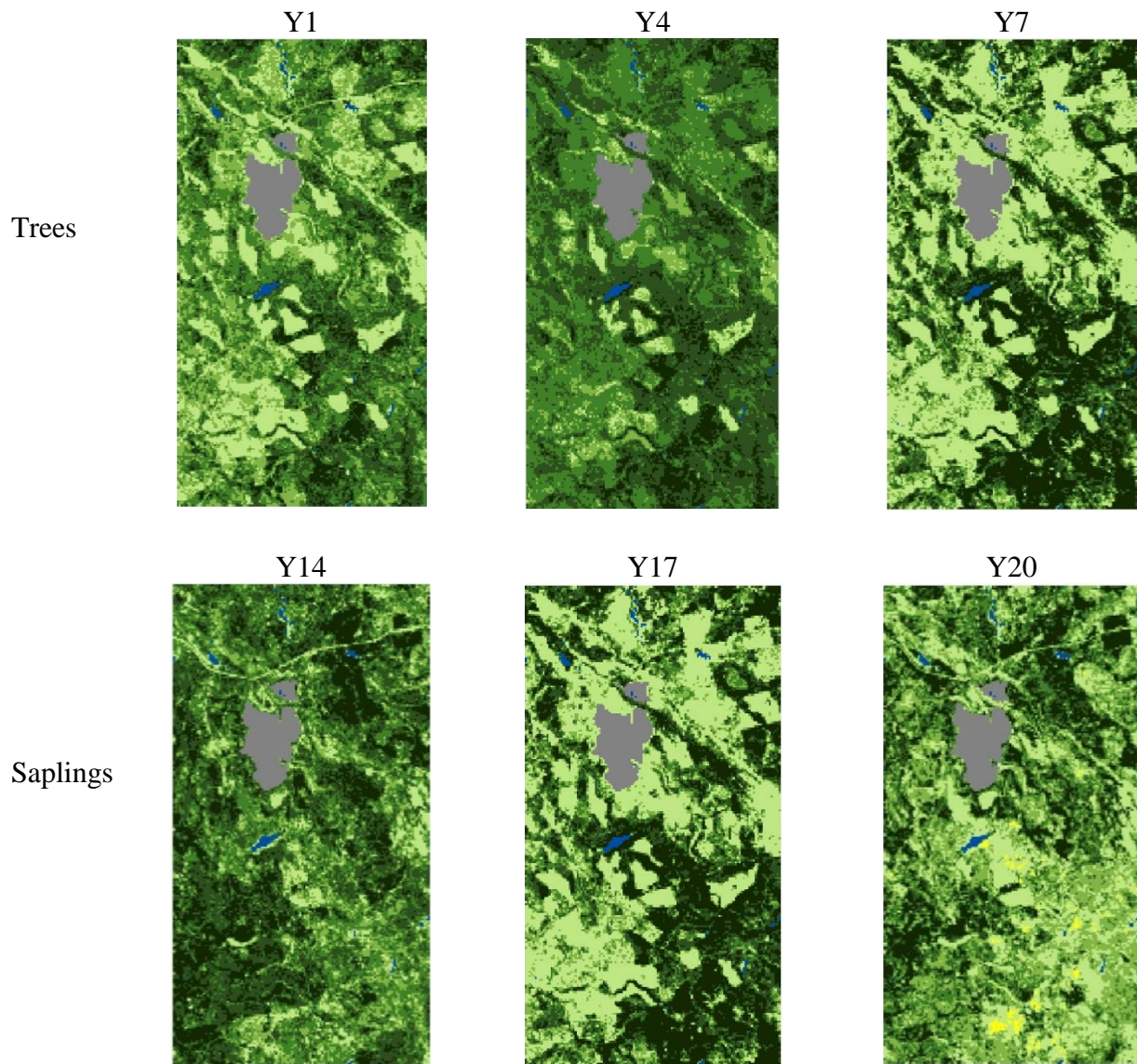
Model						Adj.	Adj.
No.	k	RSS	AIC _C	ΔAIC _C	ω _i	R ²	PRESS
Y14=log[Stem density (stems/0.25ha)+1.0]:							
6	5	47.91	-14.22	0.00	0.99	0.69	0.61
8	4	75.34	14.69	28.90	<0.01	0.52	0.44
3	8	89.07	36.02	50.23	<0.01	0.39	0.24
Y15=Mean DBH (cm):							
4	4	79.92	18.76	0.00	0.44	0.11	0.04
5	5	79.32	20.57	1.81	0.18	0.10	<0.01
7	5	80.56	21.64	2.87	0.10	0.08	<0.01
Y16=log[Mean basal area (cm ²)+1.0]:							
7	5	24.64	-60.09	0.00	0.52	0.15	0.02
8	4	26.02	-58.66	1.43	0.25	0.12	<0.01
4	4	27.13	-55.78	4.31	0.06	0.08	0.02
Y17=Mean canopy height (m):							
5	5	76.03	17.65	0.00	0.65	0.29	0.20
4	4	81.31	19.95	2.31	0.20	0.25	0.19
2	8	73.40	22.66	5.01	0.05	0.28	0.06
Y18=Mean volume (cm ³):							
4	4	185490659	1030.13	0.00	0.46	0.19	0.12
5	5	183123024	1031.57	1.44	0.22	0.19	0.08
2	8	167275797	1032.77	2.64	0.12	0.22	<0.01
Y19=log[Total basal area (m ² /0.25 ha)+1.0]:							
5	5	82.01	-153.07	0.00	0.65	0.59	0.54
8	4	6.84	-150.8	2.24	0.21	0.57	0.54
6	5	6.81	-148.82	4.25	0.08	0.57	0.52
Y20=log[Total volume (m ³ /0.25 ha)+1.0]:							
5	5	10.05	-121.96	0.00	0.97	0.64	0.59
2	8	10.18	-113.65	8.31	0.02	0.62	0.52
6	5	11.70	-11.47	10.48	0.01	0.58	0.53

¹See Table 2.6 for plausible models; k=number of parameters, RSS=regression residual sums-of-squares, AIC_C=Akaike's Information Criteria corrected for small sample sizes, ΔAIC_C=difference from minimum AIC_C, ω_i=Akaike's model weight.

Table 2.14. Model parameter estimates for sapling metrics for selected model(s) based on results from Table 2.12.

Model			
No. ¹	ω_i	Model (parameter estimate SE are in “()” below parameters)	
Y14=log[Stem density (stems/0.25ha)+1.0]:			
6	0.99	Y14=7.20 + 0.99(X1) – 0.05(X3) – 0.08(X6)	
		(0.18) (0.08) (0.06) (0.05)	
Y15=Mean DBH (cm):			
4	0.44	Y15=3.34 + 0.08(PRIN1P) – 0.26(PRIN2P)	
		(0.13) (0.07) (0.09)	
5	0.18	Y15=3.34 + 0.08(PRIN1P) – 0.26(PRIN2P) + 0.07(PRIN3P)	
		(0.13) (0.07) (0.09) (0.1)	
7	0.10	Y15=3.78 + 0.21(X2) – 0.01(X5) + 0.04(X8)	
		(0.52) (0.08) (0.07) (0.13)	
Y16=log[Mean basal area (cm ²)+1.0]:			
7	0.52	Y16=2.84 + 0.15(X2) – 0.02(X5) + 0.06(X8)	
		(0.29) (0.05) (0.04) (0.07)	
8	0.25	Y16=2.41 + 0.08(PRIN1X) + 0.10(PRIN2X)	
		(0.08) (0.03) (0.06)	
Y17=Mean canopy height (m):			
5	0.65	Y17=3.50 + 0.02(PRIN1P) – 0.44(PRIN2P) + 0.21(PRIN3P)	
		(0.13) (0.06) (0.09) (0.10)	
Y18=Mean volume (cm ³):			
4	0.46	Y18=2285.1 + 197.3(PRIN1P) – 499.0(PRIN2P)	
		(201.8) (100.0) (134.4)	
5	0.22	Y18=2285.1 + 197.3(PRIN1P) – 499.0(PRIN2P) – 140.0(PRIN3P)	
		(202.1) (100.1) (134.6) (152.7)	
Y19=log[Total basal area (m ² /0.25 ha)+1.0]:			
5	0.65	Y19=0.86 – 0.10(PRIN1P) – 0.12(PRIN2P) + 0.20(PRIN3P)	
		(0.04) (0.02) (0.03) (0.03)	
Y20=log[Total volume (m ³ /0.25 ha)+1.0]:			
5	0.97	Y20=1.16 – 0.11 (PRIN1P) – 0.22(PRIN2P) + 0.26(PRIN3P)	
		(0.05) (0.02) (0.03) (0.04)	

¹See Table 2.6 for plausible models; ω_i =Akaike’s model weight.








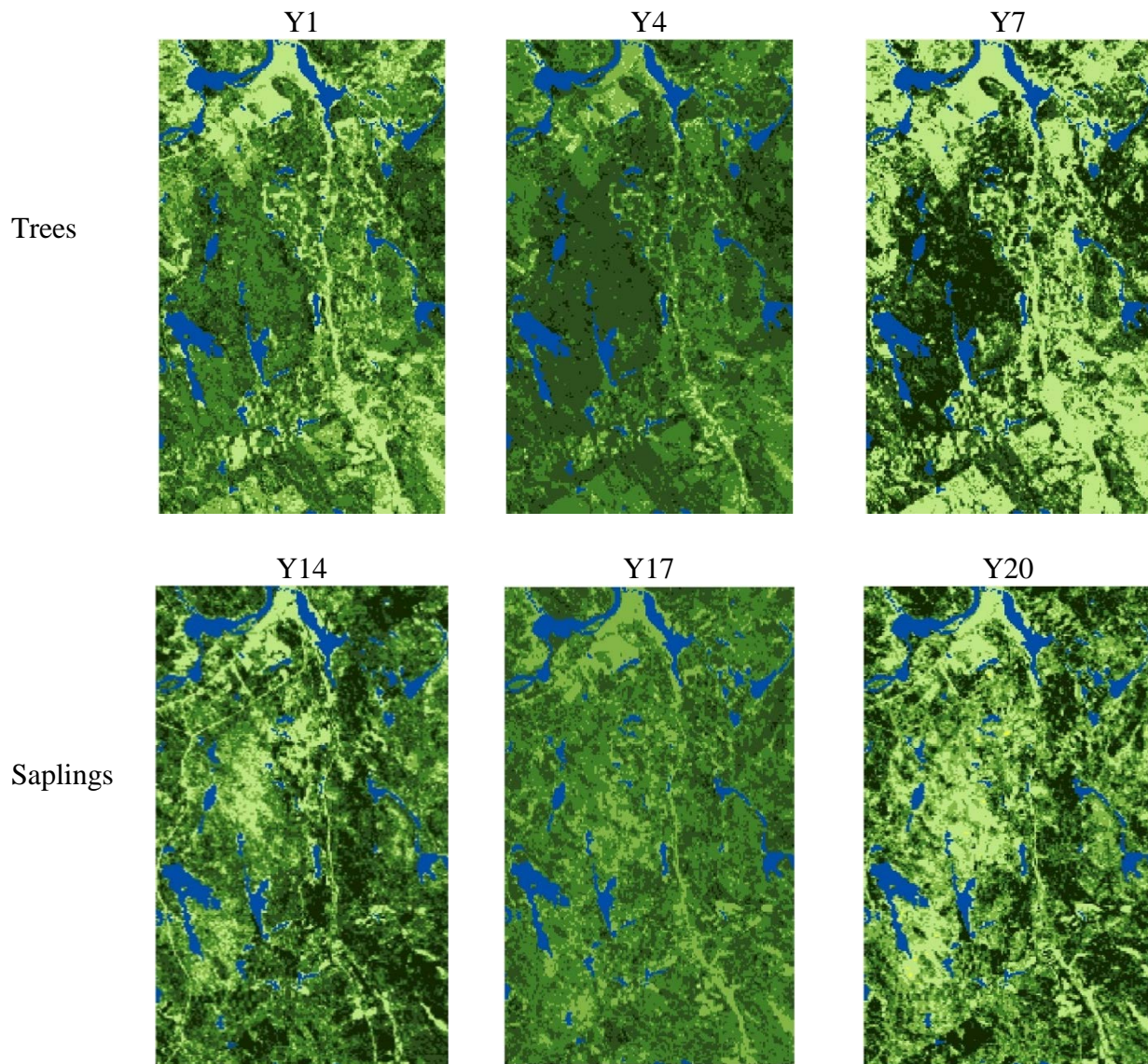
	Y1	Y4	Y7	Y14	Y17	Y20
	0-25	0-3	0-10	0-250	0-1.5	0-1
	25-100	3-6	10-20	250-500	1.5-3.0	1-2
	100-250	6-12	20-30	500-1000	3.0-4.0	2-3
	250-500	12-15	30-50	1000-2000	4.0-5.0	3-4
	500+	15+	50+	2000+	5.0+	4+

Figure 2.10.a. Predicted maps for stem densities (Y1, 14), mean canopy heights (Y4, Y17) and total volumes (Y7, Y20) at International Paper (blue=water, gray=sphagnum bog); see Table 2.1 for definitions of Y1, Y4, Y7, Y14, Y17, and Y20.








	Y1	Y4	Y7	Y14	Y17	Y20
	0-25	0-3	0-10	0-250	0-1.5	0-1
	25-100	3-6	10-20	250-500	1.5-3.0	1-2
	100-250	6-12	20-30	500-1000	3.0-4.0	2-3
	250-500	12-15	30-50	1000-2000	4.0-5.0	3-4
	500+	15+	50+	2000+	5.0+	4+

Figure 2.10.b. Predicted maps for stem densities (Y1, 14), mean canopy heights (Y4, Y17) and total volumes (Y7, Y20) at Moosehorn National Wildlife Refuge (blue=water, gray=bog); see Table 2.1 for definitions of Y1, Y4, Y7, Y14, Y17, and Y20.

maps to assist with better classifying the point-intercepts at the center of 50×50 m cells as needed by ECOSEARCH.

Discussion

Although the LiDAR that was acquired in 2003 for this study at the nominal post-spacing of 2 m which is considered by today's standard "low-density" (Jones et al. 2009), this post-spacing was more than adequate to empirically model forest-stand metrics collected in the field with LiDAR-derived explanatory variables, at least at the scale of 50×50 m plots. Not only were we able to model and predict most overstory (i.e., tree) metrics adequately, but as importantly for using ECOSEARCH, we were able to reliably model understory (i.e., saplings) densities (Y14), total basal area (Y17), total volume (Y20), and able to back-compute adequately mean sapling DBH (Y15), mean sapling volume (Y18) and mean sapling basal area (Y16). LiDAR systems currently are acquiring post-spacing at approximately 1.4 m, or even at 0.7 m, which may not be necessary in forests unless individual trees and crown mappings are desired, which currently, is not necessary for ECOSEARCH, but should not be discounted in future versions.

As is evidenced in Figs. 2.9.a – 2.9.c, improvement in modeling could be made if outliers for some of the metrics (i.e., Y2, Y3, and Y4 for trees and Y14, Y16, and Y17 for saplings) could be accommodated, but not removed. Although we used univariate multiple linear regression methods for the modeling effort, assuming a normal or at least log-normal distribution, there exists a plethora if not dizzying array of other modeling methods that could be explored and used to improve the models (e.g., generalized additive models – Guisan et al. 2006, machine learning methods – Fielding 1999, segmented or piecewise regression – Toms and Lesperance 2003, see also those described in Franklin 2009). Also, given the "rich" quantity of data provided by LiDAR there are many ways to define various LiDAR-derived explanatory

variables (e.g., Hall et al. 2005). However, all of these additional potential explanatory variables will most likely be highly correlated. This multicollinearity problem would still need to be dealt with and deciding which LiDAR-derived variables to use, which to ignore, and how to summarize is not trivial (Elith and Leathwick 2009).

Intensity values that accompany each LiDAR return can provide gray-scale images that also can be used to assist with interpreting habitat structure for ECOSEARCH (Figs. 2.6.a and 2.6.b). Actually, being able to distinguish returns (i.e., “hits”) from hardwood from softwood returns is an active area of research using intensity values (e.g., Kim et al. 2008). If intensity values are found useful, this could eliminate the need to use color infrared digital imagery for ECOSEARCH. Another option to explore is quantifying the percentage of LiDAR canopy “hits” within each 50×50 m cell using a digitized and georectified color infrared image (or QuickBird imagery). These “hits” could then be used to separate the vertical profiles into those striking hardwoods and softwoods, at least for the overstory canopy. These could then be further binned, tallied, and used as refined explanatory variables in the regression modeling, and possibly allow density and volume estimates, say, to be separated into the two tree types. This process is illustrated in Fig. 2.11 for three different mixtures of tree types with a 50×50 m stand or plot showing the vertical profile bins for both combined, and separated into hardwoods only and softwoods only. Predicting the understory species composition will be complicated, if it can be done at all, and most likely need to be model-based (e.g., MacKenzie et al. 2009).

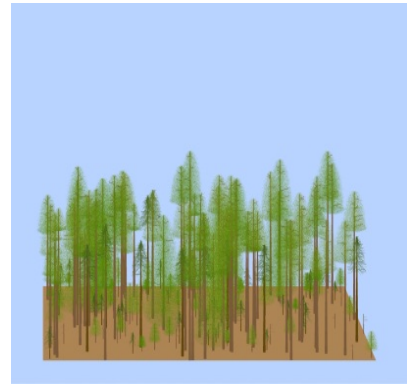
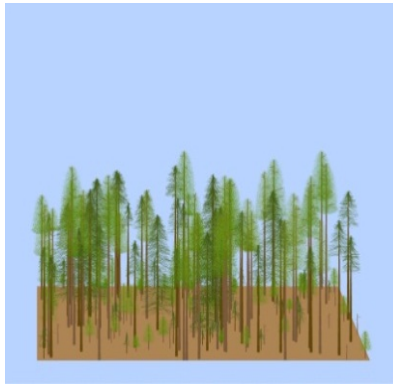
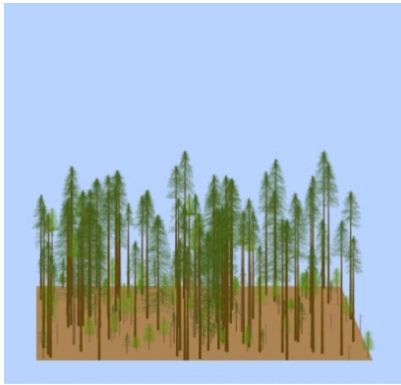
Although not a part of this effort (i.e., to actually use ECOSEARCH), the results of acquiring LiDAR for an area and this modeling effort can be used to assist with interpreting images for the habitat structure component required by ECOSEARCH. Simultaneously, the wall-to-wall predictions for various forest stand metrics also should be useful to not only for

Trees Hardwood:Softwood Proportion

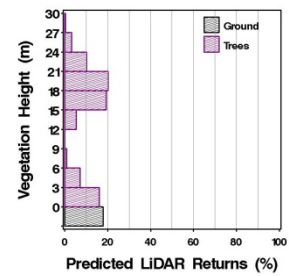
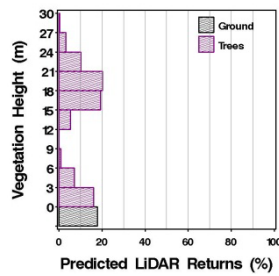
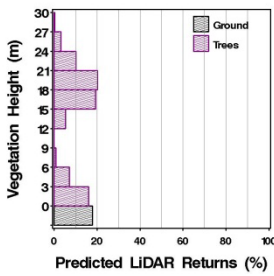
10:90

50:50

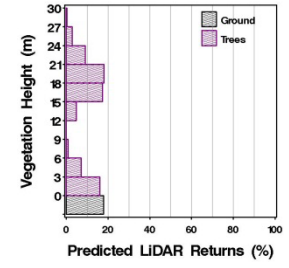
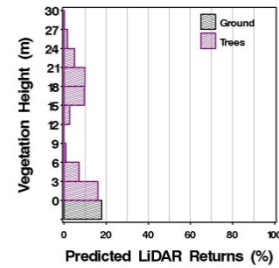
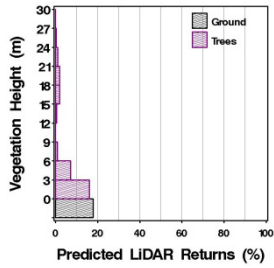
90:10



Combined Vert. Profile



Hardwood Only



Softwood Only

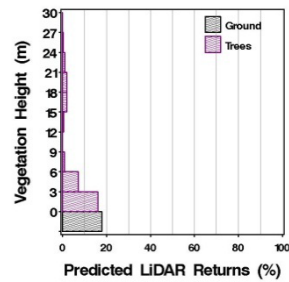
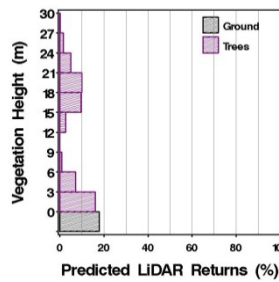
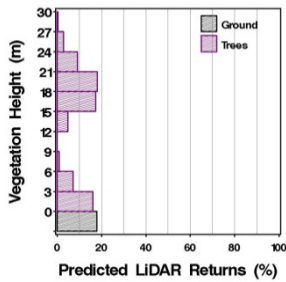


Figure 2.11. Example associations of binning LiDAR when individual tree type is known or proportion of hardwoods:softwoods is estimated from fusion of LiDAR with image-classified and geo-rectified data (e.g., Quickbird imagery at 2.4 m pixels across a 50 m pixel); top panel is 10:90, middle panel is 50:50, and bottom panel is 90:10 hardwoods:softwoods).

wildlife resource managers using ECOSEARCH but also should prove useful to foresters needing a complete inventory for several applications (e.g., fire fuel modeling, succession modeling).

Finally, we recommend that all LiDAR acquisitions should be calibrated with field data as done in this study. With the exception of two days in which a field assistant was used to record data, all field data collected here were collected by a single observer across 16 days in a single year, averaging 4-5 per study plots per day using the WQ. Although not quantified, most time was spent traversing and locating study plots. Once at the study plot, using a WQ approach took 1-2 hours to measure and quantify the trees (overstory) and the saplings (understory), which is really an insignificant amount of time considering the costs of LiDAR acquisitions. Currently, LiDAR acquisitions cost around \$200-\$500 USD per 2.6 km² (1 mi²) and depend on nominal post-spacing of LiDAR returns, acquisition area, distance to nearest staging airport, and amount of post-processing done by the vendor (e.g., ground/non-ground classification). As demonstrated in this chapter, being able to predict reasonably well both the over- and understory made the “invisible” in images “visible” with LiDAR and should improve greatly image interpretation to be used for ECOSEARCH analyses.

Literature Cited

- Aitchison, J. 1986. The statistical analysis of compositional data. Chapman and Hall, London, England.
- Anderson, H-E., J.R. Foster, and S.R. Reutebuch. 2003. Estimating forest structure parameters on Fort Lewis Military Reservation using airborne laser scanner (LIDAR) data. Pages 45-53 *In* Precision Forestry: Proceedings of the Second International Precision Forestry

- Symposium, 15-17 June 2003. Institute of Forest Resources, University of Washington, Seattle, Washington.
- Avery, T.E., and H.E. Burkhart. 2002. Forest measurements, 5th edition. McGraw-Hill, New York, New York.
- Becker, N.G. 1969. Regression problems when the predictor variables are proportions. *Journal of the Royal Statistical Society* 31:107-112.
- Brandtberg, T., T.A. Warner, R.E. Landenberger, and J.B. McGraw. 2003. Detection and analysis of individual leaf-off tree crowns in small footprint, high sampling density LiDAR data from the eastern deciduous forest in North America. *Remote Sensing of Environment* 85:290-303.
- Brower, J., J. Zar, and C. von Ende. 1989. Field and laboratory methods for general ecology, 3rd edition. Wm. C. Brown Publishers. Dubuque, Iowa.
- Burnham, K.P., and D.R. Anderson. 2002. Model selection and multi-model inference, 2nd edition. Springer-Verlag, Inc., New York, New York.
- Catana, A.J. 1963. The wandering quarter method of estimating population density. *Ecology* 44:349-360.
- Christensen, N.L., A.M. Bartuska, J.H. Brown, S. Carpenter, C. D'Antonio, R. Francis, J.F. Franklin, J.A. MacMahon, R.F. Noss, D.J. Parsons, C.H. Peterson, M.G. Turner, and R.G. Woodmansee. 1996. The report of the Ecological Society of America committee on the scientific basis for ecosystem management. *Ecological Applications* 6:665-691.
- Datta, S. 2005. Estimating the mean life time using right censored data. *Statistical Methodology* 2:65-69.

- DeGraaf, R.M., J.B. Hestbeck, and M. Yamasaki. 1998. Associations between breeding bird abundance and stand structure in White Mountains, New Hampshire and Maine, USA. *Forest Ecology and Management* 103:217-233.
- Dessecker, D.R. and D.G. McAuley. 2001. Importance of early successional habitat to Ruffed Grouse and American Woodcock. *Wildlife Society Bulletin* 29:456-465.
- Donoghue, D.N.M., P.J. Watt, N.J. Cox, and J. Wilson. 2007. Remote sensing of species mixtures in conifer plantations using lidar height and intensity data. *Remote Sensing of Environment* 110:509-522.
- Dueser, R.D., J.L. Dooley, R. Taylor, and G.J. Taylor. 1988. Habitat structure, forest composition and landscape dimensions as components of habitat suitability for the Delmarva fox squirrel. Pages 414-421 *In* Management of amphibians, reptiles, and small mammals in North America (R.C. Szaro, K.E. Severson, and D.R. Paton. Editors). USDA Forest Service Technical Report RM-166, Fort Collins, Colorado.
- Elith, J., and J. Leathwick. 2009. The contribution of species distribution modeling to conservation prioritization. Pages 70-93 *In* Spatial conservation prioritization: quantitative methods and computational tools (A. Moilanen, K.A. Wilson, and H.P. Possingham. Editors). Oxford University Press. Oxford, United Kingdom.
- Engeman, R.M., R.T. Sugihara, L.F. Pank, and W.E. Dusenberry. 1994. A comparison of plotless density estimators using Monte Carlo simulations. *Ecology* 75:1769-1779.
- Evans, D.L., S.D. Roberts, and R.C. Parker. 2006. LiDAR : a new tool for forest measurements. *Forestry Chronicle* 82:211-218.
- Falkowski, M.J., A.M.S. Smith, A.T. Hudak, P.E. Gessler, L.A. Vierling, and N.L. Crookston. 2006. Automated estimation of individual conifer tree height and crown diameter via

- two-dimensional spatial wavelet analysis of lidar data. *Canadian Journal of Remote Sensing* 32:153-161.
- Fielding, A.H. (Editor). 1999. *Machine learning methods for ecological applications*. Kluwer Academic Publishers. Norwell, Massachusetts.
- Frazer, G.W., J.A. Trofymow, and K.P. Letzman, 1997. A method for estimating canopy openness, effective leaf area index, and photosynthetically active photon flux density using hemispherical photography and computerized image analysis techniques. Information Report BC-X-373. Pacific Forestry Centre. p. 73.
- Franklin, J. 2009. *Mapping species distributions: spatial inference and prediction*. Cambridge University Press, Cambridge, United Kingdom.
- Geographic Resource Solutions, Inc. (2012). Densitometer. <http://www.grsgis.com/densitometer.html>. Accessed 6 February 2012.
- Gobakken, T., and E. Næssett. 2005. Weibull and percentile models for lidar-based estimation of basal area distributions. *Scandinavian Journal of Forest Research* 20:490-502.
- Golden Software, Inc. 2002. Golden Software, Inc. Golden, Colorado.
- Goodwin, N.R., N.C. Coops, C. Bater, and S.E. Gergel. 2007. Assessment of sub-canopy structure in a complex coniferous forest. *Proceedings of the ISPR Workshop Laser Scanning 2007 and Silverlaser 2007*, Espoo, 12-14 September 2007, Finland.
- Graham, M.H. 2003. Confronting multicollinearity in ecological multiple regression. *Ecology* 84:2809-2815.
- Grumbine, R.E. 1994. What is ecosystem management? *Conservation Biology* 8:27-38.

- Guisan, A., T.C. Edwards Jr., and T. Hastie. 2002. Generalized linear and generalized additive models in studies of species distributions: setting the scene. *Ecological Modelling* 157:89-100.
- Hall, S.A., I.C. Burke, D.O. Box, M.R. Kaufmann, and J.M. Stoker. 2005. Estimating stand structure using discrete-return lidar an example from low density, fire prone ponderosa pine forests. *Forest Ecology and Management* 208:189-209.
- Haugerud, R.A. and D.J. Harding. 1999. Some algorithms for virtual deforestation (VDF) of lidar topographic survey data. *International Archives of the Photogrammetry, Remote Sensing, and Spatial Sciences XXXIV, Part 3/W4:211-218.*
- Hirzel, A., and A. Guisan. 2002. Which is the optimal sampling strategy for habitat suitability modelling. *Ecological Modelling* 157:331-341.
- Holmgren, J., A. Persson, and U. Soderman. 2008. Species identification of individual trees by combining high resolution lidar data with multi-spectral images. *International Journal of Remote Sensing* 29:1537-1552.
- Jones, T., M. Woods, and K. Lim. 2009. Quantifying diameter and basal area distributions of uneven-aged tolerant hardwood stands using low density LiDAR. *Proceedings from Silvilaser 2009, 14-16 October 2009, College Station, Texas.*
- Ke, Y., L.J. Quackenbush, and J. Im. 2010. Synergistic use of quickbird multispectral imagery and lidar data for object-based forest species classification. *Remote Sensing of Environment* 114:1141-1154.
- Kim, S., G. Schreuder, R.J. McGaughey, and H-E. Anderson. 2008. Individual tree species identification using lidar intensity data. *Remote Sensing of Environment* 113:1575-1586.

- Koch, B., U. Heyder, and H. Weinacker. 2006. Detection of individual tree crowns in airborne lidar data. *Photogrammetric Engineering and Remote Sensing* 72:357-363.
- Küchler, A.W. 1964. Potential natural vegetation of the conterminous United States. New York, NY: American Geographic Society Special Publication No. 36.
- Li, Y., H.-E. Andersen, and R. McGaughey. 2008. A comparison of statistical methods for estimating biomass from light detection and ranging data. *Western Journal of Applied Forestry* 23:223-231.
- Lim, K., P. Treitz, K. Baldwin, I.K. Morrison, and J. Green. 2003. LiDAR remote sensing of biophysical properties of tolerant northern hardwood forests. *Canadian Journal of Remote Sensing* 29:658-678.
- Martinuzzi, S., L.A. Vierling, W.A. Gould, M.J. Falkowski, J.S. Evans, A.T. Hudak, and K.T. Vierling. 2009. Mapping snags and understory shrubs for a lidar-based assessment of wildlife habitat suitability. *Remote Sensing of Environment* 113:2533-2546.
- McKenzie, D., C.L. Raymond, and S.A. Cushman. 2009. Modeling understory vegetation and its response to fire. Pages 391-414 *In* Models for planning wildlife conservation in large landscapes (J.J. Millsaugh and F.R. Thompson, III, Editors). Elsevier, Inc., Burlington, Massachusetts.
- Meng, X., L. Wang, and N. Currit. 2009. Morphology-based building detection from airborne lidar data. *Photogrammetric Engineering and Remote Sensing* 75:437-442.
- Meyer, P., K. Staenz, and K.I. Itten. 1996. Semi-automated procedures for tree species identification in high spatial resolution data from digitized colour infrared-aerial photography. *ISPRS Journal of Photogrammetry and Remote Sensing* 51:5-16.

- MicroImages, Inc. 2012. MicroImages, Inc., Lincoln, Nebraska. www.microimages.com.
- Accessed on 26 March 2012.
- Myers, R.H. 1990. Classical and modern regression with applications, 2nd edition. PWS-Kent Publishers. Boston, Massachusetts.
- Neter, J., M.H. Kutner, C.J. Nachtshein, and W. Wasserman. 1996. Applied linear statistical models, 4th edition. Irwin, Inc. Chicago, Illinois.
- Oliver, C.D., and B.C. Larson. 1996. Forest stand dynamics, update edition. John Wiley and Sons, Inc. New York, New York.
- Peng, C.H. 2000. Growth and yield models for uneven-aged stands: past, present, and future. *Forest Ecology and Management* 132:259-279.
- Persson, A., J. Holmgren, and U. Söderman. 2002. Detecting and measuring individual trees using an airborne laser scanner. *Photogrammetric Engineering and Remote Sensing* 68:925-932.
- Piñeiro, G., S. Perelman, J.P. Guerschman, and J.M. Paruelo. 2008. How to evaluate models: observed vs. predicted or predicted vs. observed? *Ecological Modeling* 216:316-322.
- Pretzsch, H., P. Biber, and J. Dursky. 2002. The single tree-based stand simulator SILVA: construction, application, and evaluation. *Forest Ecology and Management* 162:3-21.
- Ralph, C.J., S. Droege, and J.R. Sauer. 1995. Managing and monitoring birds using point counts: standards and applications. Pages 161-169 *in* *Monitoring Bird Populations by Point Counts* (C.J. Ralph, J.R. Sauer, and S. Droege, Eds.). U.S. Department of Agriculture, Forest Service General Technical Report PSW-GTR-149.

- Rooker Jensen, J.L.R., K.S. Humes, T. Conner, C.J. Williams, and C.J. DeGroot. 2006. Estimation of biophysical characteristics for highly variable mixed-conifer stands using small-footprint lidar. *Canadian Journal of Forest Research* 36:1129-1138.
- SAS Institute. 2009. *The SAS System for Windows*, ver. 9.1. SAS Institute, Inc., Cary, North Carolina.
- Short, H.L., J.B. Hestbeck, and R.M. DeGraaf. 2001. *New England wildlife: a model for ecosystem management – ECOSEARCH (version 1)*. U.S. Forest Service, Northeastern Forest Experiment Station, GTR NE-283, Radnor, Pennsylvania.
- Snee, R.D. 1977. Validation of regression models: methods and examples. *Technometrics* 19:415-428.
- Toms, J.D., and M.L. Lesperance. 2003. Piecewise regression: a tool for identifying ecological thresholds. *Ecology* 84:2034-2041.
- Toutin, T., and P. Cheng. 2002. QuickBird – a milestone for high-resolution mapping. *Earth Observation Magazine* 11:14-18.
- Whittingham, M.J., P.A. Stephens, R.B., Bradbury, and R.P. Freckleton. Why do we still use stepwise modeling in ecology and behavior? *Journal of Applied Ecology* 75:1182-1189.
- Woods, M., K. Lim, and P. Trietz. 2008. Predicting forest stand variables from LiDAR data in the Great Lakes-St. Lawrence forest of Ontario. *Forestry Chronicle* 84:827-839.
- Zhang, K., and D. Whitman. 2005. Comparison of three algorithms for filtering airborne lidar data. *Photogrammetric Engineering and Remote Sensing* 71:313-325.

CHAPTER 3. PREDICTING BREEDING SONGBIRD ABUNDANCE IN MIXED FORESTS OF MAINE (NORTHWOODS) WITH LiDAR

Abstract

Wildlife typically structure themselves across a landscape as a function of vegetation composition and structure, both vertical and horizontal. One challenge modelers of wildlife-habitat relationships have is the ability to quantify this structure not just at the study plot level, where field-collected data are typically quantified and related to animal surveys, but also to be able to do so spatially and explicitly across a landscape of interest so that predictions of wildlife occurrence and habitat can be made. We explored LiDAR as a remote sensing technology for its capability to characterize vegetation structure in a forest and its ability to predict bird occurrence and abundance. Using regression analyses, our results indicate that several bird species can be modeled with LiDAR-derived explanatory variables ($\text{Adj. } R^2 \geq 0.40$) and LiDAR can be considered as one data-layer for various decision-support systems such as ECOSEARCH, which are natural-history models for predicting New England wildlife habitat.

Introduction

ECOSEARCH is a computer program that uses a suite of natural-history based wildlife-habitat models to spatially and explicitly predict occurrences (i.e., habitat maps) for 331 New England wildlife species as a function of environmental attributes (Short et al. 2001). Predictions are centered on a grid of 50×50 m cells (i.e., rasters) across an entire landscape of interest in a point-intercept context as opposed to artificial habitat polygons comprising broad habitat classes such as a mature forest. Pragmatically, the predicted habitat map for each species is done at 50×50 m pixel resolution using the center of each grid cell as a longitude-latitude (i.e., XY) point, however a continuous map could be derived at essentially every XY point (e.g., every 1 meter) across the landscape. The goal of ECOSEARCH is to provide resource managers with

a tool to assess the current status of habitat simultaneously for several species across a broad landscape. Having reliable maps of current habitat for each species also allows managers to use simulations to project the potential impacts of various management activities and help guide policy. The ability to make reliable predictions of habitat is one of several criteria required to effectively monitor and quantify the success of ecosystem management which is the accepted paradigm for managing ecosystems (Grumbine 1994, Christensen et al. 1996).

Currently, ECOSEARCH is based on natural-history models that take advantage of well-known habitat relationships between habitat structure and wildlife occurrences and abundances, particularly for birds (e.g., James 1971, Cody 1981, DeGraaf et al. 1998). Giorgi (1999) demonstrated that ECOSEARCH can give useful and reasonable predictive accuracies in some areas of New England (e.g., 60% overall classification accuracy rate). Several future directions for improving ECOSEARCH were pointed out by Short et al. (2001). One of those directions was to move the species models from natural-history based occurrence-only models to statistically-based models that can provide predictions of probability of occurrence. ECOSEARCH also could be augmented by using statistical models that predict other wildlife demographics (e.g., abundance, nest survival). Regardless, using statistically-based models provides opportunities to assess modeling uncertainties, both in the predictions as well as the models and their parameters (Claeskens and Hjort 2008). For example, locating areas in a predicted landscape of habitats where bias and precision are least (or greatest) could be used to improve the statistical models by identifying better sets of predictor variables. This process of continuous improvement in models and modeling products falls within the realm of adaptive management and is a requirement for ecosystem management (Walters 1986).

We demonstrated in Chapter 2 that reliable estimates of several over- and understory forest-stand metrics can be spatially predicted across a broad landscape with LiDAR using 50×50 m cells as the mapping unit in the mixed forests typical of Maine (see Chapter 1 for overview of LiDAR). LiDAR was used to assess its potential to improve estimates of the vertical habitat structure that is one of four GIS data layers required by ECOSEARCH. Short et al. (2001) pointed out that new higher-resolution remote sensing technologies have the potential to improve ECOSEARCH, both in its predictive ability and through gains in efficiency (e.g., automation). One question that naturally arises is whether we can develop reasonable models that predict species occurrence or abundance directly with LiDAR?

Applications of LiDAR in research and monitoring are increasing in a wide-range of disciplines including forestry (Reutebuch et al. 2005), bathymetry (Hilldale and Raff 2007), fault detection (Harding and Berghoff 2000), and urban planning (Priestnal et al. 2000). Many authors often mention incidentally that LiDAR also can be used to map habitat, but they usually do not provide details on how to accomplish this (e.g., Lefsky et al. 2002). Actual applications of modeling wildlife directly with LiDAR, and based on field-calibrated data, are only now beginning to be reported. For example, Pittman et al. (2009) found reasonable relationships between LiDAR-derived bathymetric variables (e.g., slope, roughness) and fish metrics (e.g., richness, biomass) off the coast of Puerto Rico (best model adjusted $R^2 > 0.46$). Nelson et al. (2005) located and mapped potential habitat of the Delmarva fox squirrel (*Sciurus niger cinereus*) in Delaware across 78% of field test sites based on relationships between LiDAR data and canopy characteristics as determined by a habitat suitability model. Although results are mixed, researchers also are beginning to explore the potential of LiDAR to map understory lichens (Korpela 2008), riparian salmon habitat (McKean et al. 2008), and beetle assemblages

(Muller and Brandi 2009). As Vierling et al. (2008) pointed out, the potential for LiDAR to improve habitat mapping is only beginning to “shed new light on habitat characterization.”

LiDAR is finding the most use and success in modeling and assessing bird-habitat relationships. One of the earliest studies to recognize the potential for LiDAR to characterize bird habitat was done by Davenport et al. (2000) in the United Kingdom. Although they did not model bird metrics directly as a function of LiDAR, they did ascertain that LiDAR can provide maps of crop heights (accuracy better than 0.1 m) as a way to characterize Skylark (*Alauda arvensis*) habitat which typically favor vegetation heights in the range of 0.2-0.6 m. Hinsley et al. (2002) recognized the potential for LiDAR to not only characterize habitat for species occurrence or abundance but also to characterize habitat quality. They successfully related LiDAR-derived canopy structural metrics to mean chick masses for Great Tits (*Parus major*) and Blue Tits (*Parus caeruleus*) in England woodlands, where increase in mean mass was equated with better habitat ($R^2 > 0.46$, several > 0.80). From another study done in England, Broughton et al. (2006) were able to derive a canopy-height metric with LiDAR and statistically compare this metric between mapped territories of Marsh Tits (*Poecile palustris*) and random pseudo-territories. They found several significant differences in mean LiDAR-derived canopy heights (most p-values < 0.02). Working in temperate forests in Maryland, Goetz et al. (2007) were able to relate satellite-based full-waveform LiDAR data, including canopy heights, to bird species richness, showing a slight decline in overall richness with increasing mean canopy heights. Other recent studies also have had good success in relating bird occurrence, abundance, or richness to LiDAR-derived metrics, e.g. Clawges et al. (2008) in aspen/pine forests of the Black Hills of South Dakota, Smith et al. (2008) in mixed forests of southern Vermont, and Seavey et al. (2009) in a California riparian forest. However, not all studies relate bird metrics to LiDAR-

derived vegetation metrics. Goodale, et al. (2007) found that LiDAR ground-returns, including their intensities, were able to quantify the micro-topography (i.e., elevation, slope, texture) of coastal habitats of Nova Scotia. These topographic metrics have been found to be useful for characterizing Piping Plover (*Charadrius melodus*) habitat (Burger 1994).

Goals and Objectives

Habitat models derived from LiDAR technology offer great advantage to natural resource managers from traditional methodologies. LiDAR, especially when used with other imagery such as QuickBird (Hyde et al. 2006), provides the opportunity to map habitats with fine-scale metrics across broad landscapes. Having these models available and incorporated into tools such as ECOSEARCH should be invaluable to managers, especially if proposed national and periodic LiDAR acquisitions become standard protocol (Stoker et al. 2007).

Updating models and their predicted maps could be done periodically thus allowing periodic habitat assessments and projections to be made. To date, no models of which we are aware of have been developed for the Northwoods of Maine. Therefore, the overall goals of this research were to improve our understanding of bird-habitat relationships in the Northwoods of Maine and to further our understanding of the potential for LiDAR technologies to enhance habitat mapping of forest birds. The specific objective was to develop and assess empirical models that predict forest bird abundance directly from LiDAR-derived explanatory variables.

Study Area

We selected two study sites in Maine that are typical of mixed forests in the northeastern USA representing two diverse forest management objectives. The first study site, located approximately 30 km east-northeast of Bangor, Maine, was on private land formerly owned by International Paper, Inc. (IP) and encompasses approximately 7680 ha (Chap. 2, Fig. 2.1). The

second study site, located approximately 10 km south-southwest of Calais, Maine, was on the Baring Unit of Moosehorn National Wildlife Refuge (MH) and encompasses approximately 10,350 ha (Chap. 2, Fig. 2.1). The IP site is classified as northern hardwoods-spruce forest (*Acer-Betula-Fagus-Picea-Tsuga*) by Küchler (1964) and is actively managed for forestry products. The MH study site falls within the northeastern spruce-fir-forest classification (*Picea-Abies*) (Küchler 1964) and is actively managed to ensure the presence of stands of early successional forests in a mosaic of stands which provides important habitat for the American Woodcock (*Scolopax minor*) (Dessecker and McAuley 2001). Although the Baring Unit of MH has been cutting 40-60 ha per year in 10-ha blocks since about 1979 to maintain some early successional stages on a rotational schedule, this unit also contains a 2000-ha wilderness area that receives no active management. Both study sites also support the goal of maintaining wildlife diversity by minimizing the impacts of their management activities.

Methods

Bird Surveys

Breeding bird survey points (50-m radius) were established at MH (n=114) and IP (n=100, but only 99 fell within the LiDAR acquisition area, see below) in 1995 and 2001, respectively (Chap 2, Fig. 2.2.a. and 2.2.b). The points were primarily established for long-term monitoring and to assess management activities. Criteria used to establish the survey points included coverage of the full range in heterogeneity of forest composition (i.e., proportion of hardwood-to-softwood) and structure (early successional-to-mature forest stands). Survey points were located approximately ≥ 250 m apart and were at least 100 m from main bodies of water. This approach, as opposed to selecting random points, was done to maximize the potential for successful modeling efforts (Hirzel and Guisan 2002) and to represent the range of successional

stages (Oliver and Larson 1996). Counting and recording birds followed accepted protocol at the time the surveys were established (Ralph et al. 1995), with surveys being conducted nearly annually at each point through 2010 (no surveys were conducted in 2008 at IP). The number of birds observed or heard for each species within the survey points was recorded at three distances from the point center (0-25 m, 25-50 m, >50 m) and at three time-intervals (0- 3 min, 3-5 min, and 5-10 min); flyovers also were recorded. Surveys were typically done from 6:00-10:00 EDT under light to moderate wind, and little or no rain. Points were only surveyed once a year by the same observer at each study site, at least for the years 2002, 2003, and 2004.

Because LiDAR was acquired in June, 2003, full leaf-on (see Chapter 2), and the bird surveying protocol did not attempt to account for detection probabilities or occurrence (e.g., Rosenstock et al. 2002, MacKenzie et al. 2006), we derived a response variable using an index to abundance. While we recognized the challenges with using indices (e.g., Betts et al. 2005), Johnson (2008) makes a reasonable argument for their defense in many cases. Bird occurrence, abundance, and detection typically varies from year-to-year at any given survey point (Sutherland and Baillie 1993). Therefore, as an index to abundance, we first tallied the number of birds seen or heard ≤ 50 m from the point center, across all 10 minutes of the survey time at each point by species for the survey years 2002, 2003, and 2004. We then averaged these three years of survey data for each species to derive a mean abundance index at each survey point. Flyovers were not included. This index accompanied with modeling efforts described below should help answer the following questions: “Given the vegetation structure at a particular survey point as characterized by LiDAR, how many birds of each species might we expect to see or hear?” , and, “Can we empirically model that relationship?” We also computed species richness and species diversity (Shannon-Weaver) for all passerines detected at each survey point

and assessed the average of these indices and their relationship to the same LiDAR-derived explanatory variables.

LiDAR

Acquisition and processing

Chapter 1 of this dissertation provides a general description of LiDAR technology. Chapter 2 of this dissertation provides a detailed description of the acquisition and processing of LiDAR (including virtual removal of buildings and classifying water and bogs). A justification for summarizing the LiDAR to 50×50 m cells, including within 50-m radii bird survey points, also was described in Chapter 2. Therefore, in this chapter, we only describe how we arrived at a suite of LiDAR-derived explanatory variables to relate to the bird response variables (mean bird abundance as mean count/0.25 ha) in our empirical models. Unless stated otherwise, all processing of LiDAR was done using the data step and macro facilities provided in SAS (SAS Institute, Inc., 2009).

LiDAR-derived explanatory variables

Because of the rich amount of information available in LiDAR point-clouds, a major challenge is how to summarize the data into a few uncorrelated, yet meaningful, variables that can be used as predictor variables in our modeling efforts. In Chapter 2, we described how we summarized the three-dimensional (3D) LiDAR point-clouds into 1-m vertical height bins within each 50×50 m cell (i.e., forest plot). We labeled these canopy closures (CC) with CC0 being proportion of returns on the ground, CC1 being the proportion of returns between the ground and 1 m, etc. to CC30 being proportion of LiDAR being between 27 and 30 m above the ground. These CC values represent canopy closure at each vertical height profile; in reality they are the “penetration” and return of LiDAR pulses as described in Chapter 1. We combined these 1-m

CCs' into 10 3-m vertical profiles labeled P0 to P10, with P0=CC0 (Chap 2, Table 2.3). The P0 to P10 variables were then used either individually or combined to accommodate multicollinearity and then used as explanatory variables to model various forest stand metrics. For computing LiDAR-derived explanatory variables for modeling birds we pooled the 1-m CC's into those described and labeled as X1 to X10 in Table 3.1.a, with X0=P0. Here X0 to X5 sum to 1.0 (i.e., 100%), whereas X0 plus X6 to X10 sum to 1.0 because of their sensitivity to early successional stages (DeGraaf et al. 1992). This computational structure helped us to accommodate those bird species that might be more sensitive to fine-scale partitioning in the lower understory or broader partitioning in the upper canopy (X1-X5) versus allowing for those birds that may partition themselves more evenly across vertical vegetation layers (Ehrlich et al, 1988, DeGraaf and Yamasaki 2001).

For birds and most other wildlife species, use of a particular habitat is not determined by only the habitat within the immediate location of their territory or home range; a species habitat selection reflects how the territory location is juxtaposed in the overall landscape (Johnson 1980). We illustrate his concept in Fig. 3.1 which depicts a 50×50 m stand of trees with a fixed structure isolated in a landscape (top panel), juxtaposed in a landscape of like stands (middle panel), and the same stand juxtaposed within dissimilar stands (bottom panel). Many studies that model bird occurrence or other demographic parameters generally restrict their quantification to the structure within the survey point (e.g., 50-m radius survey point) and either disregard how that survey point is juxtaposed in the landscape (e.g., Kirk and Hobson 2001) or in cases where the surrounding landscape is considered to only use coarser-scaled explanatory variables (e.g., Mitchell et al. 2001, Crozier and Niemi 2003). Therefore, as a way to accommodate both the fine-scale metrics provided by LiDAR at each 50×50 m cell (centered within each bird survey

Table 3.1.a. Description of LiDAR-derived explanatory variables for modeling bird species abundance derived from the center 50×50 m cell of 3×3- and 5×5 blocks of 50×50 m cells (see Fig. 3.2 for visual reference).

Scale ¹	Variable(s)	Description ²
Center	X0	Proportion LiDAR classified on ground
	X1	(0 < CC ≤ 1 m above ground)
	X2	(1 < CC ≤ 2 m above ground)
	X3	(2 < CC ≤ 4 m above ground)
	X4	(4 < CC ≤ 9 m above ground)
	X5	(9 < CC ≤ 30 m above ground)
	X6	(0 < CC ≤ 2 m above ground)
	X7	(2 < CC ≤ 6 m above ground)
	X8	(6 < CC ≤ 12 m above ground)
	X9	(12 < CC ≤ 18 m above ground)
	X10	(18 < CC ≤ 30 m above ground)
3×3 Block	X11	Mean of X0 from 9 50-m cells
	X12	SD of X0 from 9 50 m-cells
	X13	RMD of surrounding 8-m cells for X0
	X14-X18	Mean of X1-X5 for 9 50-m cells respectively
	X19-X23	SD of X1-X5 for 9 50-m cells respectively
	X24-X28	RMD of surrounding 8-m cells for X1-X5 respectively
	X29-X33	Mean of X6-X10 for 9 50-m cells respectively
	X34-X38	SD of X6-X10 for 9 50-m cells respectively
	X39-X43	RMD of surrounding 8-m cells for X6-X10 respectively
5×5 Block	X44	Mean of X0 from 25 50-m cells
	X45	SD of X0 from 25 50-m cells
	X46	RMD of surrounding 24 50-m cells for X0
	X47-X51	Mean of X1-X5 for 25 50-m cells respectively
	X52-X56	SD of X1-X5 for 25 50-m cells respectively
	X57-X61	RMD of surrounding 24 50-m cells for X1-X5 respectively
	X62-X66	Mean of X6-X10 for 25 50-m cells respectively
	X67-X71	SD of X6-X10 for 25 50-m cells respectively
	X72-X76	RMD of surrounding 24 50-m cells for X6-X10 respectively

¹In reference to 50×50 m cells (see Figure 3.2).

²CC = canopy closure at each vertical height bin (1-m increments) is the proportion of all LiDAR data falling within the height intervals, RMD=root mean squared difference of surrounding cells with center cell.

point) and how they might vary in the surrounding landscape, we derived the explanatory

variables X11 - X76 as listed Table 3.1.a. Here, we consider these X's as being arranged and

summarized in a 3×3 and 5×5 grid of 50×50 m cells juxtaposed on 50-m radii bird survey points

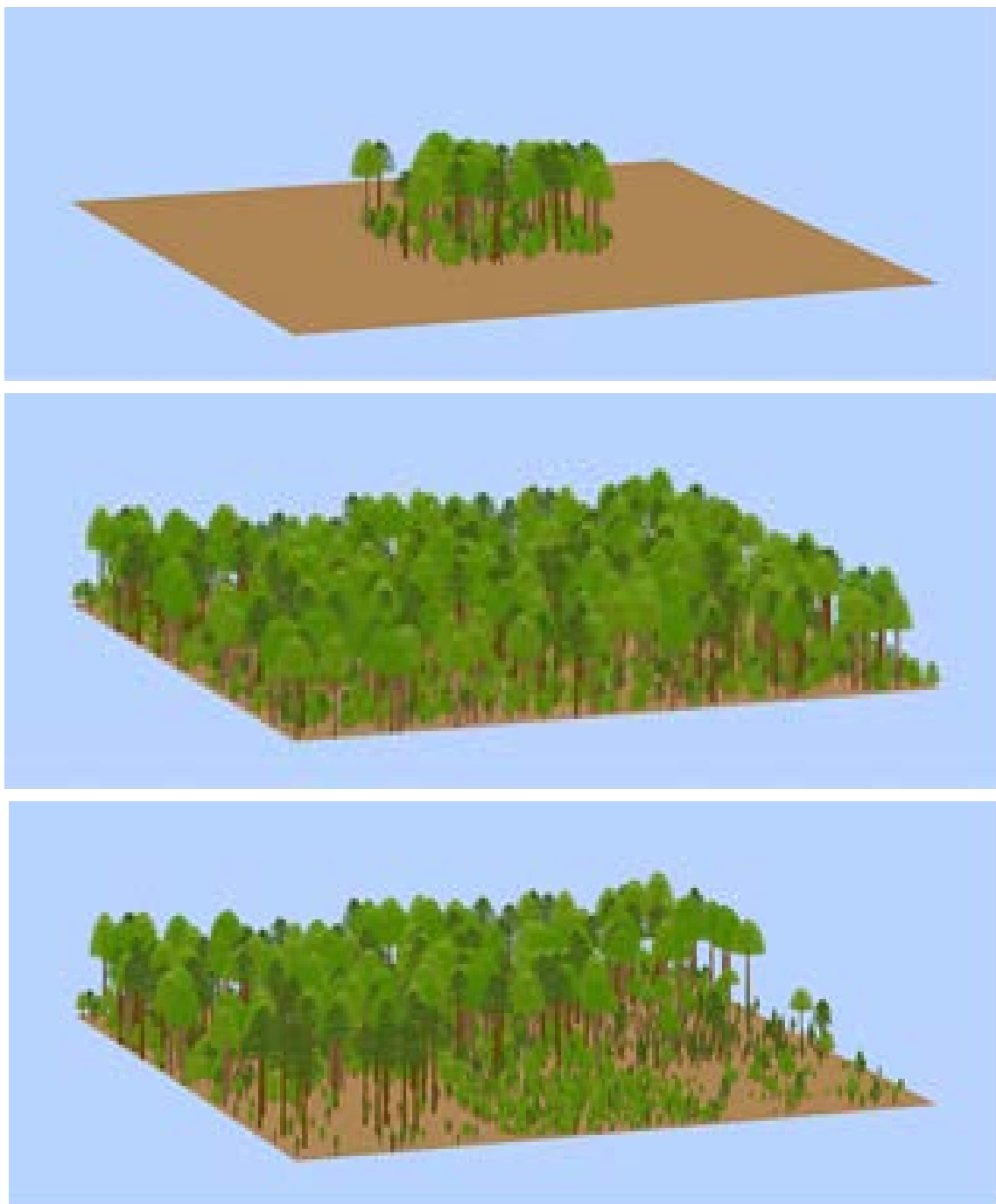


Figure 3.1. Forest plot (50×50 m, top panel) juxtaposed within a homogeneous landscape of like plots (middle panel) and within a heterogeneous landscape (bottom panel).

(Fig. 3.2, left panels). The two landscapes in Fig. 3.2 represent a relatively homogenous stand (top panel) and a heterogeneous stand (bottom panel). The right panels in Fig 3.2 depict the

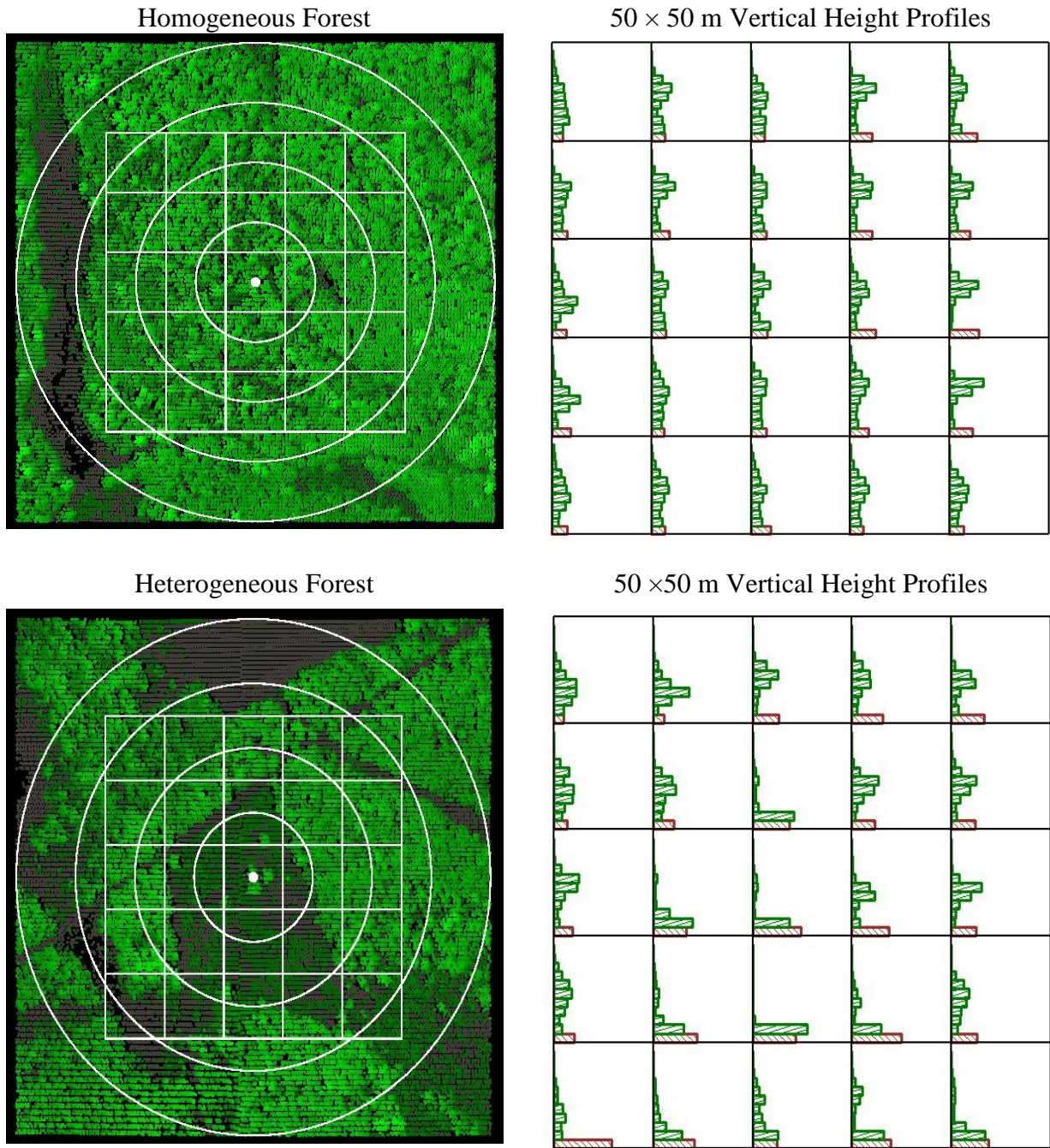


Figure 3.2. An example of 50×50 m vertical height profiles in a homogeneous forest and a heterogeneous forest. Left panels illustrate bird survey points with 25 50×50 m cells and concentric 50-m radii juxtaposed on LiDAR-derived canopy heights from short (dark) to tall (light); right panels illustrate vertical height profiles for corresponding 50×50 m cells in left panel (bottom red bar represents ground with other bars being increasing proportion of LiDAR falling within 0-3 m, 3-6m, etc. up to 30-m height bins).

vertical profile of binned LiDAR in 3-m height intervals for presentation purposes for each of the 25 50×50 m cells (center cell in right panel corresponds with center cell in left panel). Figure 3.2 encapsulates the scale of a 250×250 m block, and we can see that LiDAR-derived variables X11 to X76 in Table 3.1.a quantify not only the mean structure surrounding the center 50×50 m cell, but also the variation among cells as quantified by the standard deviation (SD) using the variables X0 - X10. As another potential metric to quantify the variation we computed a root-mean-squared difference (RMD) for the variables X0 - X10 in the surrounding eight cells of a 3×3 grid and surrounding 24 cells in a 5×5 grid relative to the center cell.

Seavey et al. (2009) had reasonable success in modeling the probability of bird species occurrence for several riparian forest birds using the means and SD's of all first-return LIDAR data at five-radii concentric around bird survey point-count locations in a California riparian forest (10 bird species had an area-under-the-curve (AUC) > 0.8 for at least one scale). To assess the potential for related variables to explain variation in bird abundance at our study sites, we also computed these same metrics in concentric 50-m radii bands surrounding the bird survey points out to 200-m radius (variables X77 - X90 in Table 3.1.b and depicted in Fig. 3.2, left panels). Table 3.2 presents summary statistics across both study sites (n=99 at IP, n=114 at MH) for the variables X0 - X10 and for selected variables X77- X90 and illustrates the reasonable range and good coverage in these metrics as required for modeling purposes (Hirzel and Guisan 2002).

As pointed out in the modeling efforts in Chapter 2 and by Graham (2003), among others, multicollinearity among explanatory variables warrants concern and should be addressed. Before deriving a suite of plausible models we conducted an assessment to investigate the amount of redundancy among the explanatory variables listed in Tables 3.1.a-b by examining

Table 3.1.b. Description of LiDAR-derived explanatory variables for modeling bird species abundance derived from concentric radii bands (see Fig. 3.2 for visual reference).

Scale (m) ¹	Var.	Description
50	X77	Mean first-return LiDAR height within 50-m radii
	X78	SD first-return LiDAR heights within 50-m radii
100	X79	Mean first-return LiDAR heights within 100-m radii
	X80	SD first-return LiDAR heights within 100-m radii
	X81	Mean first-return LiDAR heights between 50- and 100-m radii
150	X82	SD first-return LiDAR heights between 50- and 100-m radii
	X83	Mean first-return LiDAR heights within 150-m radii
	X84	SD first-return LiDAR heights within 150-m radii
200	X85	Mean first-return LiDAR heights between 100- and 150-m radii
	X86	SD first-return LiDAR heights between 100- and 150-m radii
	X87	Mean first-return LiDAR heights within 200-m radii
	X88	SD first-return LiDAR heights within 200-m radii
	X89	Mean first-return LiDAR heights between 150- and 200-m radii
	X90	SD first-return LiDAR heights between 150- and 200-m radii

¹In reference to concentrically increasing 50-m radii (see Fig. 3.2).

simple pair-wise correlations. Table 3.3.a illustrates the strong positive correlations for X's that are in close proximity in the vertical profile, whereas those farthest apart are negatively correlated for the center 50×50 m cell. Strong pair-wise correlations also exist among X's in the surrounding 3×3 grid cells (Table 3.3.b) and 5×5 grids cells (Table 3.3.c), with extremely high correlations not only among SD's and RMD's but also among means with their corresponding SD's. We also found strong correlations among the concentric radii band variables (Table 3.3.d). Although there are strong correlations among many of the potential LiDAR-explanatory variables, we did not reduce the dimensionality (e.g., via principal component analysis) because we wanted to improve our ability to interpret the models from the natural-history perspective of a bird. We do this in part by posing parsimonious models, with minimally correlated explanatory variables within each model, and competing the models among each other other (see below plausible models).

Table 3.2. Summary statistics of selected explanatory variables combined across IP (n = 99) and MH (n = 114) for the central 50×50 m cell and surrounding concentric 50 m radii (see Fig. 3.2 for visual reference).

Var. ²	Mean	SD	Canopy closure (CC) percentiles ¹				
			0	25	50	75	100
X0	0.279	0.200	0.064	0.154	0.213	0.331	0.994
X1	0.042	0.037	0.000	0.014	0.030	0.054	0.206
X2	0.067	0.055	0.000	0.027	0.045	0.094	0.279
X3	0.115	0.090	0.000	0.047	0.091	0.165	0.531
X4	0.199	0.148	0.000	0.096	0.161	0.284	0.669
X5	0.040	0.070	0.000	0.000	0.007	0.046	0.383
X6	0.109	0.087	0.004	0.046	0.078	0.157	0.387
X7	0.203	0.141	0.000	0.094	0.164	0.289	0.643
X8	0.209	0.159	0.000	0.093	0.201	0.306	0.748
X9	0.160	0.160	0.000	0.003	0.003	0.307	0.565
X10	0.040	0.070	0.000	0.000	0.007	0.046	0.383

First-return LiDAR heights (m)							
X77	7.1	4.2	0.0	3.7	7.1	10.7	15.2
X78	4.4	1.9	0.2	3.0	4.7	5.8	9.9
X79	7.1	3.6	0.0	4.8	6.8	9.9	15.2
X80	5.0	1.6	0.2	4.0	5.3	6.0	9.7
X83	7.1	3.2	0.0	5.0	6.9	9.7	14.6
X84	5.2	1.4	0.2	4.5	5.6	6.2	9.3
X87	7.1	2.9	0.1	5.0	6.9	9.2	14.1
X88	5.5	1.2	0.9	4.7	5.7	6.3	8.6

¹CC = canopy closure at each vertical height bin is the proportion of all LiDAR data falling within the height intervals.

²See Table 3.1.a and 3.1.b for definitions.

Table 3.3.a. Correlations among relevant combinations of explanatory variables, center 50×50 m cell (see Fig. 3.2 for visual reference).

Var. ¹	X1	X2	X3	X4	X5	Var. ¹	X6	X7	X8	X9	X10
X0	0.35	0.08	-0.14	-0.53	-0.25	X0	0.20	-0.29	-0.59	-0.41	-0.25
X1		0.79	0.44	-0.32	-0.27	X6		0.44	-0.53	-0.54	-0.28
X2			0.75	-0.15	-0.26	X7			-0.04	-0.58	-0.34
X3				0.22	-0.31	X8				0.13	-0.12
X4					-0.25	X9					0.44

¹See Table 3.1.a. and 3.1.b for definitions.

Table 3.3.b. Correlations among relevant combinations of explanatory variables, surrounding 3×3 grid of 50×50 m cells (see Fig. 3.2 for visual reference).

Var. ¹	X11	X15	X16	X17	X18	Var. ¹	X11	X31	X32	X33	X34
X14	0.30	0.79	0.44	-0.28	-0.56	X29	0.14	0.49	-0.47	-0.56	-0.32
X15	0.00		0.83	0.04	-0.62	X30	-0.34		0.16	-0.61	-0.37
X16	-0.21			0.44	-0.64	X31	-0.69			0.18	-0.08
X17	-0.57				-0.19	X32	-0.42				0.53
X18	-0.53					X33	-0.28				
		X12	X13								
X11		0.19	0.18								
X12			0.94								
		Var. ²					Var. ³				
		SD	RMD	SvR			SD	RMD	SvR		
X14		0.70	0.63	0.90		X29	0.68	0.67	0.90		
X15		0.75	0.75	0.90		X30	0.70	0.65	0.90		
X16		0.74	0.69	0.90		X31	0.59	0.52	0.90		
X17		0.65	0.62	0.90		X32	0.53	0.50	0.92		
X18		0.15	0.12	0.93		X33	0.88	0.49	0.51		

¹See Table 3.1.a. and 3.1.b for definitions.

²SD=standard deviations X19-X23 and RMD=root mean differences X24-X28 respectively, SvR: corresponding SD versus RMD.

³SD=standard deviations X34-X38 and RMD=root mean differences X39-X43 respectively, SvR: corresponding SD versus RMD.

Data Analysis and Modeling

Plausible models

As indicated in Chapter 2, stepwise regression methods have been shown to have biases, among other concerns (Whittingham et al. 2006). Therefore, we used an Information-Theoretic (IT) model development and selection approach (Burnham and Anderson 2002) to assess empirical models relating bird species mean abundances to the potential suite of LiDAR-derived explanatory variables in Tables 3.1.a - 3.1.b. The IT approach advocates more forethought in the development of a suite of competing models (i.e., hypotheses) than what is required by stepwise regression or other similar methods (Burnham and Anderson 2002). We derived a suite of 25 plausible models that are parsimonious (i.e., reduced the number of parameters involved as much

Table 3.3.c. Correlations among relevant combinations of explanatory variables, surrounding 5×5 grid of 50×50 m cells (see Fig. 3.2 for visual reference).

Var. ¹	X44	X47	X48	X49	X50	Var. ¹	X44	X62	X63	X64	X65
X44	0.30	0.77	0.42	-0.23	-0.56	X62	0.11	0.52	-0.42	-0.58	-0.34
X48	-0.05		0.84	0.18	-0.61	X63	-0.38		0.26	-0.60	-0.41
X49	-0.26			0.58	-0.61	X64	-0.74			0.21	-0.03
X50	-0.59				-0.20	X65	-0.43				0.57
X51	-0.55					X66	-0.29				
		X45	X46								
X44		0.40	0.34								
X45			0.89								
		Var. ²					Var. ³				
		SD	RMD	SvR		SD	RMD	SvR			
X47		0.77	0.67	0.87	X62	0.78	0.70	0.86			
X48		0.83	0.72	0.86	X63	0.71	0.60	0.82			
X49		0.76	0.62	0.85	X64	0.56	0.42	0.83			
X50		0.65	0.59	0.84	X65	0.48	0.42	0.87			
X51		0.09	0.06	0.88	X66	0.89	0.83	0.90			

¹See Table 31.a. and 3.1.b for definitions.

²SD=standard deviations X52-X56 and RMD=root mean differences X57-X61 respectively, SvR: corresponding SD versus RMD.

³SD=standard deviations X67-X71 and RMD=root mean differences X72-X76 respectively, SvR: corresponding SD versus RMD.

Table 3.3.d. Correlations among relevant combinations of explanatory variables, surrounding concentric 50-m radii (see Fig. 3.2 for visual reference).

Radii (m)	Var. ¹	X78		Radii (m)	Var.	X80	X81	X82	
50	X77	0.76		100	X79	0.69	0.99	0.67	
					X80		0.68	0.99	
					X81			0.67	
150		X84	X85	X86	200	X88	X89	X90	
	X83	0.66	0.98	0.61		X87	0.60	0.96	0.52
	X84		0.66	0.98		X88		0.57	0.94
	X85			0.63		X89			0.53

¹See Table 3.1.a. and 3.1.b for definitions.

as possible) and minimized the amount of correlations among X0 - X71 explanatory variables included within each model (Table 3.4.a). We did not include any RMD variables in any model as they were found to be nearly collinear with corresponding SD's. As a separate suite of models using variables X77-X90, we derived 17 plausible models for similar reasons (Table 3.4.b.).

Table 3.4.a. Plausible bird models using 50×50 m cells at three different scales (see Fig. 3.2 for visual reference).

Scale	Mod. No.	k	Model explanatory variables ¹	Description
Ctr.	1	2	β_0	Null model
	2	3	$\beta_0 + \beta_1(X_0)$	Ground only
	3	6	$\beta_0 + \beta_1(X_0) + \beta_2(X_1) + \beta_3(X_3) + \beta_4(X_5)$	Ground, shorter low-mid canopy only
	4	5	$\beta_0 + \beta_1(X_0) + \beta_2(X_2) + \beta_3(X_4)$	Ground, taller lower canopy to tall canopy
	5	6	$\beta_0 + \beta_1(X_0) + \beta_2(X_6) + \beta_3(X_7) + \beta_4(X_{10})$	Ground, emphasis on even canopy strata
	6	6	$\beta_0 + \beta_1(X_0) + \beta_2(X_8) + \beta_3(X_9) + \beta_4(X_{10})$	Ground, emphasis on even upper-canopy
	7	3	$\beta_0 + \beta_1(X_6)$	Tall understory only
3×3	8	4	$\beta_0 + \beta_1(X_{11}) + \beta_2(X_{12})$	Ground (mean, SD) only among 3×3 cells (9 cells)
	9	7	$\beta_0 + \beta_1(X_{11}) + \beta_2(X_{12}) + \beta_3(X_{14}) + \beta_4(X_{16}) + \beta_5(X_{18})$	Ground, mean shorter low-mid canopy
	10	5	$\beta_0 + \beta_1(X_{11}) + \beta_2(X_{12}) + \beta_3(X_{15}) + \beta_4(X_{17})$	Ground, mean shorter mid-upper canopy
	11	7	$\beta_0 + \beta_1(X_{11}) + \beta_2(X_{12}) + \beta_3(X_{19}) + \beta_4(X_{21}) + \beta_5(X_{23})$	Ground, variation in shorter low-mid canopy
	12	5	$\beta_0 + \beta_1(X_{11}) + \beta_2(X_{12}) + \beta_3(X_{20}) + \beta_4(X_{22})$	Ground, variation in shorter mid-upper canopy
	13	6	$\beta_0 + \beta_1(X_{11}) + \beta_2(X_{12}) + \beta_3(X_{29}) + \beta_4(X_{31}) + \beta_5(X_{33})$	Ground, mean taller low-mid canopy
	14	5	$\beta_0 + \beta_1(X_{11}) + \beta_2(X_{12}) + \beta_3(X_{30}) + \beta_4(X_{32})$	Ground, mean taller mid-upper canopy
	15	7	$\beta_0 + \beta_1(X_{11}) + \beta_2(X_{12}) + \beta_3(X_{34}) + \beta_4(X_{36}) + \beta_5(X_{38})$	Ground, variation in taller low-mid canopy
	16	6	$\beta_0 + \beta_1(X_{11}) + \beta_2(X_{12}) + \beta_3(X_{35}) + \beta_4(X_{37})$	Ground, variation in taller mid-upper canopy
5×5	17	4	$\beta_0 + \beta_1(X_{44}) + \beta_2(X_{45})$	Repeat of model 8 for 5×5 (25 cells)
	18	7	$\beta_0 + \beta_1(X_{44}) + \beta_2(X_{45}) + \beta_3(X_{47}) + \beta_4(X_{49}) + \beta_5(X_{51})$	Repeat of model 9 for 5×5 (25 cells)
	19	6	$\beta_0 + \beta_1(X_{44}) + \beta_2(X_{45}) + \beta_3(X_{48}) + \beta_4(X_{50})$	Repeat of model 10 for 5×5 (25 cells)
	20	7	$\beta_0 + \beta_1(X_{44}) + \beta_2(X_{45}) + \beta_3(X_{52}) + \beta_4(X_{54}) + \beta_5(X_{56})$	Repeat of model 11 for 5×5 (25 cells)
	21	6	$\beta_0 + \beta_1(X_{44}) + \beta_2(X_{45}) + \beta_3(X_{53}) + \beta_4(X_{55})$	Repeat of model 12 for 5×5 (25 cells)
	22	7	$\beta_0 + \beta_1(X_{44}) + \beta_2(X_{45}) + \beta_3(X_{62}) + \beta_4(X_{64}) + \beta_5(X_{66})$	Repeat of model 13 for 5×5 (25 cells)
	23	6	$\beta_0 + \beta_1(X_{44}) + \beta_2(X_{45}) + \beta_3(X_{63}) + \beta_4(X_{65})$	Repeat of model 14 for 5×5 (25 cells)
	24	7	$\beta_0 + \beta_1(X_{44}) + \beta_2(X_{45}) + \beta_3(X_{67}) + \beta_4(X_{69}) + \beta_5(X_{71})$	Repeat of model 15 for 5×5 (25 cells)
	25	6	$\beta_0 + \beta_1(X_{44}) + \beta_2(X_{45}) + \beta_3(X_{68}) + \beta_4(X_{70})$	Repeat of model 16 for 5×5 (25 cells)

¹See Table 3.1.a. and 3.1.b for definitions.

Table 3.4.b. Plausible bird models using concentric 50-m radii (see Fig. 3.1 for visual reference, model numbers are a continuation of those from Table 3.4.a.).

Radii scale	Mod. no.	k	Model explanatory variables ¹	Description
50	26	3	$\beta_0 + \beta_1(X77)$	Mean first-return LiDAR height within 50-m radii
	27	3	$\beta_0 + \beta_1(X78)$	SD of first-return LiDAR heights within 50-m radii
100	28	3	$\beta_0 + \beta_1(X79)$	Mean first-return LiDAR heights within 100-m radii
	29	3	$\beta_0 + \beta_1(X780)$	SD of first-return LiDAR heights within 100-m radii
	30	7	$\beta_0 + \beta_1(X79) + \beta_2(X0) + \beta_3(X1) + \beta_4(X3) + \beta_5(X5)$	Model 28 with center 50-m cell shorter low-mid canopy
150	31	7	$\beta_0 + \beta_1(X79) + \beta_2(X0) + \beta_3(X6) + \beta_4(X7) + \beta_5(X10)$	Model 29 with center 50-m cell taller low-mid canopy
	32	3	$\beta_0 + \beta_1(X83)$	Mean first-return LiDAR heights within 150-m radii
	33	3	$\beta_0 + \beta_1(X84)$	SD of first-return LiDAR heights within 150-m radii
	34	7	$\beta_0 + \beta_1(X83) + \beta_2(X0) + \beta_3(X1) + \beta_4(X3) + \beta_5(X5)$	Model 32 with center 50-m cell shorter low-mid canopy
	35	7	$\beta_0 + \beta_1(X83) + \beta_2(X0) + \beta_3(X6) + \beta_4(X7) + \beta_5(X10)$	Model 32 with center 50-m cell taller low-mid canopy
200	36	3	$\beta_0 + \beta_1(X87)$	Mean first-return LiDAR heights within 200-m radii
	37	3	$\beta_0 + \beta_1(X88)$	SD of first-return LiDAR heights within 200-m radii
	38	7	$\beta_0 + \beta_1(X87) + \beta_2(X0) + \beta_3(X1) + \beta_4(X3) + \beta_5(X5)$	Model 36 with center 50-m cell shorter low-mid canopy
All	39	7	$\beta_0 + \beta_1(X87) + \beta_2(X0) + \beta_3(X6) + \beta_4(X7) + \beta_5(X10)$	Model 37 with center 50-m cell taller low-mid canopy
	40	4	$\beta_0 + \beta_1(X77) + \beta_2(X81)$	50 m radii with 50-100-m radii band
	41	5	$\beta_0 + \beta_1(X77) + \beta_2(X81) + \beta_3(X85)$	Mean first return LiDAR heights 50 m, 50-100-m, 100-150 m radii bands
	42	6	$\beta_0 + \beta_1(X77) + \beta_2(X81) + \beta_3(X85) + \beta_4(X89)$	Mean first return LiDAR heights 50 m, 50-100m, 100-150 m, 150-200 m radii bands

¹See Table 3.1.a. and 3.1.b for definitions.

Therefore, in total, we compared 42 models under an IT framework, with minimal correlations among explanatory variables and with number of parameters ≤ 7 . A brief description of each model is provided in Tables 3.4.a. and 3.4.b. with respect to what each model is attempting to explain with respect to the variation in observed mean bird abundance.

Statistical modeling

Univariate multiple regression techniques (Neter et al. 1996) were used to model the relationship between mean bird abundance and the LiDAR-derived explanatory variables. We modeled each of the bird species abundance separately and log-transformed to reduce influences of extreme mean values and only for species which we felt there was an adequate frequency of occurrence across survey points (≥ 10). The value 1.0 was added to all mean abundances prior to log-transformation to accommodate mean abundances of zero. The IT model selection process (Burnham and Anderson 2002) was used to evaluate evidence for which of the 42 plausible models best described variation in mean bird abundance. We used ΔAIC_C and Akaike's weights (ω_i) to judge model adequacy among competing models. We assessed the adequacy of "best" model(s) fit with two statistics: adjusted R^2 , and adjusted PRESS R^2 , the latter being a measure of "fit" that involved computing an adjusted R^2 by removing one observation at a time (Myers et al. 2002). We also plotted observed mean bird abundance versus LiDAR-predicted abundance to further assess model fit for the "best" model and assess biases, if any (Piñeiro et al. 2008). We used PROC REG (SAS Institute, Inc. 2009) to fit each of the multiple regression models. We report the top three competing models for each bird species and when applicable, made predictions across both study sites for each

50×50 m cell. If there were more than one competing model, we used Akaike's weights (ω_i) to derive a weighted prediction but only when cumulative weights became > 0.5 . To avoid potential confounding of results because two different bird observers were used at the two study sites (the same bird observer was used at each site in 2002, 2003, and 2004), and because the suite of potential bird species varies somewhat from the MH site (near the Maine coast) and the IP site (interior Maine), we modeled the bird species separately at each site and qualitatively compared modeling results. Mean species richness and diversity (Shannon-Weaver) for detected passerines also were modeled similarly.

Results

Bird Surveys

We detected 78 passerine species across the IP and MH study sites for the years 2002, 2003, and 2004, with unweighted mean frequency of occurrences among survey points varying from 0 to a high of 74 (Table 3.5; acronyms for species codes are listed in Table C.1). Within each study site, several species occurred on greater than 80% of the survey points based on having been observed in at least one year (Table 3.5). Several species only met the requirement for modeling by occurring on ≥ 10 points at one or the other study sites, but not both. In total, 46 and 25 species had sufficient frequencies of occurrence to model at IP and MH respectively (i.e., 71 species-site combinations).

Models

Of the 71 species-site combinations that we attempted to model, only 16 had a single model surface as the best model by having an Akaike's weight (ω_i) > 0.5 (bolded in Table C.2). All but one of these 16 species also had $\text{Adj. } R^2 > 0.2$ for the top model,

Table 3.5. Bird species frequency of occurrence at International Paper (IP; n = 99) and Moosehorn National Wildlife Refuge (MH; n = 114) for species that were detected ≥ 1 in either 2002, 2003, or 2004.

Mean occurrence ≥ 10 of bird points				Mean occurrence < 10 of bird points			
Species ¹	IP	MH	Mean	Species ¹	IP	MH	Mean
MAWA	85	62	74	WBNU	17	0	9
OVEN	75	64	70	CEDW	10	7	9
WTSP	84	41	63	LISP	15	0	8
BCCH	77	49	63	BHVI	0	16	8
BAWW	80	42	61	DEJU	12	3	8
NAWA	84	32	58	SOSP	12	0	6
COYE	81	30	56	MODO	10	1	6
REVI	77	30	54	RCKI	8	2	5
HETH	75	24	50	GCFL	5	5	5
BTNW	75	25	50	RTHU	3	4	4
YRWA	69	24	47	PIWO	3	4	4
YBSA	69	15	42	MOWA	7	0	4
NOPA	63	18	41	GRAJ	7	0	4
AMRO	71	10	41	GRCA	5	0	3
RBNU	68	9	39	WOTH	3	0	2
PUFI	58	6	32	SAVS	3	0	2
BLBW	46	18	32	PISI	3	0	2
BTBW	49	12	31	NOWA	2	2	2
BLJA	57	4	31	COGR	2	1	2
GCKI	48	11	30	AMGO	3	1	2
VEER	47	11	29	WIWA	2	0	1
SOVI	57	0	29	TRES	1	0	1
CAWA	35	18	27	RWBL	0	1	1
PAWA	37	11	24	PHVI	2	0	1
YBFL	40	3	22	OSFL	2	0	1
CSWA	39	4	22	INBU	2	0	1
BRCR	29	15	22	EVGR	2	0	1
HAWO	35	6	21	EWPH	1	0	1
WIWR	33	4	19	EAKI	1	1	1
DOWO	30	7	19	CORA	1	0	1
YSFL	30	5	18	CONI	1	0	1
PIWA	25	10	18	CMWA	1	0	1
EAWP	25	9	17	BOCH	2	0	1
LEFL	21	11	16	BBWO	1	0	1
AMRE	25	4	15	BBCU	1	1	1
SCTA	14	11	13	AMWO	0	1	1
SWTH	20	3	12	AMCR	2	0	1
BBWA	19	5	12	YWAR	1	0	1
ALFL	19	4	12				
RBGR	15	6	11				

¹Species codes using American Ornithologists' Union (AOU), are defined in Table C.1. 3.2).

with 4 of 16 having Adj. $R^2 > 0.4$ (bolded in Table C.2). Thirty-two of the 71 modeling efforts for species-site combinations had Adj. $R^2 > 0.2$ for the top model, albeit not necessarily with an $\omega_i > 0.5$, with four having Adj. $R^2 > 0.5$ (bolded in Table C.2). Mean species richness and diversity did not have a single model surface as best model using the same criteria of $\omega_i > 0.5$. However, both species richness and diversity at the IP study site yielded models with Adj. $R^2 > 0.6$ indicating that LiDAR can predict reasonably well these diversity metrics at least at some study sites. Although these modeling results for each individual species might not be considered outstanding with respect to the percent variation explained, they do indicate that for at least some species at one of the two sites, or both, a suite of plausible models tested with LiDAR-derived explanatory yield some predictive ability (e.g., 22 species-site combinations had Adj. PRESS $R^2 > 0.2$, bolded in Table C.2). Plotting observed mean abundance versus LiDAR-predicted mean abundance indicates further that for several species a reasonable 1-to-1 correspondence was found (Fig. 3.3.a – 3.3.f). Further visual inspection of these plots indicate that for several species, if not most, LiDAR-derived explanatory variables tended to over-predict abundance involving small observed mean counts, especially zero mean counts, and to under-predict larger counts at both study sites. Bivariate plots of observed diversity metrics versus LiDAR-predicted metrics indicate no biases at the IP study site and no predictive ability at the MH site (Fig. 3.4).

Other than the 16 models that had $\omega_i > 0.5$, interpretation of the appropriate model scale becomes difficult because most of the remaining top three models were derived from varying scales (Table C.2). Because our goal was to develop and assess models for their predictive ability that could potentially be incorporated into an updated version of

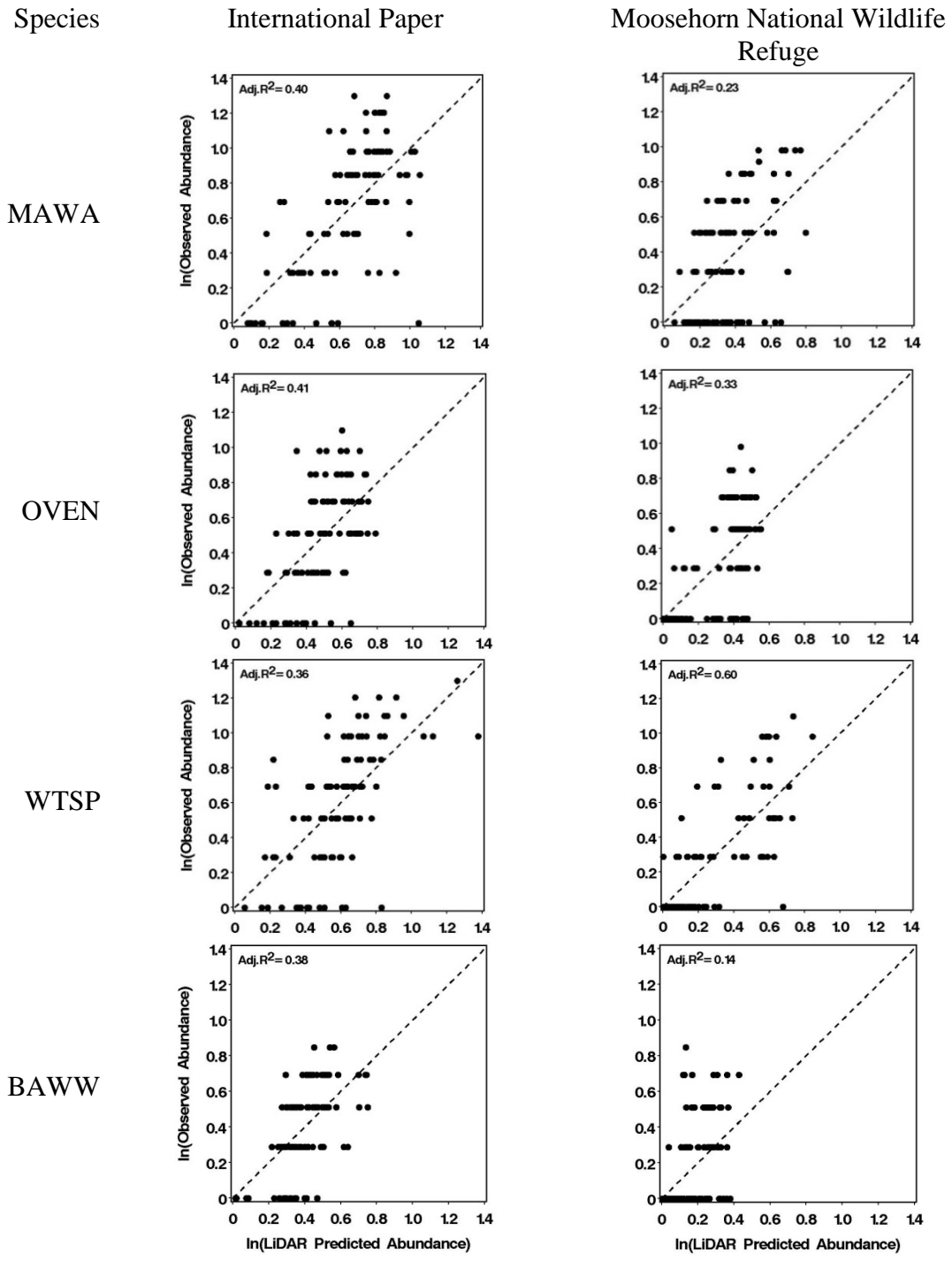


Figure 3.3.a. Observed versus LiDAR-predicted bird abundance at two forest study sites in Maine (dashed lines indicate 1-to-1 correspondence, species codes are in Table C.1.).

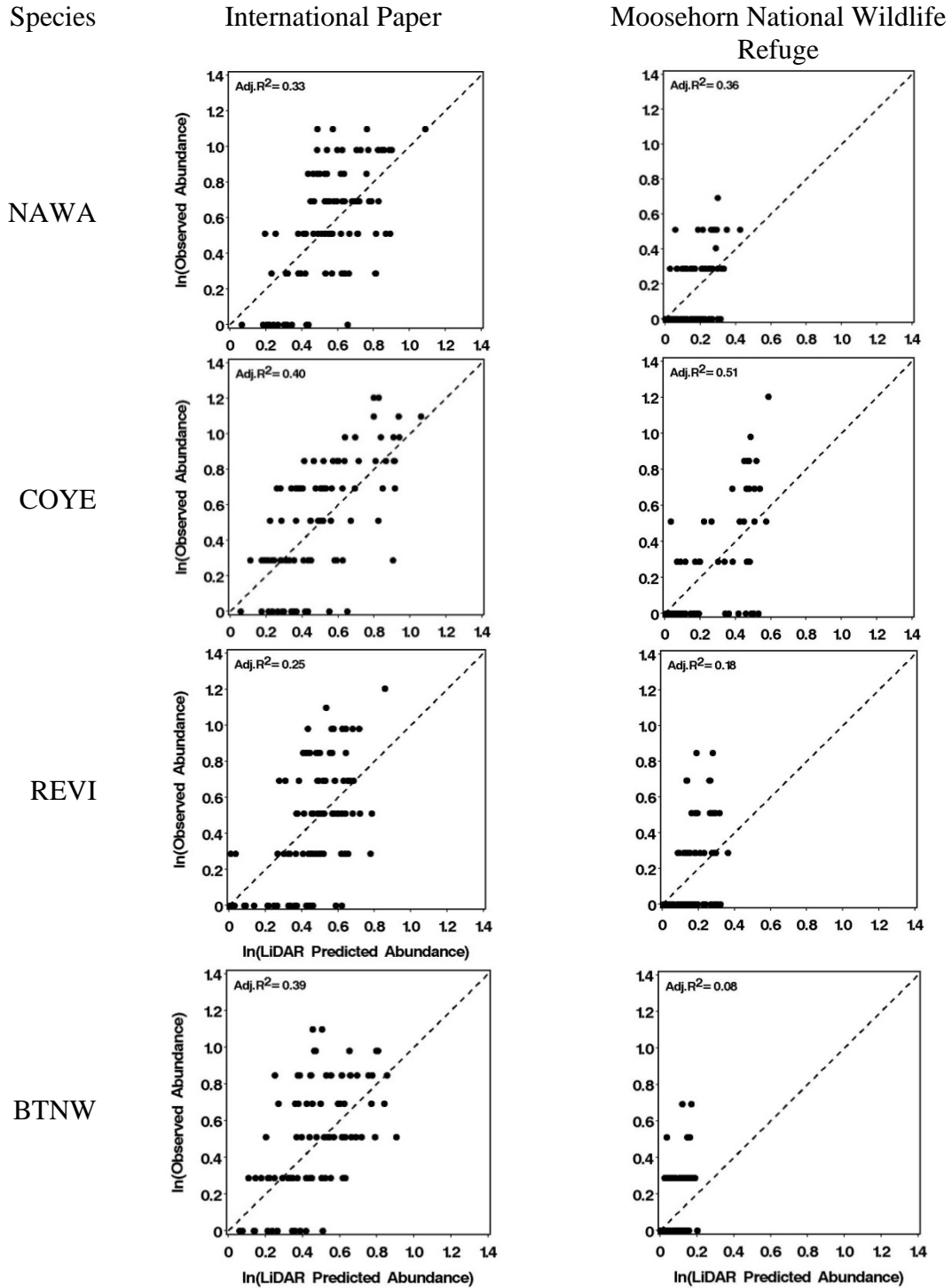


Figure 3.3.b. Observed versus LiDAR-predicted bird abundance at two forest study sites in Maine (dashed lines indicate 1-to-1 correspondence, species codes are in Table C.1.).

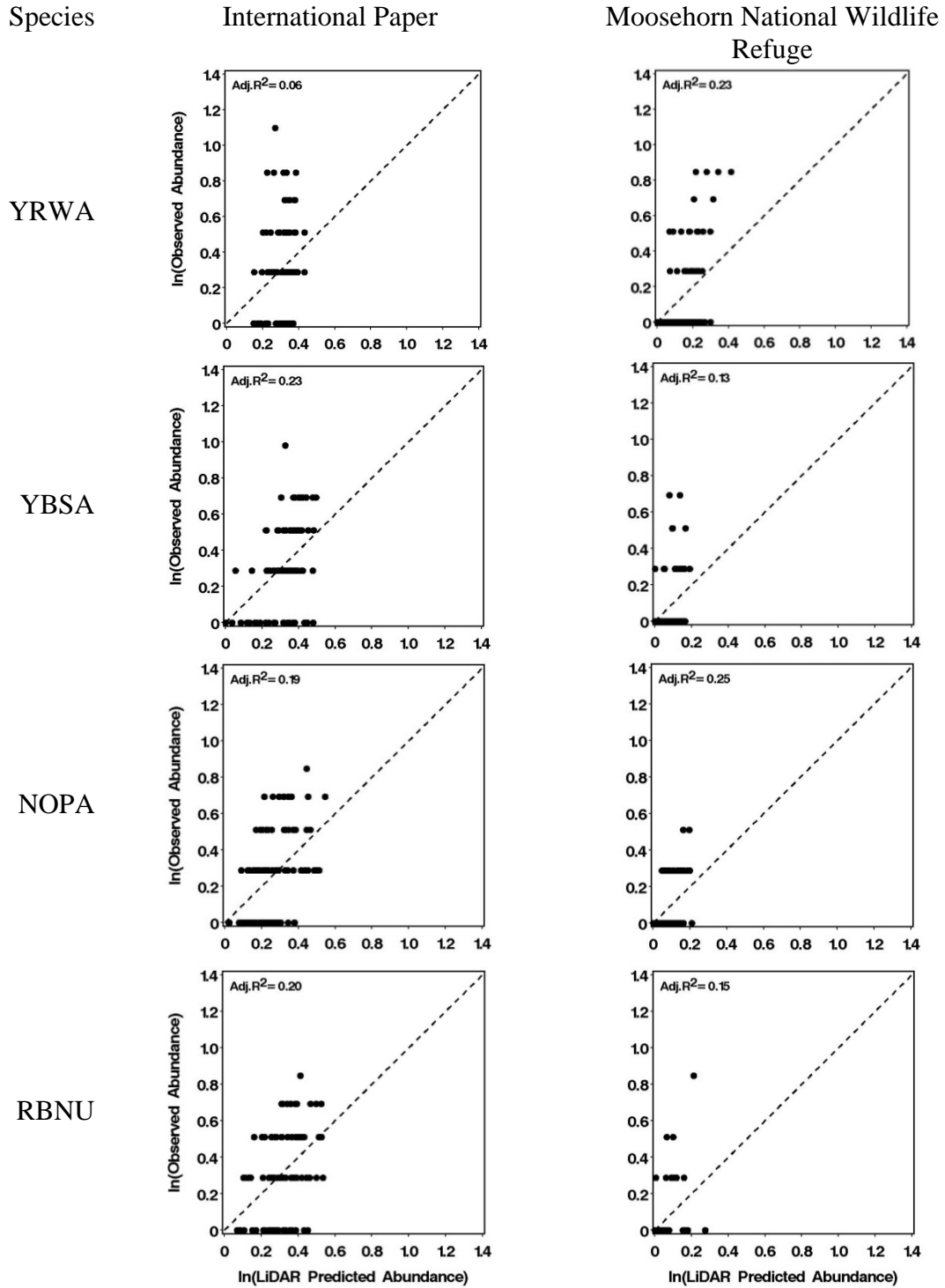


Figure 3.3.c. Observed versus LiDAR-predicted bird abundance at two forest study sites in Maine (dashed lines indicate 1-to-1 correspondence, species codes are in Table C.1.).

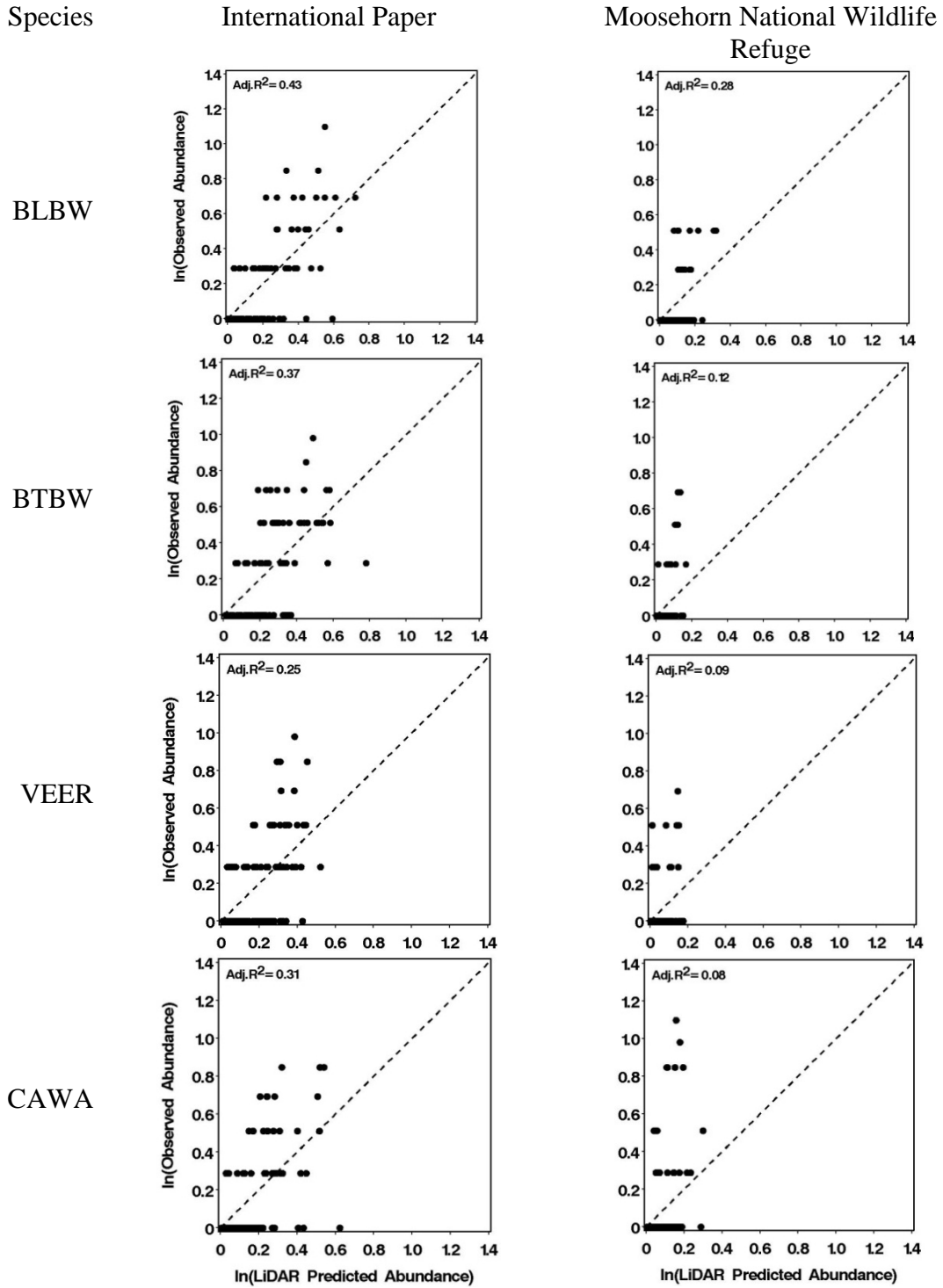


Figure 3.3.d. Observed versus LiDAR-predicted bird abundance at two forest study sites in Maine (dashed lines indicate 1-to-1 correspondence, species codes are in Table C.1.).

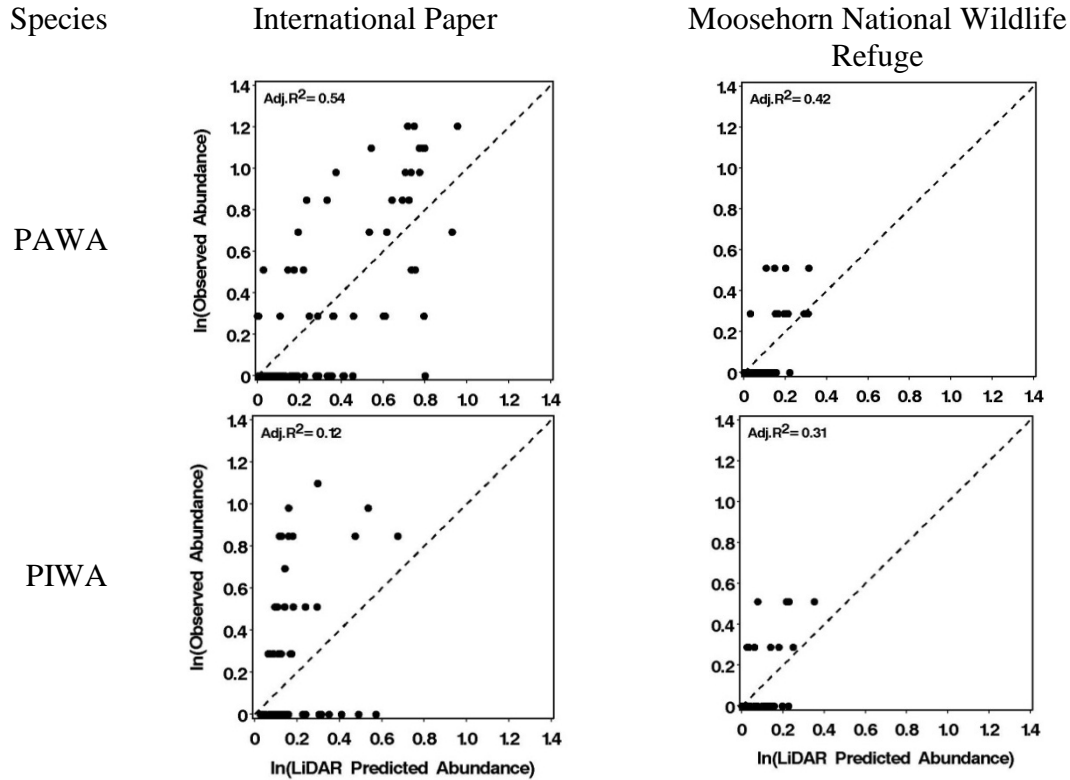


Figure 3.3.e. Observed versus LiDAR-predicted bird abundance at two forest study sites in Maine (dashed lines indicate 1-to-1 correspondence, species codes are in Table C.1.).

ECOSEARCH, we computed and report in Table C.3 the model coefficients with their respective standard errors (SE) for the top model only as ranked by ΔAIC_C (regardless of ω_i). We report in Table 3.6 the scale and directionality of model parameters for each of the 32 species-site combinations with $Adj. R^2 > 0.2$. We chose not to model average across models because doing so is still an active area of research in statistics (Claiskens and Hjort 2008) and regardless of the model, the $Adj. R^2$ values were nearly the same for the top three models (Table C.2).

Table 3.6 reveals that 13, 10, and 4 of the species-site combinations indicate reasonable models at the 5×5 grid, 3×3 grid, and the center cell respectively. The remaining five of the 32 species-site combinations with 50-m radii (two species-site combinations) and 100-m radii (three species-site combinations) are potentially useful

Species

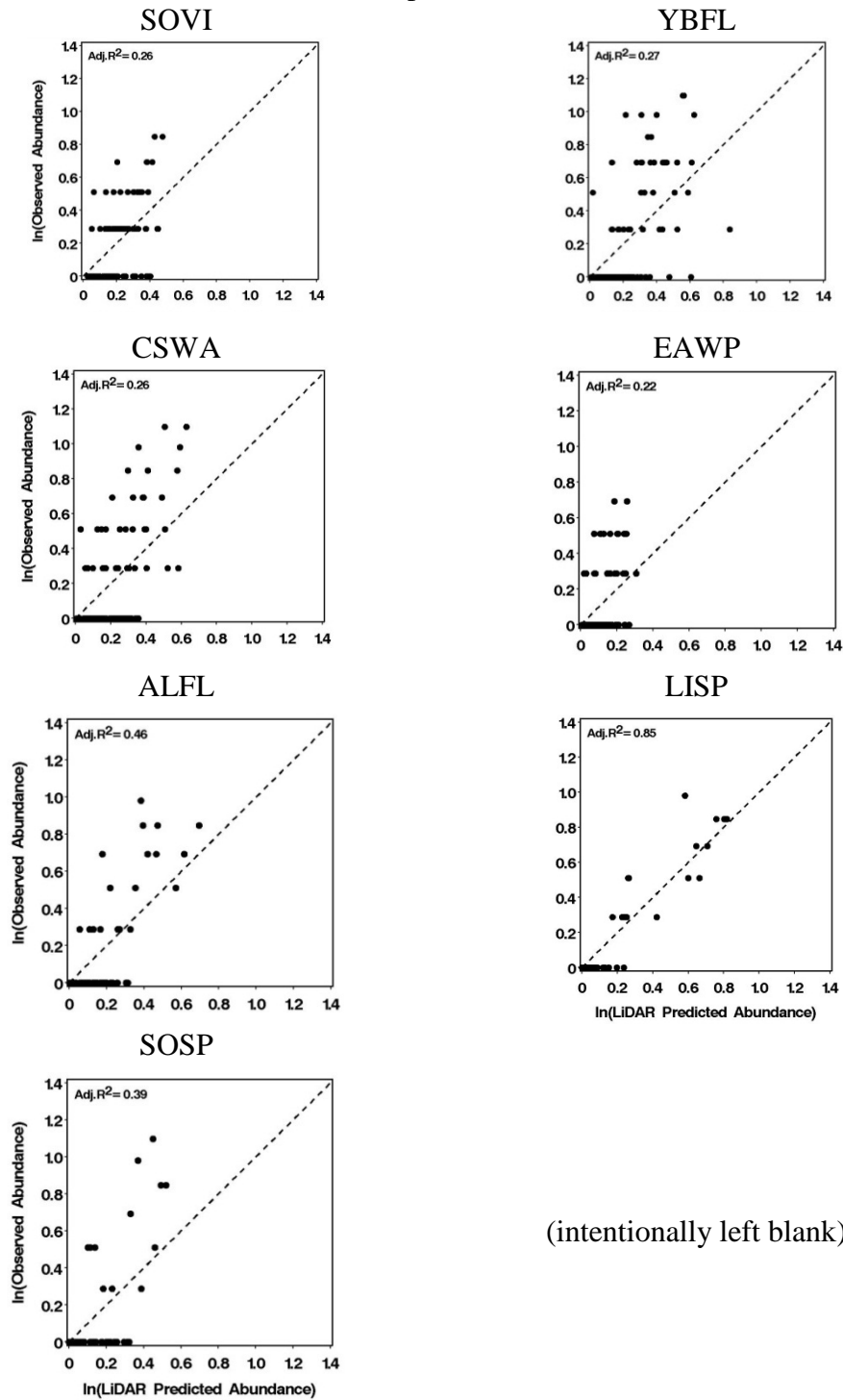


Figure 3.3.f. Observed versus LiDAR-predicted bird abundance at International Paper only (dashed lines indicate 1-to-1 correspondence, species codes are in Table C.1.).

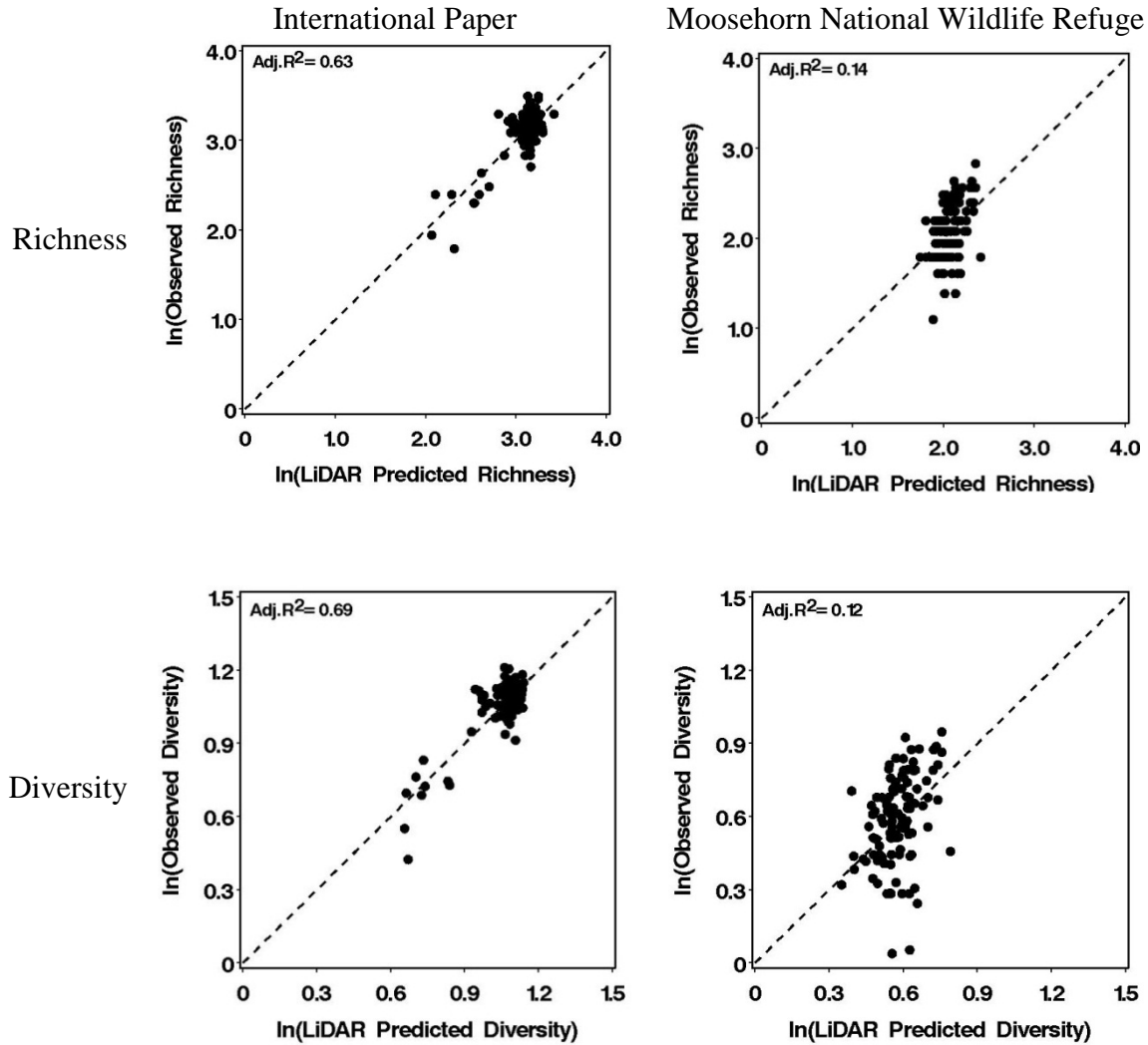


Figure 3.4. Observed vs LiDAR-predicted species richness and diversity at two forest study sites in Maine (dashed lines indicate 1-to-1 correspondence).

models. This indicates that, in general, the scale of the model varies with species-site combinations, with most requiring that consideration should be taken for LiDAR-derived explanatory variables outside the center 50×50 m cell.

It was somewhat disconcerting that consistency between sites for each species was not found. For example, Magnolia Warbler (MAWA) revealed models at the 3×3 grid scale as being useful at both IP and MH, albeit slightly less so at MH. However, the directionality of the coefficients for X11 and X12 were opposite, negative at IP, positive

Table 3.6. Summary of best bird models for which Adj. R² were greater than 0.20.

Species ¹	Site ²	Model no. ³	Scale	Adj. R ²	Parameter directions
MAWA	IP	14	3×3 (150 m)	0.40	-X11, +X12, -X30, -X32
	MH	13	3×3 (150 m)	0.23	+X11, -X12, +X29, +X31, +X33
OVEN	IP	24	5×5 (250 m)	0.41	-X44, +X45, -X67, -X69, -X71
	MH	3	Center (50 m)	0.33	-X0, -X1, -X3, -X5
WTSP	IP	22	5×5 (250 m)	0.36	+X44, +X45, +X62, +X64, +X66
	MH	30	100 m radii	0.60	-X79, +X0, +X1, +X3, +X5
BAWW	IP	9	3×3 (150 m)	0.38	+X11, +X12, +X14, +X16, +X18
NAWA	IP	19	5×5 (250 m)	0.33	+X44, -X45, +X48, +X50
	MH	30	100 m radii	0.35	-X79, +X0, -X1, +X3, +X5
COYE	IP	15	3×3 (150 m)	0.40	+X11, +X12, +X34, +X36, +X38
	MH	3	Center (50 m)	0.51	+X0, +X1, +X3, -X5
REVI	IP	24	5×5 (250 m)	0.25	-X44, +X45, -X67, -X69, -X71
BTNW	IP	40	Center (50 m) + 100 m radii	0.39	-X77, +X81
YRWA	MH	23	5×5 (250 m)	0.23	-X44, +X45, -X63, +X65
YBSA	IP	21	5×5 (250 m)	0.23	-X44, +X45, -X53, +X55
NOPA	MH	6	Center (50 m)	0.25	+X0, -X8, +X25, +X10
RBNU	IP	13	3×3 (150 m)	0.20	+X11, +X12, +X29, +X31, +X33
BLBW	IP	14	3×3 (150 m)	0.43	+X11, -X12, +X30, +X32
	MH	27	50 m radii	0.28	+X78
BTBW	IP	23	5×5 (250 m)	0.37	+X44, +X45, +X63, +X65
VEER	IP	10	3×3 (150 m)	0.25	+X11, -X12, +X15, +X17
SOVI	IP	26	50 m radii	0.26	+X77
CAWA	IP	18	5×5 (250 m)	0.31	-X44, -X45, -X47, -X49, -X51

Table 3.6. Continued.

Species ¹	Site ²	Model no. ³	Scale	Adj. R ²	Parameter directions
PAWA	IP	11	3×3 (150 m)	0.54	+X11, +X12, +X19, +X21, -X23
	MH	9	3×3 (150 m)	0.42	+X11, -X12, +X14, -X16, -X18
YBFL	IP	21	5×5 (250 m)	0.27	+X44, -X45, -X53, +X55
CSWA	IP	18	5×5 (250 m)	0.26	+X44, +X45, +X47, -X49, +X51
PIWA	MH	13	3×3 (150 m)	0.31	-X0, +X8, -X9, +X10
EAWP	IP	28	100 m radii	0.22	+X79
ALFL	IP	18	5×5 (250 m)	0.46	+X44, -X45, +X47, +X49, +X51
LISP	IP	19	5×5 (250 m)	0.85	+X44, -X45, -X48, +X50
SOSP	IP	18	5×5 (250 m)	0.39	-X44, +X45, +X47, -X49, -X51
SR	IP	18	5×5 (250 m)	0.63	-X44, +X45, +X47, -X49, -X51
	MH	6	Center (50 m)	0.14	-X0, -X8, +X9, +X10
SD	IP	9	3×3 (150 m)	0.69	-X11, +X12, +X14, -X16, +X18
	MH	6	Center (50 m)	0.12	-X0, -X8, +X9, +X10

¹Species codes using American Ornithologists' Union (AOU), are defined in Table C.1; SR=species richness, SD=species diversity (Shannon-Weaver).

²IP=International Paper, MH=Moosehorn National Wildlife Refuge.

³Model number and descriptions are listed in Tables 3.4.a. and 3.4.b.

at MH. This also created opposite directionality of coefficients in the remaining models that summarized the mean vertical canopy profile (variables X29-X33), positive at MH, negative at IP. For the Common Yellowthroat (COYE) we found inconsistent scales, with models at IP being useful at the 3×3 grid whereas only the center cell model being needed at MH, with both sites having good predictive ability (i.e., Adj. $R^2 > 0.40$ at both sites). Other inconsistencies can be found among the other species-site combinations in Table 3.6. Here, inconsistency does not necessarily translate into poor models per se, but rather emphasizes that the best models and the scale of the model vary between sites.

Discussion

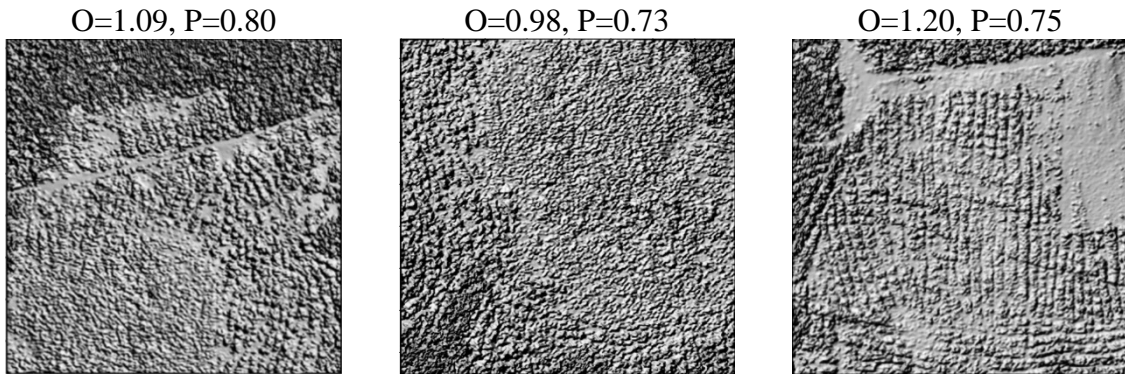
Investigating wildlife-habitat relationships in many habitats has a long history in wildlife ecology and management and continues to occupy a great deal of time, effort and resources (Morrison et al. 2006). Our results indicate that LiDAR can successfully model the mean abundance of several bird species in the Northwoods of Maine. However, interpreting such models from a natural-history perspective is challenging due to inconsistencies among top models. This challenge is exacerbated within study sites due to varying scales but with equally competitive models surfacing in their predictive ability. If the proximate goal is to develop a suite of predictive models, this is fine, especially if parsimonious models can be selected, or models averaged. However, if the ultimate goal is to understand the habitat-relationships, the model-selection framework will make these interpretations more challenging.

For common species with reasonable habitat models, managers can apply the results of these models in their forest management and planning. For example, the models for Palm Warbler (PAWA) indicated the best model at IP to be at the 3×3 grid

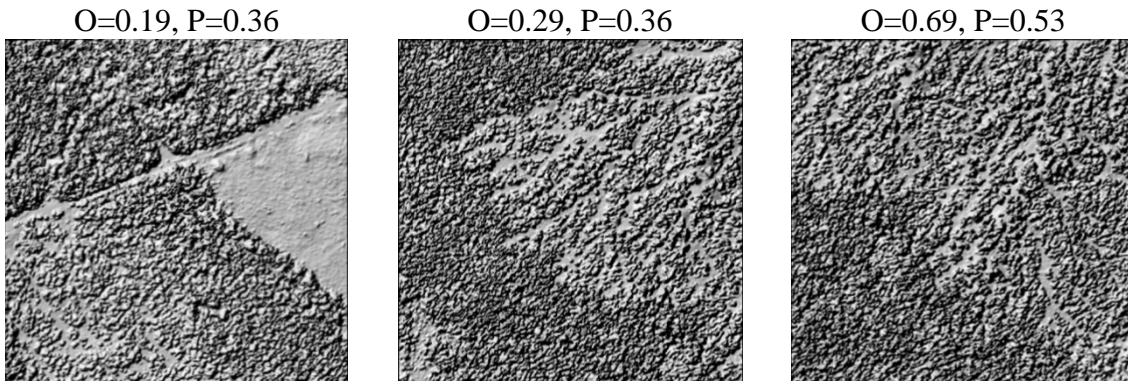
scale (model 11, Table 3.4.a) with all coefficients being positive for X11, X12, X19, and X21 (which summarize the mean and variation of low canopy out to 150 m) and negatively correlated with variation in taller canopies out to 150 m (Table 3.6). As discussed in Appendix B, interpreting these parameters and the habitat structure can sometimes be more easily done visually. Figure 3.5 presents a shaded-relief of first-return LiDAR data in a 400×400 m block for three replicate bird survey points with declining mean abundance for PAWA (top to bottom). For each of the shaded-relief images in Fig. 3.5, we present the LiDAR-derived 3-m vertical profiles for each 50×50 m cell for a 5×5 grid in Fig. 3.6 (here these 5×5 grid cells represent a 250×250 m block, less in size than the blocks presented in Fig. 3.5). From these vertical profiles in Fig. 3.6, it is apparent that mean abundance of PAWA declines with increasing mean canopy height (and variation in heights) and slightly less apparent with increasing variation in the understory, at least as represented by the 0-3 m profile (modeling was done using the X's shown in Table 3.1.a). Processing these vertical profile variables for each 50×50 m cell through the forest metric models developed in Chapter 2, we predicted the various forest metrics required by the SAS program described in Appendix B. We then rendered in 3D what these cells might look like for increasing mean abundance of PAWA (Fig. 3.7). As with the images presented in Figs. 3.5 and 3.6, the visualization provided in Fig. 3.7 provides an opportunity to improve interpretation of “habitat” for PAWA, especially when referenced with the empirical models and their coefficients as presented in Table C.3.

The models presented in Table C.3 can be incorporated into an updated version of ECOSEARCH, although not a trivial process and not without extensive programming

High PAWA abundance (log transformed mean counts)



Medium PAWA abundance (log transformed mean counts)



Low PAWA abundance (log transformed mean counts)

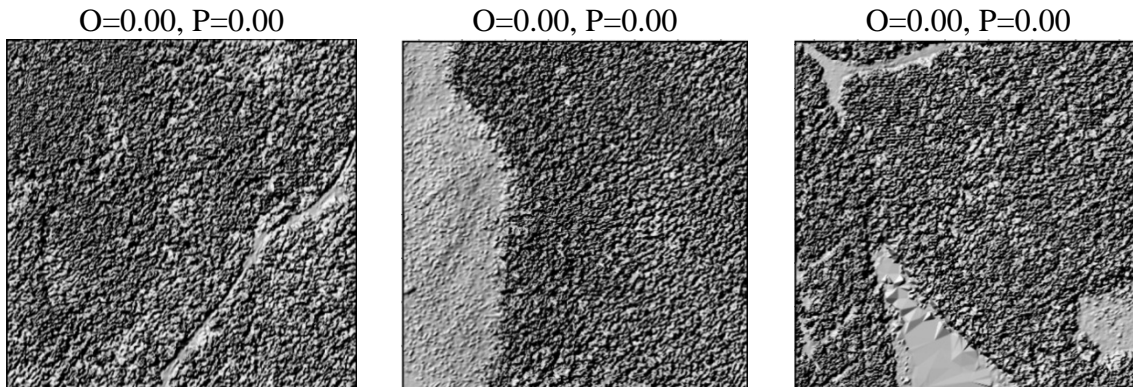
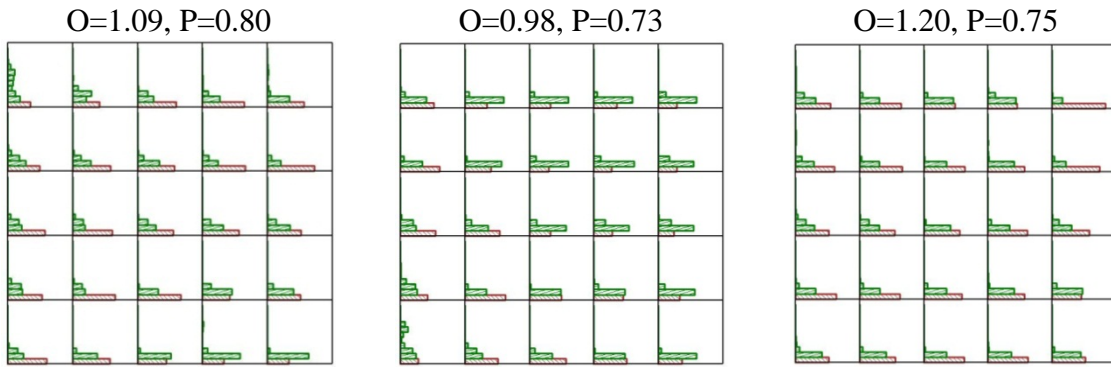
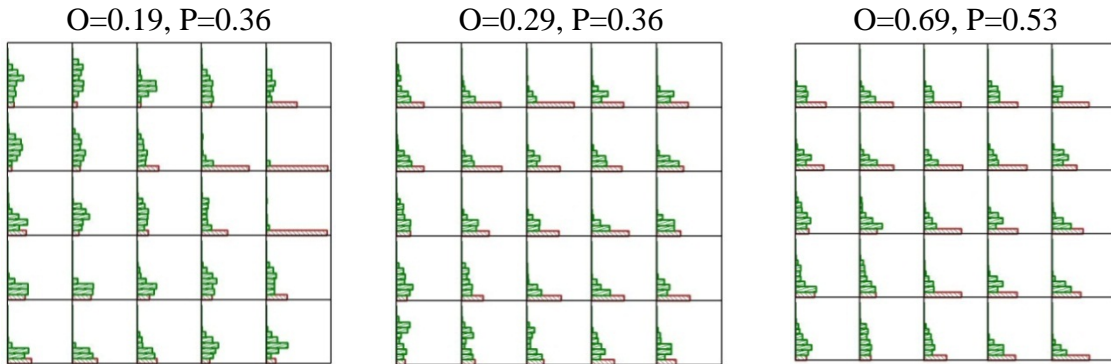


Figure 3.5. LiDAR-derived TIN-interpolated shaded-relief surface model for nine example bird survey points for 3 levels of Palm Warbler (PAWA) abundance at International Paper lands in Maine (O=observed, P=predicted; images are 400×400 m centered on 50 m radii bird survey point, see Table C.1 for species code).

High PAWA abundance (log transformed mean counts)



Medium PAWA abundance (log transformed mean counts)



Low PAWA abundance (log transformed mean counts)

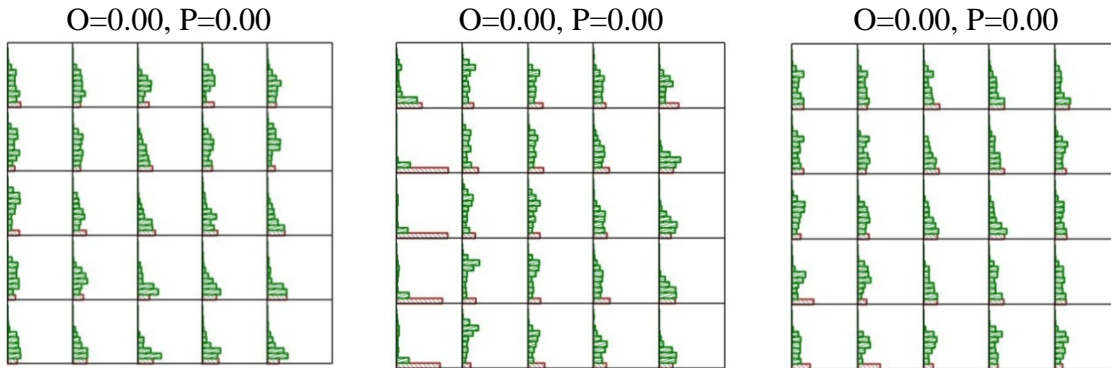
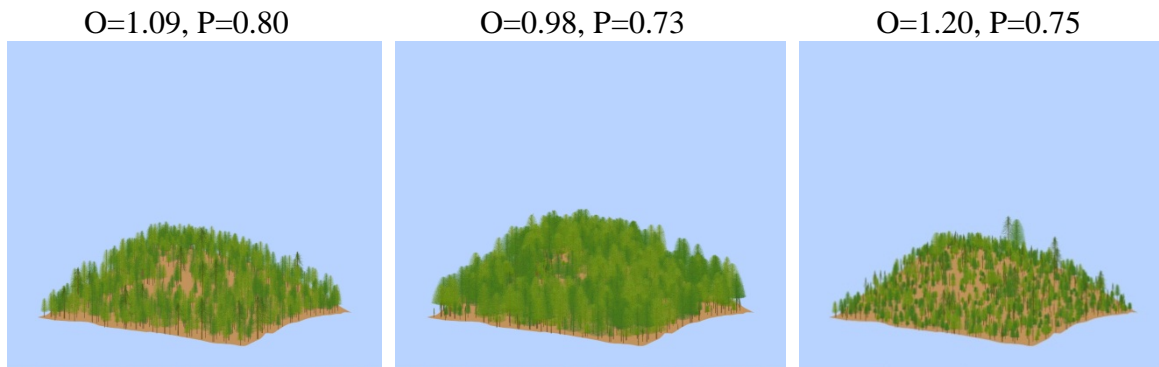
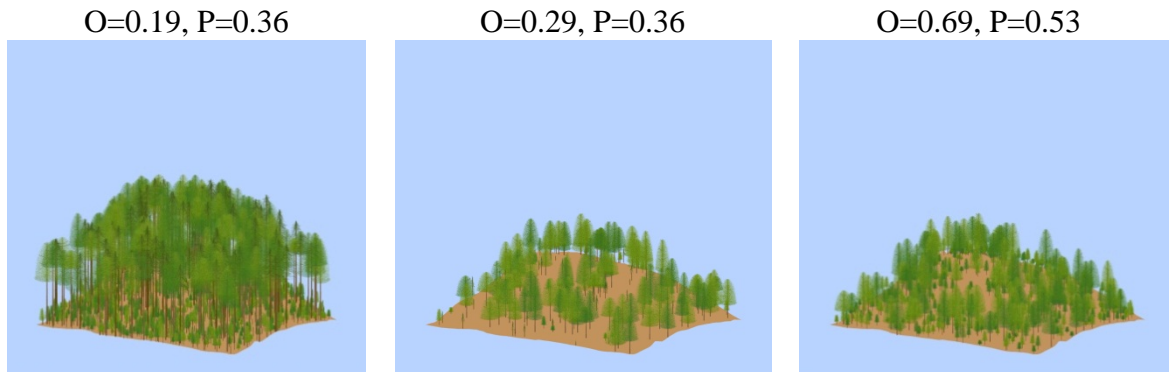


Figure 3.6. LiDAR-derived vertical height profiles at 9 example bird survey points for 3 levels of Palm Warbler (PAWA) abundance at International Paper lands in Maine (O=observed, P=predicted; cells are 50×50 m with center cell centered on 50 m radii bird survey point, see Table C.1 for species code).

High PAWA abundance (log transformed mean counts)



Medium PAWA Abundance (log transformed mean counts)



Low PAWA Abundance (log transformed mean counts)

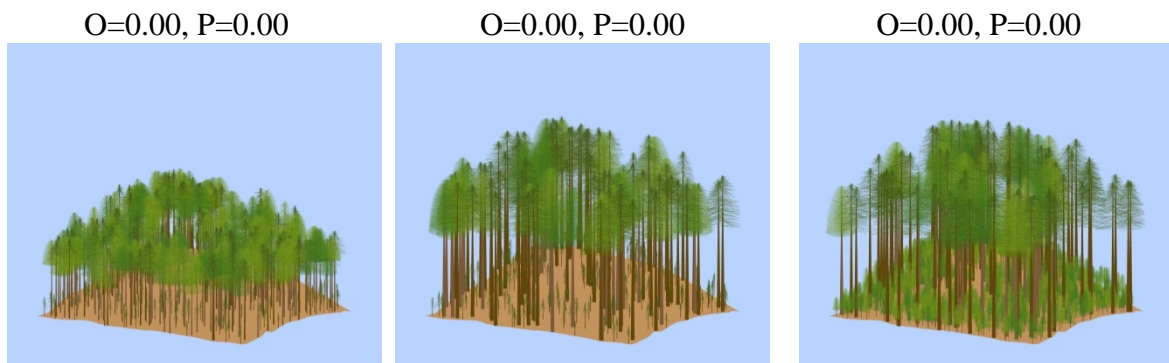
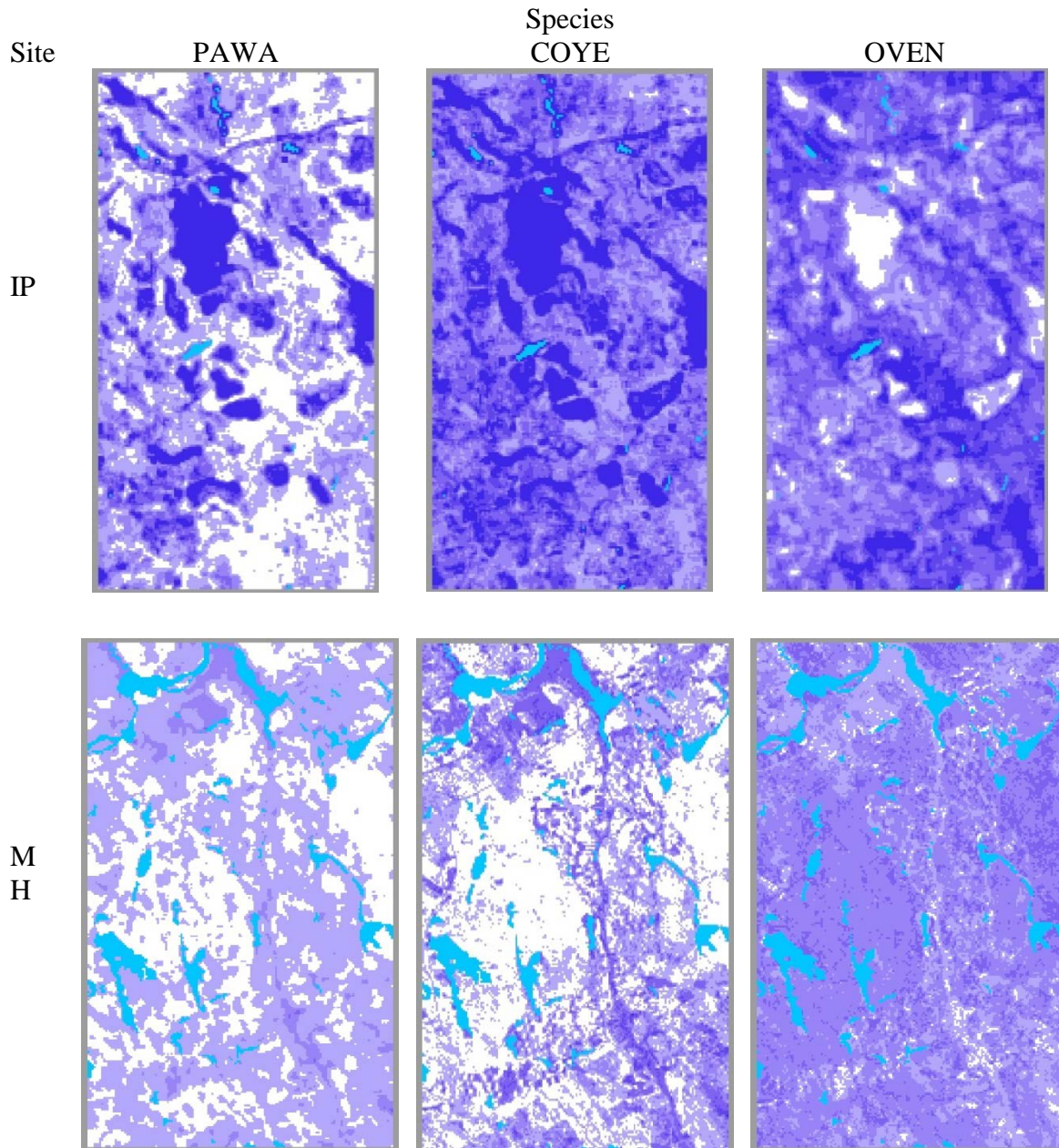


Figure 3.7. Three-dimensional visualization of simulated Palm Warbler at the center 50×50 m stands from Figure 3.5 using SAS program described in Appendix B (assumed mixed softwoods and hardwoods).

(e.g., processing and summarizing LiDAR data). Also, the models were built using LiDAR flown during leaf-on conditions, which would most likely preclude their use for LiDAR flown in leaf-off conditions. We applied the models for Palm Warblers, Common Yellowthroats, and Ovenbirds across the entire acquisition areas at IP (30,720 50×50 m cells) and MH (41,396 50×50 m cells), accommodating water and bogs, at both study sites to generate “habitat” maps of mean abundance (Fig. 3.8). Recognizing that abundance may not equate to habitat quality (Van Horne 1983), these 50-m pixel habitat maps are similar to the product maps currently generated by ECOSEARCH except LiDAR-predicted abundance estimates are provided instead of non-statistically based occurrence.

There are most likely numerous ways to improve the modeling effort. We used simple univariate multiple linear regression methods under an IT framework. As pointed out in Chapter 2, there is a large suite of alternative modeling methods available (e.g., Franklin 2009, Drew et al. 2011). However, all of these methods still require that both the response variable of interest and LiDAR-derived explanatory variables are quantified accurately and precisely. Multicollinearity among the explanatory variables would still need to be addressed, which is not always straightforward (Elith and Leathwick 2009). Often times a great deal of effort is expended to improve the accuracy and precision of explanatory variables, and using the latest fashionable modeling method, but ignore the left-hand side of the model (i.e., the precision and accuracy of the response variable itself). Other improvements should include more reliable and consistent estimates of bird abundance on the survey points, either by using distance-based approaches or having several bird surveyors survey each point multiple times within a survey season, or use




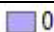

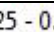
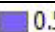
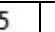
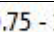
Predicted bird abundance (number of birds/0.25 ha)						Water
						

Figure 3.8. Example predicted maps for PAWA, COYE, and OVEN at International Paper (IP) (6.4×12.0 km) and Moosehorn National Wildlife Refuge (MH) (7.9×13.1 km); not drawn to scale, cells represent 50×50 m (0.25 ha), species codes for PAWA, COYE, and OVEN are in Table C.1.

both approaches. We feel the forest metric models presented in Chapter 2 and these bird abundance models are a good first step in developing spatially-explicit predictions across a landscape and can be viewed as a base-line approach to improving ECOSEARCH. Further improvement might include incorporating known natural history parameters, other GIS data layers, utilizing higher-resolution imagery, and eventually incorporating population demographics and species interactions. Intraspecific variation, temporal and environmental stochasticity, conditions in overwintering areas, migratory routes, and now climatic change also can limit the predictive capacity of any model.

Literature Cited

- Betts, M.G., N.P.P. Simon, and J.J. Nocera. 2005. Point count summary statistics differentially predict reproductive activity in bird-habitat relationship studies. *Journal of Ornithology* 146:151-159.
- Broughton, R.K., S.A. Hinsley, P.E. Bellamy, R.A. Hill, and P. Rothery. 2006. Marsh tit *Poecile palustris* territories in a British broad-leaved wood. *Ibis* 148:744-752.
- Burger, J. 1994. The effect of human disturbance on foraging behavior and habitat use in Piping Plover (*Charadrius melodus*). *Estuaries and Coasts* 17:695-701.
- Burnham, K.P., and D.R. Anderson. 2002. Model selection and multi-model inference, 2nd edition. Springer-Verlag, Inc., New York, New York.
- Christensen, N.L., A.M. Bartuska, J.H. Brown, S. Carpenter, C. D'Antonio, R. Francis, J.F. Franklin, J.A. MacMahon, R.F. Noss, D.J. Parsons, C.H. Peterson, M.G. Turner, and R.G. Woodmansee. 1996. The report of the Ecological Society of America committee on the scientific basis for ecosystem management. *Ecological Applications* 6:665-691

- Claeskens, G., and N.L. Hjort. 2008. Model selection and model averaging. Cambridge University Press, Cambridge, United Kingdom.
- Clawges, R., K. Vierling, L. Vierling, and E. Rowell. 2008. The use of airborne lidar to assess avian species diversity, density, and occurrence in a pine/aspen forest. *Remote Sensing of Environment* 112:2064-2073.
- Cody, M.L. 1981. Habitat selection in birds: the roles of vegetation structure, competitors, and productivity. *BioScience* 31:107-113.
- Crozier, G.E., and G.J. Niemi. 2003. Using patch and landscape variables to model bird abundance in a naturally heterogeneous landscape. *Canadian Journal of Zoology* 81:441-452.
- Davenport, I.J., R.B. Bradbury, G.Q.A. Anderson, G.R.F. Hayman, J.R. Krebs, D.C. Mason, J.D. Wilson, and N.J. Veck. 2000. Improving bird population models using airborne remote sensing. *International Journal of Remote Sensing* 21:2705-2717.
- DeGraaf, R.M., M. Yamasaki, W.B. Leak, and J.W. Lanier. 1992. New England wildlife: management of forested habitats. Northeastern Forest Experiment Station, GTR NE-144, Radnor, Pennsylvania.
- DeGraaf, R.M., J.B. Hestbeck, and M. Yamasaki. 1998. Associations between breeding bird abundance and stand structure in the White Mountains, New Hampshire and Maine, USA. *Forest Ecology and Management* 103:217-233.
- DeGraaf, R.M., and M. Yamasaki. 2001. New England wildlife: habitat, natural history, and distribution. Hanover, NY: University Press New England. 482pp.

- Dessecker, D.R. and D.G. McAuley. 2001. Importance of early successional habitat to ruffed grouse and American woodcock. *Wildlife Society Bulletin* 29:456-465.
- Drew, C.A., Y.F. Wiersma, and F. Huettmann. (Editors). 2011. Predictive species and habitat modeling in landscape ecology: concepts and applications. Springer, New York, New York.
- Ehrlich, P.R., D.S. Dobkin, and D. Wheye. 1988. The birder's handbook: a field guide to the natural history of North American birds, the essential companion to your identification guide. Simon and Schuster, Inc., New York, New York.
- Elith, J., and J. Leathwick. 2009. The contribution of species distribution modeling to conservation prioritization. Pages 70-93 *In* Spatial conservation prioritization: quantitative methods and computational tools (A. Moilanen, K.A. Wilson, and H.P. Possingham. Editors). Oxford University Press. Oxford, United Kingdom.
- Franklin, J. 2009. Mapping species distributions: spatial inference and prediction. Cambridge University Press, Cambridge, United Kingdom.
- Giorgi, K.S.H. 1999. Evaluation of ECOSEARCH: a wildlife-habitat model for predicting species occurrence. M.S. Thesis, Wildlife and Fisheries Conservation, University of Massachusetts, Amherst, Massachusetts.
- Graham, M.H. 2003. Confronting multicollinearity in ecological multiple regression. *Ecology* 84:2809-2815.
- Grumbine, R.E. 1994. What is ecosystem management? *Conservation Biology* 8:27-38.
- Harding, D.J., and G.S. Berghoff. 2000. Fault scarp detection beneath dense vegetation cover: airborne lidar mapping of the Seattle fault zone, Banbridge Island, Washington State. *Proceedings of the American Society of Photogrammetry and*

- Remote Sensing Annual Conference, May, 2000, Washington, District of Columbia.
- Hilldale, R.C., and D. Raff. 2007. Assessing the ability of airborne lidar to map river bathymetry. *Earth Surface Processes and Landforms* 33:773-783.
- Hinsley, S.A., R.A. Hill, D.L.A. Gaveau, and P.E. Bellamy. 2002. Quantifying woodland structure and habitat quality for birds using airborne laser scanning. *Functional Ecology* 16:851-857.
- Hirzel, A., and A. Guisan. 2002. Which is the optimal sampling strategy for habitat suitability modelling. *Ecological Modelling* 157:331-341.
- Hyde, P., R. Dubayah, W. Walker, J.B. Blair, M. Hofton, and C. Hunsaker. 2006. Mapping forest structure for wildlife habitat analysis using multi-sensor (LiDAR, SAR/InSAR, ETM+, Quickbird) synergy. *Remote Sensing of Environment* 102:63-73.
- James, F.C. 1971. Ordinations of habitat relationships among breeding birds. *The Wilson Bulletin* 83:215-236.
- Johnson, D.H. 1980. The comparison of usage and available measurements for evaluating resource preference. *Ecology* 61:65-71.
- Johnson, D.H. 2008. In defense of indices: the case of bird surveys. *Journal of Wildlife Management* 72:857-868.
- Kirk, D.A., and K.A. Hobson. 2001. Bird-habitat relationships in jack pine boreal forests. *Forest Ecology and Management* 147:217-243.
- Korpela, I.S. 2008. Mapping understory lichens with airborne discrete-return lidar data. *Remote Sensing of Environment* 112:3891-3897.

- Küchler, A.W. 1964. Potential natural vegetation of the conterminous United States. American Geographic Society Special Publication No. 36. New York, New York.
- Lefsky, M.A., W.B. Cohen, G.G. Parker, and D.J. Harding. 2002. Lidar remote sensing for ecosystem studies. *BioScience* 52:19-30.
- MacKenzie, D.I., J.D. Nichols, J.A. Royle, K.H. Pollock, L.L. Bailey, and J.E. Hines. 2006. Occupancy estimation and modeling: inferring patterns and dynamics of species occurrence. Academic Press, Burlington, Massachusetts.
- McKean, J.A., D.J. Isaak, C.W. Wright. 2008. Geomorphic controls on salmon nesting patterns described by a new, narrow-beam terrestrial-aquatic lidar. *Frontiers in Ecology and Environment* 6:125-130.
- Mitchell, M.S., R.A. Lancia, and J.A. Gerwini. 2001. Using landscape-level data to predict the distribution of birds on managed forests: effects of scale. *Ecological Applications* 11:1692-1708.
- Morrison, M.L., B.G. Marcot, and R.W. Mannan. 2006. Wildlife-habitat relationships: concepts and applications. Island Press, Washington, District of Columbia.
- Muller, J., and R. Brandi. 2009. Assessing biodiversity by remote sensing in mountainous terrain: the potential of lidar to predict forest beetle assemblages. *Journal of Applied Ecology* 46:897-905.
- Myers, R.H. 1990. Classical and modern regression with applications, 2nd edition. PWS-Kent Pub. Boston, Massachusetts.
- Nelson, R., C. Keller, and M. Ratnaswamy. 2005. Locating and estimating the extent of Delmarva fox squirrel habitat using an airborne lidar profiler. *Remote Sensing of Environment* 96:292-301.

- Neter, J., M.H. Kutner, C.J. Nachtshein, and W. Wasserman. 1996. Applied linear statistical models, 4th edition. Irwin, Inc. Chicago, Illinois.
- Oliver, C.D., and B.C. Larson. 1996. Forest stand dynamics, update edition. John Wiley and Sons, Inc. New York, New York.
- Piñeiro, G., S. Perelman, J.P. Guerschman, and J.M. Paruelo. 2008. How to evaluate models: observed vs. predicted or predicted vs. observed? *Ecological Modeling* 216:316-322.
- Pittman, S.J., B.M. Costa, and T.A. Battista. 2009. Using lidar bathymetry and boosted regression trees to predict the diversity and abundance of fish and corals. *Journal of Coastal Research* SI(53):27-38.
- Priestnall, G., J. Jaafar, and A. Duncan. 2000. Extracting urban features from lidar digital surface models. *Computers, Environment and Urban Systems* 24:65-78.
- Ralph, C.J., S. Droege, and J.R. Sauer. 1995. Managing and monitoring birds using point counts: standards and applications. Pages 161-169 *in* *Monitoring Bird Populations by Point Counts* (C.J. Ralph, J.R. Sauer, and S. Droege, Eds.). U.S. Department of Agriculture, Forest Service General Technical Report PSW-GTR-149.
- Reutebuch, S.E., H-E. Anderson, and R.J. McGaughey. 2005. Light detection and ranging (LIDAR): an emerging tool for multiple resource inventory. *Journal of Forestry* 103:286-292.
- Rosenstock, S.S., D.R. Anderson, K.M. Giessen, T. Leukering, and M.F. Carter. 2002. Landbird counting techniques: current practices and an alternative. *The Auk* 119:56-53.

- SAS Institute. 2009. The SAS System for Windows, ver. 9.1. SAS Institute, Inc., Cary, North Carolina.
- Seavey, N.E., J.H. Viers, and J.K. Wood. 2009. Riparian bird response to vegetation structure: a multiscale analysis using lidar measurements of canopy height. *Ecological Applications* 19:1848-1857.
- Short, H.L., J.B. Hestbeck, and R.M. DeGraaf. 2001. New England wildlife: a model for ecosystem management – ECOSEARCH (version 1). Northeastern Forest Experiment Station, GTR NE-283, Radnor, Pennsylvania.
- Smith, K.M., W.S. Keeton, T.M. Donovan, and B. Mitchell. 2008. Stand-level forest structure and avian habitat: scale dependencies in predicting occurrence in a heterogeneous forest. *Forest Science* 54:36-46.
- Stoker, J., J. Parrish, D. Gisclair, D. Harding, R. Haugerud, M. Flood, H-E. Anderson, K. Schuckman, D. Maune, P. Rooney, K. Waters, A. Habib, E. Wiggins, B. Ellingson, B. Jones, S. Nechero, A. Nayegandhi, T. Saultz, and G. Lee. 2007. Report of the first national lidar initiative meeting, February 14-16, 2007, Reston, Virginia.
- Sutherland, W.J., and S.R. Baillie. 1993. Patterns in the distribution, abundance, and variation of bird populations. *Ibis* 135:209-210.
- Van Horne, B. 1983. Density as a misleading indicator of habitat quality. *Journal of Wildlife Management* 47:893-901.
- Vierling, K.T., L.A. Vierling, W.A. Gould, S. Martinuzzi, and R.M. Clawges. 2008. Lidar: shedding new light on habitat characterization and modeling. *Frontiers in Ecology and Environment* 6:90-98.

Walters, C.J. 1986. Adaptive management of renewable resources. McGraw-Hill, New York, New York.

Whittingham, M.J., P.A. Stephens, R.B., Bradbury, and R.P. Freckleton. 2006. Why do we still use stepwise modeling in ecology and behavior? *Journal of Applied Ecology* 75:1182-1189.

CHAPTER 4. OPTIMIZATION OF HABITAT MANAGEMENT BASED ON LiDAR-DERIVED FOREST-STAND AND BREEDING-BIRD MODELS: A CASE STUDY FROM THE NORTHWOODS OF MAINE

Abstract

Wildlife managers seek ways to utilize empirical models to predict wildlife species occurrences or abundances as a function of environmental attributes across broad landscapes. Managers generally rely on such models and various optimization algorithms to evaluate various management scenarios. For this study, we explored LiDAR-derived canopy-height profiles for classifying small forest stands (0.25 ha) into successional age classes based on hypothetical, but realistic known vertical canopy profiles. We applied several bird-habitat models that use LiDAR-derived explanatory variables to predict the amount of habitat for six focal bird species under various management scenarios across two study sites in Maine. We assessed the impact of selected management scenarios utilizing a simple Euclidean distance (ED) metric measuring the distance between the predicted amount of bird habitat and a specific goal for each bird species. We consider as optimal the scenario with the minimum ED.

Introduction

Developing predictive wildlife-habitat models should be viewed as more than just a process for studying the habitat requirements and relationships of and among suites of species of interest (Millspaugh and Thompson 2009). Although much can and should be learned about wildlife and their habitat requirements from the empirical modeling process, many wildlife managers often would like to know how the models can be used as part of decision-support tools. Realistically, most ecosystems are difficult to manage. Thus, models should have practical utility and applications in real-world situations.

Unless one can demonstrate that a model has utility in its applications, the models often end up as merely an academic exercise, regardless of the strength of its predictability.

A decision-support tool called ECOSEARCH (Short et al. 2001) was developed for New England forests. It allows for specific impact assessments in pre- and post-treatment scenarios and predicts long-term trajectories of habitat under varying management scenarios. ECOSEARCH is a computer program that currently uses natural-history based models to make spatially-explicit predictions of species occurrences at a 50-m pixel resolution across a landscape.

Short et al. (2001) provided three examples of how ECOSEARCH might be applied. The first example was a site-specific impact assessment to wildlife that resulted from the conversion of a wooded swamp to a recreational lake with an adjoining golf course. The second example demonstrated how ECOSEARCH can be used in the development of a management plan for a wildlife refuge in which several hectares are actively managed annually on 10-ha forest stands on a 40-year harvest rotation specifically to benefit one species while assessing potential impacts to other species. A third example assessed five management options on a national forest from a multi-use perspective and evaluated their relative impacts to all modeled species. Practical applications such as illustrated in these examples are useful to managers, allowing for regular updates under an adaptive management paradigm as new information is acquired and incorporated, usually with improved models (Walters 1986).

In Chapters 2 and 3 of this dissertation, we developed empirical models utilizing the information provided by LiDAR data. We were able to model and predict several over- and understory forest stand metrics commonly used by both foresters and wildlife

managers to determine the vertical canopy structure layer required by ECOSEARCH (Chapter 2). We also demonstrated the utility of models based on LiDAR-derived explanatory variables to predict the mean abundance of several bird species. These bird models can be used to either supplement the natural-history models in ECOSEARCH or as stand-alone models in an updated version of ECOSEARCH.

Goals and Objectives

In this study, we assessed an extension of the third ECOSEARCH example described above. Here, we utilized LiDAR-derived canopy profiles and LiDAR-predicted bird models developed in Chapters 2 and 3, respectively, to investigate how these models can be used to assess multiple real-world management scenarios. The specific objective of this study was to empirically assess various harvest schedules and their spatial patterning on LiDAR-predicted bird abundance in the Northwoods of Maine. We also make an assessment of harvest schedules to determine which spatial arrangement optimizes the amount of habitat for a suite of bird species under specified and quantifiable goals.

Study Area

A detailed description of the study areas in Maine for International Paper (IP) and Moosehorn National Wildlife Refuge (MH) are presented in Chapter 2. The two study sites are considered to be representative of what is typically considered as the Northwoods mixed-forests.

Methods

LiDAR and Processing

In Chapters 1-3 we presented a detailed account of LiDAR technology, data acquisition, and processing to predict forest stand metrics and mean bird abundance. We assume the reader is familiar with how the LiDAR was summarized into canopy closure estimates within each 50×50 m cell. The explanatory variables for the forest-metric modeling (i.e., P variables) and the explanatory variables for the bird modeling (i.e., X variables) were computed from the canopy closure (CC) variables CC0, CC1, ..., CC30. These CC variables are 1-m increments in the percentages of the total number of LiDAR returns on the ground (CC0), with CC1 being the percent of returns between the ground and 1 m above the ground, CC2 between 1 and 2 m, to 30 meters (CC30). For the forest metric models we defined the variables P0 = percent of ground returns, P1 = percent of returns between 0 and 3 m above ground, P2 = percent of returns between 3 and 6 m above ground, etc. in 3-m intervals to P10 = percent of returns between 27- and 30-m (Table 2.3). Vertical profile levels for bird models were similarly defined except using different vertical height profile limits (i.e., X0 = percent of ground returns, X1 = percent of ground returns between 0 and 1 m above ground, X2 = percent of ground returns 1 to 2 m, etc.; see Table 3.1.a). The P variables are used below to classify 50×50 m cells into forest-age classes and the X variables are used to predict bird abundances under various management scenarios of harvest schedules and spatial patterning of those harvest schedules.

Hypothetical Age Classes

Before we could empirically assess varying harvest schedules and habitat spatial patterns on birds at IP and MH, we needed to classify all 50×50 m cells at the two study sites into vertical profile age classes (i.e., current age structure in 2003, the year that LiDAR was acquired). This classification was necessary to allow backcasting and forecasting among age classes spatially and explicitly on each 50 ×50 m cell as a function of a particular harvest schedule. We first generated a hypothetical stand of trees that was sequenced across a successional gradient using DeGraaf et al. (1992) and Hunter and Schmiegelow (2010) as a guide for a 150-year trajectory in forest succession that is typical of the Northwoods (see also Aber 1979). We assumed stands of softwoods only, hardwoods only, and mixed-woods have similar vertical structural profiles at each age class (Fig. 4.1). We next partitioned the successional gradient for the first 100 years of succession into 10-year age classes. The first age class (1 to 10 years) was further partitioned into 0-1 year, 2-5 years, and 6-10 years post-harvest. We considered age classes from 101 - 150 years post-harvest as the final age class because this is considered the climax sere (i.e., mature forest) for this region; the climax forest is characterized by dynamic vertical profiles that is in relatively consistent flux (Hunter and Schmiegelow 2010).

Vertical Canopy Profiles

We derived hypothetical vertical profiles for each age class using the bottom panel in Fig. 4.1 as a guide and assigned a percent canopy closure to each three-m vertical height layer up to 30 m (Table 4.1). In Table 4.1, the hypothetical canopy closure estimates (P1 to P10) sum to 100 percent implying P0 = 0 percent for bare

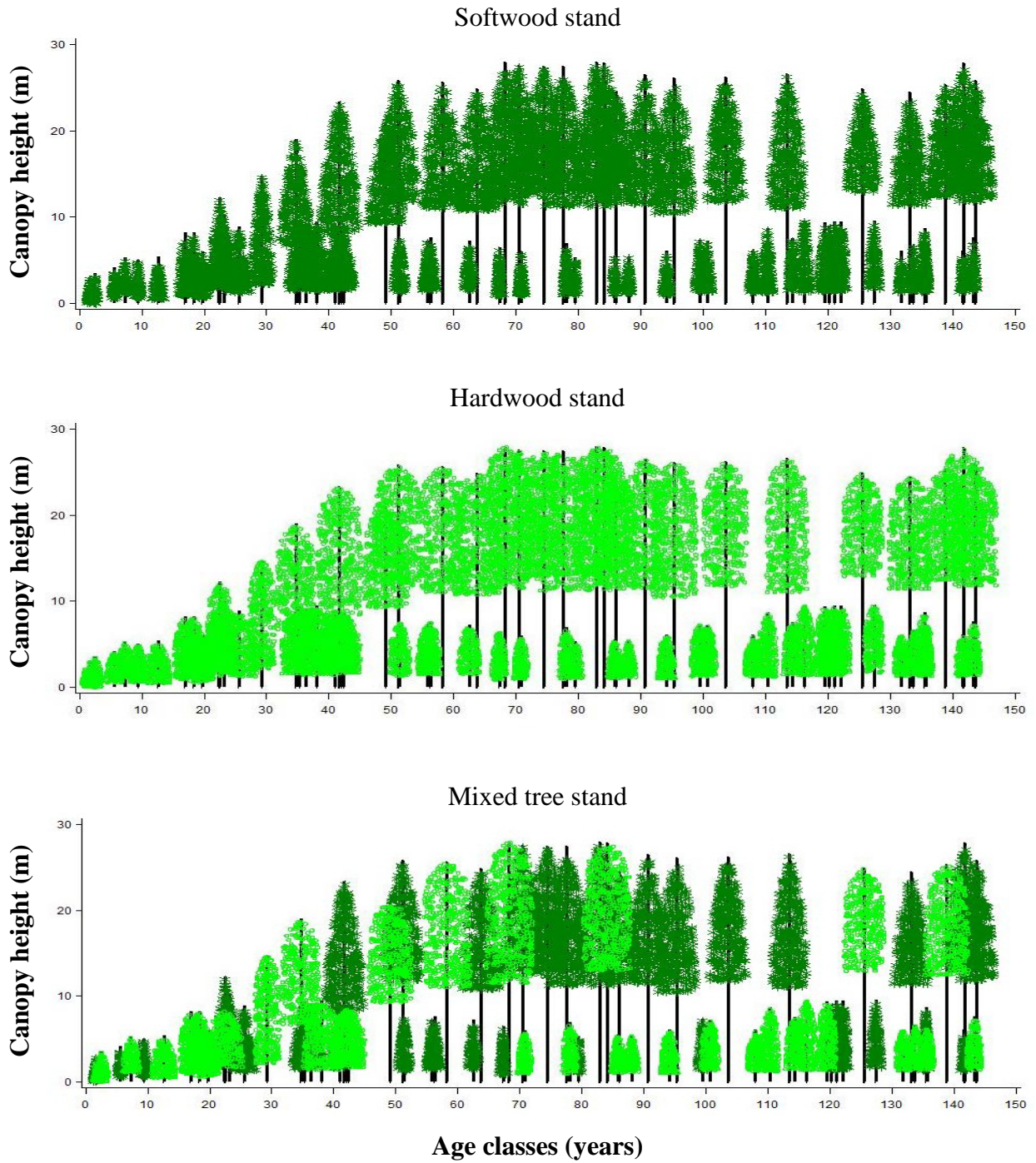


Figure 4.1. Hypothetical forest stand succession for softwood (top), hardwood (middle), and mixed hardwood-softwood (bottom). All three forest types are assumed to have the same vertical canopy profiles across time, up to and including the climax conditions at approximately 100 to 150 years (DeGraaf et al. 1992).

Table 4.1. Percent of LiDAR returns expected from hypothetical vertical canopy profiles for incremental increasing successional age classes assumed from the mixed softwoods-hardwood trajectory in bottom panel of Fig. 4.1.

Age class (years)	Canopy height (m)									
	0-3 (P1)	3-6 (P2)	6-9 (P3)	9-12 (P4)	12-15 (P4)	15-18 (P5)	18-21 (P6)	21-24 (P7)	24-27 (P8)	27-30 (P10)
0-1	100	0	0	0	0	0	0	0	0	0
2-5	90	10	0	0	0	0	0	0	0	0
6-10	35	45	20	0	0	0	0	0	0	0
10-20	20	30	30	20	0	0	0	0	0	0
21-30	15	20	20	25	20	0	0	0	0	0
31-40	15	15	10	20	20	20	0	0	0	0
41-50	10	10	10	15	20	20	15	0	0	0
51-60	10	10	10	15	15	15	15	10	0	0
61-70	5	5	10	10	15	20	20	10	5	0
71-80	5	5	5	5	10	20	20	15	10	5
81-90	10	5	5	5	10	20	20	15	5	5
91-100	10	10	5	5	10	20	20	10	5	5
101-150	10	10	10	10	15	10	15	10	5	5

ground. However, to classify each 50×50 m cell into the 13 age classes, we needed to account for the observed canopy closure at each 50×50 m cell as estimated by the LiDAR data, and hence the percent bare ground. Therefore, we adjusted each hypothetical age class P values as a function of the observed P0 (which is computed from LiDAR) for each 50×50 m cell. As an example, Fig. 4.2 illustrates what the vertical profiles for each of the 13 age classes would be for a 50×50 m cell having P0 = 10 percent bare ground. The sum of the purple-hashed bars (P1-P10) representing canopy, and the black-hashed bars, representing the 10 percent bare ground, sum to 100 percent. Therefore, as the amount of bare ground changes across the 50×50 m cells, the overall profile shape would stay the same but P1 to P10 values would increase (or decrease) consistently and inversely with the increase or decrease in percent of bare ground (P0 value). Although undoubtedly selective harvesting of individual trees within 50×50 m cells occurs causing

Age Class (years)

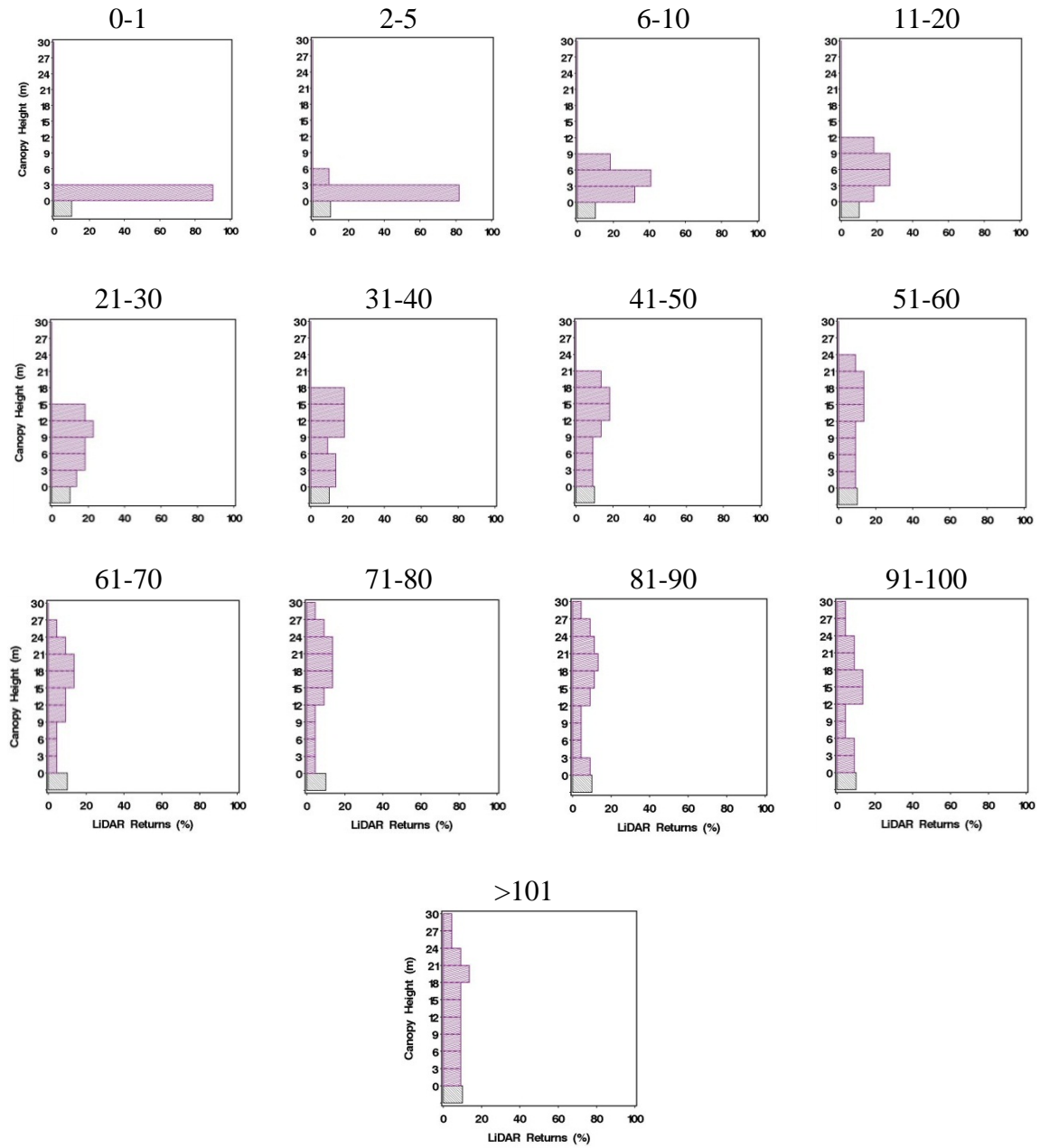


Figure 4.2. Vertical vegetation profiles (%) for hypothetical forest stand succession in Fig. 4.1 (purple bars are 3-m vertical profiles, bottom black-hashed bar is percent ground, assumed to be 10% for all age classes; all bars combined sum to 100%).

vertical profiles to change independent of natural succession, adjusting for the observed LiDAR estimated value of P0 at each cell accommodates site-specific vertical profiles due to potential differences in topography, soils, moisture, and the presence of other woody species (Hedman and Binkley 1988). We assume that the proportion of bare ground (P0) observed at a 50×50 m cell using LiDAR is a manifestation of conditions at that site, therefore the P0 remains constant as the forest matures. This assumption is unlikely, but without site-specific information and forest growth rates for each 50×50 m cell, we were forced to make this assumption.

Classifying 50×50 m Cells

We used Euclidean distances (ED) to classify the current 50×50 m cells across the entire study sites at IP and MH into age classes using the LiDAR data and summarized into the P variables (excluding 50×50 m cells classified as water or bog). ED for each 50×50 m cell and age-class combination was computed using

$$ED = \sqrt{(P0_o - P0_h)^2 + \dots + (P10_o - P10_h)^2}$$

as the measured distance between the observed LiDAR-derived vertical height profile variables $P0_o$ to $P10_o$ (Table 2.3, Chapter 2) and their analogous hypothetical vertical profiles $P0_h$ to $P10_h$ (Table 4.1). We adjusted the percent values in Table 4.1 with each cell's observed $P0_o$ as illustrated in Fig. 4.2 and describe above. The ED was computed for each of the 13 age classes for each 50×50 m cell with assignment to an age class based on the minimum of the 13 computed ED's.

Harvest Schedules and Spatial Pattern

Although there is essentially a near-infinite number of combinations of harvest schedules and spatial allocations of those schedules, we explored some hypothetical scenarios that are considered a micro-approach to management of forest stands in this region (Hunter 1999). We took a factorial approach to define the management scenarios. The scenarios consisted of combinations of two harvest rotations (80- and 90-year), two block types (mosaic, strip), two allocation patterns (random, systematic), with each combination implemented at two scales of like-cells (50-m scale being a single 50×50 m cell and 150 m scale being a 3×3 grid of like 50×50 m cells) (Fig. 4.3). The 80-year rotation was done in 5-year harvest increments with the 90-year rotation done in 10-year increments (Fig. 4.3). We also examined a hypothetical 10-year rotation at each scale representing near-continuous early successional age classes (not illustrated in Fig. 4.3). Allocation for the 10-year rotation was done in a 3×3 pattern with years 1-9 being randomly allocated to each cell and at both the 50-m and 150-m scale. Each of the harvest schedules and patterns in Fig. 4.3 were repeated as a block across the entire grid of 50×50 m cells for a particular management scenario across the IP and MH study sites. For example, the 80-year rotation in a systematic mosaic of cuts is composed of 4×4 blocks of 50×50 m cells (or 3×3 grid of like 50×50 m cells at the 150 m scale) (top left grid in Fig. 4.3). This 4×4 block was then repeated and juxtaposed across each study site with a new start-cell for the 5-year increments within each 4×4 block (see Fig. 4.3 illustrating four 4×4 blocks). The other scenarios were juxtaposed similarly, accommodating their unique pattern as necessary (e.g. strip cuts). These combinations of schedules and patterns resulted in 18 different management scenarios, all hypothetical.

80-Year Rotation (5-Year Cuts)

Systematic mosaic cuts

20	40	60	80	5	10	15	20	80	45	40	5	65	70	75	80
15	35	55	75	40	35	30	25	75	50	35	10	60	55	50	45
10	30	50	70	45	50	55	60	70	55	30	15	25	30	35	40
5	25	45	65	80	75	70	65	65	60	25	20	20	15	10	5

Random mosaic cuts

50	30	40	10	40	25	15	80	45	65	15	35	20	55	70	65
75	15	20	25	5	65	75	10	25	20	55	65	45	15	50	10
35	5	45	60	30	50	55	60	40	80	5	70	40	35	75	60
70	80	65	55	20	45	70	35	10	75	30	50	25	80	30	5

Systematic strip cuts

5	10	15	20	25	30	35	40	45	50	55	60	65	70	75	80
5	10	15	20	25	30	35	40	45	50	55	60	65	70	75	80
5	10	15	20	25	30	35	40	45	50	55	60	65	70	75	80
5	10	15	20	25	30	35	40	45	50	55	60	65	70	75	80

Random strip cuts

70	35	75	50	80	5	15	30	65	45	20	40	55	60	25	10
70	35	75	50	80	5	15	30	65	45	20	40	55	60	25	10
70	35	75	50	80	5	15	30	65	45	20	40	55	60	25	10
70	35	75	50	80	5	15	30	65	45	20	40	55	60	25	10

90-Year Rotation (10-Year Cuts)

Systematic mosaic cuts

30	40	90	70	60	10	90	80	70
20	50	80	80	50	20	40	50	60
10	60	70	90	40	30	30	20	10

Random mosaic cuts

70	50	60	60	80	30	50	30	80
80	30	20	70	40	50	20	40	70
90	40	10	20	10	90	60	90	10

Systematic strip cuts

10	20	30	40	50	60	70	80	90
10	20	30	40	50	60	70	80	90
10	20	30	40	50	60	70	80	90

Random strip cuts

20	70	60	10	40	80	90	50	30
20	70	60	10	40	80	90	50	30
20	70	60	10	40	80	90	50	30

Figure 4.3. Hypothetical harvest-schedules and spatial patterns for management scenarios juxtaposed on the landscape within either square blocks (top four configurations) or harvest strips (bottom four configurations). Values within cells represent stand age since last cutting for stand age classes through 80 or 90 years. Systematic, for both mosaic patterns and strips, implies an ordered sequence of harvests with a random start cell for mosaics and strip for strip cuts; random implies random assignment of harvests within a block, or random assignment of strips. Note: the dimensions of the individual cells can represent either a single 50×50 m cell or a 3×3 array of like 50×50 m cells.

We used the vertical profiles for each hypothetical age-class as describe above for classifying each 50×50 m cell with each harvest schedule and pattern, adjusting for the observed and unique LiDAR-derived P0 values. For each study site, this provided us these 5-year profiles, we averaged the allocated age class vertical profiles with the previous age class profiles (e.g., profiles for 60-year age-class was computed as the average profiles of the 51-60 and 61-70 age-classes; age-class 65 would be the 61-70 age class). For the 90-year rotation, we used the the upper year to define the age class (e.g., age class 50 would be the 41-50 age-class profiles).

Predicting Bird Abundance

For each of the 50×50 m cells assigned a specific age class profile for each harvest schedule and pattern (i.e., management scenario), we computed the explanatory variables used in the bird models as described in Chapter 3 (i.e., X variables listed in Table 3.1.a). To compute the X's from the hypothetically-derived P's for each 50×50 m cell, we back-computed the 1-m vertical profiles CC1 to CC30 (see Table 2.3) by an equal allocation of the each of the P values (e.g., if P1 = 0.21 or 21%, then CC1 = 0.07, CC2 = 0.07, and CC3 = 0.07). From these CC values, we then computed the various predictor variable X's as given in Chapter 3, Table 3.1.a.

To maximize the potential of predicting habitat for various species and assess ways to select the optimal management scenario, we used the bird species from Chapter 3 that had both good predictive models and represented species with varying types of vegetation structural requirements. For the IP study site we used models for Magnolia Warbler (MAWA), Ovenbird (OVEN), Common Yellowthroat (COYE), Lincoln's Sparrow (LISP), and Palm Warbler (PAWA). For the MH study site we used the same

species except Yellow-rumped Warbler (YRWA) was used instead of LISP. Species codes are defined in Appendix A.1 and the models used and their coefficients are listed in Table C.3. We defined the total amount of habitat available at each site and for each species as the percentage of all 50×50 m cells that the bird-habitat models predicted the mean abundance (number/0.25 ha) to be greater than 0.5 birds/0.25 ha for the IP site and greater than 0.25 birds/ha for the MH. We used these mean abundance cut-off values as opposed to 0.0 birds/0.25 ha because most of the models for these species tended to over-predict their abundance at low field-observed abundances (Chapter 3). Predicted bird abundances using the models were then done for each of the 18 management scenario and for the status in the year 2003 as a point of reference.

Assessing Optimal Management Scenario

To assess which of the harvest and spatial pattern combinations is “best” (i.e., optimal) requires specification of quantifiable objectives. One way to make this assessment is to define how much habitat, as a percent of the landscape, is desired or required for each bird species. For our assessment, we examined three (very) hypothetical goals. Goal A was assumed to have 80, 80, 80, 80, and 50 percent of the 50×50 m cells across the landscape to have mean abundance greater than 0.5 birds per 0.25 ha for MAWA, OVEN, COYE, LISP, and PAWA respectively at IP. Goal A at MH was the same except for MAWA, OVEN, COYE, YRWA, and PAWA respectively, except using the mean abundance of 0.25 birds per 0.25 ha. Because PAWA tends to favor early successional tracts of forest stands (see Chapter 3), goal B was allocated as 50, 50, 50, 50, and 30 percent to soften the amount required for each species at both sites by having less reduction in required habitat for PAWA (50-30=20% change versus 30%

change for the other focal species (i.e., 80-50=30%). The third goal, C, was the unrealistic but for comparative purposes was 100 % for each species. All three goals are only hypothetical and used here for illustrative purposes.

As a way to score each of the scenarios for each goal, we computed the ED between the predicted percent habitat and the percentage specified for each goal using

$$ED = \sqrt{(b_1 - g_1)^2 + \dots + (b_i - g_i)^2}$$

where b_i = predicted percent habitat and g_i = habitat goal percentage for the i th focal bird species (five focal birds species for each site in our example, $i=1$ to 5). To assess which harvest and pattern scenario best met the specific goal, we ranked the ED values from the smallest to the largest with the smallest ED representing the scenario closest to the specified goal.

Results

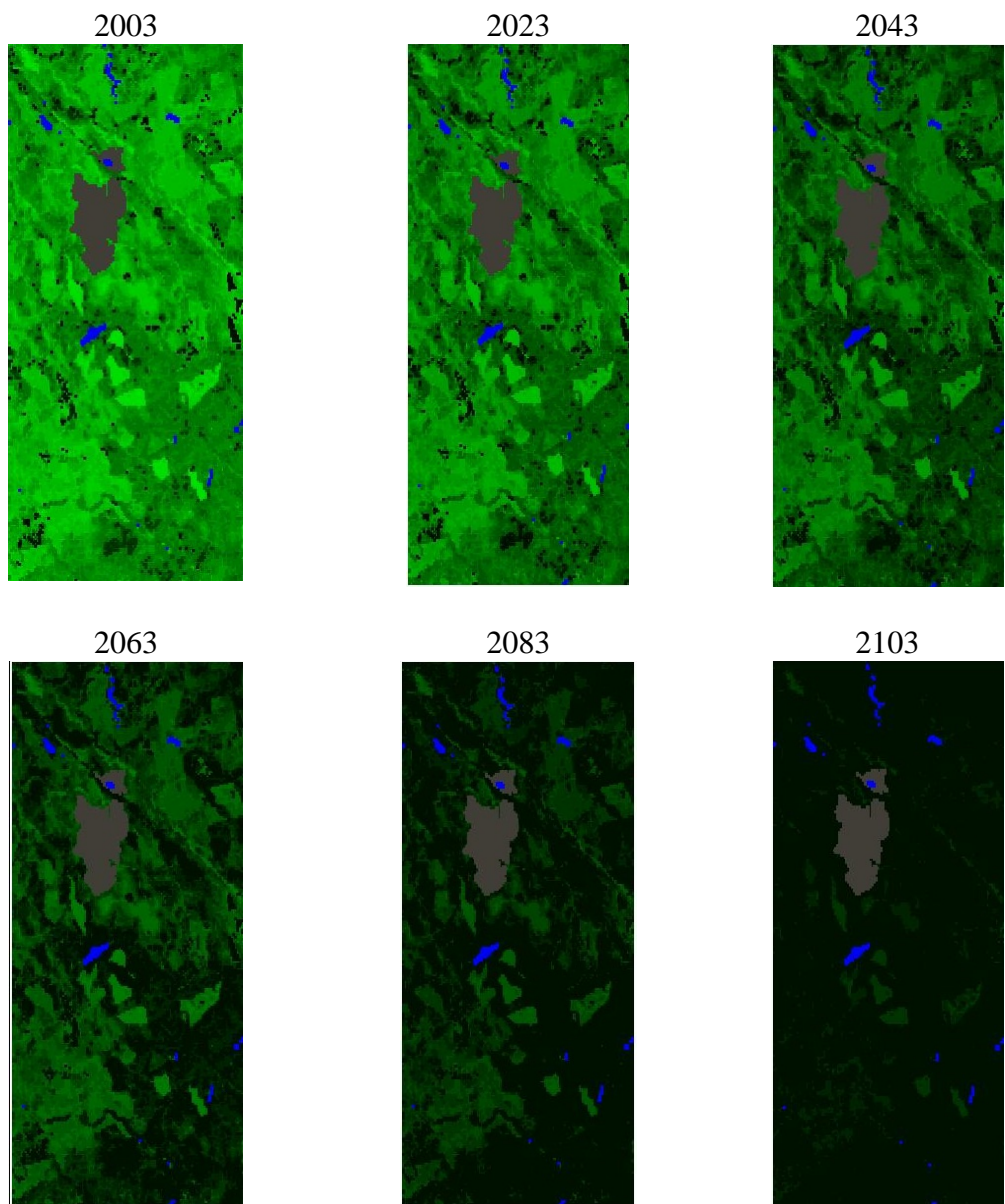
Classification results for the year 2003 LiDAR data yielded 92% and 85% of the 50×50 m cells at IP and MH, respectively, to be younger than 50 years (Table 4.2). Early successional stands (≤ 5 years since last the cut) accounted for nearly 10% of the study sites at both IP and MH. These classification results seem reasonable since IP is a commercial forest with few stands reaching >80 years. Although having an un-managed wilderness, MH is not too far removed in time from being historically cut-over and/or naturally burned (refuge was established in 1937 and actively managed thereafter). Applying and plotting in a map these age classes across the study sites reveals a dynamic mosaic of varying age classes and areas (Figs. 4.4.a. and 4.4.b. for IP and MH respectively). These figures naturally correlate well with canopy height models presented

Table 4.2. Summary of classification and enumeration of the number of 50×50 m cells from International Paper (IP) and Moosehorn National Wildlife Refuge (MH) study sites into successional age classes based on LiDAR-derived 3-m vertical vegetation profiles from 2003 acquisition year (age classes vertical profiles are per Table 4.1).

Age class (years)	IP		MH	
	Count	Forest (%)	Count	Forest (%)
0-1	848	2.86	939	2.42
2-5	2535	8.55	2340	6.04
6-10	5599	18.89	5419	13.99
10-20	3957	13.35	6358	16.42
21-30	4801	16.20	10546	27.23
31-40	5559	18.76	6690	17.28
41-50	3919	13.22	4129	10.66
51-60	615	2.08	1006	2.60
61-70	743	2.51	501	1.29
71-80	60	0.20	22	0.06
81-90	179	0.60	81	0.21
91-100	557	1.88	193	0.50
101-150	263	0.89	502	2.45
Subtotal	29635	100.00	38726	100
Water	148		2670	
Bog	937		0	
Total	30720		41396	

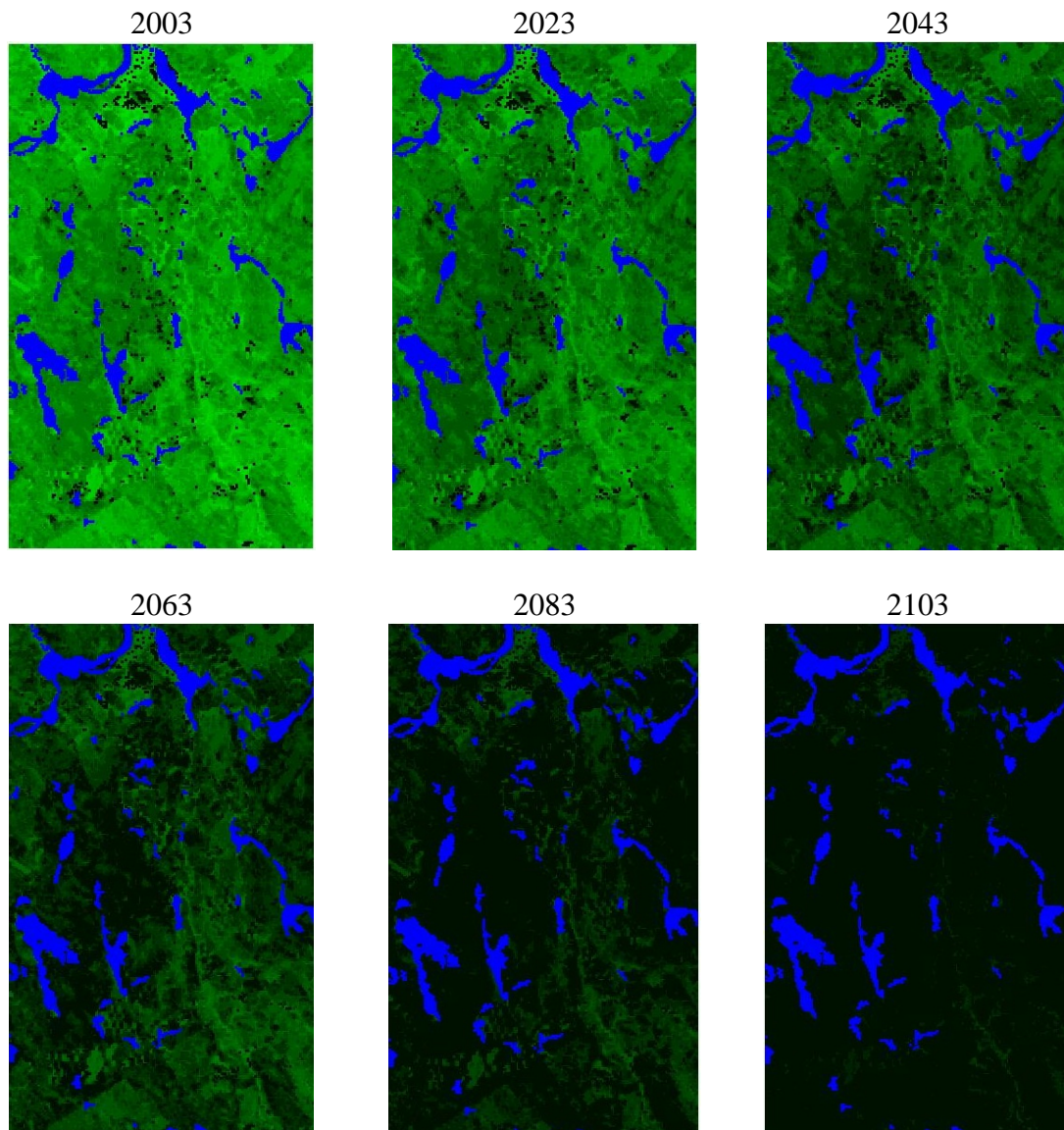
in Chapter 2 (Figs. 2.6.a. and 2.6.b). Simulating immediate termination of all harvesting on all 50×50 m cells reveals that by 2103 (when all cells at both IP and MH reach climax age class of >101) a SE to NW aging gradient at IP (Fig. 4.4.a) and a W-SW to E-NE aging gradient at MH (Fig. 4.4.b).

The predicted percent habitat for each species in the year 2003 at each study site shows varying results, with several species having a high percentage of moderately to high predicted abundance across the entire landscape where they occurred (Table 4.3). MAWA, OVEN, and COYE were predicted to occur with > 0.5 birds/0.25 ha on > 50% of the 50×50 m cells at both IP and MH, with MAWA, OVEN, and COYE being extremely ubiquitous at IP. MAWA and OVEN also were ubiquitous at MH, but with



Age class (years)							
1	2-5	6-10	11-20	21-30	31-40	41-50	51-60
61-70	71-80	81-90	91-100	>101	Water	Bog	

Figure 4.4.a. Projected forest stand ages for International Paper over a 100-year period from 2003 (LiDAR acquisition year) to 2103, in 20-year increments (study site is 6.4×12.0 km).



Age class (years)							
1	2-5	6-10	11-20	21-30	31-40	41-50	51-60
61-70	71-80	81-90	91-100	>101	Water		

Figure 4.4.b. Projected forest stand ages for Moosehorn National Wildlife Refuge over a 100-year period from 2003 (LiDAR acquisition year) to 2103, in 20-year increments (study site is 7.9×13.1 km).

Table 4.3. Percent of 50×50 m cells at International Paper (IP) and Moosehorn National Wildlife Refuge (MH) for each level of increasing predicted mean species abundance (number/0.25 ha) using models developed in Chapter 3 using 2003 LiDAR acquisition.

Site	Species ¹	Mean number of birds /0.25 ha					
		0	0.0-0.50	0.5-1.0	1.0-1.5	1.5-2.0	>2.0
IP	MAWA	0.1	15.2	40.2	33.6	10.4	0.6
	OVEN	1.7	8.5	46.4	36.7	6.7	0.1
	COYE	0.1	36.6	40.1	12.5	8.3	2.5
	LISP	41.8	53.0	3.1	2.1	0.0	0.0
	PAWA	27.4	46.3	14.1	8.8	2.4	0.9
MH		0.0	0.0-0.25	0.25-0.50	0.50-0.75	0.75-1.0	>1.0
	MAWA	2.0	30.8	47.3	14.7	3.9	1.2
	OVEN	2.6	28.5	57.4	11.4	0.1	0.0
	COYE	42.8	30.9	13.86	10.8	1.7	0.0
	YRWA	3.1	19.2	67.9	9.4	0.4	0.0
	PAWA	35.9	59.2	4.9	0.0	0.0	0.0

¹See Table C.1 for species codes.

lower predicted abundance. LISP and PAWA at IP, and YRWA and PAWA at MH, had the least amount of predicted habitat. The results somewhat parallel the results for the percent of 50×50 m cells in each age class (Table 4.2). As with our findings here, Titterington et al. (1979) found a great deal of overlap among seral stages with respect to bird abundance, with tendencies for some species abundances to be highest on early-stages (e.g., COYE), some highest in mid-stages (e.g., MAWA), and other species highest on late-stages (e.g., YRWA).

When predicting the amount of habitat for each of the five focal species under each hypothetical harvest schedule and spatial pattern, revealed little effect on the amount of habitat for MAWA and OVEN at IP (Table 4.4.a). COYE at IP had the maximum amount of habitat under the current conditions (64%), with approximately half that amount for each of the harvest schedules. The predicted amount of habitat at IP for PAWA fluctuated widely under varying management scenarios, from a low of 9% to a

Table 4.4.a. Percent of 50×50 m cells with predicted mean abundance (number of birds/0.25 ha) > 0.50 for five bird species based on “best” model selected in Chapter 3 under hypothetical management scenarios at International Paper.

Scenario ¹			Species ²				
Scale	Rotation	Harvest pattern of cuts	MAWA	OVEN	COYE	LISP	PAWA
50 m	NA	Current status in 2003	84.8	89.8	63.4	5.2	26.3
	Indef.	All cells ≥ 91-100	91.6	96.4	33.8	6.1	9.3
	10 yrs	Random mosaic	95.1	87.1	38.0	4.3	48.8
	80 yrs	Systematic mosaic	84.4	95.8	26.6	5.9	20.9
		Random mosaic	84.4	95.8	27.6	5.8	21.1
	90 yrs	Systematic strips	84.2	96.0	27.4	5.9	21.3
		Random strips	84.5	95.7	27.7	5.8	21.0
		Systematic mosaic	84.2	96.3	27.5	5.9	18.8
		Random mosaic	84.2	96.4	27.2	6.2	18.5
	150 m	10 yrs	Systematic strips	84.4	96.2	27.5	6.0
Random strips			84.5	96.3	27.3	5.9	18.5
80 yrs		Random mosaic	94.9	87.2	38.1	4.4	49.2
		Systematic mosaic	83.8	95.9	27.8	5.9	20.3
		Random mosaic	82.6	95.7	27.5	5.9	19.4
		Systematic strips	85.0	95.8	27.3	5.8	23.1
90 yrs		Random strips	85.0	96.0	28.0	6.0	21.2
		Systematic mosaic	84.4	96.3	27.7	6.1	19.0
		Random mosaic	84.7	96.4	27.4	5.9	18.5
		Systematic strips	85.1	96.4	27.4	6.0	19.0
		Random strips	84.3	96.4	27.0	5.7	18.2

¹Scale refers to size of planned contiguous age-class harvest pattern of 50×50 m cells (either in 1×1=50 m blocks or 3×3=150 m blocks); rotation refers to number of years between harvest for any particular 50×50 m cell, NA=not applicable, 10 year rotation implies no 50×50 m cell ever exceeds age class 10, see Fig. 4.4 for hypothetical harvest patterns.

²Species codes are defined in Table C.1.

high of 49%. The predicted amount of habitat for LISP at IP was always < 7%

regardless of the management scenario.

Predicted amount of habitat under the hypothetical management scenarios at MH revealed extreme amounts for all five species (Table 4.4.b). MAWA had the smallest range, but still ranged from a high of 97% to a low of nearly 42 %. The other four species ranged from lows of nearly 0 % of predicted habitat to 99%, although most

Table 4.4.b. Percent of 50×50 m cells with predicted mean abundance (number of birds/0.25 ha) > 0.25 for five focal bird species based on “best” model selected Chapter 3 under hypothetical management scenarios at Moosehorn National Wildlife Refuge.

Scenario ¹			Species ²				
Scale	Rotation	Harvest pattern of cuts	MAWA	OVEN	COYE	YRWA	PAWA
50 m	NA	Current status in 2003	67.2	68.8	26.3	77.7	7.9
	Indef.	All cells ≥ 91-100	54.5	85.4	9.3	88.3	1.1
	10 yrs	Random mosaic	96.9	0.0	99.9	7.5	99.9
		Systematic mosaic	46.5	69.2	27.9	80.8	7.3
	80 yrs	Random mosaic	46.9	69.2	27.9	80.7	7.4
		Systematic strips	47.7	68.9	28.1	80.9	7.5
		Random strips	45.9	69.3	27.8	80.7	7.6
		Systematic mosaic	42.5	74.5	22.4	85.9	1.3
	90 yrs	Random mosaic	42.7	74.2	22.5	85.6	1.3
		Systematic strips	43.5	74.1	22.6	85.6	1.3
		Random strips	42.9	74.4	22.8	85.6	1.3
		Systematic mosaic	42.5	74.5	22.4	85.9	1.3
150 m	10 yrs	Random mosaic	96.9	0.0	99.9	7.4	99.9
		Systematic mosaic	46.7	69.0	28.1	80.4	7.7
	80 yrs	Random mosaic	44.0	74.0	23.4	80.4	9.3
		Systematic strips	50.5	64.7	32.7	79.6	8.9
		Random strips	43.7	71.1	25.8	81.6	6.8
		Systematic mosaic	43.2	74.6	22.4	85.5	1.3
	90 yrs	Random mosaic	42.5	74.6	22.3	85.9	1.3
		Systematic strips	42.6	73.8	22.8	85.9	1.3
		Random strips	41.8	74.4	22.4	85.8	1.2

¹Scale refers to size of planned contiguous age class harvest pattern of 50×50 m cells (either in 1×1=50-m blocks or 3×3=150-m blocks); rotation refers to number of years between harvest for any particular 50×50 m cell, NA=not applicable, 10-year rotation implies no 50×50 m cell ever exceeds age-class 10, see Fig. 4.4 for hypothetical harvest patterns.

²Species codes are defined in Table C.1.

falling consistently at around 70-, 25-, 80-, and 7 % for OVEN, COYE, YRWA, and PAWA respectively. Several management scenarios brought the amount of habitat for PAWA to less than 2%.

We computed and ranked each of the hypothetical management scenarios for each of the three management goals at each site. Results revealed variation in rankings using ED as a ranking metric (Table 4.5). For goals A and C at IP, larger block sizes (150 m scale) using an 80-year rotation in either a systematic or random mosaic assignment of schedules within blocks had the smallest ED value, implying these scenarios were closest to reaching their respective criteria, relative to the other management scenarios. Goal B attempted, at least hypothetically, to lower the amount of habitat required for all focal species to more realistic levels, including that for PAWA's. However, since PAWA's goal was only lowered by 20% (50 to 30%) while the others were lowered 30% (80 to 50%), this could actually result in an increase in the amount habitat for PAWA. The results presented in Table 4.5 reveals that for Goal B's criteria, that using a 10-year rotation in 150-m grids of like schedules had the lowest ED at IP. However, although the amount of habitat for PAWA increases under this scenario (Table 4.4.a), the amount of predicted habitat for LISP remained low at around 4% (Table 4.4.a.). Similar scenarios were found to be optimal for each goal at MH, with 80-year rotations using grids of 150 m like 50×50 m cells having the smallest ED for goals A and B (Table 4.5.).

Discussion

This study demonstrated the utility of LiDAR-derived spatial information in the Northwood's of Maine. The spatially-explicit vertical profile information that can be summarized from data acquired from LiDAR allowed us to assess various but reasonable management scenarios for a set of three specific bird-habitat goals given the current status of the forest stand in 2003 (i.e. when the LiDAR data were acquired). Although our assessments are based on hypothetical but reasonable vertical canopy profiles for

Table 4.5. Comparison of Euclidean distances for percent occurrence (%) of five bird species based on the results from three hypothetical management goals at International Paper (IP) and Moosehorn National Wildlife Refuge (MH) (Tables 4.4.a. and 4.4.b). The bolded values are the minimum two Euclidian distances for each of the three hypothetical management goals at the two study sites.

Scenario ¹			IP goals ²			MH goals ³		
Scale	Rotation	Harvest pattern of cuts	A	B	C	A	B	C
50 m	NA	Current status in 2003	1.059	0.830	1.414	0.901	0.764	1.267
		Indef. All cell \geq 91-100	1.071	0.988	1.377	1.030	0.956	1.347
		10 yrs Random mosaic	1.074	0.781	1.431	1.387	0.994	1.715
		80 ys Systematic mosaic	1.007	0.905	1.322	0.839	0.758	1.196
		Random mosaic	1.008	0.902	1.324	0.840	0.757	1.197
		Systematic strips	1.008	0.901	1.325	0.842	0.755	1.201
		Random strips	1.008	0.902	1.324	0.837	0.756	1.194
		90 yrs Systematic mosaic	1.001	0.916	1.323	0.904	0.862	1.234
		Random mosaic	1.010	0.917	1.323	0.901	0.859	1.231
		Systematic strips	1.010	0.917	1.323	0.902	0.858	1.234
		Random strips	1.012	0.919	1.324	0.902	0.859	1.233
		150 m	10 yrs	Random mosaic	1.075	0.778	1.432	1.387
80 yrs Systematic mosaic	1.005			0.903	1.321	0.835	0.752	1.194
Random mosaic	0.995			0.903	1.310	0.852	0.770	1.205
Systematic strips	1.012			0.894	1.331	0.823	0.716	1.193
Random strips	1.013			0.902	1.331	0.847	0.779	1.197
90 yrs Systematic mosaic	1.011			0.914	1.325	0.904	0.860	1.235
Random mosaic	1.014			0.920	1.326	0.905	0.862	1.235
Systematic strips	1.016			0.918	1.330	0.900	0.858	1.231
Random strips	1.011			0.922	1.323	0.901	0.863	1.231

¹Scale refers to size of planned contiguous age class harvest pattern of 50×50 m cells (either in 1×1=50 m or 3×3=150 m), rotation refers to number of years between harvest for any particular 50×50 m cells (NA=not applicable, 10-year rotation implies no 50×50 m cell ever exceeds age class 10, see Fig. 4.4 for hypothetical harvest patterns).

²Goal A=(80,80,80,80,50), Goal B=(50,50,50,50,30), and Goal C=(100,100,100,100,100) percent habitat for MAWA, OVEN, COYE, LISP, and PAWA respectively (see Table C.1 for definitions of species code list).

³Goal A=(80,80,80,80,50), Goal B=(50,50,50,50,30), and Goal C=(100,100,100,100,100) percent habitat for MAWA, OVEN, COYE, YWRA, and PAWA respectively (see Table C.1 for species code list).

successional stages grouped into age classes, we were able to backcast and forecast successional development on each of the 50×50 m cells across the entire landscape for each of the two study sites. We also demonstrated the utility of applying bird-habitat models that use LiDAR-derived explanatory variables to predict bird abundance under various management scenarios that impact the forest age classes of each 50×50 m cell over time. From these predicted landscapes and bird abundances, assuming reasonable bird-habitat models are available, we showed that the total amount of habitat at varying predicted bird abundances can be summarized and assessed. As part of this assessment we further illustrated that an optimal suite of harvest cut-schedules and spatial patterns can be ascertained using a simple ED metric from which managers can use as one of several planning tools. Thus, this basic optimization approach utilizing LiDAR-derived vegetation profiles with supporting stand-age classes and LiDAR-predicted bird abundance can be incorporated further into a more encompassing decision-support tool such as ECOSEARCH.

Optimization and prioritization of conservation approaches across landscapes are currently a very active area of research, especially in situations with competing and conflicting goals (Moilanen et al. 2009). We used a simple metric (ED) for assessing which goal is optimal under limited and planned management scenarios, focusing on amounts of bird habitat as primary goals. Actual management prescription would need to consider cost-to-benefit ratios and logistics. We acknowledge that there are many more elaborate methods for assessing optimality, primarily using linear and nonlinear programming methods (Buongiorno and Gilless 2003) but also heuristically-derived ones as well (Michalewicz and Fogel 2000). Euclidean distance as used in this study can be

considered a reasonable metric to use at least for scenario planning. Of most interest to managers is to not just conduct “what-if” scenarios (e.g., specific impact assessments), or searching out an optimal scenario(s) among an a prior list of scenarios as was done in this study, but to seek which combinations from a near-infinite set of combinations produce optimal management prescriptions, knowing full-well there might be competing optimums (i.e., maximums for some criteria are minimums for others) across a “fitness” landscape (Kauffman 1993). Further improvements should come from exploring these alternative assessment approaches and metrics in the context of not only applying LiDAR-derived models, but as enhancements to the models and applications.

Literature Cited

- Aber, J.D. 1979. Foliage-height profiles and succession in northern hardwood forests. Ecology 60:18-23.
- Buongiorno, J., and J.K. Gilles. 2003. Decision methods for forest resource management. Academic Press, San Diego, California.
- DeGraaf, R.M., M. Yamasaki, W.B. Leak, and J.W. Lanier. 1992. New England wildlife: management of forested habitats. U.S. Department of Agriculture, Northeastern Forest Experiment Station, General Technical Report NE-144, Radnor, Pennsylvania.
- Hedman, C.W., and D. Binkley. 1988. Canopy profiles of some Piedmont hardwood forests. Canadian Journal of Forest Research 18:1090-1093.
- Hunter, M.L.Jr. (Editor). 1999. Maintaining biodiversity in forest ecosystems. Cambridge University Press, Cambridge, United Kingdom.

- Hunter, M.L., and F. Schmiegelow. 2010. *Wildlife, Forests and Forestry: Principles of Managing Forests for Biological Diversity*, 2nd edition. Prentice Hall, Houston, Texas.
- Kauffman, S.A. 1993. *The origins of order: self-organization and selection in evolution*. Oxford University Press, Inc., New York, New York.
- Michalewicz, Z., and D.B. Fogel. 2000. *How to solve it: modern heuristics*. Springer-Verlag, Berlin Heidelberg, Germany.
- Millsaugh, J.J., and F.R. Thompson. (Editors). 2009. *Models for planning wildlife conservation in large landscapes*. Academic Press, Burlington, Vermont.
- Moilanen, A., K.A. Wilson, and H.P. Possingham. 2009. *Spatial conservation prioritization: quantitative methods and computational tools*. Oxford University Press, Inc., New York, New York.
- Short, H.L., J.B. Hestbeck, and R.M. DeGraaf. 2001. *New England wildlife: a model for ecosystem management – ECOSEARCH (version 1)*. U.S. Department of Agriculture, Northeastern Forest Experiment Station, General Technical Report NE-283, Radnor, Pennsylvania.
- Titterton, R.W., H.S. Crawford, and B.N. Burgason. 1979. Songbird responses to commercial clear-cutting in Maine spruce-fir forests. *Journal of Wildlife Management* 43:602-609.
- Walters, C.J. 1986. *Adaptive management of renewable resources*. McGraw-Hill, New York, New York.

CHAPTER 5. CONCLUSIONS AND FUTURE DIRECTIONS

Conclusions

This research assessed and found that LiDAR can be used as the base remote sensing technology for forested areas in the Northwoods of Maine because it is capable of estimating reasonably well the vertical vegetation structure layer required by habitat-species mapping models such ECOSEARCH (Short et al. 2001). LiDAR data also provide the opportunity to derive other metrics across a forested landscape, either directly or indirectly through empirical models, that have been shown useful for resource managers. In addition to the well-known capability of LiDAR to derive high-resolution digital elevation models (Maune 2007), we also assessed and found LiDAR-derived explanatory variables, when developed and used in empirical models, capable of making accurate and reasonably precise predictions for several over- and understory forest metrics spatially and explicitly across broad landscape. These LiDAR-predicted metrics can be viewed as supplementing or even supplanting field-based forest inventories, depending on specific objectives and requirements. We also sought and determined that LiDAR-derived explanatory variables, when like-wise developed and used in empirical models, are capable of predicting occurrence abundance indices for several species of birds. For these LiDAR and empirically based models, we demonstrated how they can be combined and assist with assessing various management scenarios in a simple optimization context by specifying habitat goals and assessing which management scenario(s) appears to most likely meet those goals.

LiDAR, therefore, has at least two encompassing attributes that should make it the standard operandi to be used as a tool for managers. First, it provides a detailed high-

resolution DEM which allows the ability to characterize the topography beneath canopies as well as in open areas (e.g., microtopography). This allows for a multitude of applications including the topographic data layer required by ECOSEARH, change-detection from erosion (Thoma et al. 2005), locating depressions under canopies that might be vernal pools (Grant 2005), among many other applications (Vosselman and Maas 2010). The second justification for LiDAR acquisitions as standard operandi is its ability to provide spatially-explicit predictions of forest stand metrics for inventory purposes and as with topographic changes, change-detection of forest metrics and associated habitat for wildlife can be conducted spatially and explicitly across a landscape. These can then lead into specific habitat assessments for at least some bird species.

Although costs of LiDAR acquisitions remain high on a cost per ha basis (\pm \$50.00/100 ha), involving multiple stakeholders from various disciplines in acquisitions can add value and reduce costs for all by spreading out costs. Although national LiDAR acquisitions are being investigated (Stoker et al. 2007), often these multi-party acquisitions may and usually do not satisfy all stakeholders needs (e.g., leaf-on versus leaf-off acquisitions). Also, it is well known that policy and group dynamics can hinder groups and organizations from coming together for a common goal.

Future Directions

One future and important direction is the acquisition of high-resolution imagery simultaneously with LiDAR. Fusing (i.e., combining analytically) these two data sources should allow for more accurate mapping of vegetation composition, which is currently difficult to determine from LiDAR alone. Also, acquiring high-density LiDAR with the

high-resolution imagery has the potential for identifying individual tree crowns, thus allowing for mapping individual trees and their heights (Ke et al. 2010). Having this level of detail would allow the use of individual-based modeling efforts across the entire landscape (Liu and Ashton 1995). Also, this level of detail could further improve the models directly for ECOSEARCH, reduce manual interpretation of aerial images by taking advantage of the classified digital imagery, and derive enhanced LiDAR/imagery explanatory variables for modeling efforts. Even if individual crowns, thus individual trees, are not delineated, in the least, the level of detail provided by the combined imagery and LiDAR could enhance nonindividual-based stand growth models such as LANDIS (Mladenoff 2004).

With respect to assessing which management scenario(s) is optimal for the landscape at-hand and future projections, using such metrics as a simple Euclidean distances, at this time, should be viewed as an approach only. Other methods are available and should also be explored (Hof and Bevers 1998, Moilanen et al. 2005). However, as with most optimization efforts, the curse of dimensionality quickly catches-up and voids large projects as as undoable. Also, these efforts are not trivial to implement, especially from a computational perspective.

It is important to compare ECOSEARCH, version 1, predictions of bird occurrences (and others species) with those modeled here using LiDAR-derived explanatory variables, at least as occurrences. Also, ECOSEARCH, Version 1, should be updated to Version 2 that can begin to include the models developed here, at least for species that had reasonable models. Future work also could benefit from assessing not only mean abundance from averaging across years, but make better use of counting birds

within a year by using distance-based approaches (Buckland et al. 2001). Extending the modeling effort to other species and other demographics than just occurrence or abundance (e.g., nest success, chick mortality) should be explored and would require collecting field data across multiple years to calibrate and verify models. Updating ECOSEARCH would require modifying software, either the SAS programs written as part of this dissertation project, or convert them, and the FORTRAN programs ECOSEARCH is currently written to C++. Conversion to other software such as R (R Development Core Team 2005) should be explored. Finally, as LiDAR data sets become more readily available and large with decreased point-spacing, hence denser XYZ point-clouds, computation for all future LiDAR processing also should be done on parallel processing systems to speed processing times.

As summarized in this Chapter, the studies conducted as part of this dissertation should only be considered a starting point for taking advantage of a rapidly changing and improving remote sensing technology, LiDAR, with applications of its full potential only now beginning to be realized.

Literature Cited

- Buckland, S.T., D.R. Anderson, K.P. Burnham, J.L. Laake, D.L. Borchers, and L. Thomas. 2001. Introduction to distance sampling: estimating abundance of biological populations. Oxford University Press. Oxford, United Kingdom.
- Grant, E.H.C. 2005. Correlates of vernal pool occurrence in the Massachusetts, USA landscape. *Wetlands* 25:480-487.
- Hof, J., and M. Bevers. 1998. Spatial optimization for managed ecosystems. Columbia University Press. New York, New York.

- Ke, Y., L.J. Quackenbush, and J. Im. 2010. Synergistic use of QuickBird multispectral imagery and LiDAR data for object-based forest species classification. *Remote Sensing of Environment* 114:1141-1154.
- Liu, J., and P.S. Ashton. 1995. Individual-based simulation models for forest succession and management. *Forest Ecology and Management* 73:157-175.
- Maune, D.G. (Editor). Digital elevation model technologies and applications: the DEM user's manual, 2nd edition. American Society of Photogrammetry and Remote Sensing, Bethesda, Maryland.
- Mladenoff, D.J. 2004. LANDIS and forest landscape models. *Ecological Modelling* 180:7-19.
- Moilanen, A., A.M.A. Franco, R.I. Early, R. Fox, B. Wintle, and C.D. Thomas. 2005. Prioritizing multiple-use landscapes for conservation: methods for large multispecies planning problems. *Proceedings of the Royal Society-Biological Sciences* 272:1885-91.
- R Development Core Team. 2005. R: a language and environment for statistical computing. Vienna, Austria: R Foundation for Statistical Computing, <http://www.R-project.org>. Accessed 12 February 2012.
- Short, H.L., J.B. Hestbeck, and R.M. DeGraaf. 2001. New England wildlife: a model for ecosystem management – ECOSEARCH (version 1). Northeastern Forest Experiment Station, GTR NE-283, Radnor, Pennsylvania.
- Stoker, J., J. Parrish, D. Gisclair, D. Harding, R. Haugerud, M. Flood, H-E. Anderson, K. Schuckman, D. Maune, P. Rooney, K. Waters, A. Habib, E. Wiggins, B. Ellingson, B. Jones, S. Nechero, A. Nayegandhi, T. Saultz, and G. Lee. 2007.

Report of the first national lidar initiative meeting, February 14-16, 2007, Reston, Virginia.

Thoma, D.P., S.C. Gupta, M.E. Bauer, and C.E. Kirchoff. 2005. Airborne laser scanning for riverbank erosion assessment. *Remote Sensing of Environment* 95:493-501.

Vosselman, G., and H-G. Maas. (Editors). 2010. Airborne and terrestrial laser scanning. CRC Press. Boca Raton, Florida.

APPENDIX A. AN EVALUATION OF THE WANDERING POINT-QUARTER METHOD TO ESTIMATE FOREST STAND STRUCTURE WITHIN STUDY PLOTS

Introduction

As part of an assessment of light detection and ranging (LiDAR) to predict forest structure and to model wildlife habitat, we needed a field-based method and actual field data to characterize study plots and to calibrate with LiDAR-derived data. Many approaches and field methods have been used to characterize forest structure (e.g., Avery and Burkhart 2002, Husch et al. 2003). For example, foresters have developed several methods to estimate various forestry metrics (e.g., cords of wood/ha) at the stand level (Helms 1998). For our evaluation, we are interested only in metrics on 50×50 m plots (0.25 ha) because most of the bird species that we will model have territories that are much smaller than a forest stand (DeGraaf and Yamasaki 2001) and this is currently the unit-size in ECOSEARCH. However, measuring all trees (≥ 10 cm diameter at breast height or dbh) and saplings (< 10 cm dbh) within each plot may be unnecessary and unrealistic, particularly for forest stands with high stem densities.

In recent years, several methods and scales have been used to relate plot- or stand-level forest metrics to LiDAR data. Næsset et al. (2011), for example, used a single 8-m radius circular plot and sampled all trees with a dbh > 4 cm. Martinuzzi et al. (2009) measured all trees on several 11.35-m radius plots. Stephens et al. (2012), on the other hand, assessed only a sample of total tree heights on several 13.82-m radius circular plots. In all three of these recent studies, LiDAR-derived explanatory variables were related to forest metrics (e.g., mean dbh, canopy heights) within the circular plots.

Before LiDAR's inception, James and Shugart (1970) advocated a different approach to characterize forest structure in wildlife habitat studies. Their approach has been used in many wildlife studies and involve five or more 0.04-ha circular plots located randomly within a stand of trees. A modification of this approach was used by DeGraaf et al. (1998), who centered 0.04-ha circular subplots on 50-m radius circular points used for breeding bird surveys. DeGraaf and his coauthors then measured and characterized all trees within the subplots, and saplings were quantified on four 0.01-ha subplots located 20 m in each cardinal direction from the bird survey point center. To characterize and monitor forests (particularly health) across large extents of the U.S., the Forest and Inventory Analysis (FIA) program of the U.S. Forest Service also uses a variation of this approach by using four 0.017-ha circular subplots systematically nested within a larger 0.605-ha circular plot (Bechtold and Scott 2005). Another approach used in wildlife studies is to randomly deploy a 2-m wide belt transect across the study plot and to quantify all tree and sapling stems encountered within the transect (Penfound and Rice 1957). One shortcoming of either method is that it can be challenging to deploy circular subplots or belt transects in the field.

The wandering point-quarter plotless method (hereafter WQ; Catana 1963, Engeman et al. 1994) has been shown in simulation studies to be efficient and effective for sampling trees and estimating stand-level metrics (e.g., density), where stands can be from ≈ 1 ha to 100's of ha's. One advantage of the WQ is that subplots or transects are not required to be marked-out prior to taking tree measurements. Other advantages are that the method provides a more systematic sample of trees within each quadrant (thereby providing a more representative sample), requires only a tape measure and compass to

navigate between trees (and eliminates the need to bend the tape measure around trees), and, for small density plots, it selects trees for characterizing that might be missed using either the circular-plot or belt-transect methods. Because of LiDAR's blanket coverage across a 50×50 m plot, LiDAR returns would most likely hit some of the trees that might be missed by using circular-subplots or belt-transect methods whereas the WQ would at least sample and characterize some of these.

We conducted a simulation analysis before we deployed the WQ in the field for the LiDAR studies described in Chapters 2 and 3. The simulation helped us assess how well the WQ estimated various stand structural metrics (e.g., stem density, mean canopy height) within a 50×50 m (0.25-ha) plot compared to the belt-transect method. As a related comparison, we also compared forest metrics derived from FIA methodology with the WQ within an 88×88 m plot (0.77 ha), which is similar in size to the area of a standard FIA circular plot.

Methods

Sampling Methods

The WQ starts at a random point within a forest stand or plot of interest (e.g., center point of a bird survey circular plot). The observer measures the distance from the random point to the nearest tree within a 90-degree arc and then takes measurements on various characteristics from the selected tree (e.g., dbh, canopy height, species, status [alive or dead]). This tree is then used as the next “random” point from which the observer measures the distance to the next nearest tree within a 90-degree arc, and so on. Figure A.1 illustrates this process using the WQ within each of four quadrants (northeast, northwest, southwest, southeast) of a 50×50 m study plot. The process of selecting trees

can be terminated when the next tree occurs outside of the study plot (i.e., censored) or after a pre-determined number of trees have been characterized (i.e., a representative sample of trees within the quadrant has been described). For our needs, this process was repeated within each of the four quadrants and done separately for trees and saplings. Stem density estimates for the WQ are calculated as the area (2500 m^2) divided by the square of the mean distance between stems. Within each quadrant, we terminated the number of stems sampled after encountering six trees (12 for saplings). Censored distances (asterisks in Fig. A.1) were incorporated into the estimated mean distance of a study plot following the methods described in Datta (2005) for estimating the mean of right-censored values using PROC SURVIVE of SAS (SAS 2009). However, an informal analysis indicated that this was unnecessary and that the distance to the edge of the plot was a reasonable approximation in most cases.

Figure A.2 illustrates the belt-transect method that we selected for comparison with the WQ. The method involves two belt transects, each 2 m wide, with one transect running west to east and the other south to north, intersecting at the center. This belt-transect method is a slight modification of the methodology recommended by Penfound and Rice (1957) but is useful for this simulation as it attempts to provide a wider spatial coverage across the study plot. Density of trees for the belt-transect method is calculated as the number of trees encountered divided by the area (here 196 m^2) of the belt transects. Trees at the intersection of the two belt transects are counted only once. In the example in Fig. A.2, we show trees that were selected by the WQ only (thick open circles), by the belt-transect method only (solid circles), by both methods (asterisks), and by neither method (thin open circles). In this example, the WQ sampled more trees ($n = 18$) than

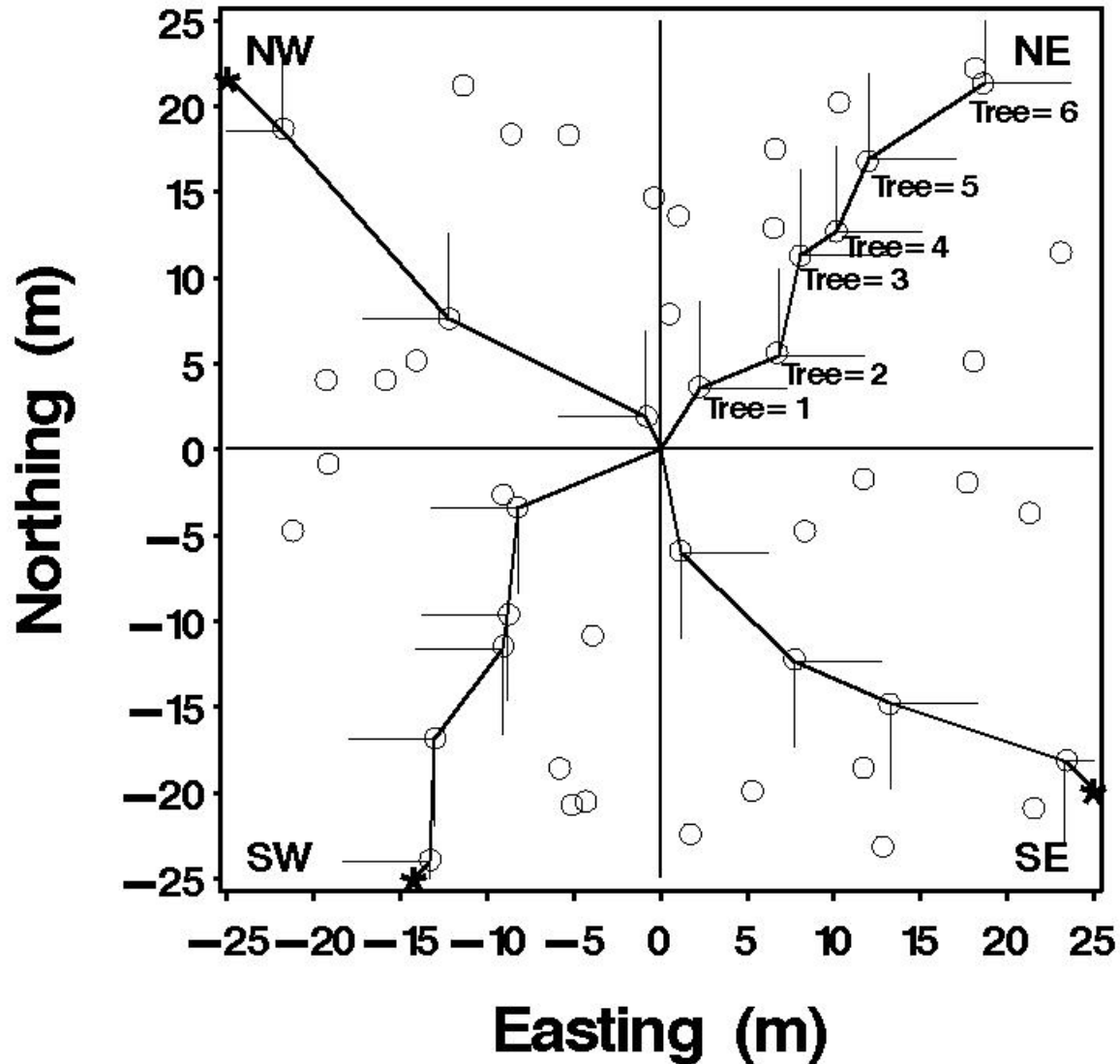


Figure A.1. Illustration of conducting a Wandering Quarter (WQ) sampling method within a 50×50 m plot (0.25 ha) of trees (total trees in plot = 50, n=18 selected for WQ, with 3 distances censored and represented by *).

the belt-transect method (n = 5 trees), and thus the WQ provided more individual tree measurements (e.g., canopy heights) than the belt-transect method.

Figure A.3 illustrates a slight modification of the FIA method. The method involves four 0.017-ha FIA circular subplots within an 88×88 m plot (0.77 ha). One circular subplot was placed at the plot center, and the remaining three subplots were

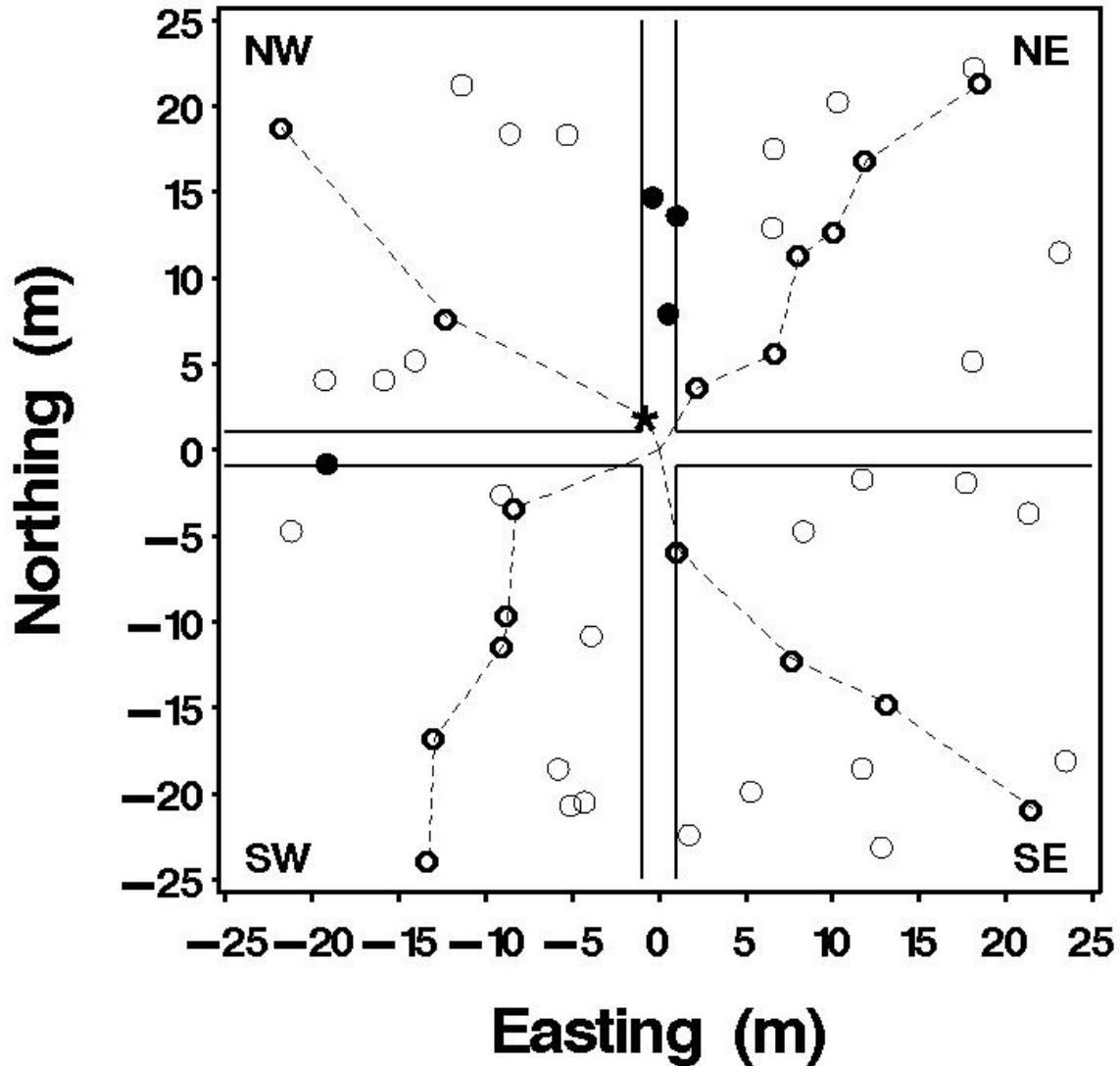


Figure A.2. Belt transect (BT) versus Wandering Quarter (WQ) sampling within a 50×50 m plot (0.25 ha) of trees: centered crossing S-N and W-E lines represent 2 m wide BT; thick open circles are selected trees using WQ only, solid circles are selected with BT only, stars are selected in both WQ and BT, with thin open circles being unsampled (N=50 total random distribution of trees, n=18 sampled for WQ, n=5 for BT).

located in a triangle, equidistant from the plot center. Stem density for the FIA method would be calculated as the number of stems encountered within the four circular subplots divided by 680 m^2 ($4 \times 0.017 \text{ ha}$). In the simulated data sets described below for the 88×88 m plots, we terminated sampling using the WQ after encountering 12 tree stems and 18 sapling stems within each quadrant. In Fig. A.3, we show trees that were selected

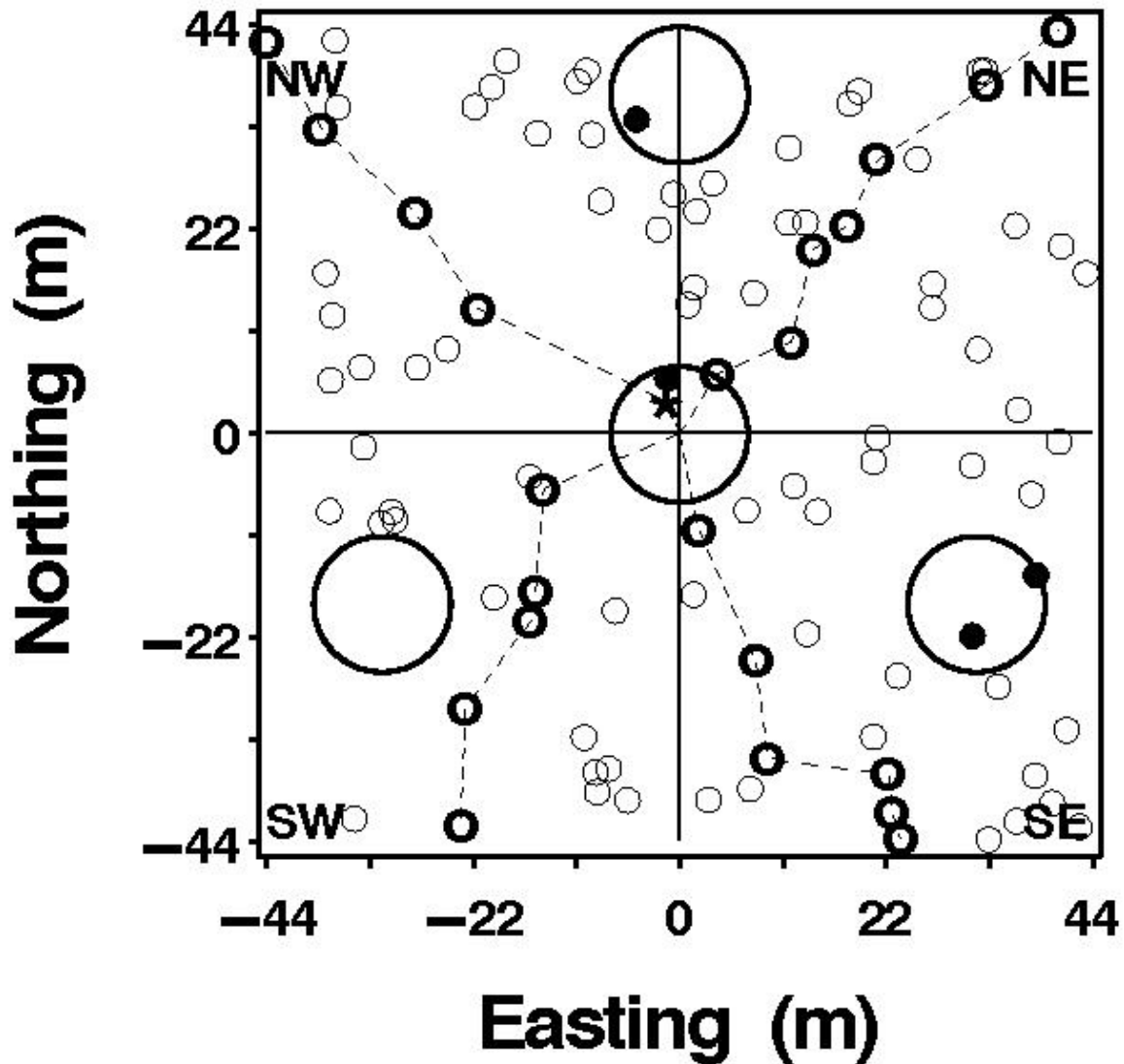


Figure A.3. Forest Inventory and Analysis (FIA) plots versus Wandering Quarter (WQ) sampling within a 88×88 m plot (0.77 ha): large circles represent location of 7.31 m radius FIA plots; thick open circles are selected using WQ only, solid circles are selected with FIA, stars are selected in both WQ and FIA, thin open circles being unsampled by either method (N=100 total random distribution of trees, n=23 sampled for WQ, n=5 for FIA).

by the WQ only (thick open circles), by the FIA method only (solid circles), by both methods (asterisks), and by neither method (thin open circles). In this example, the WQ sampled more trees (n = 23 trees) than the FIA method (5 trees).

Simulation of Plot Data to Sample

Using DeGraaf et al. (1998) as a guide for tree and sapling stem densities for mixed forests in Maine, we simulated the placement of trees and saplings at nine density levels and three spatial distributions (random, quasi-uniform, and clustered). For random distribution, we used 1, 3, 5, 10, 25, 50, 100, 250, and 500 tree stems per 50×50m plot and 1, 3, 5, 10, 50, 250, 1000, 1500, and 2500 sapling stems per 50×50m plot. For quasi-uniform distribution of trees and saplings, we attempted to derive equivalent ranges in stem densities as we used for random distributions by generating trees (or saplings) equally spaced in a 500×500 m grid with decreasing spacing between stems as densities increase. For each stem placed in the XY grid, we randomly jittered the exact XY position between ± 0.0 to 0.75 m because no stand is likely to be exactly uniform, but some can be nearly so (e.g., orchards or plantations). We then randomly positioned (both in location and orientation) a 50×50 m plot over this grid of locations to generate a quasi-uniform distribution of trees or saplings. For clumped distributions of trees or saplings within a 50×50 m plot, we generated random positions of clustered centroids within the plot, with the number of clusters being proportional to the density levels used for the random distribution. For each cluster, we then randomly selected a number of individual stems between 1 and 5, and then for each stem within a cluster, we randomly generated an XY value ± 0.0 to 2.0 m away from the cluster centroid. We repeated these processes for placement of tree and sapling stems in the 88×88 m FIA plots except we used tree densities of 1, 3, 5, 10, 25, 100, 500, 1000, and 1500 stems per 88×88 m plots, and sapling densities of 1, 3, 5, 10, 100, 500, 2000, 4000, and 7500 stems per 88×88 m plots. We therefore simulated 1080 stands from which to sample and compare the WQ and belt-

transect methods (50×50 m plots) and the WQ and the FIA (88×88 m plots) methods (i.e., 9 density levels × 3 distributions × 2 types [trees, saplings] × 10 replications at 2 scales [50×50 m, 88×88 m]). For each simulated tree or sapling, we also randomly assigned a canopy height from a normal distribution with a mean of 15 m and standard deviation of 4.47 m to assess biases, if any, for each sampling method.

Statistical Methods

We used simple correlations, linear regressions, and bivariate plots to examine the relationships and to assess any biases between the actual simulated densities (i.e., total stems/plot) and those estimated for each method and spatial distribution. We also examined biases in the estimated mean canopy heights by plotting the observed differences between the estimated and actual mean canopy heights with increasing stem density for each of the methods and spatial distributions. As an assessment of the efficiency among the three sampling methods, we plotted the number of trees actually sampled with increasing stem density for each method and distribution. An additional advantage of the WQ is that the WQ also can be used to estimate the spatial distribution (i.e., clumpiness) of stems within plots because it measures the distances between stems. Therefore, for the WQ only, we computed the coefficient of dispersion, which is the ratio of the variance of distances to the mean distance (Brower et al. 1989). For this ratio, a randomly dispersed population follows a Poisson distribution and would have a ratio equal to 1.0. Ratios substantially less than 1.0 imply a uniformly dispersed population, and ratios substantially greater than 1.0 imply clumped dispersion. We used SAS (SAS 2009) for all programming and analyses.

Results

Correlations between the actual number of trees and the estimated number of trees from both the WQ and the belt-transect method within 50×50 m plots were high ($r > 0.94$; Fig. A.4, Table A.1). Biases existed for both methods across the range of total trees (1 to ~500 stems/0.25 ha), but the biases were relatively consistent and subtle across the three distributions (i.e., both methods tended to overestimate stem densities at low densities and underestimate stem densities at higher densities). When considering only plots with <125 trees (Fig. A.5, Table A.1), the WQ still maintained a strong correlation between actual number of trees and estimated number of trees across all three distributions, whereas the belt-transect method experienced more variability and lower (albeit still strong) correlations. Both methods indicated some biases, especially for clumped distributions, by slightly underestimating the number of trees as the density of total trees increased. For saplings, the correlation between total stems and estimated stems was high, but larger biases were indicated, particularly for clumped distributions using either method (Table A.2). However, across the range of total saplings (1 to 2500 stems), these biases were fairly trivial, even for plots with <125 stems (Table A.2).

As with comparisons involving the belt-transect method on 50×50 m plots, we found high correlations and consistent but subtle biases between the total number of trees and estimated number of trees on the 88×88 m plots for the WQ and FIA across the three distributions (Fig. A.6, Table A.3). Biases tended to increase slightly with clumped distributions for plots with <125 total trees (Fig. A.7, Table A.3). Although not summarized herein, results were similar for saplings on the 88×88 m plots. Again, when

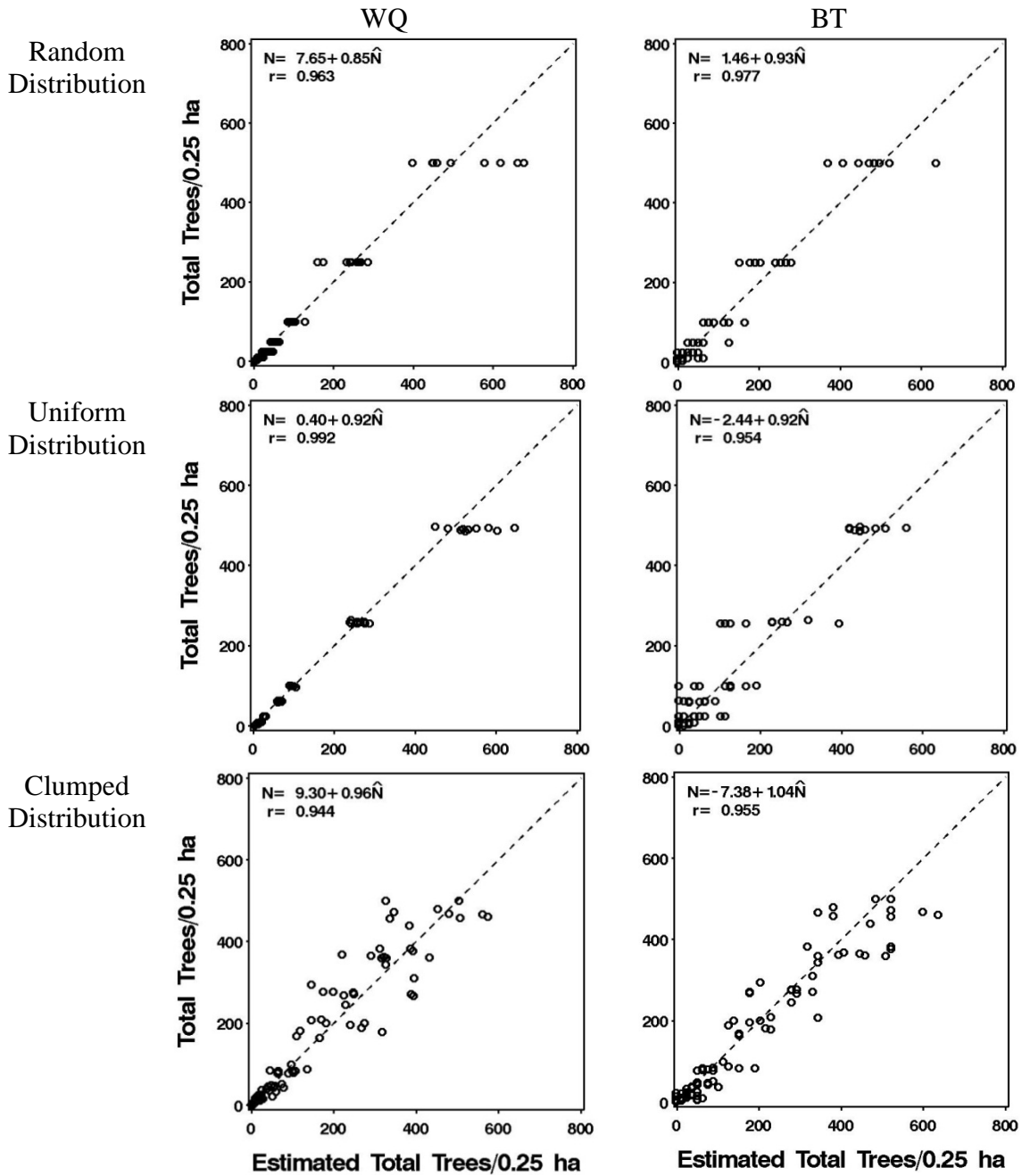


Figure A.4. Comparison of the relationship between simulated population size of total trees (all N levels) and estimated total trees for two sampling methods (WQ=Wandering Quarter, BT=Belt Transect) for three spatial distributions within 50×50 m plots (0.25 ha); dashed line is 1-to-1 correspondence.

Table A.1. Parameter estimates and correlations evaluating the linear relationship between simulated population size of total trees (N) within 50×50 m plots and estimated population size using a Wandering Quarter (WQ) method and a Belt Transect (BT) method for three spatial distributions.

N	Method	Distribution	Intercept (SE)	Slope (SE)	r
1 to ≈500	WQ	Random	7.65 (5.42)	0.85 (0.03)	0.963
		Uniform	0.40 (2.53)	0.92 (0.01)	0.992
		Clumped	9.30 (8.10)	0.96 (0.04)	0.944
		Mean	5.78 (3.35)	0.91 (0.02)	0.966
	BT	Random	1.46 (4.11)	0.93 (0.02)	0.977
		Uniform	-2.44 (5.85)	0.92 (0.03)	0.954
		Clumped	7.38 (7.94)	1.04 (0.03)	0.955
		Mean	2.13 (3.70)	0.96 (0.02)	0.962
<125	WQ	Random	-4.68 (1.14)	0.96 (0.02)	0.980
		Uniform	-6.95 (0.62)	1.08 (0.01)	0.995
		Clumped	2.57 (0.80)	0.80 (0.05)	0.910
		Mean	-3.02 (0.51)	0.95 (0.02)	0.962
	BT	Random	1.52 (3.06)	0.96 (0.07)	0.855
		Uniform	4.04 (5.53)	0.73 (0.12)	0.590
		Clumped	4.98 (5.27)	1.18 (0.12)	0.817
		Mean	3.51 (2.74)	0.96 (0.06)	0.754

considering the full range of total stems (1-1500 for trees, and 1-7500 for saplings), the biases were fairly trivial, especially for the WQ.

Efficiency and questions involving how many trees to sample on a single study plot are important considerations when selecting and evaluating field methodologies, especially when some metrics (e.g., canopy heights) are more difficult and more time-consuming to measure than others (e.g., dbh). Both the belt-transect method and the FIA tend to undersample with <100 total trees and oversample with >100 total trees (Fig. A.8). To avoid oversampling, the WQ terminates sampling after 6 trees within each quadrant thus providing up to 24 trees sampled per plot within a 50×50 m plot (48 trees with an 88×88 m plot). In general, and from a statistical perspective, having at least 24

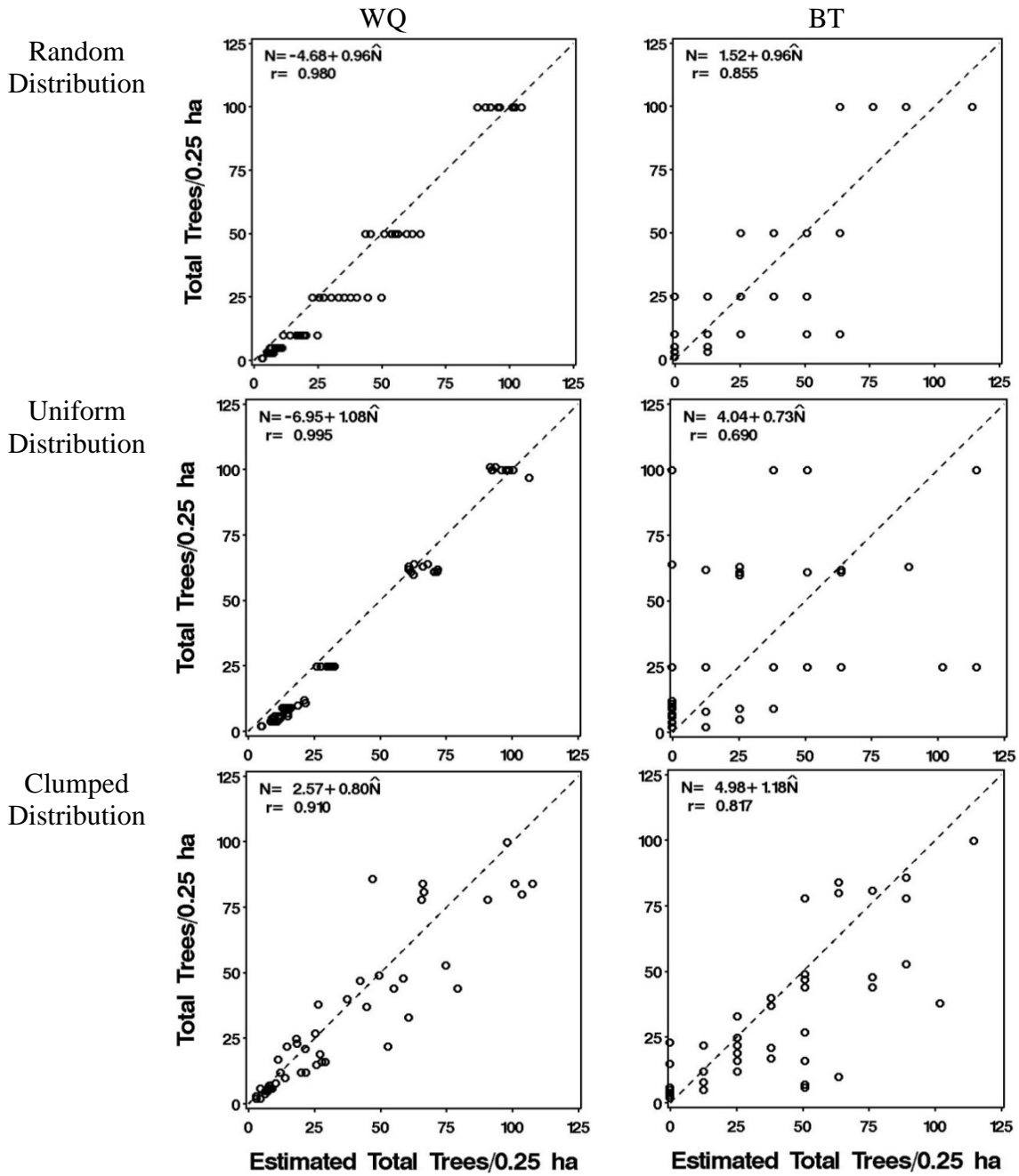


Figure A.5. Comparison of the relationship between simulated population size of total trees (only N levels < 125) and estimated total trees for two sampling methods (WQ=Wandering Quarter, BT=Belt Transect) for three spatial distributions within 50×50 m plots (0.25 ha); dashed line is 1-to-1 correspondence.

Table A.2. Parameter estimates and correlations evaluating the linear relationship between simulated population size of total saplings (N) within 50×50 m plots and estimated population size using a Wandering Quarter (WQ) method and a Belt Transect (BT) method for three spatial distributions.

N	Method	Distribution	Intercept (SE)	Slope (SE)	r
1 to ≈2500	WQ	Random	11.81 (21.01)	0.95 (0.02)	0.982
		Uniform	-5.09 (10.00)	1.04 (0.01)	0.996
		Clumped	42.86 (27.70)	0.93 (0.03)	0.968
		Mean	16.53 (12.06)	0.97 (0.01)	0.982
	BT	Random	-7.53 (11.80)	1.01 (0.01)	0.994
		Uniform	-1.59 (6.10)	1.01 (0.01)	0.999
		Clumped	20.37 (15.82)	0.97 (0.02)	0.990
		Mean	3.75 (6.89)	1.00 (0.01)	0.994
<125	WQ	Random	-3.48 (3.26)	0.97 (0.02)	0.986
		Uniform	-6.31 (1.01)	1.06 (0.01)	0.996
		Clumped	-5.68 (3.26)	1.02 (0.03)	0.978
		Mean	-5.16 (1.38)	1.02 (0.01)	0.987
	BT	Random	2.58 (3.44)	0.90 (0.03)	0.963
		Uniform	3.32 (5.64)	0.87 (0.05)	0.902
		Clumped	9.90 (5.47)	1.00 (0.05)	0.938
		Mean	5.27 (2.86)	0.92 (0.03)	0.934

units sampled form a population of units, at least provides reasonable information on summary statistics (i.e., means, standard deviatons).

For mean canopy heights, the WQ did not indicate any biases based on mean differences between observed and simulated canopy heights across any of the three distributions (Fig. A.9). The belt-transect method, however, was unable to estimate mean canopy heights for many of the plots that had a low number of total trees. In the few situations in which the belt-transect method could estimate mean canopy heights for low density plots, there was a lot of variation in the estimates (Fig. A.9). Both the WQ and the belt-transect method provided better estimates of mean canopy height as the total number of stems samples increased, indicating that it may not be necessary to collect

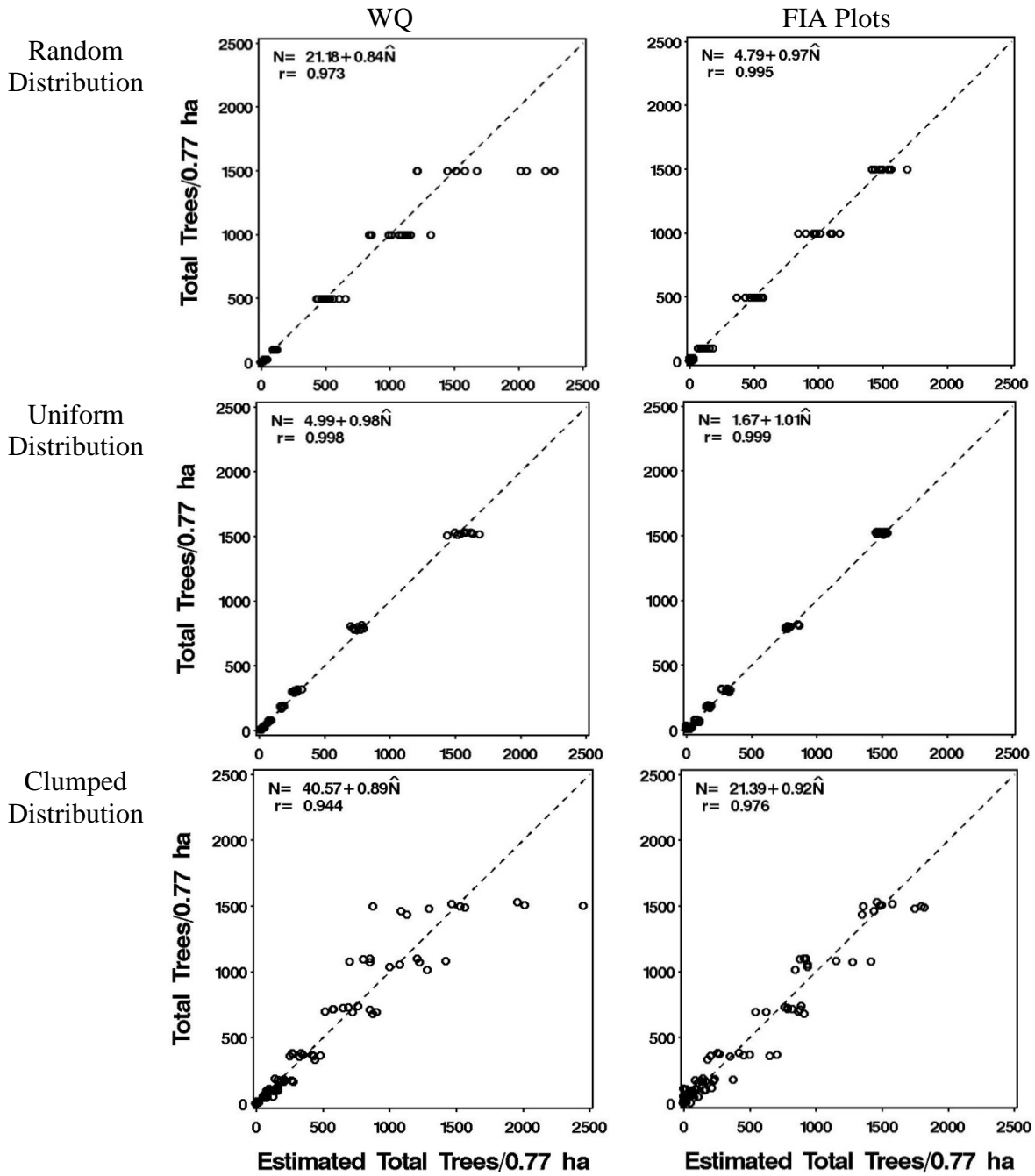


Figure A.6. Comparison of the relationship between simulated population size of total trees (all N levels) and estimated total trees for two sampling methods (WQ=Wandering Quarter, FIA=Forest Inventory and Analysis) for three spatial distributions within 88×88 m plots (0.77 ha); dashed line is 1-to-1 correspondence.

Table A.3. Parameter estimates and correlations evaluating the linear relationship between simulated population size of total trees (N) within 88×88 m plots and estimated population size using a Wandering Quarter (WQ) method and Forest Inventory and Analysis Plots (FIA) method for three spatial distributions.

N	Method	Distribution	Intercept (SE)	Slope (SE)	r
1 to ≈1500	WQ	Random	21.18 (15.20)	0.84 (0.02)	0.973
		Uniform	4.99 (4.40)	0.98 (0.01)	0.998
		Clumped	40.57 (23.38)	0.89 (0.03)	0.944
		Mean	22.25 (9.41)	0.90 (0.01)	0.972
	FIA	Random	4.79 (6.32)	0.97 (0.01)	0.995
		Uniform	1.67 (2.67)	1.01 (0.01)	0.999
		Clumped	21.39 (15.43)	0.92 (0.02)	0.976
		Mean	9.28 (5.63)	0.97 (0.01)	0.990
<125	WQ	Random	-3.69 (0.96)	0.90 (0.02)	0.986
		Uniform	-5.85 (0.77)	0.98 (0.02)	0.992
		Clumped	3.11 (3.41)	0.73 (0.04)	0.936
		Mean	-2.14 (1.21)	0.87 (0.02)	0.971
	FIA	Random	5.01 (2.06)	0.75 (0.04)	0.922
		Uniform	9.38 (2.27)	0.72 (0.06)	0.880
		Clumped	23.86 (6.00)	0.53 (0.09)	0.680
		Mean	12.75 (2.25)	0.67 (0.04)	0.827

information on more than 24 stems per 50×50 m plot. Similar conclusions can be drawn when comparing the WQ with the FIA method on the 88×88 m plots (Fig. A.10). At least some estimates of mean canopy height can be collected for plots with lower tree stem densities using the WQ than the FIA method, but this advantage quickly diminishes as the total number of trees increases (Fig. A.10).

One advantage of WQ is that it provides distances between stems. We therefore made an assessment of the distribution of stem locations within a study plot using the ratio of variance of distances to mean distances (Fig. A.11). This ratio is centered at 1.0 for random distributions, >1.0 for clustered distributions, <1.0 for uniform distributions (Brower et al. 1989). For plots with a small number of total trees (and thus sample sizes), generalities should be used with caution. There are other metrics that can be considered

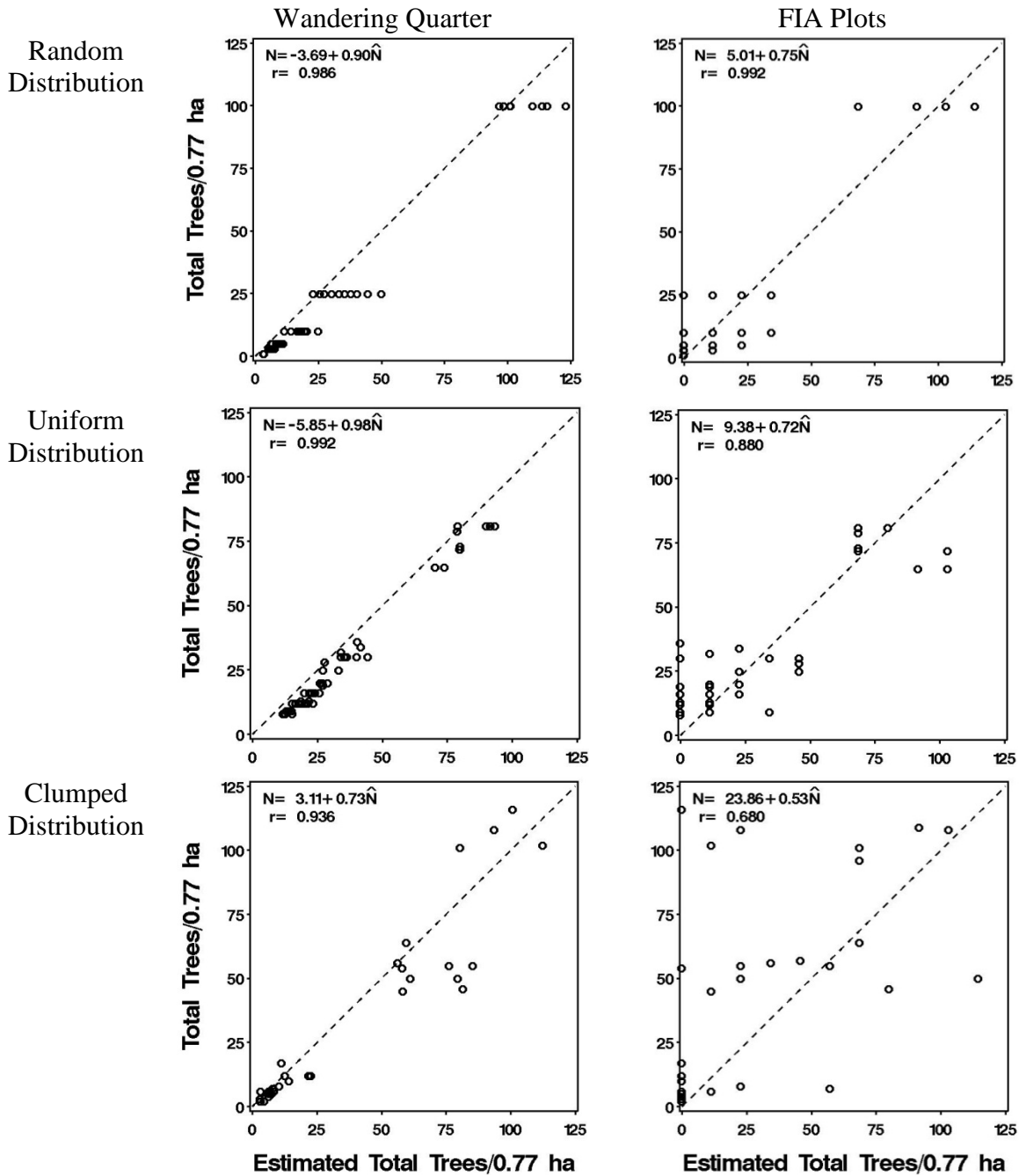


Figure A.7. Comparison of the relationship between simulated population size of total trees (all N levels < 125) and estimated total trees for two sampling methods (WQ=Wandering Quarter, FIA=Forest Inventory and Analysis) for three spatial distributions within 88×88 m plots (0.77 ha); dashed line is 1-to-1 correspondence.

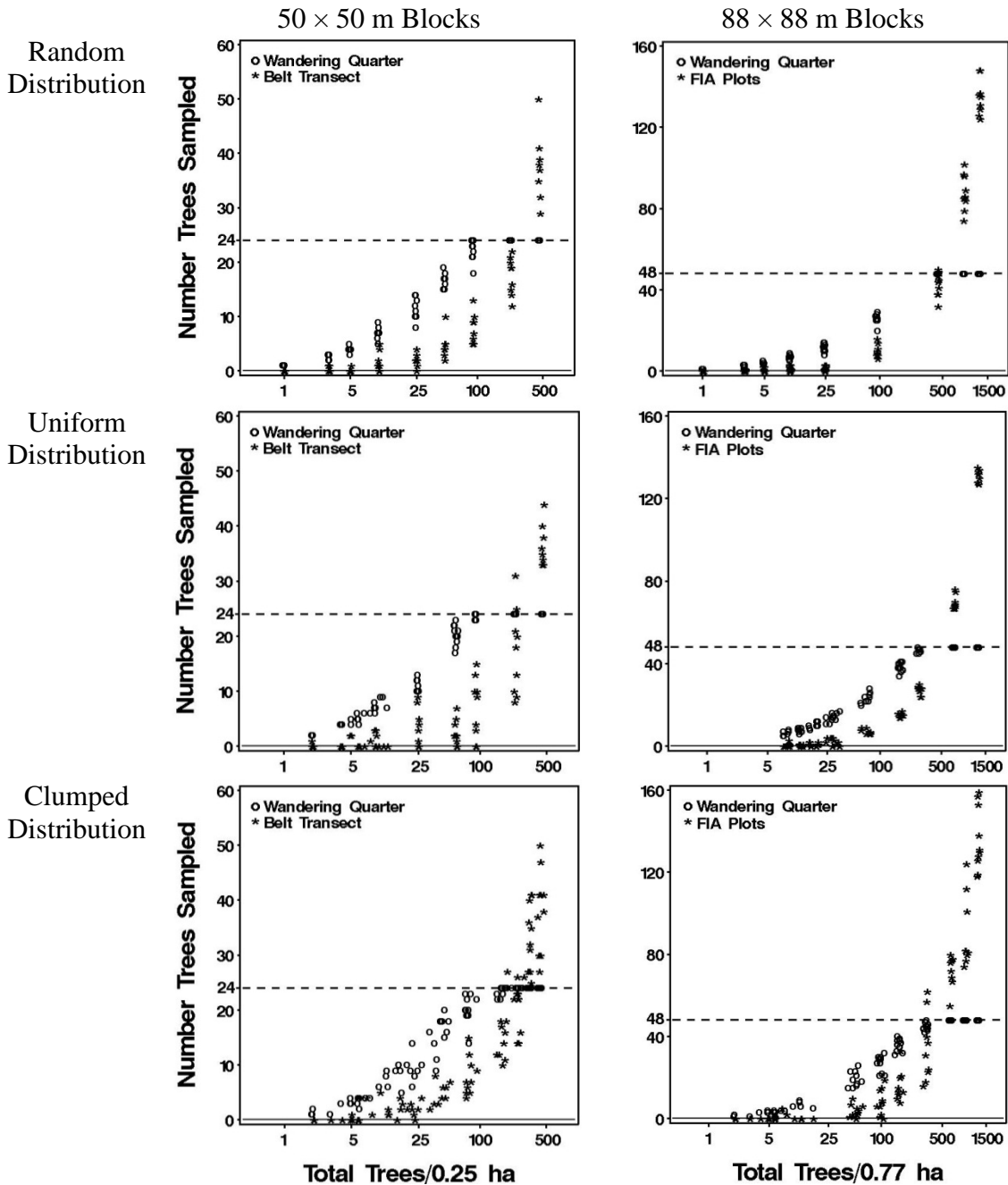


Figure A.8. Comparison of sampling intensities between Wandering Quarter (WQ) and Belt Transect (0.25 ha plots) and WQ and Forest Inventory and Analysis (FIA) plots (0.77 ha plots) sampling methods for increasing simulated total trees for three spatial distributions (dashed-line represents maximum number of stems sampled by WQ across the four quadrants).

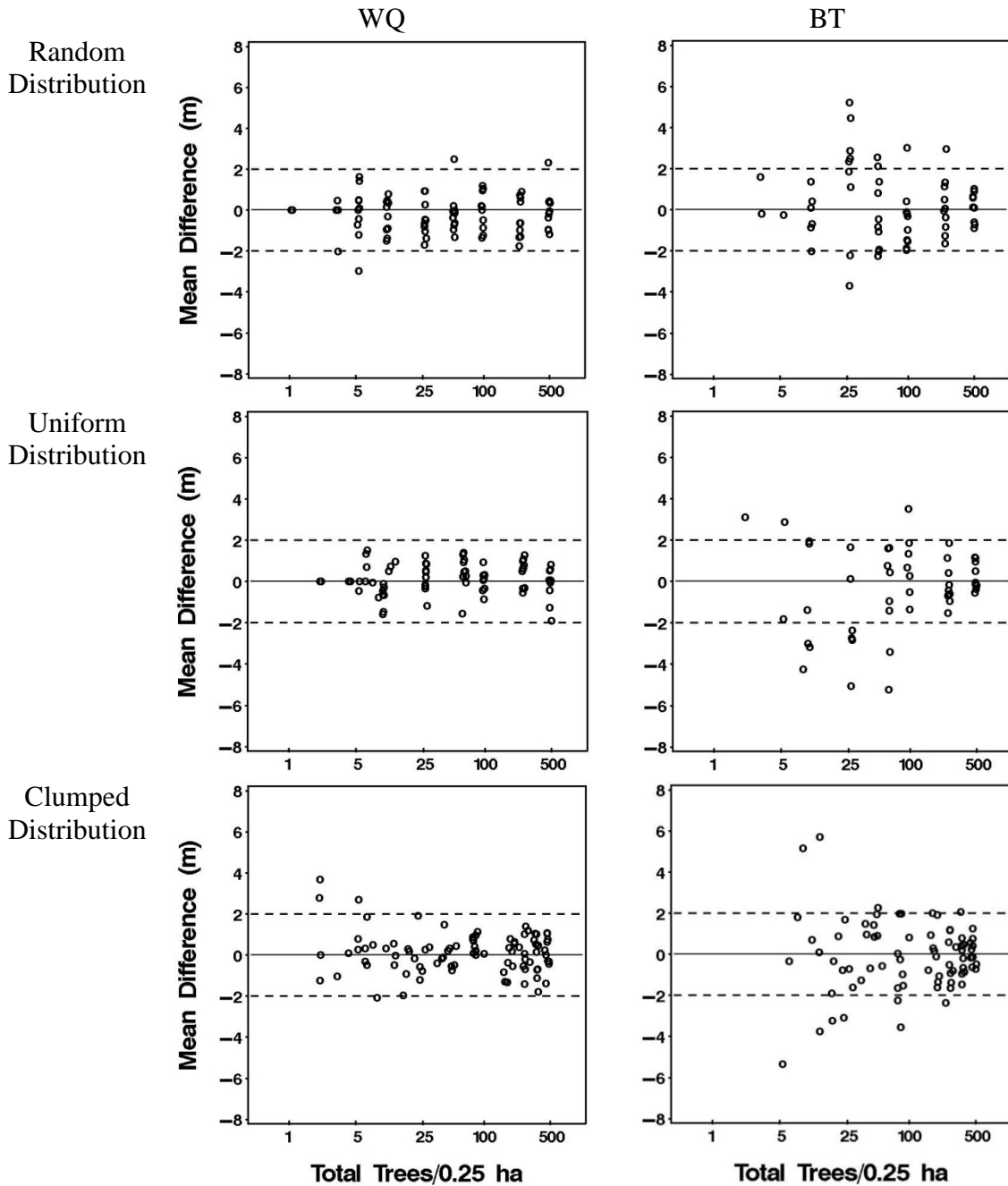


Figure A.9. Comparison of mean difference between sampled mean canopy heights and simulated population mean canopy heights within 50×50 m plots (0.25 ha) for Wandering Quarter (WQ) and Belt Transect (BT) methods for three spatial distributions (dashed-lines are ± 2 m for reference only).

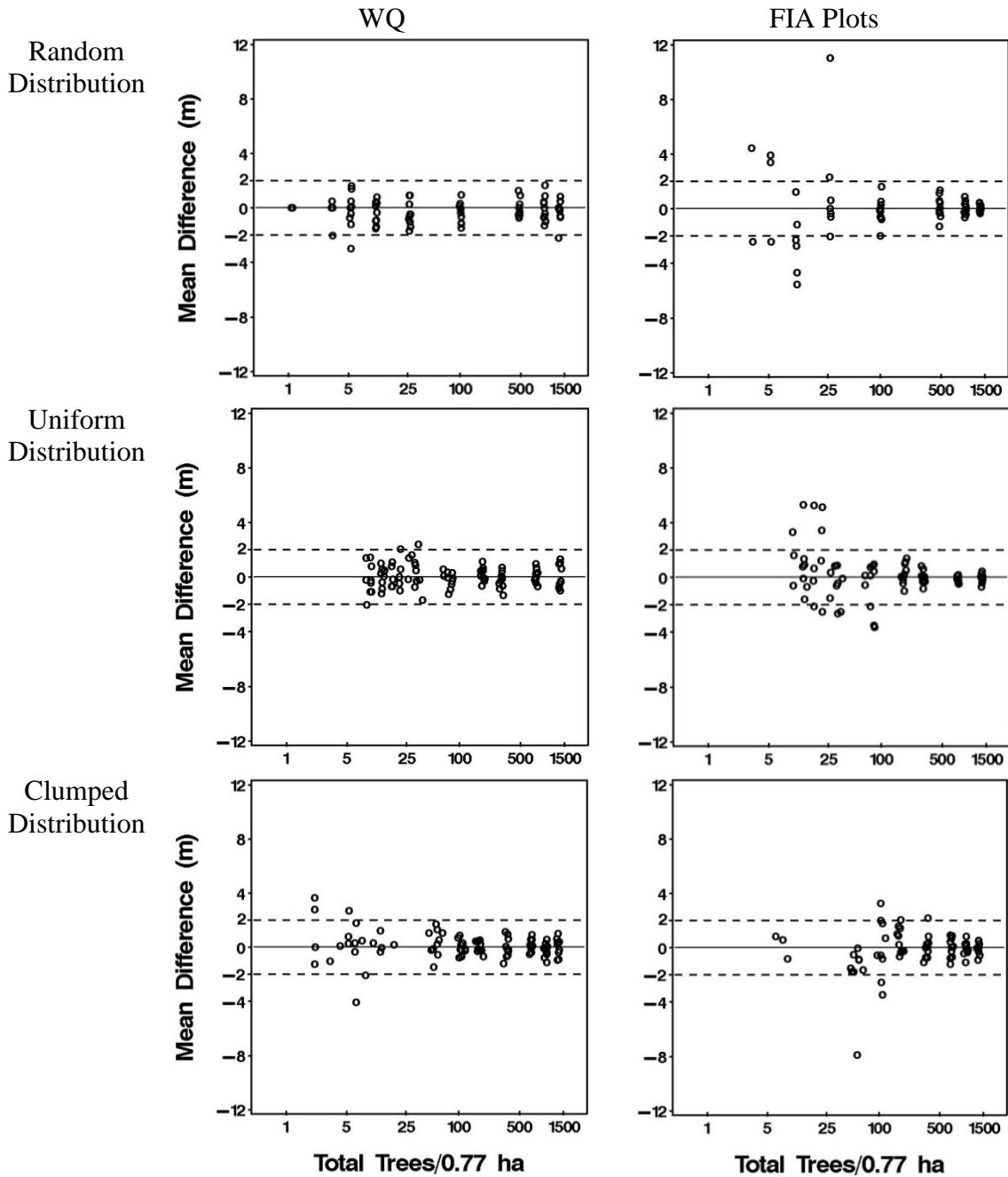


Figure A.10. Comparison of mean difference between sampled mean canopy heights and simulated population mean canopy heights within 88×88 m plots (0.77 ha) for Wandering Quarter (WQ) and Forest Inventory and Analysis (FIA) methods for three spatial distributions (dashed-lines are ± 2 m for reference only).

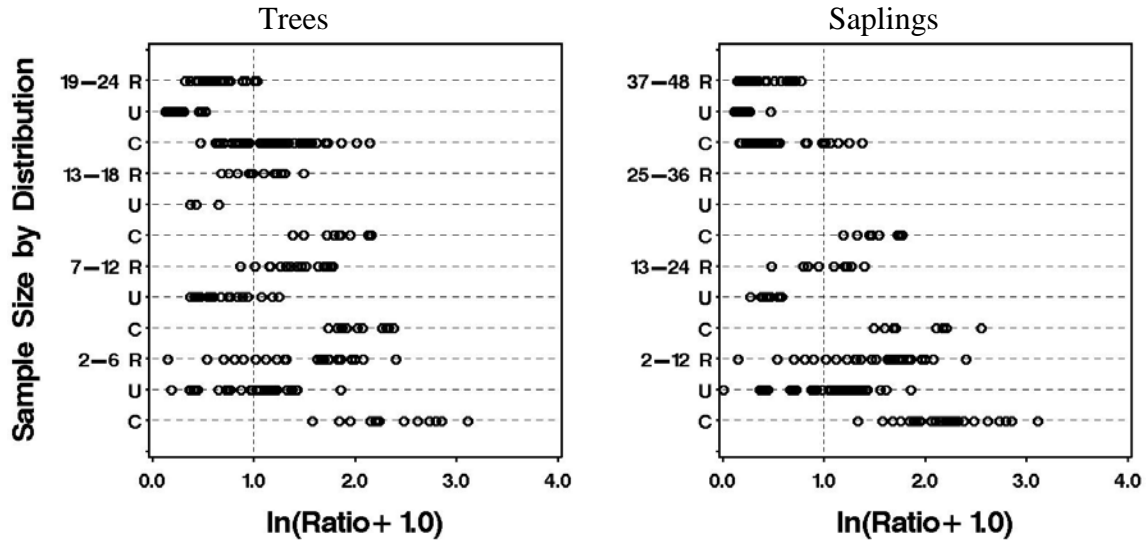


Figure A.11. Distribution of variance-to-mean ratio distances for trees and saplings sampled from known random (R), uniform (U), and clumped (C) spatial distributions within 50×50 m plots (0.25 ha) as a result of increasing sample sizes using Wandering Quarter sampling method: here Ratio=variance of distances between trees (or saplings) to their respective mean distance (note: numbers of saplings sampled for uniform and random increased from 13-24 range to 37-48 range; vertical dashed-line represents variance-to-mean ratio of 1.0 implying random distribution of stems).

and probably should (e.g., see Dale 1999), but the results in Fig. A.11 can be viewed as a guide to the type of information provided by the WQ that the BT and FIA methods do not provide (unless supplemented with other methodology). From Fig. A.11, the ratio computed from sampled stems from both known random and uniform distribution centered at 1.0 for small sample sizes, shifting to < 1.0 for larger sample sizes. The ratio for clustered distributions was > 1.0 for small sample sizes shifting to being centered on 1.0 with increasing sample sizes. This may be a reflection of the ratio of variance-to-mean is not the best metric to quantify spatial distribution. Also, as number of stems sampled increases so does the density of stems, hence the distributions of stems at the scale of a 50×50 m plot may indeed become more “uniform” due to lack of space for stems to physically be.

Discussion

The WQ performed equally as well as, or even slightly better than, the belt-transect and FIA methods, but all approaches had some subtle biases or shortcomings, particularly for clumped distributions with few total trees or saplings. The WQ has some apparent advantages over the belt-transect or FIA methods, including (1) individual trees in XY positions can be mapped or remapped by using the WQ given that the distance and angles are recorded, (2) mean characteristics of individual trees can be summarized for plots with low numbers of total trees or saplings, and (3) within-plot spatial distributions can be estimated given that distances between a sample of stems measured. Therefore, based on evidence from this simulation study, we believe the WQ will provide adequate information within 50×50 m study plots to relate field-collected data to LiDAR-derived data.

Literature Cited

- Avery, T.E., and H.E. Burkhart. 2002. *Forest Measurements*, 5th edition. McGraw-Hill, New York, New York.
- Bechtold, W.A., and C.T. Scott. 2005. The forest inventory and analysis plot design. Pages 27-42 *in* The Enhanced Forest Inventory and Analysis Program-National Sampling Design and Estimation Procedures (W.A. Bechtold and P.L. Patterson, Eds.). U.S. Department of Agriculture, Forest Service, Southern Research Station Gen. Tech. Rep. SRS-80, Asheville, North Carolina.
- Brower, J., J. Zar and C. von Ende. 1989. *Field and Laboratory Methods for General Ecology*, 3rd edition. Wm. C. Brown Publishers, Dubuque, Iowa.

- Catana, A.J. 1963. The wandering quarter method of estimating population density. *Ecology* 44:349-360.
- Datta, S. 2005. Estimating the mean life time using right censored data. *Statistical Methodology* 2:65-69.
- DeGraaf, R.M., J.B. Hestbeck and M. Yamasaki. 1998. Associations between breeding bird abundance and stand structure in the White Mountains, New Hampshire and Maine, USA. *Forest Ecology and Management* 103:217-233.
- DeGraaf, R.M., and M. Yamasaki. 2001. *New England Wildlife: Habitat, Natural History, and Distribution*. University Press of New England, Hanover, New Hampshire.
- Engeman, R.M., R.T. Sugihara, L.F. Pank, and W.E. Dusenberry. 1994. A comparison of plotless density estimators using Monte Carlo simulation. *Ecology* 65:1769-1779.
- Helms, J.A. (Ed.). 1998. *The Dictionary of Forestry*. Society of American Foresters, Bethesda, Maryland.
- Husch, B., T.W. Beers, and J.A. Kershaw, Jr. 2003. *Forest mensuration*, 4th edition. John Wiley and Sons, Inc., Hoboken, New Jersey.
- James, F.C., and H.H. Shugart. 1970. A quantitative method of habitat description. *Audubon Field Notes* 24:727-736.
- Martinuzzi, S., L.A. Vierling, W.A. Gould, M.J. Falkowski, J.S. Evans, A.T. Hudak, and K.T. Vierling. 2009. Mapping snags and understory shrubs for a LiDAR-based assessment of wildlife habitat suitability. *Remote Sensing of Environment* 113:2533-2546.

- Næssett, E., T. Gobakken, S. Solberg, T.G. Gregoire, R. Nelson, G. Stahl, and D. Weydahl. 2011. Model-assisted regional forest biomass estimation using LiDAR and InSAR as auxiliary data: a case study from a boreal forest area. *Remote Sensing of Environment* 115:3599-3614.
- Penfound, W.T., and E.L. Rice. 1957. An evaluation of the arms-length method in forest sampling. *Ecology* 38:660-661.
- SAS Institute. 2009. The SAS System for Windows, ver. 9.1. SAS Institute, Inc., Cary, North Carolina.
- Stephens, P.R., M.O. Kimberley, P.N. Beets, T.S.H. Paul, N. Searles, A. Bell, C. Brack, and J. Broadley. 2012. Airborne scanning LiDAR in a double sampling forest carbon inventory. *Remote Sensing of the Environment* 117:348-357.

APPENDIX B. A SAS PROGRAM FOR THREE-DIMENSIONAL VISUALIZATION OF FOREST HABITAT

Background and Justification

Modeling wildlife-habitat relationships often requires quantification of vegetation structure and other variables from sampling units across an entire landscape in which animal surveys have been conducted (e.g., breeding bird point-count surveys; Ralph et al. 1995). In the development of predictive models, the sampling design typically includes study plots that are small (e.g., 50×50 m), that are centered on animal survey locations, and that are representative of the overall landscape (i.e., encompass the heterogeneity of habitat types or vegetation within the landscape) (Hirzel and Guisan 2002). In forests, quantification of habitats typically includes structural measurements on a sample of individual trees, which are then summarized for each study plot and used in empirical modeling of animal demographics (e.g., bird abundance, nest survival). The ability to visualize structure (and general composition) of an entire forest stand from actual field data or simulated data would be useful to forest managers, biologists, and policy planners. Although ground-level photographs or aerial imagery may allow researchers to interpret the habitat conditions on a study plot, it often is difficult to visualize the vegetation structure or composition at that site from only a photograph and is nearly impossible to visualize these characteristics for the entire stand. Similarly, envisioning forest conditions from large spreadsheets of raw field data (e.g., stem density, diameter-at-breast height [DBH], canopy heights) or summaries of those data (e.g., mean, variation) also is challenging, especially when there are hundreds of study plots or many vegetation measurements or variables involved. Forest stand growth and projections

from simulation models, either from forecasting or backcasting, also are nearly impossible to visualize from model outputs.

Wildlife-habitat models can be complex and involve one to several explanatory variables. Examining directions and magnitudes of model parameter estimates, even for good-fitting models, can be difficult to interpret, especially those with nonlinear relationships and interactions. Although analysts can easily show the relationship between an animal demographic and a suite of explanatory variables by using two- and three-dimensional response surface plots, it is much more difficult to demonstrate low, moderate, and high quality habitat at three-dimensions in a study plot or forest stand using standard graphics for response surface plots. Response surface plots also may be too complicated or intimidating for lay audiences and managers.

For our studies in Maine, we developed forest vegetation models and wildlife-habitat relationship models by using data derived from light detection and ranging (LiDAR) technology (see Chapter 2 for details on modeling forest structure and Chapter 3 for details on modeling bird abundance as a function of LiDAR-derived explanatory variables). LiDAR is an optical remote sensing technology that uses lasers to detect and measure features on the Earth's surface, including vegetation in forested areas. Airborne LiDAR is capable of providing both horizontal and vertical information on forest vegetation structure at high resolutions and vertical accuracies (Lim et al. 2003). Within our Maine study plots, the LiDAR system recorded returns along the flight path of an aircraft. The returns were then classified into vertical bins that represent the amount of vegetation within different height profiles (i.e., percent of LiDAR returns between the ground [0 m] and 3 m, between 3 m and 6 m, etc.). These vertical profiles were then

summarized and used as explanatory variables in statistical models. One advantage of LiDAR-derived models is the continuous coverage of LiDAR-derived variables across the entire study area, allowing for spatially-explicit predictions of metrics for individual plots as well as the entire forest stand covered by LiDAR (i.e., assuming reasonable models have been developed). For example, the models that we developed in Chapter 2 (forest stand models) and Chapter 3 (bird-habitat models) used LiDAR-derived explanatory variables across the entire study area, which allowed us to make large-scale predictions and to visualize the forest plots under varying model scenarios. The LiDAR acquisition for one study site (Moosehorn National Wildlife Refuge) was 7.9×13.1 km, which yielded over 41,000 sampling units (cells or study plots) that were each 50×50 m.

Several software packages are available that provide visualization tools that can be used to explore or interpret characteristics of forest vegetation and stands (e.g., McGaughey 1998, 2000; Lim and Honjo 2003; Kao et al. 2005). Many of these packages offer graphical user interfaces (GUI) that allow users to interact with their visualization and modeling efforts as well as input field-collected or simulated data. As useful as these software tools are for rendering and visualizing forest vegetation in three dimensions, we were interested in an approach that could be integrated with our empirical wildlife-habitat models that we developed using SAS statistical software (SAS 2009). Therefore, we developed a visualization tool using SAS programming code that can be embedded within other SAS code or used as a stand-alone program; our visualization approach provides a new way to visualize and compare large quantities of three-dimensional data that were field-collected, predicted, or simulated.

Methods

General Process

Figure B.1 outlines the general process used to render the data from the 50×50 m plots for three-dimensional visualization in SAS. A spreadsheet of stand-level metrics can be generated using one of several approaches. First, these metrics can be derived from field-collected or simulated forest stand data from individual 50×50 m plots. Second, the metrics can come from empirical wildlife demographic models that are a function of forest stand explanatory variables (or from LiDAR explanatory variables). In this approach, wildlife models can be executed under various scenarios (e.g., optimal or suboptimal habitat) of the explanatory variables in a factorial arrangement, and then the forest stand metrics can be computed and organized in the format of the required spreadsheet. Third, forest stand metric models can be executed (as a function of LiDAR-derived explanatory variables) and then used to predict forest stand level information (typically as means and standard deviations). In this approach, the forest stand level information can be sampled from a multivariate (log) normal distribution to populate the stand with trees and then organized in the format of the required spreadsheet. After the spreadsheet has been generated and properly formatted using SAS or another program, the data can then be used to render the study units or stand in three dimensions (see Fig. B.1 for examples).

Spreadsheet Format

The spreadsheet format (Fig. B.1) is required by the SAS program and includes 11 columns (all units are in meters). Column 1 is a numerical identifier for each

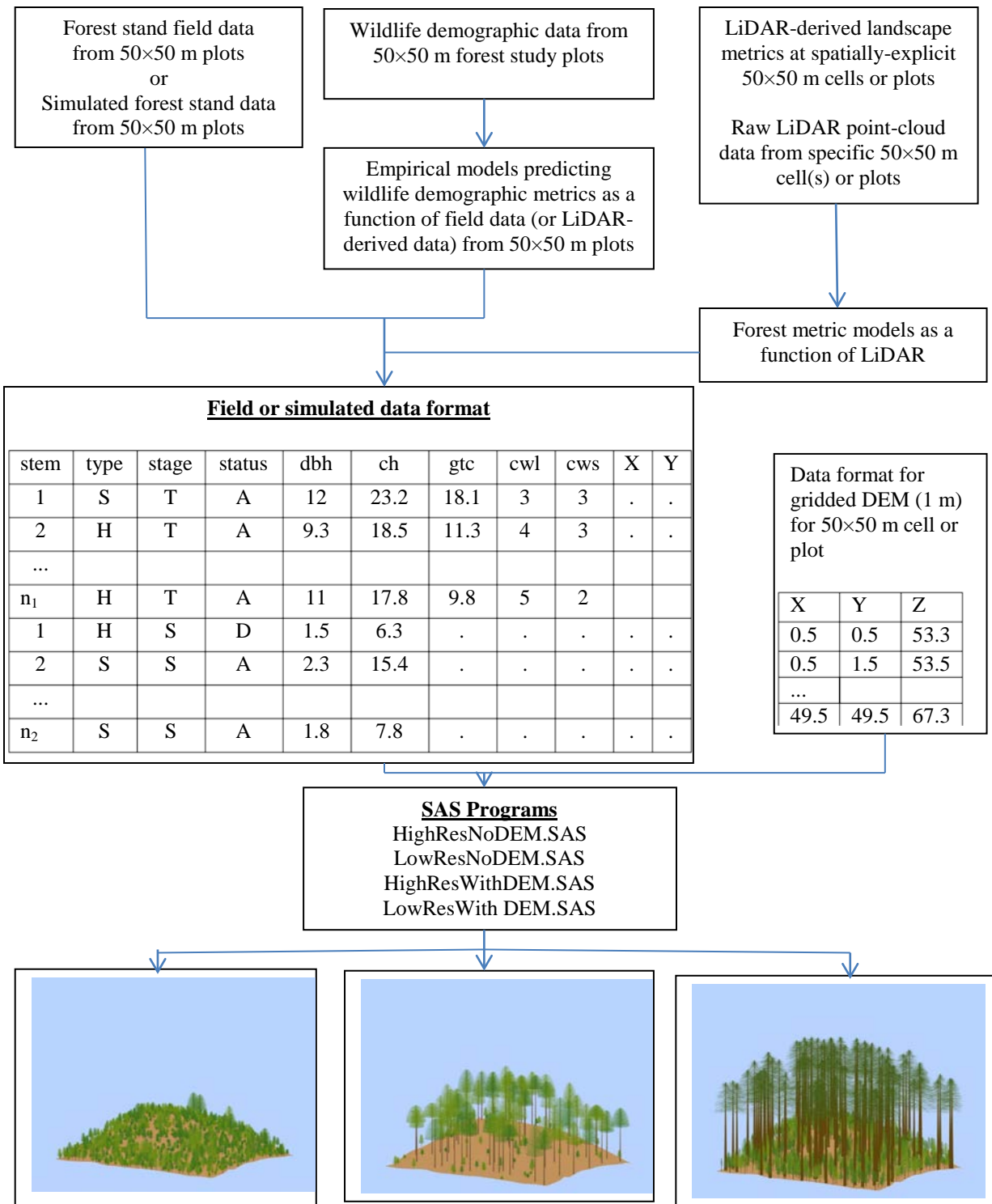


Figure B.1. Basic data flow chart illustrating three-dimensional visualization of 50x50 m plot using SAS program(s) from field or simulated data, estimated field data from empirical wildlife models, or those modeled from LiDAR-derived data (see text for details, spreadsheet units are in meters).

individual stem. Column 2 classifies each stem species into one of two broad types: softwood (S; coniferous or needle-bearing species) and hardwood (H; deciduous or leaf-bearing species). Column 3 represents the life stage of an individual stem as either a tree (T; ≥ 10 cm diameter at breast height [dbh]) or a sapling (S; < 10 cm dbh). Column 4, categorizes the stems as being either alive (A) or standing dead (D). The remaining seven columns are forest metrics (all units are in meters), including DBH, canopy height of the stem (CH), distance from ground to bottom of live canopy (GTC), canopy width as determined by the drip-line at its widest (CWL), canopy width at its narrowest (CWS), and easting and northing of individual stems within the 50×50 m plot (X and Y). GTC, CWL, and CWS are only required for trees; sapling values are generated within the program. Because LiDAR also provides estimation of accurate digital elevation models (DEM), we incorporated SAS code that allows for the processing of the underlying DEM.

SAS Programs

We developed four SAS programs using the PROC G3D procedure and the Annotate facility in SAS/GRAPH (SAS 2009). The SAS programs comprise several hundred lines of code, so the following description only gives an overview of the process while focusing on the outputs and potential outcomes. The output format can be tailored for specific needs, including high resolution output as a JPEG image and lower quality output as a graphic on a SAS graphics screen. Each output can be displayed with or without an input DEM. If no DEM is available, the forest plot is then rendered on a flat surface. Figure B.2 outlines the pseudocode of the SAS programs and the steps used to import a DEM to represent the topography, import raw tree measurement data, draw

1. Ground Data
 - a. Ground data file – Read in file, find maximum and minimum coordinates to create a boundary for the graphing area.
 - b. No ground data file – A data step creates the boundary of the graphing area using a data lines statement controlled by the user.
2. Tree Data
 - a. With easting and northings
 - b. Without easting and northings – coordinates for the vegetation are randomly generated by the program
3. Draw trunks.
4. Create canopies using random points within functional boundary.
5. Create branches for hardwoods and dead softwoods.
6. Move all created vegetation pieces to the appropriate coordinates (everything is initially created about the origin [0,0,0]).
7. Finalize ground for graphing
 - a. Ground file – data is gridded using PROC G3GRID and the data may or may not be filled with a solid color depending on the user's choice
 - b. No ground file – Ground area is filled with color
8. Background is filled with a solid color
9. All vegetation objects are placed in one data set
10. The data set containing the vegetation objects are sorted based the rotation of the graph. This helps the graph appear more realistic.
11. The background, ground, and sorted tree data are placed into one data set that will be annotated.
12. Graph the data
 - a. If using higher resolution – graph is saved as a JPEG image
 - b. If using lower resolution – graph is saved in the graphing window
13. Import graphic to other software

Figure B.2. Pseudocode of SAS programs used to render in 3D forest stand metrics. individual trees or saplings based on type, stage, or status, and position each tree in a forest stand or plot. Figure B.3 illustrates how the program (step 1) draws a single softwood or hardwood tree at a point (0,0) as a function of DBH and canopy height, (step 2) adds branches or leaves based on mean drip-line canopy width and distance from ground to bottom of live canopy, and (step 3) positions several trees in a 50×50 m study plot. To “draw” and plot a tree, we used a spheroid shape to represent the canopies. The

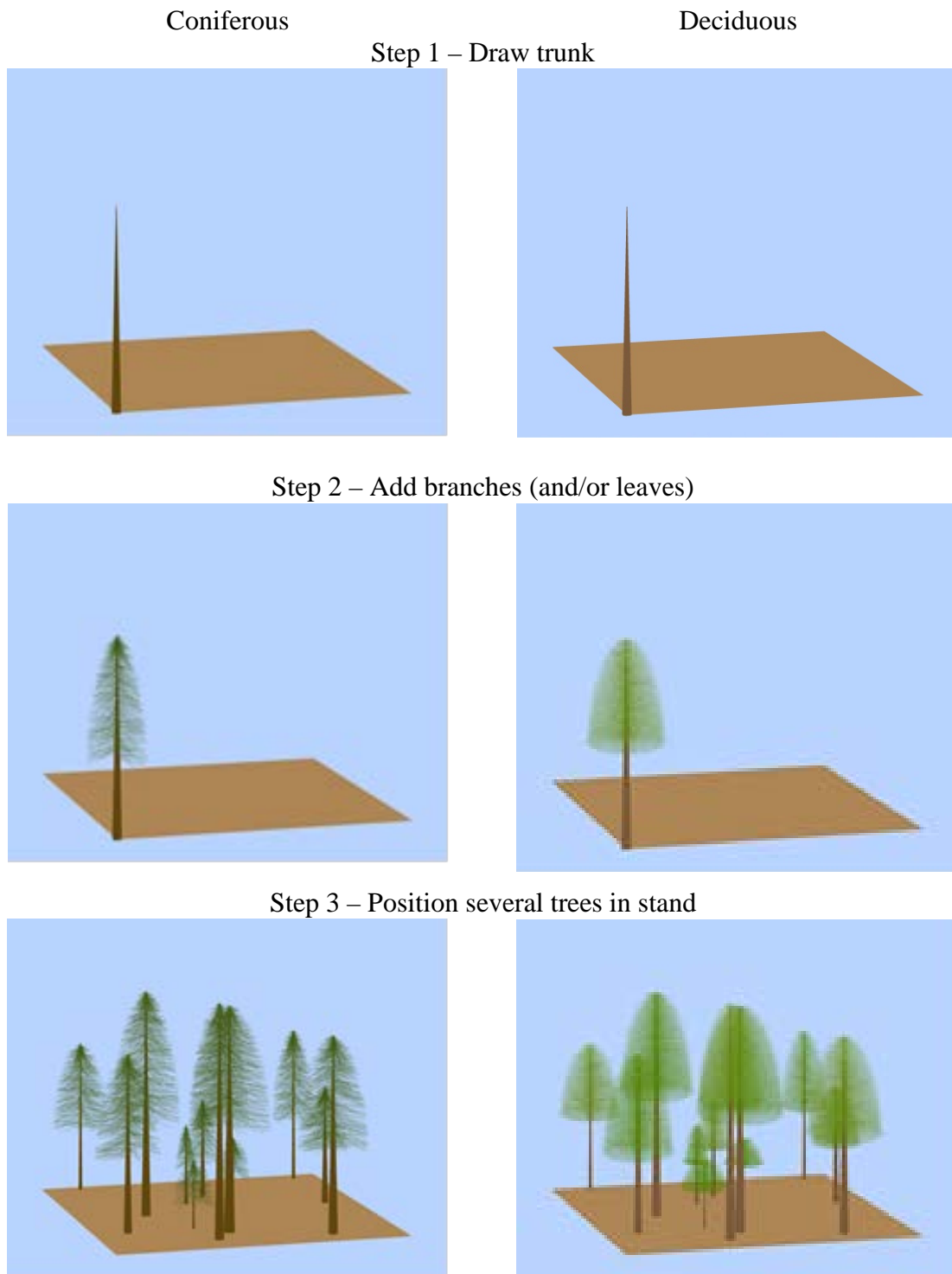


Figure B.3. Basic steps used to draw a single tree at a specific location within a 50×50 m plot, and then add additional trees as per specific data set.

SAS program itself provides more details than can be presented here. In brief, the following four variables are generated:

HRADIUS= the horizontal radius = $\frac{1}{2} \times \text{mean}(\text{CWS}, \text{CWL})$,

VRADIUS= the vertical radius= $(\text{CH}-\text{GTC})$,

V= a random number between 0 and 360,

U= a random number between 0 and 180.

Using these four variables, the following formulas are used to the create spheroid shape:

$X = \text{HRADIUS} \times \sin(V) \times \cos(U)$,

$Y = \text{HRADIUS} \times \sin(V) \times \sin(U)$

$Z = \text{VRADIUS} \times \cos(V)$.

For the upper part of the canopy, a point is only used if the value of $Z \geq 0$. The leaves for hardwood trees are plotted at the generated X, Y, and Z coordinates after randomly shifting the coordinates slightly to prevent having a uniform look around the edge of the canopy. For softwood trees (i.e., conifers) branches are generated by drawing lines from $X=0, Y=0, Z=\text{generated } Z$ to $X=\text{generated } X, Y=\text{generated } Y, \text{ and } Z=\text{generated } Z$ adjusted slightly. Based on where the line falls vertically in the canopy, Z is randomly adjusted down to give a more realistic look. For saplings we assumed $\text{CW} = \text{GTC} = \frac{1}{3}\text{CH}$.

Figure B.4 illustrates several examples of 50×50 m stands of trees positioned on an input DEM. Figure B.5 illustrates a single 50×50 m cell of mixed deciduous and coniferous trees and saplings centered in a 3×3 grid of 50×50 m cells. The cell is shown by itself, surrounded by similar vegetation, and surrounded by dissimilar vegetation;

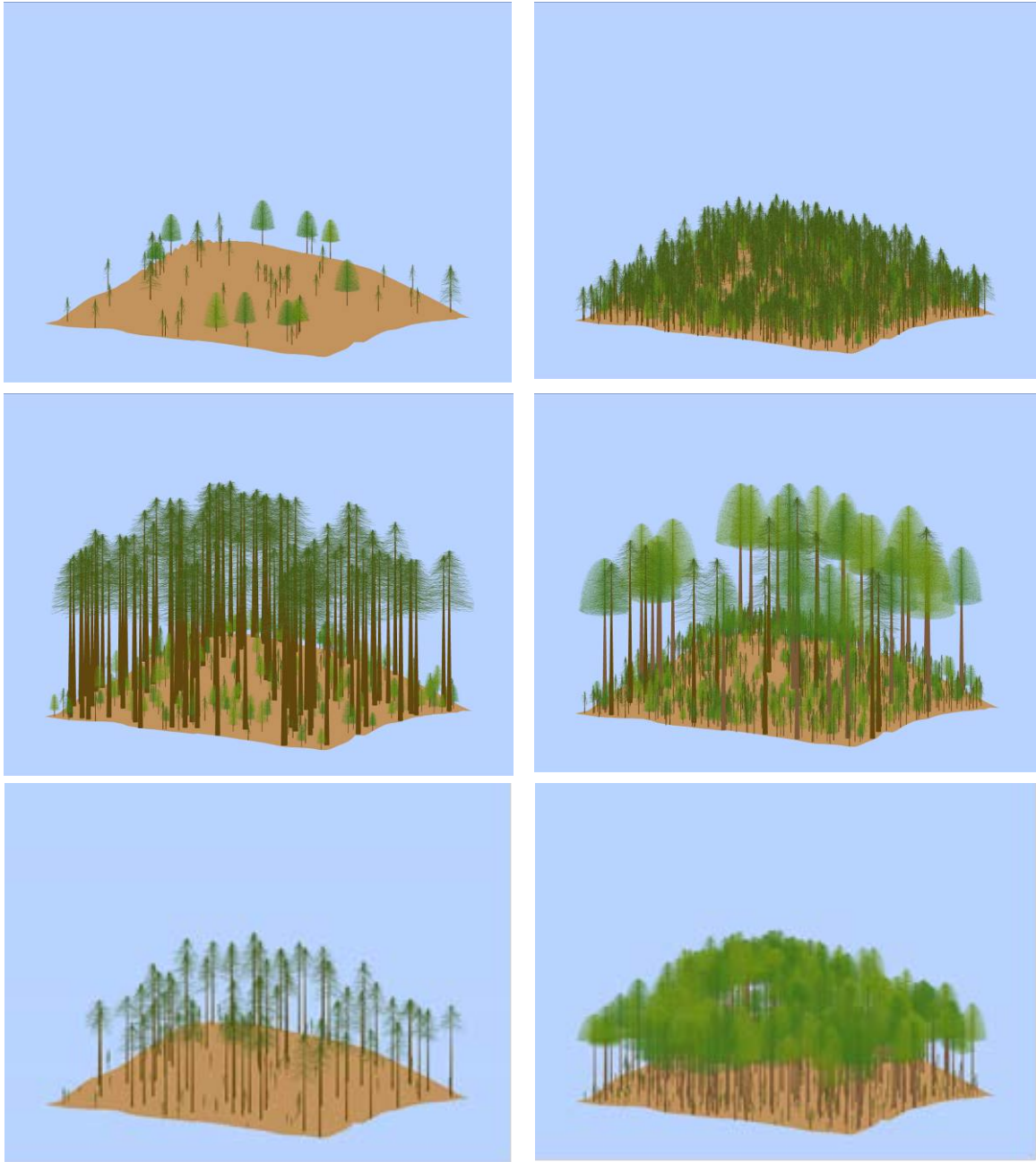


Figure B.4. Examples of 50×50 m forest plots positioned on a digital elevation model: UL represents a thinned early successional mixed-type (hardwood:softwood) plot, UR represents an early successional softwood plot, ML represents a mature softwood plot with low density understory, MR represents a mixed-type plot with moderately dense understory, LL represents highly thinned mid-story plot that maybe have experience a recent burn, and LR represents a dense mid-story plot with no understory.

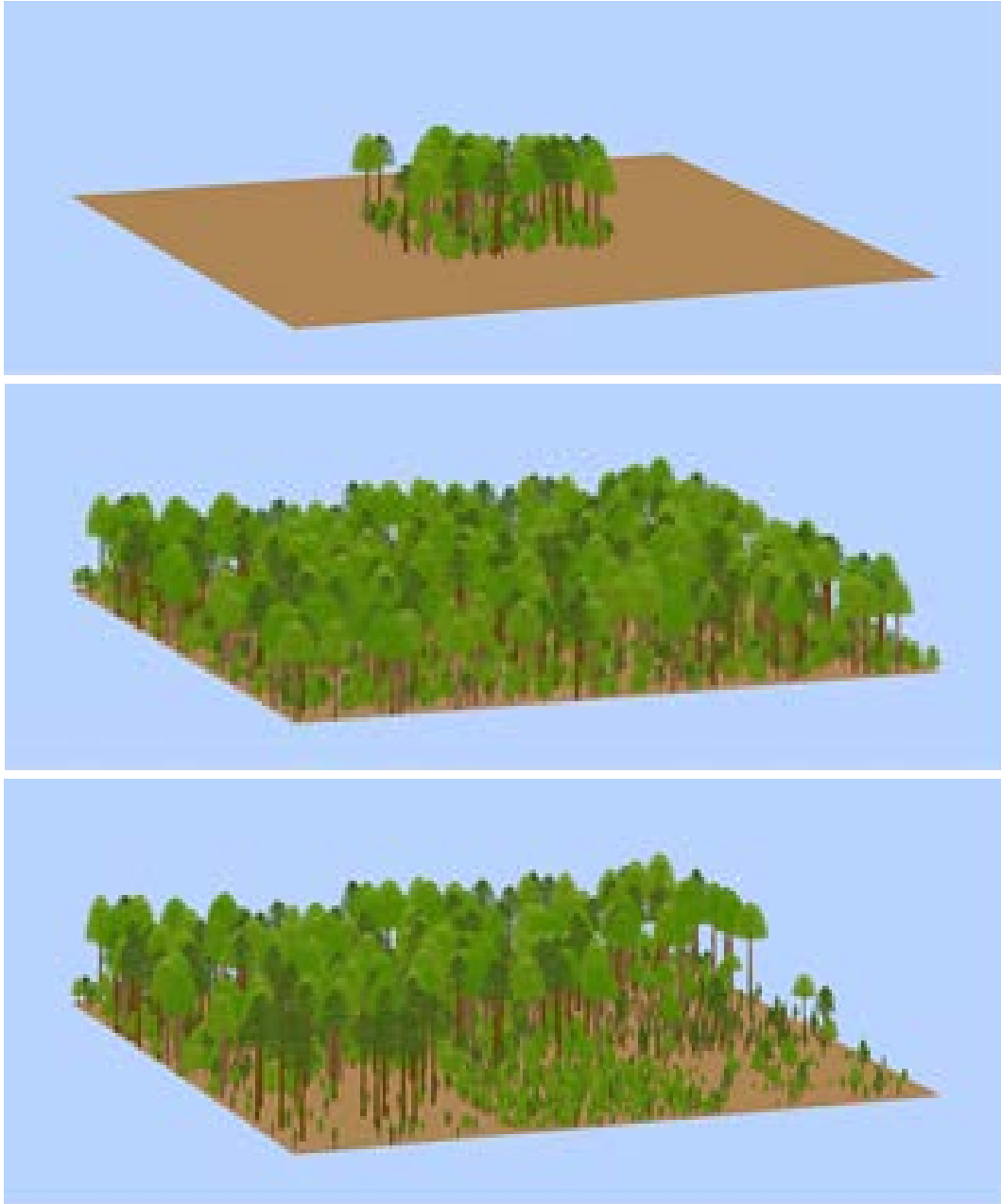


Figure B.5. Examples of tree stands juxtaposed on 50×50 m forest plots within a landscape.

these landscape scenarios can represent various levels of habitat quality for a particular wildlife species. Figure B.6 illustrates basic modifications that can be made within the SAS code. Many other modifications can be made based on specific needs (e.g., various tree species can be colored differently, different models can be used for canopy shapes).

Visualization Program Options

Vegetation Type

Trees Only (deciduous=hardwood, or, coniferous=softwood)

Saplings Only (deciduous=hardwood, or, coniferous=softwood)

Trees and Saplings Combined

Data Available for Generating Ground (i.e., DEM)?

Yes

Fill in Ground with Color

Yes – The ground is filled with a solid color that can be specified by the user.

No – The ground is plotted using PROC G3D PLOT to create a surface plot. The colors for the top and bottom surfaces of the plot are specified by the user.

No – A flat solid colored surface (polygon) is created to represent the ground.

Location of Vegetation Available

(Is the easting and northing listed in the file containing tree data?)

Yes – The vegetation is plotted at coordinates listed in the file.

No – Random coordinates are generated by the program.

Resolution of Output

High – The graph is saved as a JPEG image (details are changeable within the code).

Low – The graph is displayed in the SAS/GRAPH window.

Rotation and Tilt

Any rotation and tilt angles can be modified.

Figure B.6. General modification tools available in the visualization program developed using SAS.

Remarks

The code for the three-dimensional visualization SAS programs will be available for download as ASCII files at www.usgs.npwrc.gov. These programs will be open-source templates that can be used as stand-alone applications or modified to incorporate into other SAS analyses for specific objectives. The goal in the development of these visualization tools was not to design a graphical user interface but rather to provide an alternative and flexible approach to three-dimension visualization of vegetation structure data that can be included in assessments of wildlife-habitat models, can be used in forecasting or backcasting habitat, and can be used to evaluate habitat changes relative to management activities or natural succession. Although there is the potential for misinterpretation of visualization models (e.g., see Millspaugh et al. 2009), a major benefit of these models derived from LiDAR data is that one can visualize individual cells, a portion of the forest stand, or the whole forest stand (e.g., see above example for Moosehorn National Wildlife Refuge). Moreover, these SAS visualization tools can be used to model forest growth, to predict potential impacts to various wildlife species, and to evaluate management scenarios within the SAS environment. Archiving tens of thousands of JPEG images is not necessary because forest plots can be rendered at any location using SAS code, which can aid greatly in interpreting habitat and its potential quality for various wildlife species.

Literature Cited

Hirzel, A., and A. Guisan. 2002. Which is the optimal sampling strategy for habitat suitability modeling. *Ecological Modeling* 157:331-341.

- Kao, D.L., M.G. Kramer, A.L. Love, J.L. Dungan, and A.T. Pang. 2005. Visualizing distributions from multi-return LiDAR data to understand forest structure. *Cartographic Journal* 42:35-47.
- Lim, E., and T. Honjo. 2003. Three-dimensional visualization forest of landscapes by VRML. *Landscape and Urban Planning* 63:175-186.
- Lim, K., P. Treitz, M. Wulder, B. St-Onge, and M. Flood. 2003. LiDAR remote sensing of forest structure. *Progress in Physical Geography* 27:88-106.
- McGaughey, R.J. 1998. Techniques for visualizing the appearance of forestry operations. *Journal of Forestry* 96:9-14.
- McGaughey, R.J. 2000. EnVision-environmental visualization system. U.S. Forest Service, Pacific Northwest Research Station, Seattle, Washington, USA. <http://forsys.cfr.washington.edu/envision.html>. Accessed 14 November 2011.
- Millspough, J.J., R.A. Gitzen, D.R. Larsen, M.A. Larson, and F.R. Thompson, III. 2009. General principles for developing landscape models for wildlife conservation. Pages 1-31 *in* *Models for Planning Wildlife Conservation in Large Landscapes* (J.J. Millspough and F.R. Thompson, III, Eds.). Elsevier, Inc., Boston, Massachusetts.
- Ralph, C.J., S. Droege, and J.R. Sauer. 1995. Managing and monitoring birds using point counts: standards and applications. Pages 161-169 *in* *Monitoring Bird Populations by Point Counts* (C.J. Ralph, J.R. Sauer, and S. Droege, Eds.). U.S. Department of Agriculture, Forest Service General Technical Report PSW-GTR-149.
- SAS Institute. 2009. *The SAS System for Windows, ver. 9.1*. SAS Institute, Inc., Cary, North Carolina.

APPENDIX C. SUPPLEMENTARY MATERIAL FOR CHAPTER 3

Table C.1. Bird species observed at tow mixed forests in Maine Northwoods: species are listed alphabetically by their American Ornithologists' Union (AOU) species code.

AOU	Common name	Scientific name
ALFL	Alder Flycatcher	<i>Empidonax alnorum</i>
AMCR	American Crow	<i>Corvus brachyrhynchos</i>
AMGO	American Goldfinch	<i>Carduelis tristis</i>
AMRE	American Redstart	<i>Setophaga ruticilla</i>
AMRO	American Robin	<i>Turdus migratorius</i>
AMWO	American Woodcock	<i>Scolopax minor</i>
BAWW	Black-and-white Warbler	<i>Mniotilta varia</i>
BBCU	Black-billed Cuckoo	<i>Coccyzus erythrophthalmus</i>
BBWA	Bay-breasted Warbler	<i>Dendroica castanea</i>
BBWO	Black-backed Woodpecker	<i>Picoides arcticus</i>
BCCH	Black-capped Chickadee	<i>Poecile atricapillus</i>
BHVI	Bell's Vireo	<i>Vireo bellii</i>
BLBW	Blackburnian Warbler	<i>Dendroica fusca</i>
BLJA	Blue Jay	<i>Cyanocitta cristata</i>
BOCH	Boreal Chickadee	<i>Poecile hudsonicus</i>
BRCR	Brown Creeper	<i>Certhia americana</i>
BTBW	Black-throated Blue Warbler	<i>Dendroica caerulescens</i>
BTNW	Black-throated Green Warbler	<i>Dendroica virens</i>
CAWA	Canada Warbler	<i>Wilsonia canadensis</i>
CEDW	Cedar Waxwing	<i>Bombycilla cedrorum</i>
CMWA	Cape May Warbler	<i>Dendroica tigrina</i>
COGR	Common Grackle	<i>Quiscalus quiscula</i>
CONI	Common Nighthawk	<i>Chordeiles minor</i>
CORA	Common Raven	<i>Corvus corax</i>
COYE	Common Yellowthroat	<i>Geothlypis trichas</i>
CSWA	Chestnut-sided Warbler	<i>Dendroica pensylvanica</i>
DEJU	Dark-eyed Junco (Slate-colored)	<i>Junco hyemalis</i>
DOWO	Downy Woodpecker	<i>Picoides pubescens</i>
EAKI	Eastern Kingbird	<i>Tyrannus tyrannus</i>
EAPH	Eastern Phoebe	<i>Sayornis phoebe</i>
EAWP	Eastern Wood-Pewee	<i>Contopus virens</i>
EVGR	Evening Grosbeak	<i>Coccothraustes vespertinus</i>
GCFL	Great Crested Flycatcher	<i>Myiarchus crinitus</i>
GCKI	Golden-crowned Kinglet	<i>Regulus satrapa</i>
GRAJ	Gray Jay	<i>Perisoreus canadensis</i>
GRCA	Gray Catbird	<i>Dumetella carolinensis</i>
HAWO	Hairy Woodpecker	<i>Picoides villosus</i>
HETH	Hermit Thrush	<i>Catharus guttatus</i>
INBU	Indigo Bunting	<i>Passerina cyanea</i>

Table C.1. Continued.

AOU	Common name	Scientific name
LEFL	Least Flycatcher	<i>Empidonax minimus</i>
LISP	Lincoln's Sparrow	<i>Melospiza lincolnii</i>
MAWA	Magnolia Warbler	<i>Dendroica magnolia</i>
MODO	Mourning Dove	<i>Zenaida macroura</i>
MOWA	Mourning Warbler	<i>Oporornis philadelphia</i>
NAWA	Nashville Warbler	<i>Vermivora ruficapilla</i>
NOPA	Northern Parula	<i>Parula americana</i>
NOWA	Northern Waterthrush	<i>Seiurus noveboracensis</i>
OSFL	Olive-sided Flycatcher	<i>Contopus cooperi</i>
OVEN	Ovenbird	<i>Seiurus aurocapillus</i>
PAWA	Palm Warbler (Yellow Palm)	<i>Dendroica palmarum</i>
PHVI	Philadelphia Vireo	<i>Vireo philadelphicus</i>
PISI	Pine Siskin	<i>Carduelis pinus</i>
PIWA	Pine Warbler	<i>Dendroica pinus</i>
PIWO	Pileated Woodpecker	<i>Dryocopus pileatus</i>
PUFI	Purple Finch	<i>Carpodacus purpureus</i>
RBGR	Rose-breasted Grosbeak	<i>Pheucticus ludovicianus</i>
RBNU	Red-breasted Nuthatch	<i>Sitta canadensis</i>
RCKI	Ruby-crowned Kinglet	<i>Regulus calendula</i>
REVI	Red-eyed Vireo	<i>Vireo olivaceus</i>
RTHU	Ruby-throated Hummingbird	<i>Archilochus colubris</i>
RWBL	Red-winged Blackbird	<i>Agelaius phoeniceus</i>
SAVS	Savannah Sparrow	<i>Passerculus sandwichensis</i>
SCTA	Scarlet Tanager	<i>Piranga olivacea</i>
SOSP	Song Sparrow	<i>Melospiza melodia</i>
SOVI	Solitary vireo	<i>Vireo solitarius</i>
SWTH	Swainson's Thrush	<i>Catharus ustulatus</i>
TRES	Tree Swallow	<i>Tachycineta bicolor</i>
VEER	Veery	<i>Catharus fuscescens</i>
WBNU	White-breasted Nuthatch	<i>Sitta carolinensis</i>
WIWA	Wilson's Warbler	<i>Wilsonia pusilla</i>
WIWR	Winter Wren	<i>Troglodytes troglodytes</i>
WOTH	Wood Thrush	<i>Hylocichla mustelina</i>
WTSP	White-throated Sparrow	<i>Zonotrichia albicollis</i>
YBFL	Yellow-bellied Flycatcher	<i>Empidonax flaviventris</i>
YBSA	Yellow-bellied Sapsucker	<i>Sphyrapicus varius</i>
YRWA	Yellow-rumped Warbler (Myrtle)	<i>Dendroica coronata</i>
YSFL	Yellow-shafted flicker	<i>Colaptes auratus</i>
YWAR	Yellow Warbler	<i>Dendroica petechia</i>

Table C.2. Bird modeling results for International Paper (IP) and Moosehorn National Wildlife Refuge (MH) sorted by the most encountered species to least encountered (see Table 3.5; bolded Adj. R² indicate a reasonable best model selected based on Akaike's weights and Adj. R² ≥ 0.2).

Species ¹	Site ²	Mod. no.	k	RSS	AICc	Δ AICc	ω _i	Adj. R ²	PRESS Adj. R ²
MAWA	IP	14	6	7.98	-236.34	0.00	0.31	0.40	0.33
		19	6	8.02	-235.86	0.48	0.25	0.40	0.34
		10	6	8.05	-235.51	0.84	0.21	0.40	0.34
	MH	13	7	8.86	-276.22	0.00	0.16	0.23	0.12
		7	3	9.61	-275.70	0.51	0.13	0.19	0.16
		28	3	9.64	-275.36	0.86	0.11	0.19	0.16
OVEN	IP	24	7	5.82	-265.36	0.00	0.91	0.41	0.33
		21	6	6.25	-260.64	4.72	0.09	0.37	0.32
		22	7	6.92	-252.50	12.86	0.00	0.32	0.24
	MH	3	6	5.92	-324.43	0.00	0.19	0.33	0.28
		5	6	5.94	-324.02	0.41	0.16	0.33	0.27
		6	6	5.94	-323.97	0.46	0.15	0.33	0.27
WTSP	IP	22	7	7.70	-237.55	0.00	0.64	0.36	0.29
		18	7	7.83	-235.94	1.61	0.29	0.35	0.29
		13	7	8.18	-231.60	5.95	0.03	0.32	0.25
	MH	30	7	4.32	-357.96	0.00	0.29	0.60	0.55
		34	7	4.39	-356.22	1.74	0.12	0.59	0.54
		3	6	4.48	-356.13	1.83	0.11	0.59	0.54
BCCH	IP	8	4	9.25	-226.30	0.00	0.18	0.17	0.11
		2	3	9.49	-225.93	0.37	0.15	0.15	0.12
		17	4	9.39	-224.74	1.56	0.08	0.15	0.10
	MH	2	3	7.88	-298.38	0.00	0.21	0.05	0.02
		4	5	7.72	-296.39	1.99	0.08	0.05	<0.01
		26	3	8.02	-296.40	1.99	0.08	0.03	<0.01
BAWW	IP	9	7	3.55	-314.28	0.00	0.47	0.38	0.31
		10	6	3.67	-313.22	1.05	0.28	0.37	0.29
		19	6	3.72	-312.04	2.24	0.15	0.36	0.29
	MH	14	6	5.57	-331.35	0.00	0.20	0.14	0.07
		23	6	5.60	-330.82	0.53	0.15	0.13	0.06
		19	6	5.61	-330.50	0.86	0.11	0.13	0.06

Table C.2. Continued.

Species ¹	Site ²	Mod. no.	k	RSS	AICc	Δ AICc	ω_i	Adj. R ²	PRESS Adj. R ²
NAWA	IP	19	6	6.96	-249.99	0.00	0.54	0.33	0.25
		21	6	7.02	-249.03	0.96	0.34	0.32	0.23
		23	6	7.27	-245.65	4.34	0.06	0.30	0.21
	MH	30	7	2.40	-425.20	0.00	0.26	0.35	0.28
		31	7	2.41	-424.42	0.78	0.17	0.35	0.27
		34	7	2.44	-423.02	2.19	0.09	0.34	0.26
COYE	IP	15	7	6.44	-255.32	0.00	0.72	0.40	0.32
		24	7	6.76	-250.48	4.84	0.06	0.37	0.28
		11	7	6.78	-250.18	5.14	0.06	0.37	0.28
	MH	3	6	4.09	-366.53	0.00	0.22	0.51	0.42
		30	7	4.03	-365.94	0.59	0.16	0.51	0.41
		11	7	4.07	-364.92	1.62	0.10	0.51	0.41
REVI	IP	24	7	7.69	-237.80	0.00	0.94	0.25	0.15
		21	6	8.47	-230.47	7.32	0.02	0.18	0.09
		15	7	8.39	-229.11	8.69	0.01	0.18	0.07
	MH	22	7	4.26	-359.52	0.00	0.63	0.18	0.10
		7	3	4.75	-356.06	3.46	0.11	0.12	0.09
		23	6	4.54	-354.57	4.95	0.05	0.13	0.06
HETH	IP	29	3	7.53	-248.84	0.00	0.36	0.19	0.16
		33	3	7.62	-247.60	1.24	0.19	0.18	0.15
		8	4	7.50	-247.00	1.84	0.14	0.18	0.14
	MH	7	3	2.78	-417.26	0.00	0.39	0.08	0.06
		40	4	2.79	-414.74	2.52	0.11	0.07	0.02
		26	3	2.85	-414.25	3.02	0.09	0.06	0.03
BTNW	IP	40	4	6.66	-258.29	0.00	0.25	0.39	0.34
		23	6	6.38	-258.52	0.26	0.22	0.39	0.34
		41	5	6.65	-256.78	2.01	0.09	0.38	0.32
	MH	40	4	2.67	-419.67	0.00	0.12	0.08	0.04
		26	3	2.72	-419.57	0.10	0.12	0.08	0.05
		27	3	2.73	-419.29	0.37	0.10	0.08	0.04

Table C.2. Continued.

Species ¹	Site ²	Mod. no.	k	RSS	AICc	Δ AICc	ω_i	Adj. R ²	PRESS Adj. R ²
YRWA	IP	27	3	6.31	-266.32	0.00	0.16	0.06	0.02
		29	3	6.31	-266.30	0.02	0.16	0.06	0.02
		8	4	6.24	-265.29	1.03	0.09	0.06	0.00
	MH	23	6	4.27	-361.79	0.00	0.55	0.23	0.15
		19	6	4.30	-360.91	0.88	0.26	0.22	0.15
		18	7	4.24	-360.15	1.64	0.18	0.23	0.14
YBSA	IP	21	6	4.44	-294.39	0.00	0.20	0.23	0.17
		10	6	4.49	-293.41	0.98	0.12	0.22	0.16
		24	7	4.42	-292.52	1.87	0.08	0.23	0.14
	MH	6	6	2.01	-447.67	0.00	0.45	0.13	0.06
		42	6	2.03	-446.20	1.47	0.22	0.11	0.03
		41	5	2.09	-445.10	2.56	0.13	0.10	0.02
NOPA	IP	42	6	4.28	-297.96	0.00	0.22	0.19	0.10
		36	3	4.59	-297.76	0.20	0.20	0.16	0.13
		28	3	4.71	-295.34	2.62	0.06	0.14	0.10
	MH	6	6	1.21	-505.81	0.00	0.83	0.25	0.16
		5	6	1.28	-499.11	6.70	0.03	0.21	0.12
		26	3	1.36	-498.71	7.10	0.02	0.18	0.15
AMRO	IP	39	7	7.99	-233.97	0.00	0.12	0.13	0.02
		38	7	8.01	-233.72	0.26	0.10	0.13	0.02
		25	6	8.20	-233.69	0.28	0.10	0.12	0.03
	MH	14	6	1.32	-495.37	0.00	0.33	0.10	<0.01
		37	3	1.43	-492.74	2.63	0.09	0.05	0.01
		23	6	1.36	-491.76	3.61	0.05	0.07	<0.01
RBNU	IP	13	7	4.46	-291.69	0.00	0.16	0.20	0.08
		22	7	4.46	-291.66	0.03	0.16	0.19	0.09
		24	7	4.48	-291.21	0.47	0.13	0.19	0.08
	MH	ND ³							

Table C.2. Continued.

Species ¹	Site ²	Mod. no.	k	RSS	AICc	Δ AICc	ω_i	Adj. R ²	PRESS Adj. R ²
PUFI	IP	2	3	6.36	-265.53	0.00	0.18	0.03	0.00
		1	2	6.62	-263.67	1.86	0.07	0.00	<0.01
		7	3	6.49	-263.53	2.00	0.06	0.01	<0.01
	MH	ND ³							
BLBW	IP	14	6	3.64	-314.08	0.00	0.42	0.43	0.38
		23	6	3.68	-313.11	0.97	0.26	0.43	0.38
		6	6	3.69	-312.77	1.31	0.22	0.43	0.37
	MH	27	3	1.78	-468.23	0.00	0.45	0.28	0.24
22		7	1.66	-467.01	1.22	0.24	0.30	0.21	
13		7	1.69	-464.78	3.45	0.08	0.28	0.18	
BTBW	IP	23	6	4.25	-298.77	0.00	0.71	0.37	0.30
		21	6	4.38	-295.69	3.07	0.15	0.35	0.29
		14	6	4.44	-294.44	4.33	0.08	0.34	0.27
	MH	40	4	1.92	-456.94	0.00	0.30	0.12	0.06
42		6	1.87	-455.50	1.44	0.14	0.13	0.05	
26		3	1.99	-455.18	1.76	0.12	0.10	0.06	
BLJA	IP	26	3	6.12	-269.28	0.00	0.16	0.09	0.05
		28	3	6.18	-268.38	0.91	0.10	0.08	0.05
		8	4	6.05	-268.21	1.07	0.09	0.09	0.04
	MH	ND ³							
GCKI	IP	6	6	5.51	-273.03	0.00	0.45	0.14	0.05
		13	7	5.48	-271.20	1.83	0.18	0.14	0.01
		14	6	5.76	-268.59	4.44	0.05	0.10	0.01
	MH	32	3	2.03	-452.74	0.00	0.12	0.03	<0.01
36		3	2.04	-452.55	0.19	0.11	0.03	<0.01	
2		3	2.04	-452.23	0.51	0.09	0.02	<0.01	

Table C.2. Continued.

Species ¹	Site ²	Mod. no.	k	RSS	AICc	Δ AICc	ω_i	Adj. R ²	PRESS Adj. R ²			
VEER	IP	10	6	4.38	-295.69	0.00	0.46	0.25	0.17			
		14	6	4.47	-293.87	1.83	0.19	0.23	0.16			
		9	7	4.40	-292.96	2.73	0.12	0.24	0.13			
	MH	19	6	1.82	-458.76	0.00	0.43	0.11	0.02			
		10	6	1.86	-456.70	2.06	0.15	0.09	0.02			
		18	7	1.84	-455.65	3.11	0.09	0.09	<0.01			
SOVI	IP	26	3	3.58	-322.35	0.00	0.55	0.26	0.23			
		40	4	3.57	-320.52	1.84	0.22	0.26	0.21			
		41	5	3.55	-318.86	3.49	0.10	0.25	0.18			
	MH	ND ³										
		CAWA	IP	18	7	3.91	-304.73	0.00	0.84	0.31	0.23	
				19	6	4.25	-298.77	5.96	0.04	0.26	0.20	
21	6			4.26	-298.51	6.22	0.04	0.26	0.20			
MH		27	3	5.34	-342.73	0.00	0.26	0.08	0.04			
		15	7	5.02	-341.00	1.73	0.11	0.10	<0.01			
		30	7	5.02	-340.96	1.77	0.11	0.10	0.01			
PAWA	IP	11	7	6.41	-255.80	0.00	0.44	0.54	0.46			
		21	6	6.65	-254.47	1.33	0.23	0.53	0.46			
		12	6	6.76	-252.86	2.94	0.10	0.52	0.45			
	MH		9	7	0.86	-542.05	0.00	0.52	0.42	0.33		
			20	7	0.87	-540.42	1.63	0.23	0.41	0.31		
			18	7	0.88	-538.86	3.19	0.11	0.40	0.31		
YBFL	IP	21	6	7.51	-242.44	0.00	0.72	0.27	0.19			
		23	6	7.72	-239.65	2.79	0.18	0.25	0.16			
		22	7	7.63	-238.51	3.93	0.10	0.25	0.14			
	MH	ND ³										
			CSWA	IP	18	7	6.38	-256.15	0.00	0.60	0.26	0.14
					9	7	6.49	-254.54	1.61	0.27	0.24	0.10
20	7	6.67			-251.88	4.27	0.07	0.22	0.09			
MH	ND ³											

Table C.2. Continued.

Species ¹	Site ²	Mod. no.	k	RSS	AICc	Δ AICc	ω_i	Adj. R ²	PRESS Adj. R ²	
BRCR	IP	33	3	2.06	-377.23	0.00	0.17	0.10	0.07	
		27	3	2.07	-376.46	0.77	0.11	0.09	0.06	
		29	3	2.08	-376.12	1.11	0.10	0.09	0.06	
	MH	28	3	2.09	-449.66	0.00	0.38	0.17	0.13	
		40	4	2.09	-447.66	2.00	0.14	0.16	0.11	
		32	3	2.13	-447.42	2.23	0.12	0.15	0.11	
HAWO	IP	29	3	3.11	-336.49	0.00	0.12	0.06	0.03	
		33	3	3.12	-335.99	0.50	0.10	0.05	0.02	
		41	5	2.99	-335.92	0.57	0.09	0.07	<0.01	
	MH	ND ³								
	WIWR	IP	27	3	3.79	-316.87	0.00	0.35	0.11	0.08
			15	7	3.49	-316.07	0.80	0.23	0.15	0.05
29			3	3.88	-314.43	2.44	0.10	0.09	0.06	
MH		ND ³								
DOWO	IP	33	3	2.49	-358.24	0.00	0.08	0.01	<0.01	
		1	2	2.55	-358.20	0.05	0.08	0.00	<0.01	
		17	4	2.44	-358.07	0.17	0.07	0.02	<0.01	
	MH	ND ³								
YSFL	IP	33	3	2.74	-348.81	0.00	0.13	0.02	<0.01	
		29	3	2.75	-348.43	0.38	0.10	0.02	<0.01	
		17	4	2.69	-348.36	0.45	0.10	0.03	<0.01	
	MH	ND ³								
PIWA	IP	6	6	6.81	-252.13	0.00	0.14	0.12	0.02	
		27	3	7.29	-251.95	0.18	0.13	0.09	0.06	
		3	6	6.82	-251.88	0.25	0.12	0.12	0.03	
	MH	13	7	0.98	-527.20	0.00	0.87	0.31	0.21	
		22	7	1.03	-521.81	5.39	0.06	0.27	0.16	
		27	3	1.11	-521.47	5.73	0.05	0.24	0.19	

Table C.2. Continued.

Species ¹	Site ²	Mod. no.	k	RSS	AICc	Δ AICc	ω_i	Adj. R ²	PRESS Adj. R ²
EAWP	IP	28	3	2.68	-351.02	0.00	0.18	0.22	0.18
		31	7	2.46	-350.73	0.29	0.16	0.25	0.16
		22	7	2.46	-350.46	0.55	0.14	0.25	0.16
	MH	ND ³							
LEFL	IP	24	7	2.34	-355.52	0.00	0.32	0.12	<0.01
		22	7	2.41	-352.46	3.05	0.07	0.09	<0.01
		35	7	2.43	-351.86	3.66	0.05	0.08	<0.01
	MH	23	6	4.16	-364.58	0.00	0.32	0.16	0.08
22		7	4.11	-363.77	0.81	0.22	0.16	0.06	
24		7	4.11	-363.70	0.87	0.21	0.16	0.07	
AMRE	IP	1	2	3.45	-328.08	0.00	0.11	0.00	<0.01
		37	3	3.40	-327.63	0.45	0.09	0.01	<0.01
		40	4	3.35	-326.72	1.36	0.06	0.01	<0.01
	MH	ND ³							
SCTA	IP	28	3	1.17	-433.20	0.00	0.19	0.10	0.06
		36	3	1.18	-432.51	0.69	0.14	0.09	0.05
		32	3	1.18	-432.45	0.75	0.13	0.09	0.05
	MH	41	5	1.20	-508.30	0.00	0.29	0.10	0.05
26		3	1.26	-507.21	1.08	0.17	0.08	0.05	
42		6	1.19	-507.20	1.10	0.17	0.10	0.02	
SWTH	IP	36	3	2.02	-379.28	0.00	0.14	0.05	0.00
		26	3	2.02	-378.99	0.29	0.12	0.05	0.00
		28	3	2.03	-378.74	0.54	0.10	0.04	0.00
	MH	ND ³							
BBWA	IP	26	3	1.42	-413.63	0.00	0.25	0.09	0.04
		40	4	1.41	-412.45	1.18	0.14	0.09	0.02
		28	3	1.46	-411.05	2.58	0.07	0.06	0.02
	MH	ND ³							

Table C.2. Continued.

Species ¹	Site ²	Mod. no.	k	RSS	AICc	Δ AICc	ω_i	Adj. R ²	PRESS Adj. R ²	
ALFL	IP	18	7	2.84	-336.43	0.00	0.74	0.46	0.37	
		9	7	2.96	-332.10	4.33	0.09	0.44	0.33	
		19	6	3.07	-331.07	5.35	0.05	0.43	0.33	
	MH	ND ³								
RBGR	IP	7	3	1.10	-439.27	0.00	0.46	0.08	0.04	
		5	6	1.06	-436.35	2.92	0.11	0.09	0.00	
		3	3	1.07	-435.44	3.82	0.07	0.08	0.00	
	MH	ND ³								
WBNU	IP	30	7	1.77	-383.22	0.00	0.19	0.13	<0.01	
		31	7	1.79	-382.11	1.10	0.11	0.12	<0.01	
		6	6	1.83	-382.11	1.11	0.11	0.10	<0.01	
	MH	ND ³								
CEDW	IP	1	2	1.24	-429.89	0.00	0.14	0.00	<0.01	
		33	3	1.23	-428.56	1.32	0.07	0.00	<0.01	
		2	3	1.23	-428.46	1.42	0.07	0.00	<0.01	
	MH	ND ³								
LISP	IP	19	6	0.71	-475.26	0.00	0.46	0.85	0.82	
		22	7	0.71	-473.77	1.49	0.22	0.85	0.82	
		18	7	0.71	-473.21	2.05	0.17	0.84	0.82	
	MH	ND ³								
BHVI	IP	ND ³								
		MH	23	6	2.10	-442.40	0.00	0.17	0.14	0.08
			28	3	2.23	-442.26	0.14	0.16	0.11	0.08
32	3		2.24	-441.88	0.52	0.13	0.11	0.08		
DEJU	IP	23	6	1.23	-421.34	0.00	0.23	0.08	<0.01	
		14	6	1.25	-419.56	1.78	0.10	0.07	<0.01	
		22	7	1.23	-419.35	2.00	0.09	0.08	<0.01	
	MH	ND ³								

Table C.2. Continued.

Species ¹	Site ²	Mod. no.	k	RSS	AICc	Δ AICc	ω_i	Adj. R ²	PRESS Adj. R ²
SOSP	IP	18	7	2.79	-338.23	0.00	0.98	0.39	0.25
		23	6	3.13	-329.10	9.13	0.01	0.32	0.18
		9	7	3.13	-326.59	11.64	0.00	0.32	0.16
	MH	ND ³							
MODO	IP	29	3	0.87	-462.40	0.00	0.08	0.03	0.00
		40	4	0.85	-462.06	0.34	0.07	0.04	<0.01
		15	7	0.80	-462.03	0.37	0.07	0.07	<0.01
	MH	ND ³							
SR	IP	18	7	3.01	-330.49	0.00	0.32	0.63	0.57
		9	7	3.02	-330.15	0.34	0.27	0.63	0.57
		19	6	3.16	-328.08	2.41	0.10	0.62	0.55
	MH	6	6	8.34	-285.39	0.00	0.16	0.14	0.04
26		3	8.87	-284.90	0.49	0.13	0.11	0.08	
27		3	8.91	-284.39	0.99	0.10	0.11	0.07	
SD	IP	9	7	0.48	-511.70	0.00	0.28	0.69	0.64
		18	7	0.48	-511.71	0.00	0.28	0.69	0.64
		17	4	0.53	-509.36	2.35	0.09	0.67	0.64
	MH	6	6	3.91	-371.65	0.00	0.13	0.12	0.03
26		3	4.15	-371.59	0.06	0.13	0.10	0.06	
27		3	4.17	-370.85	0.79	0.09	0.09	0.05	

¹Species codes are in Table C.1; SR=species richness, SD=species diversity (Shannon-Weaver).

²IP=International Paper, MH=Moosehorn National Wildlife Refuge.

³ND= number of survey points with detected birds <10.

Table C.3. Estimated model parameters for best bird selected models only and with Adj.R² ≥ 0.20 at International Paper (IP) and Moosehorn National Wildlife Refuge (MH).

Species ¹	Mod.	Best model parameters (SE below parameters in “()”)
MAWA:		
IP ²	14	Y=1.53-1.46(X11)+0.28(X12)-0.46(X30)-2.29(X32) (0.37) (0.40) (0.46) (0.74) (0.64)
MH ²	13	Y=-0.21+0.42(X11)-0.72(X12)+2.88(X29)+0.73(X31)+0.56(X33) (0.26) (0.42) (0.58) (0.62) (0.47) (0.71)
OVEN:		
IP	24	Y=1.17-1.21(X44)+1.98(X45)-5.64(X67)-3.00(X69)-0.82(X71) (0.12) (0.17) (0.50) (1.28) (0.96) (1.03)
MH	3	Y=0.63-0.53(X0)-1.81(X1)-0.76(X3)-0.15(X5) (0.06) (0.21) (0.88) (0.27) (0.31)
WTSP:		
IP	22	Y=-0.63+0.77(X44)+1.16(X45)+4.77(X62)+1.55(X64)+0.36(X66) (0.39) (0.40) (0.45) (0.86) (0.87) (1.28)
MH	30	Y=-0.05-0.02(X79)+1.02(X0)+0.51(X1)+1.11(X3)+0.55(X5) (0.12) (0.01) (0.19) (0.80) (0.26) (0.32)
BAWW:		
IP	9	Y=-0.20+0.17(X11)+0.20(X12)+1.09(X14)+3.11(X16)+0.46(X18) (0.30) (0.31) (0.31) (0.83) (0.91) (0.35)
MH	14	Y=0.16-0.15(X11)-0.04(X12)+0.57(X30)-0.28(X32) (0.19) (0.27) (0.46) (0.43) (0.37)
NAWA:		
IP	19	Y=-0.24+0.69(X44)-0.22(X45)+4.78(X48)+1.54(X50) (0.14) (0.18) (0.42) (0.90) (0.38)
MH	30	Y=0.17-0.02(X79)+0.04(X0)-0.04(X1)+0.63(X3)+0.17(X5) (0.09) (0.01) (0.14) (0.60) (0.20) (0.24)
COYE:		
IP	15	Y=-0.26+1.27(X11)+0.29(X12)+3.74(X34)+1.39(X36)+3.08(X38) (0.12) (0.16) (0.51) (1.34) (1.39) (1.24)
MH	3	Y=-0.19+0.72(X0)+1.66(X1)+0.84(X3)-0.17(X5) (0.05) (0.18) (0.73) (0.22) (0.26)
REVI:		
IP	24	Y=1.02-1.04(X44)+2.56(X45)-1.30(X67)-4.72(X69)-1.46(X71) (0.14) (0.19) (0.57) (1.47) (1.11) (1.19)
MH	22	Y=0.90-0.56(X44)-0.93(X45)-2.00(X62)-1.05(X64)-1.99(X66) (0.24) (0.39) (0.41) (0.55) (0.45) (0.64)

Table C.3. Continued.

Species ¹	Mod.	Best model parameters (SE below parameters in “()”)
YRWA:		
IP	ND ³	
MH	23	Y=0.43-1.04(X44)+1.49(X45)-1.12(X63)+0.07(X65) (0.23) (0.33) (0.42) (0.53) (0.45)
BTNW:		
IP	40	Y=0.06-0.03(X77)+0.09(X81) (0.06) (0.02) (0.02)
MH	40	Y=0.03+0.02(X77)-0.01(X81) (0.04) (0.01) (0.01)
YBSA:		
IP	21	Y=0.57-0.59(X44)+0.25(X45)-5.98(X53)+0.95(X55) (0.08) (0.12) (0.36) (1.97) (0.79)
MH	6	Y=0.01-0.01(X0)+0.04(X8)+0.38(X9)-0.33(X10) (0.06) (0.13) (0.10) (0.09) (0.19)
NOPA:		
IP	42	Y=0.01-0.01(X77)+0.05(X81)-0.07(X85)+0.07(X89) (0.06) (0.02) (0.03) (0.03) (0.02)
MH	6	Y=-0.02+0.08(X0)-0.01(X8)+0.25(X9)+0.50(X10) (0.04) (0.10) (0.07) (0.07) (0.15)
RBNU:		
IP	13	Y=-0.21+0.28(X11)+0.13(X12)+0.55(X29)+1.64(X31)+1.70(X33) (0.23) (0.24) (0.35) (0.53) (0.52) (0.75)
MH	22	Y=-0.18+0.20(X44)+0.34(X45)+0.23(X62)+0.29(X64)+1.39(X66) (0.14) (0.22) (0.23) (0.32) (0.26) (0.36)
BLBW:		
IP	14	Y=-0.18+0.18(X11)-0.10(X12)+0.43(X30)+1.63(X32) (0.25) (0.27) (0.31) (0.50) (0.43)
MH	27	Y=-0.12+0.04(X78) (0.03) (0.01)
BTBW:		
IP	23	Y=-0.66+0.61(X44)+0.59(X45)+1.34(X63)+2.40(X65) (0.35) (0.38) (0.32) (0.71) (0.61)
MH	40	Y=0.01+0.02(X77)-0.02(X81) (0.03) (0.01) (0.01)

Table C.3. Continued.

Species ¹	Mod.	Best model parameters (SE below parameters in “()”)
VEER:		
IP	10	Y=-0.18+0.23(X11)-0.39(X12)+2.75(X15)+0.93(X17) (0.10) (0.13) (0.35) (0.63) (0.27)
MH	10	Y=-0.04+0.06(X11)-0.20(X12)-0.02(X15)+0.39(X17) (0.05) (0.16) (0.27) (0.30) (0.12)
SOVI:		
IP	26	Y=0.03+0.03(X77) (0.04) (0.01)
MH	ND ³	
CAWA:		
IP	18	Y=2.27-2.23(X44)-0.47(X45)-0.57(X47)-5.21(X49)-2.44(X51) (0.39) (0.41) (0.32) (1.02) (1.25) (0.46)
MH	27	Y=-0.07+0.04(X78) (0.05) (0.01)
PAWA:		
IP	11	Y=-0.17+0.86(X11)+1.97(X12)+5.66(X19)+1.52(X21)-2.26(X23) (0.11) (0.16) (0.59) (2.62) (1.49) (0.68)
MH	9	Y=0.06+0.22(X11)-0.21(X12)+1.66(X14)-0.63(X16)-0.19(X18) (0.08) (0.13) (0.18) (0.44) (0.29) (0.10)
YBFL:		
IP	21	Y=0.01+0.10(X44)-1.72(X45)-1.10(X53)+5.53(X55) (0.11) (0.16) (0.47) (2.56) (1.02)
MH	ND ³	
CSWA:		
IP	18	Y=-0.06+0.28(X44)+0.49(X45)+4.62(X47)-1.77(X49)+0.38(X51) (0.50) (0.53) (0.41) (1.31) (1.60) (0.59)
MH	ND ³	
PIWA:		
IP	6	Y=0.13-0.06(X0)+0.02(X8)-0.28(X9)+2.10(X10) (0.13) (0.18) (0.33) (0.22) (0.56)
MH	13	Y=-0.10+0.10(X11)-0.09(X12)+0.25(X29)+0.17(X31)+1.30(X33) (0.09) (0.14) (0.19) (0.20) (0.16) (0.24)

Table C.3. Continued.

Species ¹	Mod.	Best model parameters (SE below parameters in “()”)
EAWP:		
IP	28	Y=-0.06+0.03(X79) (0.03) (0.01)
MH	ND ³	
ALFL:		
IP ²	18	Y=-0.37+0.62(X44)-0.03(X45)+5.12(X47)+0.03(X49)+0.12(X51) (0.33) (0.35) (0.27) (0.87) (1.06) (0.39)
MH ²	ND ³	
LISP:		
IP	19	Y=-0.10+0.95(X44)-0.43(X45)-1.24(X48)+0.03(X50) (0.04) (0.06) (0.13) (0.29) (0.12)
MH	ND ³	
SOSP:		
IP	18	Y=0.71-0.47(X44)+0.50(X45)+2.20(X47)-3.65(X49)-0.90(X51) (0.33) (0.35) (0.27) (0.86) (1.05) (0.39)
MH	ND ³	
SR:		
IP	18	Y=3.32-1.29(X44)+1.34(X45)+2.80(X47)-0.77(X49)-0.06(X51) (0.34) (0.36) (0.28) (0.90) (1.10) (0.40)
MH	6	Y=2.12-0.47(X0)-0.10(X8)+0.25(X9)+0.90(X10) (0.12) (0.26) (0.20) (0.18) (0.39)
SD:		
IP	9	Y=1.1-0.45(X11)+0.54(X12)+0.94(X14)-0.12(X16)+0.05(X18) (0.11) (0.11) (0.12) (0.31) (0.34) (0.13)
MH	6	Y=0.63-0.35(X0)-0.07(X8)+0.14(X9)+0.53(X10) (0.08) (0.18) (0.13) (0.13) (0.27)

¹Species codes are in Table C.1.; SR=species richness, SD=species diversity (Shannon-Weaver).

²IP=International Paper, MH=Moosehorn National Wildlife Refuge.

³ND= number of survey points with detected birds <10.